

# Wind turbine operational optimization considering revenue and fatigue objectives

A thesis accepted by the Faculty of Aerospace Engineering and Geodesy  
of the University of Stuttgart in fulfillment of the requirements  
for the degree of Doctor of Engineering Sciences (Dr.-Ing.)

by

Vasileios Pettas

born in Athens, Greece

Main referee: Prof. Dr. Po Wen Cheng  
Co-referee: Prof. Dr. Carlo Luigi Bottasso

Date of defense: 23.01.2024

Stuttgart Wind Energy at the Institute of Aircraft Design  
University of Stuttgart  
2024



# Contents

<b>List of Figures</b>	<b>v</b>
<b>List of Tables</b>	<b>ix</b>
<b>Abbreviations</b>	<b>xi</b>
<b>List of Symbols</b>	<b>xiii</b>
<b>Abstract</b>	<b>xv</b>
<b>Kurzfassung</b>	<b>xvii</b>
<b>1 Introduction</b>	<b>1</b>
1.1 Motivation . . . . .	1
1.2 Research areas and research objectives . . . . .	2
1.3 Thesis structure and organization . . . . .	4
<b>2 Background</b>	<b>7</b>
2.1 Background information and related research . . . . .	7
2.2 Definitions and metrics . . . . .	14
2.3 Aeroelastic simulations and turbine definition . . . . .	18
2.4 Wind turbine control . . . . .	20
2.5 Introduction to surrogate modelling . . . . .	32
<b>3 Controller design</b>	<b>35</b>
3.1 Baseline controller design for the DTU 10 MW rwt . . . . .	35
3.2 Down-regulation . . . . .	40
3.3 Power boosting . . . . .	42
3.4 Individual blade control . . . . .	44
3.5 Summary-Conclusions . . . . .	50
<b>4 Surrogate modelling and aero-servo-elastic analysis</b>	<b>53</b>
4.1 Surrogate modelling methodology . . . . .	53
4.1.1 Input and output variable space . . . . .	54
4.1.2 Regression approaches . . . . .	56
4.2 Uncertainty quantification . . . . .	59
4.3 Aero-servo-elastic analysis . . . . .	66
4.3.1 Discussion on tradeoffs and optimization potential . . . . .	75
4.4 Summary . . . . .	78

<b>5</b>	<b>Evaluation-optimization framework</b>	<b>81</b>
5.1	Accumulation and evaluation framework . . . . .	81
5.2	Optimization problem formulation . . . . .	84
5.3	Assumptions and considerations about the method . . . . .	92
5.4	Summary . . . . .	95
<b>6</b>	<b>Data sets and definition of scenarios</b>	<b>97</b>
6.1	Presentation and analysis of data sets . . . . .	97
6.2	Definition and discussion of optimization scenarios . . . . .	107
6.3	Summary . . . . .	111
<b>7</b>	<b>Optimization results and discussion</b>	<b>113</b>
7.1	Potential . . . . .	114
7.1.1	Baseline reponse . . . . .	114
7.1.2	Potential by applying IBC . . . . .	122
7.1.3	Potential by applying down-regulation . . . . .	125
7.1.4	Potential by applying selective shutdown . . . . .	128
7.1.5	Potential by applying power boosting . . . . .	131
7.2	Optimization under fixed prices . . . . .	133
7.2.1	Fatigue damage minimization under fixed prices . . . . .	134
7.2.2	Revenue maximization under fixed prices . . . . .	146
7.2.3	Sensitivity to wind distribution uncertainty under fixed prices . . . . .	156
7.3	Optimization under fluctuating market prices . . . . .	159
7.3.1	Fatigue damage minimization under fluctuating market prices . . . . .	159
7.3.2	Revenue maximization under fluctuating market prices . . . . .	170
7.3.3	Sensitivity to day ahead forecast uncertainty under fluctuating prices . . . . .	186
7.3.4	Sensitivity to forecast horizon length under fluctuating prices . . . . .	189
7.3.5	Sensitivity to wind distribution uncertainty under fluctuating prices . . . . .	192
7.4	Discussion . . . . .	194
<b>8</b>	<b>Conclusions</b>	<b>199</b>
8.1	Summary . . . . .	199
8.2	Conclusions . . . . .	200
8.3	Recommendations for future work . . . . .	204
	<b>Appendix</b>	<b>207</b>
A.1	Code and data availability . . . . .	207
A.2	Publications . . . . .	207
	<b>Bibliography</b>	<b>209</b>

# List of Figures

- 1.1 The different components of the present work building upon each other to evaluate the research objective . . . . . 4
- 1.2 Overview of the components of the operational optimization method proposed in this work . . . . . 6
  
- 2.1 Control regions of a wind turbine. . . . . 21
- 2.2 Example maps of  $\lambda$ - $\theta$ - $C_p$  and  $\lambda$ - $\theta$ - $C_t$  . . . . . 27
- 2.3 Schematic representation of the different IPC schemes. . . . . 29
- 2.4 Possible controller trajectories for generator torque and generator speed considering power boosting . . . . . 31
  
- 3.1  $\lambda$ - $\theta$ - $C_p$  and  $\lambda$ - $\theta$ - $C_t$  maps for the DTU 10 MW rwt used for the controller design 37
- 3.2 Effect of the torque-speed ramp on region 1.5. . . . . 38
- 3.3 Block diagram of the full controller and actuators . . . . . 39
- 3.4 Steady state operational characteristics for the baseline controller . . . . . 39
- 3.5 The two trajectories considered for the derivation of down-regulation set points along with the minimum  $C_t$  trajectory . . . . . 40
- 3.6 Steady state operational characteristics for the two down-regulation trajectories 42
- 3.7 Power boosting controller trajectories for generator torque and speed . . . . . 43
- 3.8 Steady state operational characteristics for the power boosting mode . . . . . 44
- 3.9 Identified linear model and FAST simulation response around 16 m/s with 5% turbulence intensity . . . . . 46
- 3.10 Block diagram of the IBC controller . . . . . 47
- 3.11 Filter design for the IBC loop . . . . . 48
- 3.12 Indicative time series of the pitch angle of each blade along with the mean pitch value for a simulation with mean wind speed 18 m/s . . . . . 49
- 3.13 Blade root flapwise moment and pitch rate PSD at 16 m/s . . . . . 50
- 3.14 Overview of the controller structure, including the switching between modes cascaded in the decision-making loop . . . . . 51
  
- 4.1 Overview of the procedure to create, apply and validate a surrogate model. . . 54
- 4.2 Sampling of validation set based on the latin hypercube method . . . . . 57
- 4.3 Box plots of the relative error and relative absolute error . . . . . 60
- 4.4 Comparison between the surrogate response and the validation set per quantity of interest . . . . . 62
- 4.5 Relative error between the surrogate predictions and the validation dataset sorted per input variable for blade loads . . . . . 63
- 4.6 Relative error between the surrogate predictions and the validation dataset sorted per input variable for the tower bottom loads . . . . . 64

4.7	Relative error between the surrogate predictions and the validation dataset sorted per input variable . . . . .	64
4.8	Relative error between the surrogate predictions and the validation dataset sorted per input variable for the low-speed shaft loads . . . . .	65
4.9	Relative error between the surrogate predictions and the validation dataset sorted per input variable for mean power and blade pitch travel. . . . .	66
4.10	GPR surrogate response for the tower bottom DELs. . . . .	67
4.11	GPR surrogate response for the tower top/nacelle loads. . . . .	69
4.12	GPR surrogate response for the blade root loads. . . . .	71
4.13	GPR surrogate response for the low-speed shaft loads. . . . .	73
4.14	GPR surrogate response for electric power, energy, and blade pitch travel. . . .	74
5.1	Overview of the accumulation process . . . . .	82
5.2	Example output of the framework applied to evaluate different operational strategies . . . . .	83
5.3	Schematic overview of the optimization process for all cases considered . . . .	89
6.1	Example time series of the data used . . . . .	100
6.2	Wind speed PDFs and CDFs, and TI distributions over wind speeds for all years and locations considered . . . . .	101
6.3	Fitted Weibull distributions for the wind speeds at both sites using all the available data . . . . .	102
6.4	Electricity price PDFs and CDFs for all years and markets considered . . . . .	103
6.5	Percentage of time when the turbine: is not operating (upper), the mean wind speed is above baseline rated (middle), the mean wind speed is above rated and the price higher than the mean of the year (lower) for all years and sites. . . .	104
6.6	Bivariate probability of wind speed and electricity prices for all years and sites considered . . . . .	106
7.1	Contribution of wind speed and electricity prices bins to the total revenue for all years and sites considered using the baseline control mode in fluctuating market prices . . . . .	116
7.2	Contribution of wind speed and electricity prices bins to the total revenue for all years combined . . . . .	117
7.3	Contribution of wind speed and electricity prices bins to the total accumulated damage for the tower, nacelle, and low-speed shaft loads using the baseline controller in fluctuating market prices . . . . .	119
7.4	Contribution of wind speed and prices bins to the total accumulated damage for the blade loads using the baseline controller in fluctuating market prices . .	121
7.5	KPIs by applying the IBC loop per year and location considered . . . . .	122
7.6	KPIs by applying the IBC for wind speeds above the threshold considering all years for both locations . . . . .	123
7.7	KPIs by operating the turbine constantly in different power levels below the baseline for the whole period in both locations considered . . . . .	126
7.8	KPIs by applying selective shut-down based on projected revenue thresholds. .	130
7.9	Expected relative increase in revenue compared to the baseline operation by constantly applying different levels of power boosting under fluctuating prices	132

7.10	KPIs by applying constant power boosting for the whole period considered and both locations under fixed prices . . . . .	133
7.11	KPIs for revenue-neutral load minimization cases under fixed prices using both trajectories for the whole period considered for both locations and different maximum power levels . . . . .	135
7.12	KPIs for revenue-neutral load minimization under fixed prices using both trajectories per year and per location . . . . .	138
7.13	Power level per wind speed bin resulting from revenue-neutral load minimization for all locations and trajectories . . . . .	139
7.14	KPIs for load minimization cases including a revenue reduction cap of 5% for the DE site . . . . .	141
7.15	KPIs for load minimization cases including a revenue reduction cap of 5% for the DK site . . . . .	143
7.16	Power level per wind speed bin resulting from optimization using wind speed distributions for load minimization with a revenue reduction cap of 5% for all locations and trajectories . . . . .	145
7.17	KPIs for load-neutral revenue maximization cases under fixed prices using both trajectories for the whole period considered for both locations and different maximum power levels . . . . .	147
7.18	KPIs for load neutral revenue maximization under fixed prices using both trajectories per year and per location . . . . .	149
7.19	Power level per wind speed bin resulting from optimization for load-neutral revenue maximization for all locations and trajectories . . . . .	150
7.20	KPIs for revenue maximization cases including a load increase cap of 5% cases under fixed prices for the DE site . . . . .	152
7.21	KPIs for revenue maximization cases including a load increase cap of 5% cases under fixed prices for the DK site . . . . .	153
7.22	Power level per wind speed bin resulting from optimization using wind speed distributions for revenue maximization with a load increase cap of 5% for all locations and trajectories . . . . .	155
7.23	Resulting Weibull wind speed distributions by varying the originally derived coefficients by $\pm 10\%$ . . . . .	156
7.24	Results of optimization cases compared to baseline operation under fixed prices using the modified Weibull distributions . . . . .	157
7.25	KPIs for revenue-neutral load minimization cases under fluctuating prices using both trajectories for the entire period considered for both locations and different maximum power levels . . . . .	160
7.26	KPIs for revenue-neutral load minimization under fluctuating prices using both down-regulation trajectories per year . . . . .	162
7.27	Relative differences of revenue, energy, and fatigue damage for the TBMy and BRMz loads to the baseline per wind speed-price bin for the DK 2019 data considering the revenue-neutral load minimization scenario under fluctuating prices . . . . .	164
7.28	KPIs for load minimization cases including a revenue reduction cap of 5% under fluctuating prices for the DE site . . . . .	166

7.29	KPIs for load minimization cases including a revenue reduction cap of 5% under fluctuating prices for the DK site . . . . .	167
7.30	KPIs for load minimization cases including a revenue reduction cap of 5% under fluctuating prices for the DE2022 dataset . . . . .	169
7.31	KPIs for load-neutral revenue maximization cases under fluctuating prices using both trajectories for the entire period considered for both locations and different maximum power levels . . . . .	171
7.32	KPIs for load-neutral revenue maximization under fluctuating prices using both trajectories per year . . . . .	174
7.33	Relative differences of revenue, energy, and fatigue damage for the TBMy and BRMz loads to the baseline per wind speed-price bin for the DK 2015 data considering load-neutral revenue maximization under fluctuating prices . . . .	176
7.34	Relative differences of revenue, energy, and fatigue damage for the TBMy and BRMz loads to the baseline per wind speed-price bin for the DE 2018 data considering load-neutral revenue maximization under fluctuating prices . . . .	178
7.35	Relative differences of revenue, energy, and fatigue damage for the TBMy and BRMz loads to the baseline per wind speed-price bin for the DE 2022 data considering load-neutral revenue maximization under fluctuating prices . . . .	179
7.36	KPIs for revenue maximization with a load increase cap under fluctuating prices using both trajectories for the DE site . . . . .	181
7.37	KPIs for revenue maximization with a load increase cap under fluctuating prices using both trajectories for the DE2022 dataset . . . . .	183
7.38	KPIs for revenue maximization with a load increase cap under fluctuating prices using both trajectories for the DK site . . . . .	185
7.39	Example time series of wind speed, TI, and electricity prices with the added uncertainty from the DK2015 dataset . . . . .	187
7.40	Comparison of results of load neutral cumulative revenue maximization based on DA forecasts under fluctuating prices with and without uncertainty in the forecast . . . . .	188
7.41	Comparison of results for revenue-neutral cumulative fatigue damage minimization based on DA forecasts under fluctuating prices with and without uncertainty in the forecast . . . . .	189
7.42	Results of optimization cases compared to baseline operation in fluctuating prices using varying forecast horizon lengths. . . . .	190
7.43	KPIs of revenue maximization cases under fluctuating prices using the modified Weibull distributions representing the uncertainty in wind speed distribution estimation . . . . .	193

# List of Tables

2.1	Metrics definitions, abbreviations and units . . . . .	17
2.2	DTU 10 MW rwt design parameters . . . . .	19
2.3	Natural frequencies of the DTU 10 MW rwt . . . . .	19
3.1	Pitch actuator and generator speed filter modelling parameters . . . . .	36
3.2	Design characteristics of the baseline controller . . . . .	37
4.1	Variables and parameters for the simulations used to create the training set . .	56
4.2	Kernel functions and basis functions used in GPR for the different quantities of interest . . . . .	59
4.3	Evaluation metrics of the GPR and spline-based surrogate models compared to the validation set . . . . .	61
4.4	Qualitative summary of DELs' sensitivity to the controller modes and wind conditions. . . . .	76
5.1	Instantaneous and cumulative quantities included in the output of the evaluation framework . . . . .	82
5.2	Hyperparameters used for the GA and PSO algorithms as implemented in the Matlab optimization toolbox. . . . .	92
6.1	Overview of datasets used . . . . .	100
7.1	Absolute performance metrics for the baseline operation for all periods and sites considered . . . . .	114
7.2	Relative increase in blade pitch travel by applying IBC and percentage of time IBC is active for various activation thresholds considering all years for both locations . . . . .	124



# Abbreviations

AEP	Annual energy production
BR <sub>Ip</sub>	In-plane blade root moment
BR <sub>Mx</sub>	Edgewise blade root moment
BR <sub>My</sub>	Flapwise blade root moment
BR <sub>Mz</sub>	Blade root torsion
BR <sub>Oop</sub>	Out-of-plane blade root moment
BS	Band stop
CapEx	Capital expenditure
CDF	Cumulative distribution function
CfD	Contract for differences
CorRES	Correlations in renewable energy sources
CPC	Collective pitch control
DA	Day-ahead
DE	Germany
DEL	Damage equivalent load
DK	Denmark
DOE	Design of experiment
DoF	Degree of freedom
DTU	Technical university of Denmark
FAST	Fatigue, Aerodynamics, Structures, and Turbulence
GA	Genetic algorithm
GPR	Gaussian process regression
HP	High pass
IBC	Individual blade control
IEC	International Electrotechnical Commission
IPC	Individual pitch control
KPI	Key performance indicator
LCOE	Levelized cost of energy
LHM	Latin hypercube method
LP	Low pass
LSSM <sub>y</sub>	Low-speed shaft moment around y-axis
LSSM <sub>z</sub>	Low-speed shaft moment around z-axis
LSST <sub>q</sub>	Low-speed shaft torque
LTI	Linear time-invariant
LU	Luxemburg
MAE	Mean absolute error

ME	Mean error
MedAE	Median absolute error
ND	Non-dimensional
NEWA	New European wind atlas
NREL	National Renewable Energy Laboratory
O&M	Operations and maintenance
OpEx	Operating expenses
PDF	Probability density function
PI	Proportional integral
PID	Proportional integral derivative
PitchTr	Blade pitch travel
PPA	Power purchase agreement
PSD	Power spectral density
PSO	Particle swarm optimization
Rev	Revenue
rwt	Reference wind turbine
SCADA	Supervisory control and data acquisition
SISO	Single input single output
std	Standard deviation
SWE	Stuttgart Wind Energy
TBM <sub>x</sub>	Fore-aft tower bottom moment
TBM <sub>y</sub>	Side-side tower bottom moment
TBM <sub>z</sub>	Tower bottom torsion
TI	Turbulence intensity
TKE	Turbulence kinetic energy
TSR	Tip speed ratio
TTM <sub>x</sub>	Tower top roll moment
TTM <sub>y</sub>	Tower top pitch moment
TTM <sub>z</sub>	Tower top yaw moment
VAF	Variance accounted for
VSPR	Variable speed pitch regulated
WF	Wind farm
wsp	Wind speed
WT	Wind turbine

# List of Symbols

## Greek letters

$\alpha$	Wind shear power law coefficient
$\Delta$	Difference
$\kappa$	Torque controller gain
$\lambda$	Tip speed ratio
$\mu()$	Mean function of Gaussian process
$\omega_{rot}$	Rotational speed of the rotor
$\omega_g$	Rotational speed of the generator
$\omega_{g,rat}$	Rated rotational speed of the generator
$\omega_{g,1.5,max}$	Maximum rotational speed of the generator in control region 1.5
$\omega_{g,1.5,min}$	Minimum rotational speed of the generator in control region 1.5
$\omega_{NS}$	Natural frequency of the mechanical system for controller design
$\omega_N$	Natural frequency of the notch filter
$\rho$	Density
$\sigma^2$	Variance
$\theta$	Blade pitch angle
$\theta_{fine}$	Blade pitch angle for control region 2
$\xi$	Damping ratio

## Roman letters

$A$	Weibull distribution shape parameter
$A_{rot}$	Rotor area
$B$	Number of bins
$c$	Material/cross-section constant
$C_p$	Power coefficient
$c_{pen}$	Constant defining the gain of the penalty term
$C_t$	Thrust coefficient
$D$	Damage
$e$	Error
$F()$	Objective function

---

$g$	Gravitational acceleration constant
$g_i()$	Evaluation function for threshold exceedance of objectives
$i_{GB}$	Gear box ratio
$J$	Moment of inertia
$k$	Weibull distribution scale parameter
$K()$	Covariance kernel matrix
$k()$	Covariance function of Gaussian process
$K_P$	Proportional gain
$K_I$	Integral gain
$l_i$	Lower bound
$m$	Wöhler exponent
$M_a$	Aerodynamic torque
$M_g$	Generator torque
$M_{g,max15}$	Maximum generator torque in control region 1.5
$M_{g,rat}$	Rated generator torque
$M_{loss}$	mechanical torque loss in the drive train
$N$	Number of stress cycles
$N_{crit}$	Critical number of stress cycles for failure
$N_{eq}$	Equivalent number of stress cycles for the derivation of DEL
$P$	Power
$P_{rat}$	Rated power
$Q$	Quantity
$Q_{depth}$	Notch filter parameter regulating the depth
$Q_{width}$	Notch filter parameter regulating the width
$R$	Radius
$R^2$	Coefficient of determination
$S$	Load range
$T$	Thrust force
$T_h$	Forecast horizon duration
$t$	time
$u$	Wind speed
$u_i$	Upper bound
$w$	Weight
$x$	Input
$X$	Input variable space
$y$	Output

# Abstract

Wind energy holds significant importance in achieving the energy transition towards a sustainable, carbon-free energy future. The core technology has matured over the last decades, resulting in a substantial increase in installed capacity. While these advancements have led to considerable cost reductions, they have also brought about reductions in mechanisms supporting the economic viability of wind energy projects. Additionally, wind energy is required to play a more substantial role in supporting the electrical network, traditionally done by conventional generation technologies. However, wind energy differs fundamentally from these technologies in terms of cost allocation through the project's lifecycle and the ability to forecast and regulate energy production. These factors have given rise to new challenges for wind energy research, expanding its focus on topics such as enhancing grid integration, increasing profitability, and better utilization of existing farms through lifetime extension.

The objective of this thesis is to support these goals by introducing a methodology for the management of long-term operational objectives, in terms of revenue and fatigue loading, based on adaptive control considering wind conditions and electricity prices. Currently, wind turbines produce power according to the wind conditions, operating in a single mode for most of their operational life. However, wind turbines have the capability to adjust their power output. They can operate in down-regulation, producing lower power than the baseline mode, which also decreases structural loading. Moreover, they can operate in power-boosting mode, which allows for exceeding the baseline power level at higher wind speeds with a tradeoff in structural loading. Additionally, modern turbines are capable of individually adjusting the pitch angle of each blade, enabling individual pitch control (IPC), which can reduce structural loading with the penalty of increased pitch actuator usage. These functionalities require mainly software modifications and can be applied to most machines, allowing for switching between modes according to an external decision-maker. The active management of power output and fatigue loading over time (e.g, in hourly intervals) according to wind conditions and electricity prices enables operational strategies for optimizing long-term objectives. Fatigue consumption and revenue generation can be effectively redistributed over time and conditions in an optimal manner, providing additional flexibility to both wind farm owners and grid operators.

Exploring this research objective requires a multidisciplinary approach encompassing aspects of controller design, surrogate modeling, and optimization. As a first step, a multi-mode

controller is synthesized, allowing adjustment of the power level between 50% and 130% of the baseline level and the optional application of an IPC loop. Two configurations are considered to assess the impact of the choice of down-regulation trajectory on structural load reduction. The IPC loop is based on an individual blade control (IBC) approach involving an independent controller for each blade.

In the next step, a data-driven surrogate model is created based on mid-fidelity aeroelastic simulations. Two regression approaches are considered: a spline-based interpolation and a Gaussian process regression (GPR). The two methods performed very similarly with low uncertainty in their predictions, possibly due to the dense factorial sampling considered.

The surrogate model is utilized to develop an evaluation-optimization framework for long-term operational strategies. As a monitoring tool, it resembles a digital twin, enabling the tracking of fatigue consumption across all components, revenue accumulation, and other metrics potentially useful for condition monitoring purposes based on input time series of wind and prices. Two optimization approaches are developed within this framework. The first employs as input the mean wind distribution, aiming to optimize the controller mode per wind speed, thereby creating a long-term operational schedule according to wind conditions. The second approach leverages forecasts of wind speeds and electricity prices to assign the optimal control mode per time step within the designated horizon.

The proposed method is evaluated using two multi-year datasets, each representing distinct boundary conditions with regard to wind and price dynamics. Two optimization scenarios are considered, reflecting potential business cases: revenue maximization with a constraint on fatigue damage accumulation and fatigue damage minimization with constraints on cumulative revenue. This methodology is employed to assess the applicability and performance of the proposed operational approach for different objectives, considering both fixed and fluctuating market prices. Furthermore, it investigates the impact of controller design, optimization approach, and boundary conditions on the optimization outcomes.

The results indicate that the method is able to concurrently optimize the revenue and fatigue loads in the long term. The two optimization approaches exhibited differences in terms of improvements achieved and the distribution of fatigue and revenue. Fatigue reduction was possible across all wind turbine components, suggesting that it can enable lifetime extension for the entire system while maintaining profitability. Revenue maximization cases showed higher dependency on the optimization approach and the maximum power boosting level considered. For the forecast-based optimization, the length of the horizon considered proved to be critical. For all cases, the most influential factor determining the extent of improvement was found to be the boundary wind and market dynamics. Overall, this thesis demonstrates that there is potential for optimizing long-term objectives using adaptive control, and it is worth exploring it further to address current research challenges in wind energy.

# Kurzfassung

Die Windenergie ist von großer Bedeutung für die Energiewende. Technologische Weiterentwicklungen und Skalierungseffekte beim Ausbau haben zu Kostensenkungen geführt, die wiederum die Reduktion staatlicher Subventionen nach sich gezogen haben. Zudem muss die Windenergie durch die Reduktion konventioneller Kraftwerke eine größere Rolle bei der Unterstützung des Stromnetzes spielen. Dabei unterscheidet sich die Windenergie grundlegend von konventionellen Kraftwerken, in Bezug auf die Kostenzuweisung über den Lebenszyklus sowie die Fähigkeit zur Vorhersage und Regulierung der Energieerzeugung. Diese Faktoren haben zu neuen Herausforderungen für die Windenergieforschung geführt, etwa die Verbesserung der Netzintegration, die Steigerung der Rentabilität und die bessere Nutzung bestehender Anlagen durch Verlängerung der Lebensdauer.

Diese Arbeit soll einen Beitrag zur Umsetzung dieser Ziele leisten. Konkret wird eine adaptive Anlagensteuerung für langfristige Betriebsziele in Bezug auf Einnahmen und Ermüdungslasten eingeführt, wobei Windbedingungen und Strompreise berücksichtigt werden. Gegenwärtig hängt die Stromproduktion hauptsächlich von den Windverhältnissen ab und die Anlagen werden überwiegend in einem einzigen Modus betrieben. Windenergieanlagen können jedoch ihre Leistungsabgabe anpassen. Sie können gedrosselt betrieben werden, meist verbunden mit geringeren strukturellen Lasten. Alternativ können sie gezielt über Nennleistung betrieben werden, was jedoch oft mit höheren strukturellen Lasten verbunden ist. Darüber hinaus erlauben moderne Anlagen eine blattindividuelle Anstellwinkelsteuerung (IPC), die strukturelle Lasten verringern kann, wobei jedoch die Stellmotoren stärker beansprucht werden. Diese Funktionen erfordern in erster Linie Softwareanpassungen und können auf den meisten Anlagen angewandt werden, so dass die Umschaltung zwischen den Modi in Abhängigkeit von einer externen Entscheidungsinstanz möglich ist. Das aktive Management der Leistungsabgabe und der Ermüdungslasten im Zeitverlauf (z. B. in stündlichen Intervallen), abhängig von Windbedingungen und Strompreisen, ermöglicht Betriebsstrategien zur Optimierung langfristiger Ziele. Die Energieabgabe ins Netz und die Erträge können über die Zeit optimal unverteilt werden, was Windparkbesitzern und Netzbetreibern zusätzliche Flexibilität bietet.

Die Umsetzung dieses Forschungsziels erfordert einen multidisziplinären Ansatz, der Aspekte des Reglerentwurfs, der Surrogat-Modellierung und der Optimierung umfasst. In einem ersten Schritt wird ein Regler mit mehreren Betriebsmodi entwickelt, der eine Anpassung der Leistung

zwischen 50% und 130% der Leistung des Normalbetriebs und die optionale Anwendung einer IPC-Schleife ermöglicht. Es werden zwei Konfigurationen betrachtet, um die Auswirkungen der Wahl der Drosselungstrajektorie auf die strukturelle Lastreduzierung zu bewerten. Die IPC-Schleife basiert auf einem Ansatz der Einzelblattsteuerung (IBC), mit unabhängigen Reglern für jedes Blatt.

Im nächsten Schritt wird ein datengetriebenes Surrogate-Modell erstellt, basierend auf aeroelastischen Simulationen. Dabei werden zwei Regressionsansätze untersucht, die ähnliche Vorhersageergebnisse liefern. Das Surrogat-Modell wird zur Entwicklung eines Bewertungs- und Optimierungsansatzes für langfristige Betriebsstrategien herangezogen. Ähnlich einem digitalen Zwilling erlaubt das Surrogat-Modell, den zeitlichen Verlauf von Anlagenzuständen, etwa Ermüdungsfortschritt oder finanzielle Erträge, bei verschiedenen Wind- und Preiszeitreihen effizient abzuschätzen und die Betriebsstrategie zu optimieren. In dieser Arbeit werden zwei Optimierungsansätze untersucht. Der erste verwendet die mittlere Windverteilung und optimiert den Reglermodus pro Windgeschwindigkeit, um so einen langfristigen Betriebsplan entsprechend den Windbedingungen zu erstellen. Der zweite Ansatz nutzt Windgeschwindigkeits- und Strompreisprognosen, um den optimalen Modus für jeden Zeitschritt innerhalb eines festgelegten Zeithorizonts zu bestimmen.

Die vorgeschlagene Methode wird anhand von zwei mehrjährigen Datensätzen evaluiert, die jeweils unterschiedliche Randbedingungen in Bezug auf die Wind- und Preisdynamik darstellen. Es werden zwei Optimierungsszenarien betrachtet (potenzielle Geschäftsfälle): Maximierung der Erträge bei beschränkten Ermüdungslasten sowie Minimierung der Ermüdungslasten bei beschränkten Ertragsverlusten. Für diese Szenarien werden die Anwendbarkeit und Leistungsfähigkeit der entwickelten Methode bewertet, wobei sowohl feste als auch variable Marktpreise berücksichtigt werden. Darüber hinaus wird der Einfluss des Reglerentwurfs, des Optimierungsansatzes und der Randbedingungen auf die Optimierungsergebnisse untersucht.

Die Ergebnisse zeigen, dass die Methode, gleichzeitig Ertrag und die Ermüdungslasten langfristig optimieren kann. Die beiden Optimierungsansätze unterschieden sich in den erzielten Verbesserungen und der Verteilung von Ermüdungslasten und Ertrag. Die Ermüdungslasten aller Komponenten der Windenergieanlage konnten reduziert werden, was nahelegt, dass eine Lebensdauererweiterung des Gesamtsystems bei Erhalt der Rentabilität möglich ist. Für die Ertragsmaximierung zeigt sich eine stärkere Abhängigkeit vom Optimierungsansatz und der betrachteten maximalen Leistungserhöhung. Bei der prognosebasierten Optimierung erwies sich die Länge des betrachteten Horizonts als kritisch. In allen Fällen beeinflusst die Wind- und Preisdynamik das Verbesserungspotential am meisten. Insgesamt weist die Arbeit nach, dass eine adaptive Steuerung Optimierungspotential für langfristige Betriebsziele hat und sich ihre weitere Erforschung für das Voranbringen der Energiewende lohnt.

# Chapter 1

## Introduction

### 1.1 Motivation

Wind energy has emerged as a prominent renewable energy source, playing a pivotal role in the energy transition required for protecting the environment and mitigating climate change. Its higher energy density, compared to other renewable sources, and its versatility in terms of suitable locations, both onshore and offshore, have fueled significant technological advancements and widespread deployment in recent decades.

As a result, wind energy has now matured into a reliable technology, bringing about new demands and expectations. In its earlier stages, wind energy relied heavily on subsidies due to the relatively high costs associated with developing the technology at its infant stages. Additionally, there were minimal requirements placed on supporting the electrical grid. Currently, the landscape has evolved. Subsidies are diminishing or disappearing altogether, putting wind energy projects in direct competition with conventional energy sources. This shift necessitates a focus on cost reduction and revenue enhancement in order to maintain the profitability of wind energy and sustain its growth. Moreover, wind energy producers are required to play a more substantial role in grid stability by providing flexibility and ancillary services.

Thus, the objectives in wind energy research expand from the earlier objectives of optimizing the wind turbine itself by increasing the power output and reducing manufacturing costs to broader ones. These include objectives such as improving the operation to the wind farm level, increasing flexibility in power production and reducing forecasting uncertainty for better grid integration, extending the lifetime to more efficiently utilize already installed plants, increasing revenue and reducing maintenance costs to maintain profitability and attractiveness

of investment, leveraging digitalization and computational power to further improve the performance and reduce costs, reducing environmental impacts, and improving the circularity of the various components among others.

This work aligns with these evolving objectives in wind energy research. It aims to propose an operational management approach that allows for flexible wind turbine operation, focusing on optimizing long-term revenue and fatigue objectives. By utilizing existing control technologies, this approach offers an added degree of freedom for stakeholders, contributing to the broader goals of improving wind energy efficiency and profitability as well as grid integration.

In the current operational paradigm, wind turbines operate during their entire operational lifetime in one control mode, with the power output being dictated by the wind conditions. The only exception to this is when grid operators may require wind farms to curtail power production or shut down entirely for reasons related to grid stability or congestion. Modern wind farm flow control concepts have also employed the concept of down-regulation to mitigate the wake effects downstream of a wind turbine, aiming to enhance the overall performance of the entire wind farm. Furthermore, retrofit packages offered as add-ons exist in the market, offering the possibility to strategically boost the power output beyond baseline levels in specific wind conditions in order to increase power production. Moreover, control technologies focusing on structural load reductions to potentially reduce manufacturing costs, such as individual pitch control, have been developed and extensively tested in the field, but are scarcely employed in commercial wind turbines due to a lack of clear financial benefits.

The proposed operational management integrates these established control technologies and utilizes them within a novel framework for managing the revenue and fatigue damage accumulation over time in order to optimize long-term operational objectives. Taking into account the wind and pricing boundary conditions, energy production and structural fatigue budget can be distributed over conditions and over time more efficiently compared to the current monolithic operational approach. This new approach can enable pursuing various objectives such as maximizing revenue to enhance profitability, extending the operational lifetime, and enabling efficient participation in additional markets such as intraday or balancing electricity markets.

## 1.2 Research areas and research objectives

The present dissertation focuses on the method development and proof of concept of an operational management approach aiming to concurrently optimize the fatigue damage accumulation and revenue generation of a wind turbine during its entire operational lifetime. This task requires a multidisciplinary approach involving the research areas of controller design, surrogate modeling, and mathematical optimization. The different components of the method are built

on top of each other in a modular manner, as illustrated in figure 1.1.

At its core, this method involves designing a wind turbine controller capable of adjusting the power output of the wind turbine as well as employing an individual pitch control loop according to the external commands of the decision maker. Furthermore, using an aeroelastic simulator, a large dataset of simulations is created to capture the wind turbine's response under varying wind conditions for all control modes. This dataset serves as the foundation for creating a data-driven surrogate model able to predict the turbine's response for the entire spectrum of expected conditions quickly and accurately without the need to perform expensive aeroelastic simulations.

Based on this surrogate model, a numerical framework is developed to track the accumulation of key metrics over time. This framework takes into account the input wind conditions, electricity price, and the selected control mode for each time step. An optimization framework is developed around the accumulation framework. The objective is to determine the optimal control mode to assign to each time block, ultimately optimizing cumulative revenue and fatigue objectives by the end of the designated time period.

The potential of the proposed operational approach is evaluated within different scenarios, considering various combinations of revenue and fatigue objectives, that are relevant to practical business cases. These scenarios are realistically evaluated using two historical datasets with distinct wind and price dynamics.

These tools enable the assessment of the efficacy and performance of the proposed operational management method for different objectives and investigate the influence of the controller design, optimization approach, and boundary conditions on the optimization outcomes. This is the overarching research objective of the present work. An overview of the different steps and methods followed to achieve this is provided in figure 1.2.

The specific research objectives are summarized in the following list:

- **Controller design**

Develop a simple and robust wind turbine controller featuring multiple modes, utilizing already applied methods that do not require additional sensors or actuators. Explore diverse controller design approaches to derive down-regulation and power-boosting set points in combination with individual pitch control. Identify the impact of controller design choices on the aeroelastic response of the turbine regarding power production, fatigue loading, and blade pitch actuator usage, as well as the overall optimization outcomes.

- **Surrogate modeling**

Create an efficient surrogate model tailored for the application, encompassing the structural loads for all major components of the system, power production, and other

relevant metrics. Evaluate different methods for creating the surrogate model in terms of uncertainty quantification, complexity, and computational cost.

- **Optimization**

Develop and evaluate an optimization framework that incorporates various optimization approaches that are able to utilize wind speeds, in terms of mean long-term distributions or forecasts, and electricity price forecasts to optimize long-term revenue and fatigue objectives under constant or fluctuating market prices by adapting the control mode of the wind turbine.

- **Overall**

Evaluate the feasibility of managing revenue and fatigue damage accumulation across all major components of a wind turbine, by adapting the power level of the turbine and selectively applying individual pitch control based on an optimization framework used for decision-making. Quantify the expected optimization performance and its sensitivity to different combinations of objectives under different pricing mechanisms, controller configurations, optimization approaches, wind conditions, and market dynamics. Evaluate the impact of input uncertainty on the optimization's performance.

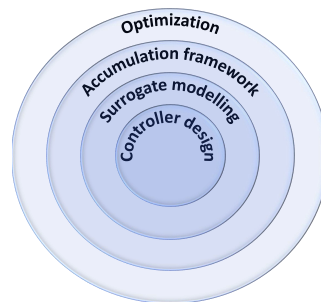


**Figure 1.1:** The different components of the present work building upon each other to evaluate the research objective

## 1.3 Thesis structure and organization

Given the multidisciplinary nature of this work, the thesis chapters are structured to consolidate all relevant information related to each discrete topic within the respective chapter. Each chapter also includes a critical discussion of the methods utilized, potential alternatives, and suggestions for further research on the topic.

**Chapter 2** compiles all the background information and knowledge essential to comprehend the methods and scope of the rest of the work. It presents background information on energy pricing mechanisms, revenue streams for wind turbines, and related research aimed at optimizing systems in directions similar to the work discussed here. Additionally, it introduces

fundamental concepts in wind energy used throughout the thesis, and it offers a summary of the state of the art in the topics of controller design and surrogate modeling. Finally, this chapter introduces the models, software, and metrics used throughout the thesis.

**Chapter 3** encompasses all aspects related to the controller’s design. It introduces the controller synthesis for the baseline operation of a reference wind turbine. Subsequently, the baseline controller is expanded to incorporate additional modes that enable down-regulation, power boosting, and individual pitch control. The rationale behind the tuning and design choices is explained, and their implications are thoroughly discussed. Lastly, the chapter explains the combination and switching between these modes.

**Chapter 4** focuses on the development of surrogate models for all controller modes based on mid-fidelity aeroelastic simulations. The design of experiment approach is motivated, and two methods for creating the surrogate model based on the simulated dataset are introduced. The two models are compared and discussed in terms of complexity, computational costs, and performance. Based on the surrogate model, a comprehensive aero-servo-elastic analysis of the response of the wind turbine under the full range of conditions is performed. This analysis compares various controller design choices and derives insights regarding their potential impact on the optimization.

**Chapter 5** introduces the evaluation-optimization framework. Based on the surrogate model, a data-driven digital twin of the wind turbine is developed. This evaluation framework tracks the instantaneous and cumulative response of the turbine in terms of fatigue damage, energy production, revenue, and other metrics. The chapter also delves into the development of the optimization framework, built upon the evaluation framework, with its primary objective being the long-term management of the wind turbine’s fatigue and revenue. The assumptions considered, the formulation of the objective functions, and the choice of optimization algorithms are presented and critically discussed.

**Chapter 6** provides an overview of the historical datasets, spanning several years, employed to assess the proposed methods. Two locations, each characterized by distinct wind conditions and electricity market dynamics, are considered in order to evaluate the proposed method under varying boundary conditions. The datasets are analyzed, and the attributes relevant to the proposed method are discussed. Furthermore, the optimization scenarios considered for the evaluation of the proof of concept are introduced and critically discussed, focusing on their potential application within real-world business cases.

**Chapter 7** consolidates the components of this study, presenting optimization results. Initially, the potential of each control mode is individually analyzed, establishing optimization bounds stemming from controller design and dataset-specific boundary conditions. Subsequently, results for various scenarios are individually and comparatively discussed, with a differentiation based on pricing mechanisms: fixed prices and fluctuating market prices. The performance

of the methods, as well as the influence of factors such as controller design, optimization approach, wind and market boundary conditions, are critically discussed. Additionally, the chapter includes uncertainty analyses to assess the sensitivity of the optimization outcomes to input uncertainty.

**Chapter 8** concludes the study by summarizing the main findings, offering high-level conclusions about the operational optimization method, and suggesting further research on the topic. For detailed comments and recommendations related to the various research topics and technical implementations, readers are referred to the respective sections within the relevant chapters.

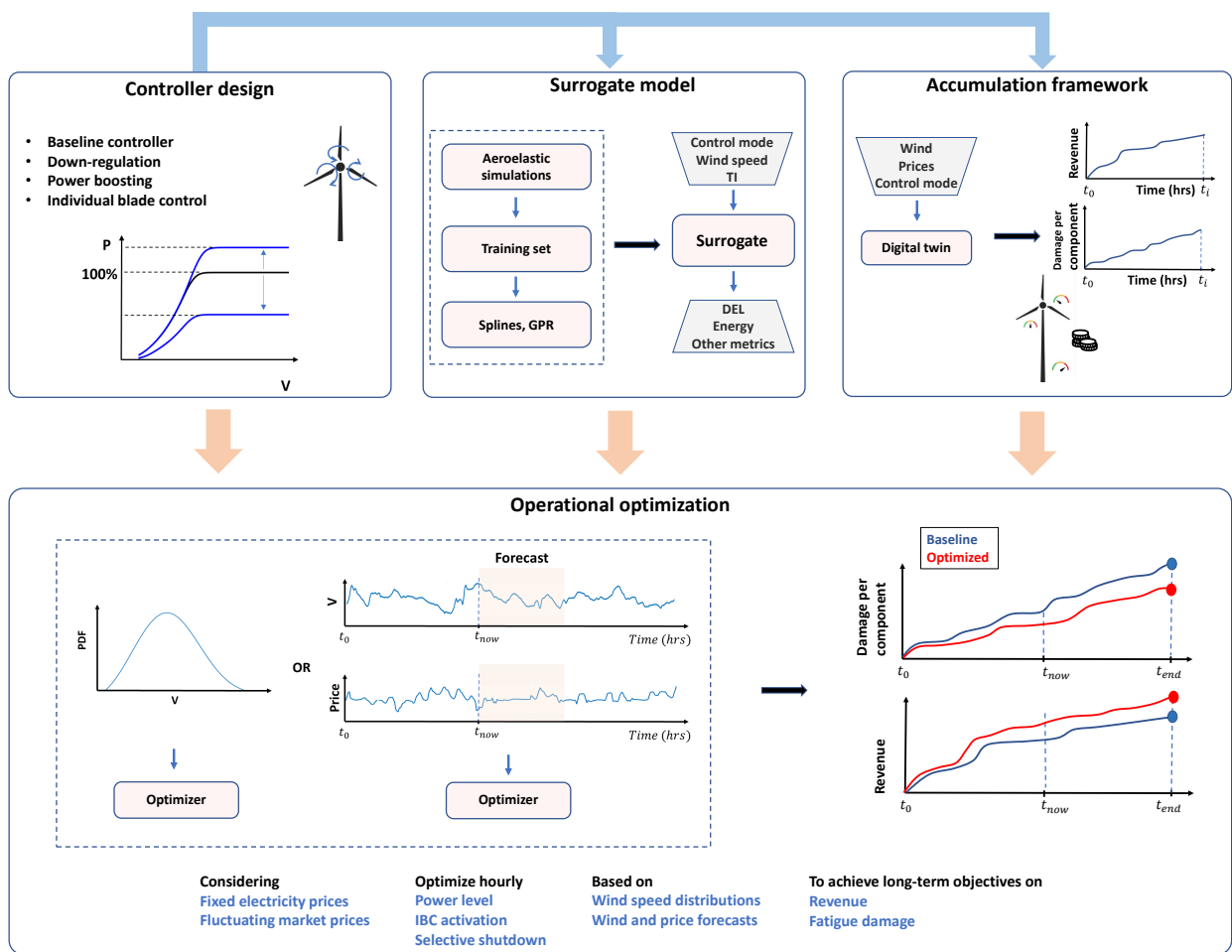


**Figure 1.2:** Overview of the components of the operational optimization method proposed in this work

# Chapter 2

## Background

This chapter provides background information related to the work done in the thesis. Related research and an overview of the state of the art are provided to explain the motivation and context of the research topics involved. Moreover, definitions of quantities, metrics, aeroelastic simulations, and the turbine model used throughout the rest of the thesis are introduced.

### 2.1 Background information and related research

In this section, background information on topics related to the proposed operational management approach to provide an understanding of the context and the motivation. Moreover, related research is discussed in relation to optimization objectives for wind farm operation and the general direction of this work. More specific discussion on the state-of-the-art regarding the technical approaches in controller design, surrogate modeling, etc., can be found in the relevant sections.

The goal of the electricity markets is to ensure efficient balancing between the generation, consumption, distribution, and pricing of electricity. Most markets can be divided into two main segments: the day-ahead (DA) or spot market and the intraday market. Within the DA market, projected consumption is estimated on an hourly basis for the following day. Subsequently, considering the hourly forecasts of renewable energy generation, conventional power producers participate in bidding, operating within the established regulatory framework, by specifying prices and trading volumes. Employing the merit order principle, the lowest bids are accepted with the aim of economically optimizing the electricity supply based on lower marginal costs. This process establishes DA prices for all market participants and determines

which power plants will be designated to deliver the required energy. To address short-term fluctuations in production or demand throughout the day, electricity is actively traded in the intraday market. The intraday market features shorter trading intervals, often extending to just a few minutes, enabling rapid adaptation to changing conditions. Moreover, additional markets exist offering grid balancing services and other ancillary services delivered by flexibility providers.

Within this market model, the pricing mechanism for wind energy producers varies. In its initial stages, wind farm operators received governmental subsidies to offset the high costs associated with wind energy. These subsidies were typically provided in the form of a fixed electricity price guaranteed for a specified number of years or energy production volume. This approach aimed to safeguard the economic viability of wind projects, especially considering the volatility in market prices and wind conditions. Such agreements are often structured as power purchase agreements (PPAs), ensuring a fixed price or employing mechanisms such as two-way contracts for differences (CfDs).

As wind energy technology has matured, cost reductions have become achievable, leading to a decrease in the reliance on subsidies. However, subsidies remain integral to the sustainability of wind energy projects. The newer subsidy schemes involve pricing mechanisms such as constant or sliding premium tariffs, which entail an additional premium on top of the DA prices and other financial instruments such as green certificates. Moreover, wind energy producers are typically not involved in the intraday or secondary markets. This trend has spurred efforts to enhance profitability in order to ensure the continuing expansion of wind energy capacity as the subsidizing mechanisms diminish.

In contrast to conventional fuel-based electricity generation, wind energy requires a high upfront capital investment and has low marginal costs. Moreover, production cannot be flexibly regulated to meet demand or precisely forecasted. Additionally, wind farms are frequently located in remote areas, posing additional challenges on the transmission grid, which can lead to curtailment requests by the grid operator to avoid local grid congestion. These facts highlight the challenges in grid integration and expansion of wind energy while maintaining profitability and attractiveness of investment.

As the fundamental technology involved in wind energy generation has matured and wind energy penetration in the mix has increased significantly, research objectives have evolved to adapt to these new requirements. In addition to the traditional objectives of decreasing manufacturing costs and increasing power production, wind energy systems have to be optimized, taking into account objectives such as grid integration, overall profitability, market structures, environmental impact, etc.

In [1], a detailed overview of the challenges of large-scale integration of renewables to the current market structures and pricing mechanisms is provided. The need for change in pricing

mechanisms to capacity-based support schemes in order to support grid integration and ensure profitability is highlighted. In the same direction, [2] discusses the issues of the current structure and recommends potential adaptations in the market structures to accommodate wind energy, such as the consideration of probabilistic bids, the introduction of alternative business models, and leveraging digitalization and artificial intelligence to explore more efficient market clearing mechanisms. [3] examines the potential profitability of turbines without subsidies in Germany through simulations of the present and future electricity systems. The need to look into revenue metrics instead of solely relying on levelized cost of energy (LCOE) and the importance of emission prices in order to maintain the profitability of wind farms is highlighted. [4] explores the cost reductions achieved in wind energy due to technological advancements and examines their impact on pricing mechanisms and overall profitability. The repercussions of this downward price trend are discussed in [5], shedding light on the uncertainties associated with future revenues and their implications on the realization and final investment decisions for offshore wind projects secured through auctions.

Through the analysis of the challenges of increasing renewables penetration in the Irish electricity market, [6] underscores the necessity and potential benefits, for all stakeholders, of transforming the markets from cost-based to value-based able to reward and incentivize flexible and reliable capacity. Additionally, [7] presents findings from a simulation study that explores potential approaches for wind energy producers to participate in balancing markets. The study suggests that such participation can offer both technical and economic advantages to the system and the producers. The study presented in [8] focused on the possible participation of wind in reserve and ancillary markets. The findings indicate that greater participation of wind energy in these markets can be beneficial for the power system and play a crucial role in maintaining the profitability of wind farms, especially as subsidies diminish.

Additionally, as the amount of installed wind capacity with relatively modern machines has increased, the topic of end-of-life decision-making has emerged. Lifetime extension, under the appropriate conditions, can lead to better use of material, accelerating the energy transition as well as increased profitability for the producers. As discussed in [9], decision-making depends on both technical and financial aspects, while novel operational approaches are required to effectively manage structural loads while maintaining profitability.

Echoing these challenges, research focusing on the design and operation of wind turbines and wind farms is adapting its goals. [10] introduces new value-based metrics for renewables, expanding beyond annual energy production (AEP) and LCOE, aiming to better capture the time-varying value of wind energy in electricity markets. In [11], these metrics are utilized within wind farm design optimization, showing how different monetary objectives influence the optimal technical design. Furthermore, [12] delves into the potential and associated technical and legislative challenges of leveraging wind farm control to enable efficient participation in

various electricity markets and ancillary services. The study highlights the importance of price-driven operation and structural load management as crucial enabling factors. [13] identifies the current prospects and grand challenges in the field of wind farm control. It emphasizes the necessity of designing and optimizing wind farms and relevant control strategies with a holistic approach, considering value-based objectives, structural load management, and non-economic objectives like environmental impact. Aligned with these objectives, [14] demonstrates the potential of designing wind turbines taking into account the environmental and societal impact, specifically in terms of generated and displaced greenhouse gas emissions across the entire lifecycle. The findings suggest that significant improvements in environmental and societal objectives can be achieved with a relatively small tradeoff in profitability. Furthermore, [15] explores the benefits of low specific power wind turbine designs on the value of wind energy. Trading maximum power output for higher production in lower wind speeds is shown to have benefits for both farm operators and the grid in terms of revenue, forecasting uncertainty, and reduced balancing and grid costs.

Focusing more on revenue objectives, several approaches have been explored in the literature. From a trading perspective, optimization methods have been proposed that can utilize probabilistic wind generation forecasts to optimize dispatching strategies while participating in both DA and balancing markets [16, 17]. In [17], a trading framework for optimal decision-making is developed to concurrently optimize trading financial products and participating in the day-ahead and intraday electricity markets in the short term. The findings suggest that revenues can be increased within specific risk and uncertainty levels compared to passive participation in the DA market. Furthermore, [18] introduces a profit maximization approach tailored for wind energy producers involved in both DA and reserve markets. This approach involves actively down-regulating the farm's output and optimally trading reserves in the reserve market, ultimately leading to increased expected revenue.

Moreover, revenue maximization has been considered in literature with respect to the operational strategy and control of wind farms. [19] suggests capacity over-installation combined with constant down-regulation to maximize profit, considering the DA market. This strategy involves increasing the wind farm's output at lower wind speeds, and its effectiveness depends on pricing mechanisms and the correlation between wind speeds and prices. In a similar approach, [20] suggests and experimentally evaluates the constant down-regulation of a wind farm by 10% to provide up-regulation reserves in the secondary frequency reserve market. The results demonstrate that this approach is technically feasible and can lead to increased revenue compared to operating the farm at full capacity while participating only in the DA market. The feasibility of this approach depends on the farm's ability to respond accurately and rapidly to up-regulation requests.

The planning of the downtime allocated for preventive maintenance, dictated by the op-

erations and maintenance (O&M) schedule, based on expected revenue is suggested in [21]. The study demonstrates that revenue can be increased when monetary-based availability objectives are considered compared to time-based or production-based approaches. Moreover, [22] introduces an operational concept for wind turbines that combines structural fatigue life estimation with revenue maximization strategies. This concept considers participation in both the DA and intraday markets, factoring in forecasts and balancing costs. The findings demonstrate the potential to improve profitability, emphasizing the importance of managing the lifetime of wind turbines. Notably, the framework is conceptually similar to the approach presented here, although the publication focuses solely on financial considerations, omitting the lifetime management aspect.

Considering research focusing more on the technical aspects of wind farm flow control, only a few publications can be found considering revenue and prices. This shows a gap that needs to be bridged between the research focused on technical implementation at the wind farm/turbine level and research focusing on bidding/dispatching strategies and other finance-oriented topics related to wind energy. On one hand, research focused on the economics of wind energy can benefit by considering more in-depth the technical capabilities and limitations of the current wind energy technology, while more technical research can better focus its objectives on addressing issues that can potentially have a major impact on the value of wind energy.

In [23], the potential of wind farm flow control to optimize revenue considering the DA prices was explored in a comparative study where different modeling and control approaches were evaluated with the same price and wind data representing current and future market scenarios. The results highlighted that revenue increases can be achieved, with the extent of the increase dependent on market conditions. Moreover, it was shown that revenue and energy increases are not necessarily proportional and that the wind and market dynamics exert a high influence on the magnitude of the revenue increase. Additionally, the study emphasized the need for models and frameworks that can consider both revenue and loads in wind farm control optimization, as most of the existing tool chains focus solely on power and neglect structural load considerations. The work presented in [24] explored the potential increase in revenue for wind farms operating within the DA markets by applying wake steering. The study considered historical data across various areas in the US. The expected increase in revenue was found between 0.8% and 1.7%, slightly higher than the expected increase in energy production.

Apart from the value-related objectives, the management of fatigue consumption is the second area of focus in this work. In the context of wind farm control research, the focus has been more on maximizing power production and providing ancillary services, while the topic of fatigue loading is less prominent [25, 26]. There have been fewer published studies, such as [27, 28, 29, 30], that focus on optimizing both power production and fatigue loading simultaneously. These studies typically employ a surrogate model to simulate the loading

of each turbine, utilizing single-turbine aeroelastic simulations and flow models of varying fidelity to account for flow interactions within the farm. The control strategies are derived from multi-objective optimization methods, employing both closed- and open-loop wind farm control approaches.

The optimization of both loads and power in wind farm control has been somewhat limited in the past. However, this approach has gained prominence in recent years due to its significance in achieving comprehensive system optimization. The integration of value-based objectives, including fatigue accumulation objectives, in wind farm control optimization and evaluating long-term operational strategies are important topics that can enable the holistic assessment of the impact of the control methods and, thus, enable wider industry adoption. The method proposed in this work, focusing on a single turbine, contributes to this direction by suggesting multi-objective optimization approaches for cumulative fatigue and revenue objectives, as well as a methodology suitable for the evaluation of the long-term impact of such methods.

Traditionally, research focused on individual wind turbines has concentrated on load reduction and power optimization, primarily oriented towards wind turbine design improvements and potential cost reductions. However, the long-term impact of implementing these strategies on fatigue and revenue, and consequently in topics such as grid integration, profitability, lifetime extension, etc., has not been extensively examined. Leveraging digital twins and condition-monitoring systems for monitoring component fatigue consumption, in combination with adaptive control strategies, can lead to reduced maintenance costs and extended lifetime for the entire turbine or of specific sub-components [31, 9]. To this end, methods implemented on the turbine controller level adapting the controller in real-time have been suggested, as shown for example in [32, 33]. These methods involve the use of real-time load measurements or model-based estimators to internally calculate and accumulate fatigue damage. Subsequently, through a predefined logic, such as targeting a specific damage accumulation level or utilizing model predictive control with a short-term prediction horizon, the control mode continuously adjusts to achieve fatigue reductions while balancing trade-offs with other objectives like power output and actuator usage. Additionally, adaptive control approaches, taking into account both fatigue and power, considering inputs such as the turbulence level [34] or based on load thresholds [35] can be found in the literature.

These approaches align with the research objectives of this work but differ fundamentally in terms of approach and evaluation methodology. In the present work, the controller mode is adapted in a quasi-static manner, with adjustments made for each consecutive hourly time block based on commands from an external decision-maker responsible for assigning the controller mode to the turbine with the aim of optimizing long-term objectives. Moreover, the results in this work are evaluated in terms of cumulative metrics for the fatigue loading of all major components, revenue, and other metrics over multiple years of operation while also considering

the effect of the pricing mechanisms.

In the context of operational management for long-term objectives, literature on the perspective discussed in the present work is rather limited. In [36], a method for selective shut-down of a wind turbine according to the projected revenue threshold is introduced. This approach considers a simplified model for fatigue damage, which is used to estimate potential lifetime extensions by the application of the method. Assuming operation with a fixed subsidy for an initial period and operation in the DA market for the lifetime extension period, the findings suggest that there is potential to increase the overall profitability. The selective shut-down approach is also considered in the present work as a fatigue reduction method in combination with down-regulation and individual pitch control. Additionally, in [37], a reliability-based method for fatigue management of a single turbine is presented, focusing on the blade loads. This approach involves down-regulation and power boosting while optimizing power levels using model predictive control. The power level is optimized for consecutive time blocks based on wind forecast horizons of a few days with the objectives of reducing fatigue damage and increasing energy production. The findings suggest significant reductions in blade fatigue damage, while potential increases in energy are not explicitly reported. Moreover, [38] outlines an operational strategy for targeting fatigue damage accumulation levels of a specific component of a single wind turbine within a wind farm while minimizing the trade-off in energy production. This approach utilizes down-regulation and optimizes power levels based on site-specific mean wind speed distributions. The potential economic benefits of the method are evaluated by considering the lifetime extension of the turbine under the assumption that the damage reductions at the tower represent the entire turbine and that fixed prices will also be valid during the extension period. These recent studies align with the research direction of the present work, underscoring the significance and potential for addressing current research challenges related to long-term operational strategies for wind turbines.

Overall, the literature review and discussions in this section underscore the necessity for operational strategies capable of concurrently managing revenue and fatigue loading in wind turbines over time. This work aims to introduce and evaluate such a methodology for a single turbine based on adaptive control, encompassing down-regulation, power boosting, and individual pitch control. The goal is to assess the method on a technical level, analyzing the tradeoffs between revenue and fatigue accumulation on the entire system under various wind and market conditions. As a foundation, the proof of concept and the example optimization scenarios detailed in this work lay the groundwork for leveraging the method in a broader context, aligning with the diverse research areas discussed in this section.

## 2.2 Definitions and metrics

In this section, definitions of quantities and metrics used throughout the thesis are provided to facilitate the understanding.

### Basic definitions

The electrical or aerodynamic power of a wind turbine ( $P$ ) can be correlated to the wind speed using the dimensionless power coefficient ( $C_p$ ) power coefficient as shown in equation 2.1.

$$P = \frac{1}{2}\rho A_{rot}v^3 C_p \Rightarrow C_p = \frac{2P}{\rho A_{rot}v^3} \quad (2.1)$$

Where  $\rho$  is the density of air,  $A_{rot}$  is the swept area of the rotor, and  $v$  is the uniform, incoming horizontal wind speed.

The aerodynamic thrust force, defined as the axial force applied by the wind on the rotor of a wind turbine, can be correlated to the wind speed using the dimensionless thrust coefficient ( $C_t$ ) using equation 2.2.

$$T = \frac{1}{2}\rho A_{rot}v^2 C_t \Rightarrow C_t = \frac{2T}{\rho A_{rot}v^2} \quad (2.2)$$

The tip speed ratio (TSR or  $\lambda$ ) is a dimensionless parameter defined by the ratio of the translational speed at the tip of the blade to the mean horizontal wind speed. It is useful as it correlates the rotor's rotational speed to the horizontal mean wind speed and provides insights into the performance and efficiency of a rotor. It is used in the aerodynamic and controller design of wind turbines. TSR can be calculated using equation 2.3.

$$TSR = \lambda = \frac{\omega_{rot}R}{v} \quad (2.3)$$

Where  $\omega_{rot}$  is the rotational speed of the rotor, and  $R$  is the rotor's radius.

The Weibull distribution is a widely used probability distribution in wind energy due to its ability to accurately model long-term wind speed distributions. It is employed to represent the wind speed frequency distribution at a specific location using historical measurement data. The distribution's versatility makes it suitable for various wind conditions encountered in different regions. The Weibull distribution is characterized by two parameters: the shape parameter ( $k$ ) and the scale parameter ( $A$ ). The shape parameter determines the skewness and coefficient of variation of the distribution. The scale parameter influences the distribution's spread and height, and is closely correlated to the mean wind speed. The probability density function (PDF) of the Weibull distribution is expressed as defined in equation 2.4

$$f(v; k, A) = \frac{k}{A} \left(\frac{v}{A}\right)^{k-1} e^{-(v/A)^k} \quad (2.4)$$

where  $v$  is the wind speed,  $k$  is the shape parameter, and  $A$  is the scale parameter.

### Structural fatigue calculations

To evaluate the structural reliability of wind turbines under the impact of stochastic cyclic loading, the concept of fatigue damage is used. Fatigue damage (D) and damage equivalent loads (DELs) serve as metrics for quantifying the fatigue impact of load series on a component. Using these, the structural strength required for each component in order to avoid structural failure due to fatigue, for a predefined lifetime duration, can be calculated. Moreover, they enable the comparison of different designs in terms of their impact on fatigue accumulation and, therefore, predicted structural lifetime. As the management of fatigue accumulation is one of the main focuses of this work, the topic is briefly introduced here.

The fatigue performance of a material is typically characterized by the S-N curve. The S-N curve shows the number of cycles (N) for various load ranges (S) a material can endure before failing. Points below the curve indicate the ‘safe’ region, while above, failure occurs. The curve itself represents the critical value. In its logarithmic form, it can be assumed linear with a slope equal to  $-1/m$  where  $m$  is referred to as the Wöhler exponent ( $m$ ). Based on this, the maximum allowed cycles for each load range are calculated using equation 2.5.

$$N = cS^{-m} \quad (2.5)$$

$c$  is a constant correlated to the exact material properties and the shape of the considered cross-section. This is usually not known, and only the manufacturer can provide exact values. When the objective is solely to compare fatigue loads for the same design,  $c=1$  can be assumed, as it is done in the present work. However, for actual design purposes, more information is required.

Damage is a simplified metric to quantify the contribution of a combined loading spectrum, encompassing multiple load ranges and cycles, to structural fatigue accumulation until failure is reached. This simplification, based on Miner’s rule [39], involves the linear addition of the different contributions, in terms of cycles counted per stress range, to determine the total accumulated damage as expressed by equation 2.6.

$$D = \sum_{i=1}^{i=j} \frac{N_i}{N_{crit,i}} = \sum_{i=1}^{i=j} \frac{N_i}{cS_i^{-m}} = \sum_{i=1}^{i=j} N_i S_i^m \quad (2.6)$$

Where  $j$  is the total amount of binned load ranges,  $S_i$  is the mean value of the  $i_{th}$  load

range bin, and  $N_i$  is the number of cycles counted for this load range. These two values can be calculated directly from the signal's loading time series, produced by measurement or simulations, using the rainflow-counting algorithm [40].

By definition, avoiding failure means that  $D \leq 1$ , which is the goal when designing components. Since the material constant  $c$  for each component is unknown, the absolute value of damage cannot be calculated. Consequently, it can only be calculated relatively compared to a reference case. Hence, for the rest of this work, the total cumulative damage calculated for the baseline case over the specified time period will be normalized to 1. This is a conservative assumption implying that the baseline operation consumes the entire damage budget.

DEL is a commonly used metric allowing the comparison of the effects of different dynamic loads for a specific time duration while removing the dependency on  $c$  explained earlier. The idea behind DEL is to define an equivalent load range so that when it is applied for a specific number of cycles  $N_{eq}$ , it results in the same damage as the total load spectrum. DELs can be calculated using equation 2.7.

$$D_{eq} = D \Rightarrow \frac{N_{eq}}{cS_{eq}^{-m}} = \sum_{i=1}^{i=j} N_i S_i^m \Rightarrow S_{eq} = DEL = \left( \sum_{i=1}^{i=j} \frac{N_i}{N_{eq}} S_i^m \right)^{1/m} \quad (2.7)$$

The value of DEL is independent of the simulation length and needs to be used cautiously. While it is effective for comparing different loading cases, DELs cannot be added linearly, e.g., the DEL from two different simulations cannot be added to calculate the total DEL. The value of  $N_{eq}$  can be arbitrarily chosen. In this work, the 1 Hz equivalent load is used. Thus,  $N_{eq}$  is equal to the duration of the signal in seconds. Based on the previous definitions, the transformation between DEL and  $D$  can be derived as shown in equation 2.8.

$$DEL = \left( \frac{D}{N_{eq}} \right)^{1/m} \Rightarrow D = DEL^m N_{eq} \quad (2.8)$$

It should be noted that within this approach, the mean of the load cycle is not considered, only the range. This is a simplified approach used to compare fatigue load levels and evaluate the influence of a proposed method comparatively. Nevertheless, it is important to be considered in real-world applications as it has been demonstrated to have a high influence on the resulting fatigue damage distribution [41, 42].

## Metrics and KPIs definitions

From a fatigue evaluation perspective, the aim of this work is to assess fatigue loading across all major wind turbine components. Thus, all the major components are considered, including the tower, nacelle, blades, and low-speed shaft. The DEL is calculated from the aeroelastic

simulations and used in the surrogate model. Within the developed accumulation framework, the DEL predictions provided by the surrogate are translated to damage and added linearly to track the fatigue accumulation of each component over time. The set of metrics defined is presented in table 2.1. Additional metrics, such as generator speed std, tip-tower clearance, etc., have been recorded from the aeroelastic simulations and are included in the surrogate model but not used within the scope of this work. The complete set of metrics is included in the publicly available repositories (see appendix A.1).

**Table 2.1:** Metrics definitions, abbreviations and units

Abbrev.	Quantity	Metric	Unit	Wöhler
BRMx	Edgewise blade root moment	DEL/D	kNm/ND	10
BRMy	Flapwise blade root moment	DEL/D	kNm/ND	10
BRMz	Blade root torsion	DEL/D	kNm/ND	10
BROop	Out of plane blade root moment	DEL/D	kNm/ND	10
BRIp	In plane blade root moment	DEL/D	kNm/ND	10
TBMx	Fore-aft tower bottom moment	DEL/D	kNm/ND	4
TBMy	Side-side tower bottom moment	DEL/D	kNm/ND	4
TBMz	Tower bottom torsion	DEL/D	kNm/ND	4
TTMx	Tower top roll moment	DEL/D	kNm/ND	4
TTMy	Tower top pitch moment	DEL/D	kNm/ND	4
TTMz	Tower top yaw moment	DEL/D	kNm/ND	4
LSSMy	Low-speed shaft moment around y-axis	DEL/D	kNm/ND	4
LSSMz	Low-speed shaft moment around z-axis	DEL/D	kNm/ND	4
LSSTq	Low-speed shaft torque	DEL/D	kNm/ND	4
Energy	Energy	$\int_{t_o}^{t_{end}} P_{el} dt$	kWh	-
PitchTr	Pitch travel	$\sum_{t_o}^{t_{end}-1}  \theta_{t+1} - \theta_t $	deg	-

The energy output is used to accumulate energy production over time and also calculate the instantaneous and cumulative revenue by multiplying it with the electricity price. Furthermore, pitch travel is used as a metric to track the pitch actuator usage in order to assess the impact of different strategies, and especially the individual pitch control loop, on the pitch system.

The key performance indicators (KPIs) utilized to evaluate the optimization results in chapter 7 include the relative differences in cumulative damage per load, cumulative energy, cumulative revenue, and cumulative pitch travel. The relative differences for all quantities are calculated compared to the baseline operation for a specified period using equation 2.9.

$$\Delta Q = 100 \frac{Q_{new} - Q_{base}}{Q_{base}} \quad [\%] \quad (2.9)$$

Moreover, two additional KPIs are introduced to evaluate the impact of the different

optimization approaches. The first, denoted as *IBC%*, indicates the percentage of time the individual blade control (IBC) loop is active. It is calculated by dividing the amount of time steps the IBC loop was active by the total amount of time steps where the wind turbine was operational (not shut down). Since in the baseline operation, IBC is not considered, the values reported are absolute values.

The second additional KPI, denoted as *Shut%*, quantifies the percentage of time that the wind turbine is intentionally shut down based on the optimization strategy. This metric evaluates the frequency of selective shutdowns requested by each optimization approach. It is defined as the difference in shutdown time between the optimized and the baseline case, divided by the total amount of time the turbine remained operational in the baseline case.

## 2.3 Aeroelastic simulations and turbine definition

The aeroelastic simulations required for this work were performed with the mid-fidelity, open-source tool FAST v8.16.00 [43, 44] provided by the National Renewable Energy Laboratory (NREL). All degrees of freedom available in the structural module ElastoDyn were enabled besides the *YawDOF* option, as the nacelle yaw is maintained constant throughout the simulations. In the aerodynamics module AeroDyn v14.04, the Beddoes dynamic stall model was activated. Additionally, the equilibrium induction-factor model, along with the Prandtl corrections for tip-loss and hub-loss calculations. Moreover, the tower shadow model was deactivated. The settings regarding the turbine configuration and the various modules used in FAST were kept consistent for all simulations.

The FAST software was compiled as an S-function and integrated within a Matlab/Simulink framework. The controller and actuators were designed in Matlab and connected to the S-function within the aforementioned simulation framework. More details on this can be found in section 3.1. Additionally, pre- and post-processing tools were also developed in Matlab for the present work.

The open-source software Turbsim v2.0.0 [45], provided by NREL, was used for generating the numerical wind fields. The grid dimensions were set to 180 by 180 meters with 31 grid points along each dimension. The time step of the wind fields was set to 0.125s. The turbulence model used was the International Electrotechnical Commission (IEC) Kaimal model by enabling the *IECKAI* option along with the IEC normal turbulence model and the default surface roughness length options in Turbsim. The power law model was used for the wind shear. All settings were kept constant for all wind fields generated. The only exceptions are the mean wind speed at the hub height and the turbulence intensity (TI), as discussed in section 4.1.1.

The DTU 10 MW reference wind turbine (rwt) [46] was chosen as a representative of a

modern multi-MW machine resembling the current generation of offshore wind turbines. The turbine is considered in an onshore configuration to reduce computational costs. The main design characteristics are presented in table 2.2. More information on the turbine model and its implementation in FAST can be found in [46, 47]. The system's main natural frequencies are presented in table 2.3

**Table 2.2:** DTU 10 MW rwt design parameters

<b>Turbine Parameters</b>	<b>Value</b>
Rotor radius	89.2 m
Hub Height	119 m
Gearbox ratio	1:50
Rated rotor speed	9.6 rpm
Rated generator speed	480 rpm
Cut in generator speed	275 rpm
Rated generator torque	2.1602E5 Nm
Rated power	10 MW
Electrical efficiency of generator	94%
Mechanical efficiency of gearbox	100%
Power losses from converter	220 kW

Although the proposed operational optimization and the size of the chosen turbine are more relevant for offshore applications, the choice to use the onshore version was motivated to reduce the computational time by excluding hydrodynamics. In a practical implementation, hydrodynamics and offshore foundations should be included. However, the response of the system, in terms of the metrics considered in this work, is not expected to differ substantially in a fixed bottom offshore configuration as the hydrodynamic loads mainly affect the substructure. Consequently, this choice is not expected to affect the optimization outcomes and the applicability of the method considered in this work.

**Table 2.3:** Natural frequencies of the DTU 10 MW rwt

Mode	Natural Frequency Hz
1 <sup>st</sup> Tower	0.26
1 <sup>st</sup> edgewise blade	0.93
1 <sup>st</sup> flapwise blade	0.61
2 <sup>nd</sup> flapwise blade	1.74

## 2.4 Wind turbine control

The wind turbine's control system encompasses several functions, including supervisory control, closed-loop operational control, and the safety system [48, 49, 50]. It relies on sensors to measure essential quantities like blade pitch angle, rotor speed, generator torque, and more. Actuators, such as the generator torque actuator, blade pitch actuators, and the mechanical brake, are employed to execute desired actions according to the logic programmed in the local wind turbine controller software.

The supervisory control loop is the higher-level layer, responsible for switching operational states and ensuring safe operation, managing the overall operation of the system. Some of its main functions include [48]:

- Managing standby operations, such as idling, locked rotor, nacelle yaw orientation, and cable unwinding
- Verifying the execution of the current operational objective and identifying faults
- Initiating the start-up process when conditions meet the requirements
- Initiating the shut-down procedure, whether normal or emergency, in response to fault detection, alarm triggers (e.g., overspeeding or high temperatures), or when wind conditions fall outside the operational range

The closed-loop operational control is responsible for the operation of the turbine, including normal operation, start-up and shut-down maneuvers. For modern multi-MW horizontal axis wind turbines with variable speed and pitch regulation (VSPR), the basic control loop has as inputs the (usually low passed) generator/rotor rotational speed, generator torque, blade pitch angle, nacelle yaw orientation, and wind direction. Additional inputs, such as tower top acceleration, hub height wind speed, load measurements in various locations, etc., can be integrated into secondary control loops aimed at reducing loads or enhancing power production. The outputs of the controller are the generator torque, blade pitch angle, and nacelle yaw angle. The generator, blade pitch motor, and nacelle yaw motor are the actuators responsible for converting these commands to mechanical work.

In normal operation, the closed-loop control is responsible for maximizing power extraction until the design power level. When this is reached, in order to limit structural loads and noise emissions, the controller focuses on keeping the power output constant and the rotor speed and generator torque within a design envelope by engaging the blade pitch system.

This work focuses only on the closed-loop control of the turbine in normal operation, excluding the start-up and shutdown maneuvers. Thus, in the following, more details will be given on these topics as they are relevant to the controller design in this work. More information on the rest of the controller's functionality can be found in [48].

The control regions of a VSPR wind turbine are shown in figure 2.1. The graphs illustrate how power, generator speed, and  $C_p$  relate to the different wind speeds and control regions. Moreover, the characteristic of the generator (torque vs. rotational speed) is shown for the different control regions.

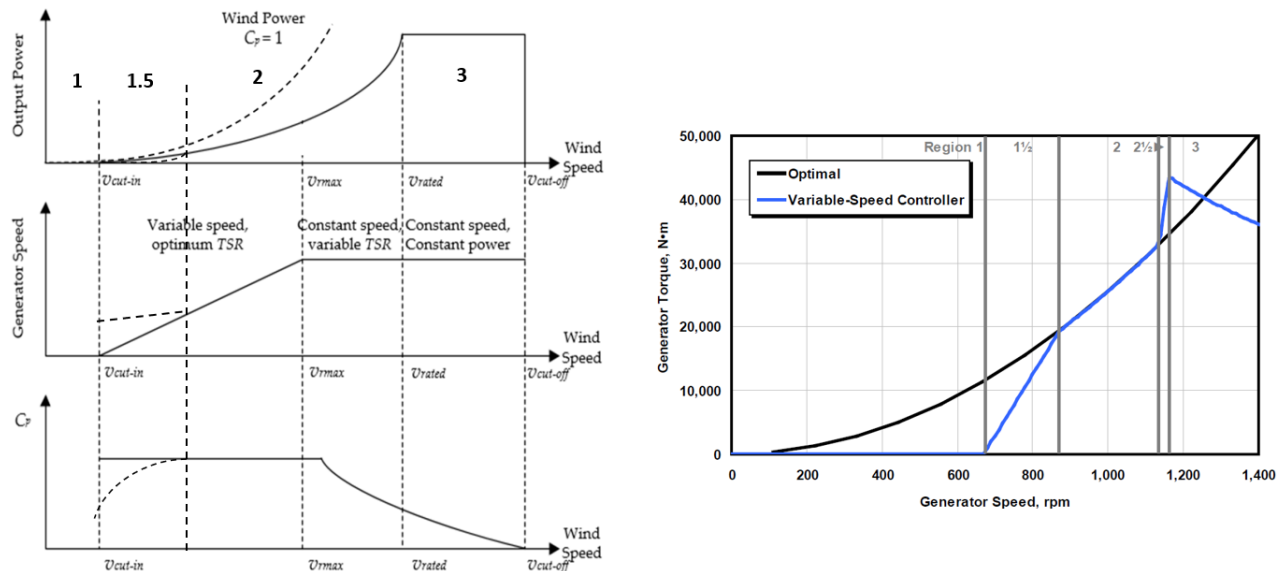


**Figure 2.1:** Control regions of a wind turbine. Left: Power, generator speed and  $C_p$  as a function of wind speed (figure modified from [51]) Right: Example of generator torque vs generator speed for the different control regions (figure modified from [52])

Ideally, a wind turbine would produce power proportional to the cube of the wind speed at every wind speed. Due to technical constraints, this is only possible for a limited range of wind speeds in Region 2. In Region 1, the wind speed is too low; hence, the aerodynamic torque is not able to match the minimum torque of the electrical generator, or it might not even be enough to overcome the rotor's inertia. In this region, the turbine is not producing electricity, and the rotor is either locked or idling.

The minimum wind speed at which the turbine can produce electrical power is called the cut-in wind speed, which denotes the lower limit of control region 1.5. In order to extract the maximum possible power from the wind, a specific rotor rotational speed ( $\omega_{rot}$ ), is necessary, determined by the aerodynamic design of the rotor to attain the designated TSR value associated with the maximum possible power  $C_p$ . In region 1.5, the optimal TSR can not be achieved, leading to sub-optimal power extraction with a reduced  $C_p$ . This occurs because the rotational speed has to be higher than the optimal in order to avoid resonance between the 3P (third harmonic of  $\omega_{rot}$ ) frequency of the rotor and the tower's first natural frequency. This is due to the common "stiff-stiff" design of steel wind turbine towers. Another reason for the minimum rotor speed requirement could be the minimum rotational speed allowed by the electrical generator.

In region 1.5, the controller's objective is to keep rotational speed above the minimum and ensure a controlled trajectory towards the optimal TSR ( $\lambda_{opt}$ ) as wind speed increases while minimizing  $C_p$  reduction and structural loading. The blade pitch angle typically remains constant at the fine pitch value, which is determined by aerodynamic design considerations. The regulation of the rotational speed is achieved by manipulating the generator torque. Two common approaches are employed for controlling the generator torque in this region. The first uses a linear ramp for the torque forcing the rotor speed on a prescribed trajectory [43, 53, 51] as shown in figure 2.1. The second employs a PI loop [54, 53, 55] that sets the rotational speed to the minimum value of region 2 where  $\lambda_{opt}$  is achieved. This PI loop is active until generator torque reaches the minimum value of region 2, effectively creating a vertical trajectory on the torque-speed graph. Both methods have advantages, with the PI loop being able to keep rotor speed closer to  $\lambda_{opt}$  leading to higher energy capture, but on the other hand, the switching between the regions and the decoupling with the PI loop for region 2.5 needs careful handling. In this work, the linear ramp method is used for simplicity.

When design  $\lambda_{opt}$  is reached, control region 2 starts. Here, the generator torque is controlled so that optimal torque is provided for each rotor rotational speed in order to maintain  $\lambda_{opt}$  and thus optimal power extraction. In this region, the controller varies only the generator torque, and the aerodynamically optimal blade pitch angle  $\theta$  is kept constant. It can be derived that for a given target  $\lambda_{opt}$  and  $C_{p,opt}$ , optimal power output and, consequently, optimal generator torque is proportional to the square of the rotational speed:

$$M_g = \frac{0.5\rho\pi R^5 i_{GB} C_{p,opt}}{\lambda_{opt}^3} \omega_{rot}^2 - M_{loss} \Rightarrow M_g = \kappa\omega_g^2 - M_{loss}, \quad M_g \in (M_{g,max15} \quad M_{g,rat}] \quad (2.10)$$

Where  $i_{GB}$  is the gear box ratio, so that  $\omega_{rot} = \omega_g i_{GB}$ .  $M_{g,rat}$  is the generator torque at rated power,  $M_{g,max15}$  is the maximum generator torque in region 1.5 and  $M_{loss}$  is the mechanical torque loss in the drive train.

More advanced techniques have also been suggested in the literature [56, 55, 57] using an estimator that is able to track the rotor effective wind speed and subsequently  $\lambda$  so that a PI loop for the generator torque can be designed to directly track the optimal TSR leading to higher energy capture. In this work, the  $\kappa\omega^2$  strategy is chosen for control region 2.

Region 2.5 is the transition region between regions 2 and 3. It is worth noting that this region is important for the wind turbine loads as the turbine is operating in maximum thrust while switching control objectives and engaging blade pitching. The generator torque and the rotational speed of the rotor have upper limits according to manufacturer specifications and noise emission legislation (often defined as tip speed restrictions), respectively. Region 2.5 is the region in which one of these limits is reached while power has not reached the rated value.

The behavior of each turbine depends on the specific aerodynamic design and upper speed and torque design limits. Region 2.5 can go from almost non-existent to spanning over a range of wind speeds of 3 m/s. It is more common, especially as rotors grow larger, that  $\omega_{rat}$  is reached first.

In region 2.5, two control approaches are commonly implemented. The simpler one is using a torque-speed linear ramp to drive the generator torque to the rated values as shown in figure 2.1). In this case, the control design variables are the choice of the torque and speed value of the first point of the ramp [43, 48]. To prevent interference between the pitch controller and speed regulation and ensure smooth transitions, various strategies can be implemented. These strategies may include imposing limits on the minimum pitch angle and setting a torque limit slightly above the rated value, after which pitching is activated.

The second approach includes a PI loop that will create a vertical line in the speed-torque map [58, 55, 53, 54]. In this method, the set point for the PI controller is the rated rotational speed  $\omega_{rat}$ , and it is activated when the  $\omega_{rat}$  is reached. In order to clearly separate the two PI loops (region 1.5 and 2.5) and the region 2 torque controller, saturation limits are applied to the output torque. Moreover, the switching of the set point is activated based on a fixed torque value close to the middle of region 2 between  $\omega_{min}$  and  $\omega_{rat}$ . This leads to a smooth transition since, until either limit is reached, the torque controller's output is saturated. In order to make sure that the pitch and torque controllers do not overlap in this region, various approaches can be found in the literature. In [54], a switching logic based on a hard switch that allows the pitch controller to start being active when the commanded value is slightly higher than the minimum along with an anti-windup term for the integrator referencing the power is used. In another approach [58, 55], known as the set point smoother, two tunable gains are used as weights on the difference of current pitch angle to the minimum and the difference of current rotational speed to rated to produce an offset to the set point of each controller. This ensures that in regions 2 and 3, only one controller is active for speed regulation while the other is saturated. In both cases, there are no tuning rules for the parameters, and it is usually done iteratively.

In region 3,  $P_{rat}$ ,  $\omega_{rat}$ , and  $M_{g,rat}$  have been reached. The controller's objective is to keep  $\omega_{rat}$  constant for every wind speed until cut-off using the blade pitch system to regulate the rotational speed. In regards to the torque controller, two modes are used. Constant power, where the torque is commanded based on the current speed  $M_g = P_{rat}/\omega_g$  and constant torque where  $M_g = M_{g,rat}$ . The most common approach for the pitch controller is a feedback PI loop with the setpoint being the rated rotational speed  $\omega_{rat}$  and saturation limits  $[\theta_{fine} \quad \theta_{max}]$ .

An additional anti-windup term on the integrator is typically implemented. This ensures that after a period of operation in below-rated conditions where the pitch controller is saturated, the integral term will not increase indefinitely. This mechanism ensures a rapid response from the

pitch controller when the turbine transitions to rated conditions. It also aids in the decoupling of the pitch and torque controllers concerning speed regulation. The anti-wind up can be implemented by feeding the saturated commanded pitch values (which has to be  $\theta_{com} > \theta_{fine}$ ) for the calculation of the integral error or setting hard limits on the integral error. Various tuning methods exist for the pitch controller in region 3, with the most common being the closed-loop shaping method. As this method is used in this work for the gain tuning of the collective pitch PI loop, it is briefly introduced here.

The scope of the PI blade pitch controller is to minimize the error of the rotational speed of the generator compared to the set point. The error is defined as:

$$e(t) = \omega_g(t) - \omega_{g,rat} \quad (2.11)$$

The commanded pitch angle value from a PI scheme will have the form:

$$\theta_{com,t_i} = K_P e_{t_{i-1}} + K_I \int_{t_0}^t e dt \quad (2.12)$$

Or equally

$$\theta_{com,t_i} = K_P e_{t_{i-1}} + \frac{K_P}{T_I} \int_{t_0}^t e dt \quad \text{where} \quad T_I = \frac{K_P}{K_I} \quad \text{and} \quad K_P, K_I, T_I \rightarrow f(\theta_{t_{i-1}}) \quad (2.13)$$

The proportional ( $K_P$ ) and integral ( $K_I$ ) gains can be calculated with the closed loop shaping method. This simple method is based on a linearized single-DOF representation of the drivetrain dynamics. Combining the single-DoF linear model (linearized for each wind speed) with the PI leads to a second-order linear model, which can have the desired dynamic response by defining a damping ratio ( $\xi$ ) and a natural frequency ( $\omega_{NS}$ ) similarly to a second order mass-spring-damper mechanical system. The drive train dynamics can be represented as:

$$J\dot{\omega}_{rot} + \frac{M_g}{i_{GB}} = M_a \Rightarrow \dot{\omega} = \frac{1}{J} M_a(\omega, \theta, u) - \frac{1}{J} \frac{P_{a,rat}}{\omega/i_{GB}} \rightarrow \dot{\omega} = f(\omega, \theta, v) \quad (2.14)$$

Where  $J$  is the moment of inertia of the whole drive train (including the hub, blades, and generator) and  $M_a$  is the aerodynamic torque. Here, constant power in region 3 is assumed.

Using Taylor's series expansion, the system can be linearized around an operating point defined by its operational states ( $\omega$ ,  $\theta$  and  $v$ ) such as:

Hence:

$$\Delta\dot{\omega} = \left. \frac{\partial f}{\partial \omega} \right|_{OP} \Delta\omega + \left. \frac{\partial f}{\partial \theta} \right|_{OP} \Delta\theta + \left. \frac{\partial f}{\partial v} \right|_{OP} \Delta v \quad (2.15)$$

Note that at the operating point  $\dot{\omega} = 0$

Solving for each partial derivative term:

$$\left. \frac{\partial f}{\partial \omega} \right|_{OP} \Delta\omega = \left[ \frac{0.5\rho A v_{op}^3}{J} \left( \frac{R}{\omega_{op} u_{op}} \frac{\partial C_p}{\partial \lambda} - \frac{C_p}{\omega^2} \right) + \frac{1}{J} \frac{P_{a, rat}}{\omega / i_{GB}} \right] \Delta\omega = a \Delta\omega \quad (2.16)$$

$$\left. \frac{\partial f}{\partial \theta} \right|_{OP} \Delta\theta = \left[ \frac{0.5\rho A v_{op}^3}{J \Omega_{op}} \frac{\partial C_p}{\partial \theta} \right] \Delta\theta = b_1 \Delta\theta \quad (2.17)$$

$$\left. \frac{\partial f}{\partial v} \right|_{OP} \Delta v = \left[ \frac{0.5\rho A v_{op}}{J \omega_{op}} (3v_{op}^2 C_{p, op} - v_{op} \omega_{op} R \frac{\partial C_p}{\partial \lambda}) \right] \Delta u = b_2 \Delta u_0 \quad (2.18)$$

The partial derivatives  $\frac{\partial C_p}{\partial \theta}$  and  $\frac{\partial C_p}{\partial \lambda}$  for each wind speed can be derived as finite differences from a lookup table derived from open loop aeroelastic simulations.

Then, the PI controller from pitch to rotor speed will have the form:

$$\Delta\theta = K_P \Delta\omega_g + K_I \int_{t_0}^t \Delta\omega_g dt = \frac{K_P}{i_{GB}} \Delta\omega + K_I \int_{t_0}^t \frac{\Delta\omega}{i_{GB}} dt \quad (2.19)$$

Combining equations 2.16 - 2.19:

$$\Delta\dot{\omega} = a \Delta\omega + b_1 \left( \frac{K_P}{i_{GB}} \Delta\omega + K_I \int_{t_0}^t \frac{\Delta\omega}{i_{GB}} dt \right) + b_2 \Delta u_0 \quad (2.20)$$

This differential equation represents a second-order system that has the following state space representation:

$$\ddot{x} + (-a - b_1 c K_P) \dot{x} + (-b_1 c K_I) x = b_2 u \quad (2.21)$$

$$y = \frac{1}{i_{GB}} \dot{x} \quad (2.22)$$

Where the state variable is  $x = \int_{t_0}^t \Delta\omega dt$ , the input (u) is  $\Delta u_0$  and the output (y) is  $\Delta\omega_g$ .

The close-loop behavior of the system can be adapted by deriving the gains based on the design  $\xi$  and  $\omega_{NS}$  omega values:

$$\omega_{NS} = \sqrt{-b_1 c K_I} \Rightarrow K_I = \frac{-\omega_{NS}^2}{b_1 c} \quad (2.23)$$

$$\xi = \frac{-a - b_1 c K_P}{2\omega_{NS}} \Rightarrow K_P = \frac{2\xi\omega_{NS} + a}{-b_1 c} \quad (2.24)$$

Another important aspect of the pitch controller is gain scheduling. At different wind speeds and blade pitch angles, the sensitivity of the aerodynamic torque to changes in the blade pitch angle varies depending on the aerodynamic design of the blades. To compensate for this change in dynamics, it is common to derive the gains for different operating points and assign a gain scheduling based on the current collective pitch angle value.

In the case of floating wind turbines, further adjustments are needed to the blade pitch controller due to instability issues arising from potential negative damping of the controller to the platform's motion. Various approaches have been considered, such as adding an additional proportional term feedbacking the tower acceleration or the platform's motion or using filters to avoid specific zones in combination with relaxing the proportional gains [59, 55].

As the PI feedback loop is limited due to the method's simplicity, there is no straightforward way to include other objectives except the tracking of the rotational speed and the first-order stability of the drivetrain system. Objectives like power maximization, reduction of overshoot in rotational speed, structural load reduction, actuator usage, etc., are very important for the overall performance of the system. Hence, it is common that after the first iteration with this method, the PI gains are further fine-tuned based on mid-fidelity aeroelastic simulations according to these objectives [60, 61].

Tuning of the PI loop with more advanced methods as well as alternative optimal control methods using techniques such as model predictive control [62], linear quadratic regulators [63, 51] and  $H_\infty$  [64] have been suggested in the literature and scarcely tested in the field. These methods have the potential to increase the controller's performance as they can inherently handle more objectives. However, they are not considered in this work as the focus is on the utilization of existing, commonly applied technologies to demonstrate the proof of concept of a novel operational management approach.

Additional loops or filters can be added to the controller to reduce loads by damping resonances. The most widely used are for damping fore-aft tower vibrations and drive train torsional vibrations [53, 48]. The first requires an accelerometer at the nacelle, which is used to measure acceleration that is converted to velocity. A proportional gain to the pitch angle based on the sensitivity of thrust to pitch angle can then be applied aiming to increase the damping of the mode. Moreover, drivetrain vibrations can occur in region 3 due to the potential coupling of the torsional mode of the drive train with the first blade in-plane mode and/or the first tower side-side mode. This phenomenon is more relevant for cases where the constant torque strategy is employed. These can be mitigated by applying a narrow band-stop filter on the measured generator speed, targeting the frequency of the drive train in order to force a small ripple on the torque controller's reaction around this frequency that will avoid resonance. High-fidelity aeroelastic simulations are essential to verify the proper functioning of these loops when they are combined. This verification ensures that the primary objectives of the control

system are maintained and that any potential unmodeled dynamics do not lead to resonances or instabilities.

For the tuning of the controller parameters, identifying the correlation between  $\lambda$ ,  $\theta$ , and  $C_p$ ,  $C_t$  is required. Since these are properties stemming from the aerodynamic and structural design of the turbine, it is common to derive look-up tables for these values based on open-loop aeroelastic simulations. This is done by using a uniform wind field for the simulations. The rotor speed and collective blade pitch angle are varied sequentially to extract the steady-state response. An example of  $\lambda$ - $\theta$ - $C_p$  and  $\lambda$ - $\theta$ - $C_t$  maps obtained with this process is shown in figure 2.2.

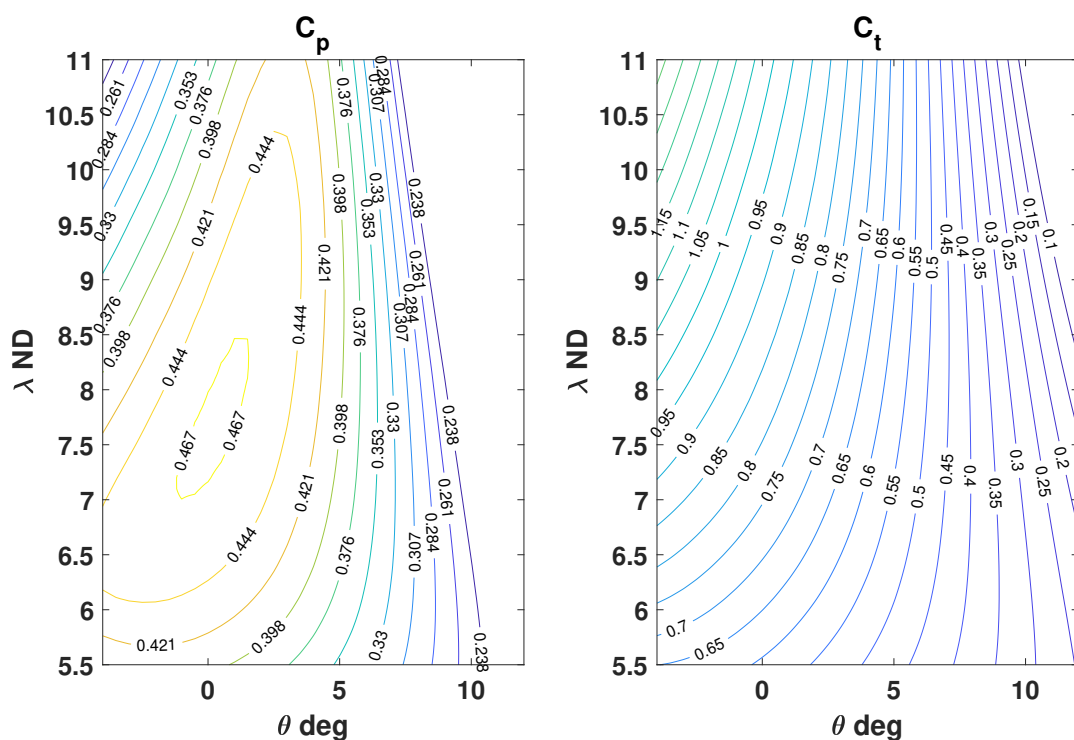


**Figure 2.2:** Example maps of  $\lambda$ - $\theta$ - $C_p$  and  $\lambda$ - $\theta$ - $C_t$

The previous discussion covered common control methods used for the baseline control of wind turbines. These methods utilize standard actuators and sensors found in most modern machines. Using additional sensors, such as nacelle-mounted lidars for wind preview [65] and actuators, such as active aerodynamic devices [66, 67] is another field of research that has shown potential for improving the control objectives. These technologies have not yet been widely adopted by the industry due to cost-effectiveness, reliability, and robustness considerations. In this work, the primary focus is on using widely applicable control technologies without hardware requirements. The only exception is the requirement for root bending moment sensors, which are essential for individual pitch control.

One advanced control method, beyond the baseline feedback control loop, aiming for load

reductions is individual pitch control (IPC). IPC is leveraging the fact that modern utility-scale VSPR wind turbines have an individual pitch actuator for each blade. Commanding a differential pitch angle to each blade according to some logic can lead to structural load reductions, focusing mainly on blade and nacelle components. This is due to large, flexible rotors experiencing different wind speeds in different angles of attack inside the rotor area, leading to imbalances in the loading of the rotor. This is caused mainly by the spatial variability of boundary layer turbulence but also due to deterministic effects such as wind shear and veer, tower shadowing, coning and tilting of the rotor.

IPC methods have been extensively researched and field tested [48, 68, 69, 70, 71, 72], and to a smaller extent applied in the industry. The reason for the scarce industrial application is, on one hand, the requirement of load sensors on the blade root due to cost and reliability considerations, and on the other hand, the longevity of the actuator and bearing due to the increased actuation, which might lead to increased maintenance costs. These challenges can be potentially addressed if the actuator and sensor requirements are accounted for in the initial design phase and if the IPC application shows clear financial benefits. The last point aligns with one of the scopes of this work, which is to show the potential optimization of long-term operational objectives by including such a technology in the system.

Various approaches to implementing IPC have been proposed in the literature. An overview of the different concepts, along with their fundamental differences and similarities, can be found in [70, 69]. The simplest approach involves a model-based cyclic pitch signal at the 1P frequency depending on the current state, such as the commanded collective pitch controller (CPC) angle. In this approach, the command for each blade depends on its azimuthal position. This method has the advantage of not requiring blade load sensors and may result in reduced pitch actuation compared to other IPC approaches. However, it has drawbacks, including lower efficiency due to model discrepancies and its limited ability to compensate for only part of the deterministic loads.

The most common application is based on the Coleman multiblade coordinate transformation [73, 74]. The main idea, stemming from the helicopter industry, is to project the loading effects of the rotating blades to a non-rotating frame with two orthogonal axes coinciding with the tilt and yaw axes of the undeflected rotor. This way, direct measurements from the blade root can be transformed into two moments in the non-rotating system. These imbalance moments can then be compensated by some control algorithm providing the compensating moment requirement. Then, using the inverse Coleman transformation, from the non-rotating to the rotating frame, these can be expressed as differential pitch angle commands for each blade, according to its azimuth angle, added on top of the CPC command as shown in figure 2.3. This approach has inherent advantages as it can capture load variations dynamically and also avoids the overlap with the speed regulation loop as the rotational speed is not accounted for

in the non-rotating frame. Moreover, the transformation itself is based on harmonics of the rotational speed so that specific frequencies can be targeted (1P, 2P, ..., nP). This is convenient for reducing unnecessary pitch actuation and targeting specific harmonics that have a higher impact on structural loads. The control can be based on single-input-single-output (SISO) PI loops for each load component due to rotor similarity, while more advanced methods have also been suggested ([75, 76, 69]). In this implementation, it is important to account for the possible delays due to actuator dynamics and aeroelastic effects, allowing for some lag in the azimuthal phase of the commands. Additional filters and/or rate/amplitude saturation limits can be applied to the differential command to restrict the amplitude and rate of the differential pitching action.

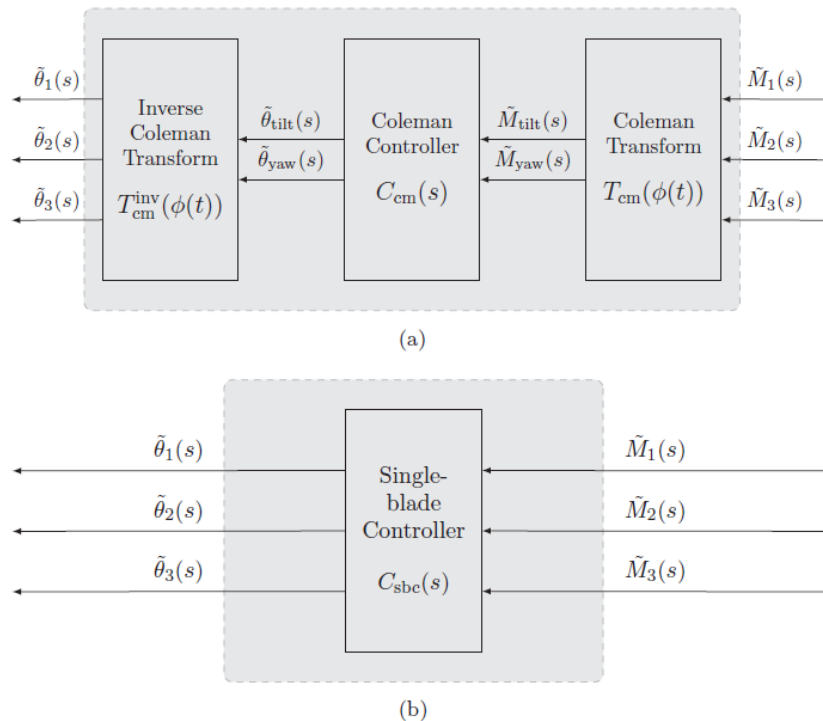


**Figure 2.3:** Schematic representation of the different IPC schemes. (a) Coleman-based (b) individual blade control (figure modified from [70])

Another common approach to IPC, which is employed in this work, is controlling each blade individually by feedbacking the measured blade root loads directly [77, 78, 79, 80]. This approach is denoted as individual blade control (IBC). IBC considers 3 completely independent SISO controllers employing as input the blade's instantaneous load and providing as output the differential pitch command as shown in figure 2.3. The benefit compared to the previous approach is that the controller is not limited to attenuating only frequencies close to the rotor speed harmonics, allowing for a broader range of load reduction possibilities and that blade loads can be targeted more efficiently. On the other hand, these methods can lead to higher pitch actuation, depending on the design approach, and may be more sensitive to noise in the

load measurements.

In order to tune the PI gains, a linear blade model per operational point can be used, including the actuator's dynamics and the pitch's sensitivity to the load of interest. Filters are applied to limit the effective bandwidth of the controller along with saturation for amplitude and rate. Depending on the implementation, tuning these filters can change the controller's behavior in terms of targeted frequencies and limiting pitch actuation, which are competing objectives. More details on the exact IBC controller implementation used in this work are given in section 3.4.

Another aspect of wind turbine operation related to the controller is down-regulation. Congestion of the electrical grid, electrical grid load balancing, O&M decisions due to degradation of specific parts, and wind farm sector management for wakes are the most common cases where the wind turbine is required to reduce the power output from the design values discussed earlier. Different naming conventions used interchangeably for the same process can be found in literature, including down-regulation, curtailment, derating, and throttling. In this work, the term down-regulation is used throughout.

To reduce the power output,  $C_p$  has to be reduced. This can be done by adjusting the operating points in terms of tip speed ratio and/or blade pitch angle. Depending on the turbine's design and the intended application, different approaches can be used which will effectively change the operating point in the  $\theta$ - $\lambda$ - $C_p$  and  $\theta$ - $\lambda$ - $C_t$  maps. For example, for wind farm control purposes, the aim would be to minimize the thrust to reduce the wake effects; for O&M applications, specific loads or avoidance zones of  $\omega$  might be targeted, etc.

The selection of trajectory for the down-regulation defines the new setpoints used by the controller. The choice between modifying the rotor speed, the pitch angle, or a combination of them to achieve the new set points affects the control regions differently [81, 82, 60, 83, 84, 85]. Choosing to keep  $\lambda$  constant (horizontal trajectory in figure 2.2) means that the fine pitch angle in region 2 has to be increased while the rotor speed trajectory over wind speeds will be the same until the reduced rated value is reached. Region 1.5 will be shorter as the torque demand will be reduced. In region 2, the main difference will be the  $\kappa$  value. Region 2.5 will also be reduced or completely eliminated depending on the level of down-regulation.

Opting for the other theoretical boundary for down-regulation (vertical trajectory in figure 2.2), which involves keeping the fine pitch angle constant, necessitates modifying the tip-speed ratio ( $\lambda$ ). This modification can mean either increasing or decreasing the targeted rotational speed per wind speed. However, this approach is not practically feasible, as it quickly reaches the upper and lower limits of rotational speed. Considering a combination of the two approaches, the reduction of TSR is the most favorable as it does not require the increase of rotational speed, and it reduces region 2.5. Caution has to be taken as the target power level decreases, which can lead to a significant extension region of 1.5 depending on the lower acceptable limit

of rotational speed.

No matter what the set point choice is, the reduction in power production comes with a reduction in structural loading [86, 87, 83]. In this work, down-regulation is used as a means for structural loads reduction, complementary to the IBC loop. Two trajectories were chosen in this work: the constant TSR approach and a trajectory combining both pitch and TSR reductions. Details on the implementation are given in section 3.2.

The final topic related to the controller's functionality is power boosting, which involves increasing the rated power of the wind turbine above the initial rated value. From a control perspective, this can be done following different strategies for the rotor speed and the generator torque, as shown in fig 2.4. One option is increasing region 2, as described by the trajectory H-D in the figure, meaning operating in optimal  $C_p$  for longer. This leads to increasing both rotational speed and torque, which are reached at a higher wind speed than the initial design value. Alternatively, only region 2.5 can be extended by increasing only the rated torque (trajectory H-A-B in the figure) or only the rated rotational speed (trajectory H-E-C in the figure) and keeping the other value constant to the nominal design. Finally, it can be done by a combination of torque and speed depending on the possible technical restrictions, as seen, for example, in the trajectories H-F-G1 and H-F-G2 included in the figure.

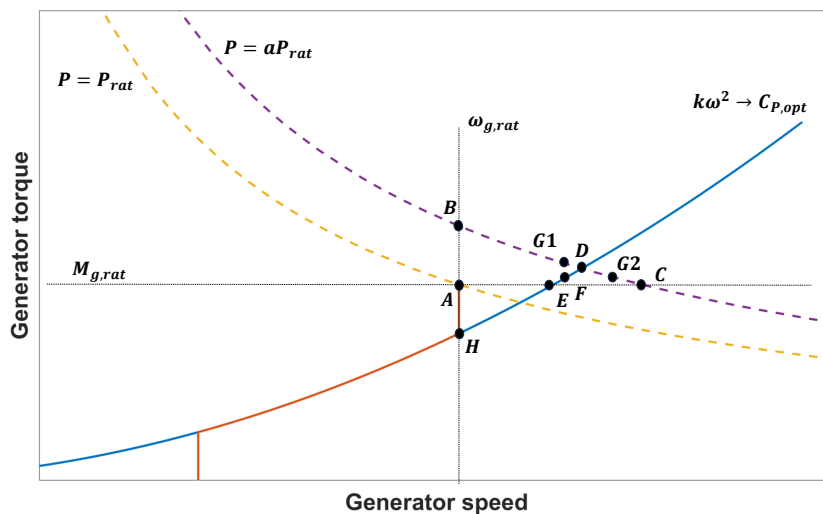


**Figure 2.4:** Possible controller trajectories for generator torque and generator speed considering power boosting

When implementing power boosting, several critical factors must be taken into account. Commonly, the upper rotational speed is limited so that a 90 m/s tip speed is not exceeded due to noise restrictions and air compressibility considerations. Hence, the approach of increasing the rotational speed can be applied only in cases of offshore wind farms where less strict limitations apply. Furthermore, the design limits of the generator and power electronics have to be considered. Electrical generators and power electronics have an upper limit of

torque and power due to limitations such as electrical and thermal stresses while having some overload capacity depending on the generator design [88]. Thus, the maximum level and duration of possible power boosting depend heavily on the design characteristics of the system. Turbine manufacturers already offer such options in new turbines or as part of retrofit packages [89, 90, 91]. The exact levels of power boosting are not clearly stated. From the available information, a level of 5-10% above nominal is deduced. In this work, it is assumed that the electrical system can handle a power boosting level of up to 30%. Details on the power boosting method followed in this work are given in section 3.3

This section provided an overview of the control system, including its description, objectives, and the most common implementation approaches. For the present work, the control task is to design a controller for the DTU 10 MW rwt (see chapter 3) that covers the baseline functionalities and also has the possibility to apply down-regulation, power boosting, and individual pitch control, without using additional actuators or sensors. The focus is on a simple and robust scheme that is easy to tune for all set points and has a similar response in all modes, allowing for smoothness in the following optimization task. Nevertheless, it is clear that more advanced methods and fine-tuning could lead to better overall performance in terms of both power production and structural loading.

## 2.5 Introduction to surrogate modelling

A surrogate model, in the context of engineering modeling, is a simplified and computationally efficient representation of a complex system or process. It serves as a substitute for the original model, approximating its behavior while reducing computational costs. Surrogate models are often constructed using statistical techniques or machine learning algorithms, leveraging available data to emulate the responses of the original system. They are particularly useful when the original model is computationally expensive or difficult to solve. By providing rapid and approximate predictions, surrogate models aid in optimization, sensitivity analysis, uncertainty quantification, and decision-making processes across various disciplines, including engineering, physics, and computer science [92].

With the increase in computational power in recent years, several applications of surrogate modeling have been suggested in the context of wind energy research for uncertainty quantification, optimization, and monitoring purposes. Different surrogate methods for lifetime load estimation of a single turbine over various inflow conditions are compared in [93], including polynomial chaos expansion, quadratic response surface, universal Kriging, importance sampling, and nearest-neighbor interpolation. It was found that universal Kriging was the most accurate method. Nevertheless, the high computational cost to create the surrogate due to the high dimensionality, as well as the longer time to produce predictions, led to the suggestion

that polynomial chaos expansion was the best tradeoff. In [94], Kriging and polynomial chaos expansion are compared, in a similar way, for estimating lifetime reliability indices over an ensemble of environmental conditions. It was found that Kriging performs better when a higher number of samples is considered, while polynomial chaos expansion performs better in more sparse sampling.

The lifetime loads of a floating wind turbine based on surrogates for a full environmental contour were evaluated in [95]. The surrogate methods used were piecewise polynomials, radial basis function networks, and artificial neural networks. The dependence of each approach on sampling method and size are discussed and compared, showing that, overall, surrogate models can be accurate enough for the purpose. Additionally, it was found that wind speed and TI were the most influential inputs for most of the fatigue loads considered. The sensitivity of loads and power response for a single onshore turbine in normal operation to the environmental conditions and aeroelastic modeling properties using an elementary effects methodology was discussed in [96]. The results showed that wind speed, TI, and shear were by far the most influential parameters. Surrogates based on Universal Kriging and non-intrusive polynomial chaos expansion are used in [97] to quantify the propagation of uncertainty from inflow condition and blade aerodynamic properties to loads and AEP. The results indicated that universal Kriging demonstrated faster convergence to the desired accuracy level than polynomial chaos expansion.

Quadratic response surfaces were used to create surrogate models for loads in [98] to accelerate site-specific load assessment according to the standards. It was found that site-specific loads could be captured with an uncertainty  $<5\%$  and that the contribution of uncertainty due to surrogate modeling is smaller than the uncertainty contribution from modeling and seed-to-seed variability when considering a reasonable training sample size. In [99], surrogate models based on fifth-order polynomial response surfaces, calibrated using least squares, were utilized to analyze the sensitivity of loads for an onshore wind turbine to various input conditions. The study revealed that wind speed and TI were the primary contributors to uncertainty, indicating their significant influence on the turbine's load response.

Polynomial chaos expansion is used for surrogate modeling of a single onshore turbine in [100]. Using the surrogate model, they propagate the uncertainty from aeroelastic simulations to annual energy production and lifetime DELs to quantify the overall uncertainty and the highest uncertainty contributors. In [101], Kriging was used to analyze the effect of wind and sea states on the loading of a floating wind turbine and quantify the uncertainty. It was shown that the mean values are captured with higher accuracy by the surrogate model, while significantly larger samples are required for the standard deviation. It was also shown that wind speed and TI were the most influential parameters. Additionally, [102] employs a surrogate-based optimization approach, utilizing a cubic polynomial regression surrogate

model, to optimize the design of an aeroelastically tailored blade tip extension. The surrogate model helps alleviate the otherwise infeasible computational costs of simulations during the optimization process. The optimized designs were validated using high-fidelity simulations, demonstrating the effectiveness of the surrogate-based optimization method.

Surrogate modeling has also been considered for wind farm optimization and uncertainty quantification studies, as when considering an entire farm, the dimensions increase highly. An approach for mapping loads of any turbine in a wind farm with arbitrary size and layout using surrogate models is presented in [103]. Polynomial chaos expansion and artificial neural networks are used for surrogate modeling. Both models were able to capture the loads response with  $<10\%$  uncertainty, with artificial neural networks being slightly more accurate but prone to overfitting. The same surrogate model is used in [104] to perform induction-based wind farm optimization for power and loads in a wind farm, showcasing its applicability. Optimization of power and loads, for two wind turbines in a row, with wake steering using surrogate models based on polynomial chaos expansion was presented in [105, 106]. The surrogate was able to capture the power and load response with an uncertainty level of 2% and 5%, respectively. In [107], surrogate models for power and loads in a wind farm considering down-regulation are presented. Different surrogate methodologies, including linear regression, artificial neural networks, and Gaussian process regression (GPR), are compared, with GPR exhibiting the best performance, yielding less than 10% error for all loads and 0.2% error for power. Artificial neural networks were also used in [108] to create a surrogate model for loads and power in a wind farm, including transient such as start-up and shut-down for failure detection and health monitoring purposes. The loads were able to be predicted with a coefficient of determination higher than 0.95 for all cases. A validation with SCADA data for power showed a mean error of 1.5% for the surrogate model.

As seen from the previous discussion, various applications of surrogate models have been successfully demonstrated in the context of wind energy research. In this work, the scope of the surrogate model is to replace the expensive aeroelastic simulations using FAST with a quick and accurate data-driven statistical model that can be used for optimization and the digital twin application. The goal is to have a model that can reproduce the statistical values derived from post-processing the output time series of the simulations in terms of quantities of interest (e.g., DEL, mean values, etc.). Therefore, the output space can be mapped thoroughly in a continuous manner to the input space, which includes the wind conditions and the controller modes. In this process, the balance between the computational cost of creating the training dataset and the prediction uncertainty has to be considered. Details on the surrogate modeling approaches followed in the present work are given in chapter 4.

# Chapter 3

## Controller design

This chapter deals with all the aspects related to the wind turbine controller design. The structure and tuning of the baseline controller for the nominal operation at the initial design values are presented. Based on this, the retuning process of the controller to achieve down-regulation and power-boosting considering structural loads and power production is presented. Next, the design and tuning of the individual blade controller loop aiming for load reductions in rated and above-rated conditions are discussed. Finally, the full controller synthesis enabling the switching and combination of the different modes is discussed, and the steady-state response of the turbine is presented.

### 3.1 Baseline controller design for the DTU 10 MW rwt

The controller described here serves as a simple control algorithm for the DTU 10 MW rwt described in section 2.2. The considered inputs are the low-pass filtered generator rotational speed and the blade pitch angle. The outputs include the commanded generator torque and the commanded collective blade pitch angle. The controller uses linear ramps for the transitions regions 1.5 and 2.5. In region 2, the  $\kappa\omega^2$  strategy is employed for tracking the optimal TSR. In region 3, the generator speed is controlled with a PI loop, including gain scheduling and an anti-windup feature. The gains are tuned with the closed-loop shaping method and manual fine-tuning. The controller and actuators were designed in Matlab/Simulink, utilizing the Sfunction version of FAST v8.16 to perform the closed-loop aeroelastic simulations.

The modeling of the mechanical pitch actuator is done with a second-order low-pass filter, including saturation limits in rate and magnitude. The measured generator speed is filtered

using a first-order low-pass filter. There is no generator torque actuator implemented, assuming instantaneous response to the commanded torque. The relevant values used are summarized in table 3.1. Additionally, damping loops for drivetrain torsion and tower fore-aft vibrations are not employed, as the simulations did not reveal any resonances, and the constant power strategy is applied in region 3.

**Table 3.1:** Pitch actuator and generator speed filter modelling parameters

Parameter	Value
Maximum pitch angle	90 deg
Minimum pitch angle	0 deg
Pitch actuator second order LP filter frequency	1.6 Hz
Pitch actuator second order LP filter damping	0.8 ND
Maximum absolute pitch rate	8 deg/s
Generator speed 1 <sup>st</sup> order LP filter corner frequency	0.25 Hz

The first step for the controller design was to perform steady-state open-loop simulations with the DTU 10 MW rwt model to derive the  $\theta$ - $\lambda$ - $C_p$  and  $\theta$ - $\lambda$ - $C_t$  maps required. This was done with all the DoFs activated using a uniform wind field of 10 m/s and considering fixed pitch angle and rotor speed. The blade pitch angle was systematically varied from -5 to 35 degrees with a step of 0.5 deg.  $\omega_{rot}$  was adjusted to yield a range of TSR values ranging from 1 to 16 with a 0.1 step. The resulting maps are presented in figure 3.1. Based on these maps, a design TSR of 7.75 was chosen along with a fine pitch angle of 0 degrees, leading to a maximum  $C_p$  value of 0.467. The choice of TSR is slightly higher than the 7.6 value reported in the design report [46], leading to a reduction of 0.0006 in  $C_p$ . This modification was made to address an issue observed with the lower TSR, which caused the rated rotational speed to be reached before the rated torque. Consequently, an uncontrolled region 2.5 emerged, where the rotor rapidly accelerated until reaching the rated speed. This behavior led to increased loads and unpredictable performance when adjusting set points for other power levels. By increasing the design TSR, region 2.5 was significantly reduced, allowing rated torque and rotational speed to be reached simultaneously. An overview of the controller design characteristics is provided in table 3.2.

The DTU 10 MW rwt features a "stiff-stiff" tower design, necessitating a minimum rotor rotational speed of over 5.1 rpm to prevent the first natural frequency of the tower from crossing with the 3P frequency. The torque-speed ramp for region 1.5 was designed such that the first point was at 5.5 rpm for the cut in wind speed. The steepness of the ramp was identified by manual testing with closed-loop aeroelastic simulations looking at the trade-off between power and loads. The effect of the ramp on the TSR values is shown in figure 3.2. After iteratively identifying 6 rpm as the target  $\omega_{rot}$  value to end region 1.5, the linear torque-speed ramp can

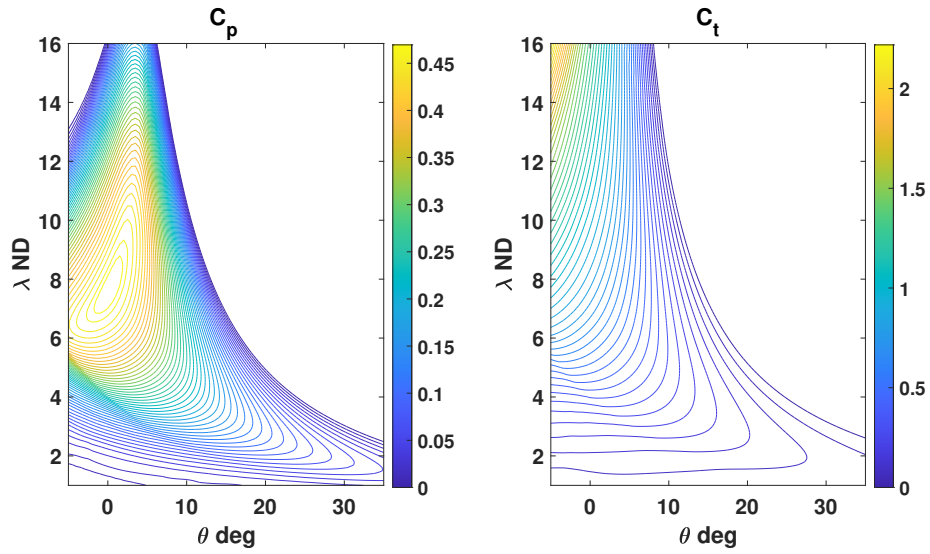


**Figure 3.1:**  $\lambda$ - $\theta$ - $C_p$  and  $\lambda$ - $\theta$ - $C_t$  maps for the DTU 10 MW rwt used for the controller design

**Table 3.2:** Design characteristics of the baseline controller

Design characteristics	Value
Tip speed ratio	7.8 ND
$C_p$	0.467 ND
Region 1.5 min rotational speed	5.5 rpm
Region 1.5 max rotational speed	6.0 rpm
Rated rotational speed	9.6 rpm
Rated wind speed	11.5 m/s
Torque constant for region 2	92.97 kNm/(rad/s) <sup>2</sup>
Cut in wind speed	4 m/s
Cut off wind speed	24 m/s
Pitch limit for switching between region 2.5-3	1 deg
Minimum pitch	0 deg
Maximum generator torque allowed above rated	110 %
Generator speed 1st order LP filter corner frequency	0.25 Hz

be defined by:

$$M_g = a_{15} + b_{15}\omega_g \quad (3.1)$$

where the coefficients  $a_{15}$  and  $b_{15}$  can be calculated by equations 3.2 and 3.3:

$$a_{15} = \frac{\kappa \omega_g^2}{\omega_{g,1.5,max} - \omega_{g,1.5,min}} \quad (3.2)$$

$$b_{15} = -a_{15} \omega_{g,1.5,min} \quad (3.3)$$

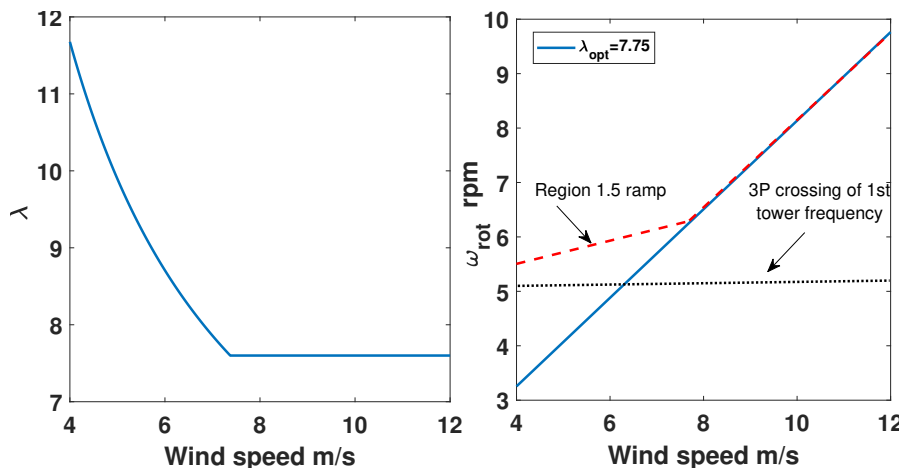


**Figure 3.2:** Effect of the torque-speed ramp on region 1.5.

In region 2, the  $\kappa\omega^2$  (see section 2.4) approach was followed with the pitch being constant to the fine pitch value. The transition between regions 1.5 and 2 is based on the measured generator torque value. In region 3, power is kept constant with the torque controller reacting to the filtered generator speed signal. The pitch controller involves a PI loop feedbacking the low-pass filtered generator speed. The gains are derived with the closed-loop shaping method described in section 2.4. The natural frequency and damping for the tuning were chosen iteratively based on loads and generator speed metrics with the values  $\omega_{NS} = 0.75 \text{ rad/s}$  and  $\xi = 0.7$  selected. No further manual fine-tuning was performed, in order to have a unified automated way to tune the controller for all the power level set-points without biases. The gain scheduling is based on the mean measured collective pitch derived with the same method for four mean pitch values 0, 7, 14, and 21 deg (roughly corresponding to wind speeds of 11, 14, 17, and 21 m/s) and linearly interpolated for the rest of the operating points. Moreover, there is an anti-windup scheme for the integral term using tracking back calculation. The idea is that in the unsaturated range, the commanded signal is fed to the integrator. In the saturation range, the difference between saturated and unsaturated values is used to generate a feedback signal to act on the integrator input [109].

The complete structure of the baseline closed-loop controller, including filters and actuators, is presented in figure 3.3. Figure 3.4 shows the steady state operational characteristics achieved with the presented baseline controller for nominal operation.

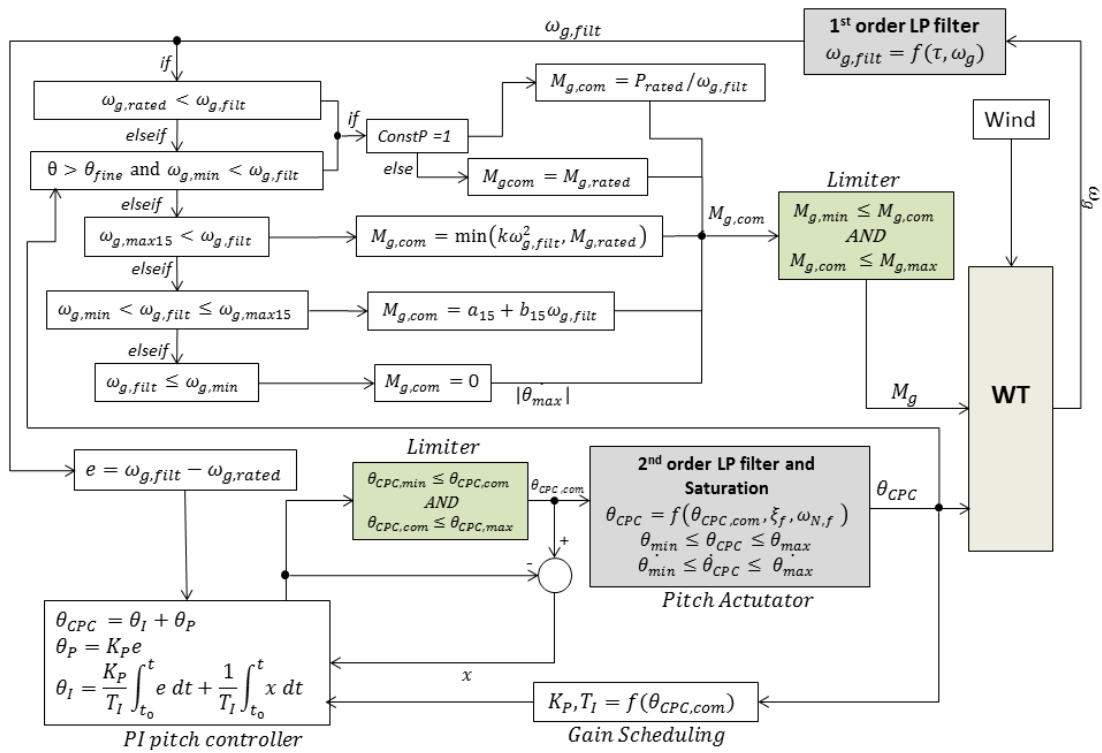


Figure 3.3: Block diagram of the full controller and actuators

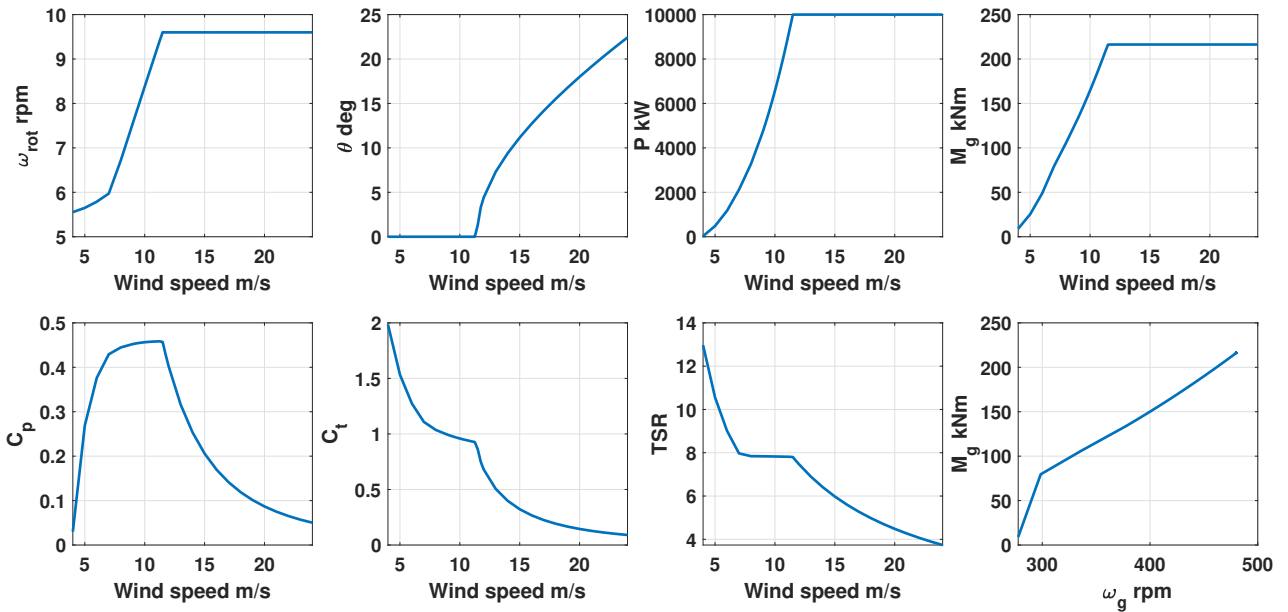
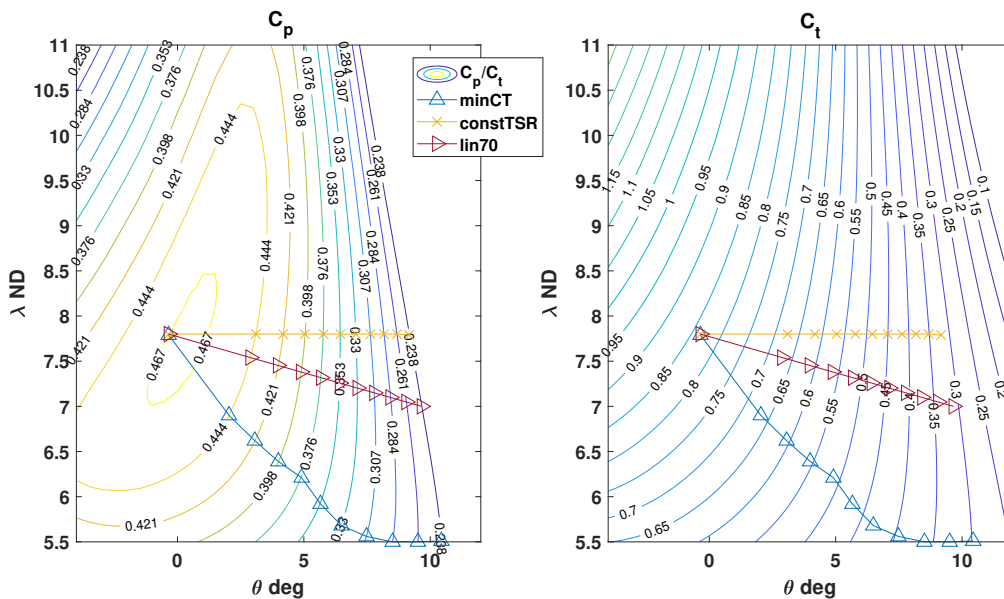


Figure 3.4: Steady state operational characteristics for the baseline controller

## 3.2 Down-regulation

This section presents the trajectories considered in defining the down-regulation set points, along with the changes in the baseline controller for achieving the desired output power level. As explained in section 2.4, the scope of the down-regulation in the whole operational range in this work is to leverage the structural load reduction that comes with reducing power. The level of power reduction was decided to be up to 50% of the nominal value.

Two approaches were considered for deriving the set-points. The first maintains the TSR constant and achieves down-regulation through pitch adjustment, denoted as "*constTSR*". The second employs a linear trajectory in the  $\theta$ - $\lambda$ - $C_p$  space, combining both pitch and TSR modifications to lower the  $C_p$ . This second approach, referred to as "*lin70*," sets the minimum target TSR to 7. This choice was made to avoid further reducing the rotational speed. Further reduction was found to limit region 2 substantially for power levels below 70%, which has detrimental effects on power and loads as the turbine operates in off-design points for a large range of wind speeds. The selection of these approaches aligns with findings reported in [84], where a comparison of various down-regulation strategies was performed across the entire operational range. The findings indicated that the constant TSR approach and the combination of pitching and rotor speed reduction led to higher load reductions in the tower and main shaft compared to other strategies. This is particularly relevant for the present application because tower and shaft loads cannot be effectively reduced with IPC. The two selected trajectories are presented in figure 3.5 alongside the minimum  $C_t$  trajectory. Contour lines in the figure show the targeted reduction in  $C_p$  in increments of 5%.



**Figure 3.5:** The two trajectories considered for the derivation of down-regulation set points along with the minimum  $C_t$  trajectory

After defining the fine pitch angle and determining the target TSR and  $C_p$  for each level of down-regulation, the controller parameters need to be adjusted accordingly. For region 2, the adjusted torque constant  $\kappa$  was recalculated for any power level based on target  $C_p$  and TSR values using equation 2.10. The new rated rotational speed required for the updated set point definition was analytically derived by computing the updated rated wind speed based on the target  $C_p$  and  $\lambda$  values.

In the full-load region, as constant power is used for every mode of the controller, the torque is again derived by the targeted rated power and instantaneous generator speed. For the PI pitch controller, the new  $\omega_{g,rat}$  set point was used, and the gains, along with the gain scheduling for different mean pitch angles, were tuned with the same process as the baseline.

In region 1.5, the rotational speed bounds that define the torque-speed ramp remain the same as the baseline configuration. This is because the improvements in terms of loads and power from fine-tuning for the lin70 trajectory were minimal, and there was no consistent pattern to generalize for every power level. The coefficients of the ramp for each power level are then derived by equations 3.2 and 3.3. This approach slightly changes the effective cut-in wind speed for different power levels depending on the aerodynamic torque achieved. In practice, this means that down-regulation can be applied down to a minimum level depending on the wind speed. Moreover, exact power tracking cannot be achieved in region 1.5 since the fine pitch angle and the off-design TSR combination can vary the resulting  $C_p$ .

All the aforementioned parameters, for all the control regions, were derived for power levels from 50% to 100% with a step of 5% and provided as a look-up table. The values in between are calculated by linear interpolation according to the requested power level. The resulting steady-state response derived from aeroelastic simulations of the turbine for the different power levels is shown in figure 3.6.

Power tracking with both trajectories is accurate for wind speeds higher than 6.5 m/s. In lower wind speeds and for both trajectories, down-regulation levels below 75% produce power higher than targeted, even increasing above the baseline. This can be explained by the TSR plots showing that the achieved TSR is closer to the targeted value, leading to increased  $C_p$ . For down-regulation levels below 75% the opposite behavior is observed. In levels below 60% the produced aerodynamic power is not enough for electricity production, shifting the cut-in wind speed. To avoid this unpredictable behavior (also observed in loads as discussed in chapter 4) and since the power output is low (below 0.6 MW), it was decided to limit down-regulation to 75% for cases with mean wind speeds equal to or smaller than 6 m/s.

The steady-state plots of  $C_t$ ,  $\theta$  and  $\omega_{rot}$  show what is also observed in the  $C_p$  maps: the rate of change in values from 100% is much higher than in lower percentages. This is important for the application considered in this work as it indicates that substantial load reductions could be obtained with small changes in power level.

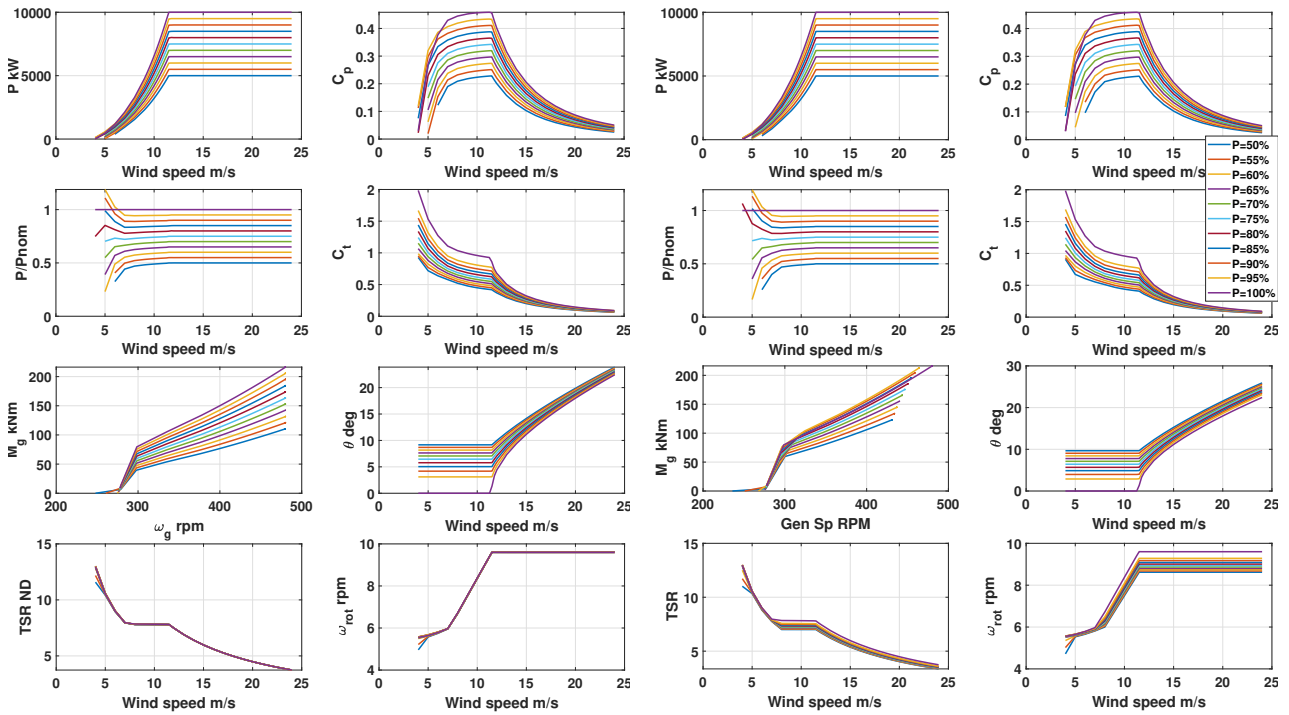


**Figure 3.6:** Steady state operational characteristics for the two down-regulation trajectories: Left columns 1 and 2: Const TSR trajectory. Right columns 3 and 4: lin70 trajectory

### 3.3 Power boosting

The design goal for the power boosting mode is to increase the power output of the turbine up to 30% of the nominal value in the wider possible range of wind speeds with the least possible increase in loads. Moreover, relevant to this work is to create a boosting scheme that behaves similarly for the different power boosting levels. The reason is to avoid cases where the loads are lower for higher power outputs that can drive the optimization process towards the specific power level.

The control strategy for power-boosting depends on the specific characteristics of the turbine, as explained in section 2.4. Figure 3.7 shows the possible trajectories based on the developed baseline controller of the DTU 10 MW rwt. Trajectory A-B shows the torque-based power boosting approach where the rated rotational speed remains constant and the torque is increased. The increased torque demand would be directly proportional to the power increase. This approach would introduce a region 2.5 where the turbine will operate with sub-optimal  $C_p$ . Trajectory A-C follows the optimal  $C_p$ , extending region 2 until the new power level is reached, increasing both torque and rotational speed. The rotational speed-based approach is described by trajectory A-D, where after rated torque is reached, the rotor would keep speeding up with the wind speed increase. This introduces an extended region 2.5 where the rotor should freely accelerate until the target rotational speed is reached. Trajectories A-E-F1 and A-E-F2 are examples of the approach increasing both speed and torque and can be adjusted to any

proportion between them.

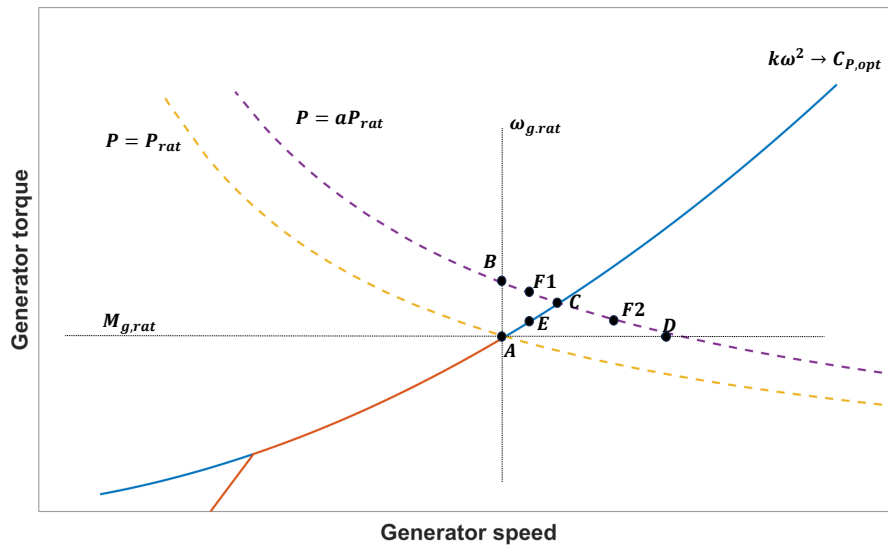


**Figure 3.7:** Power boosting controller trajectories for generator torque and speed

The decision was to extend region 2, continuing to track optimal  $C_p$  until the new rated value is reached, following the  $\kappa\omega^2$  approach. This implementation avoids creating transition regions that would vary in range depending on the power boosting level. As a result, the behavior of the turbine in terms of loads and power remains similar for all cases. Moreover, this approach was selected in order to avoid the maximum increase in rated torque and rotational speed values while maintaining maximum power extraction.

The relevant changes in the controller parameters include assigning rated values for rotational speed and generator torque as well as adapting the gains of the PI pitch controller. The rated values are derived analytically and are used as the new set point for the pitch controller and as upper bounds for the torque controller. The gain scheduling was derived for each power level as the targeted  $C_p$  levels are higher than the baseline. The necessary parameters for the power boosting mode were calculated analytically for power levels between 100-130%, with 5% increments, and provided in a look-up table. For other power levels, the values are derived through linear interpolation based on the requested power level.

The resulting steady-state operational characteristics for the power boosting mode are shown in figure 3.8. For the maximum power level, the increase in rotational speed is 8.3%, with the rotor reaching a maximum speed of 10.5 rpm and the tip having a maximum translational speed of 97.6 m/s. The maximum torque is increased by 18.8%, reaching 257 kNm. The rated wind speed is increased up to 12.6 m/s.

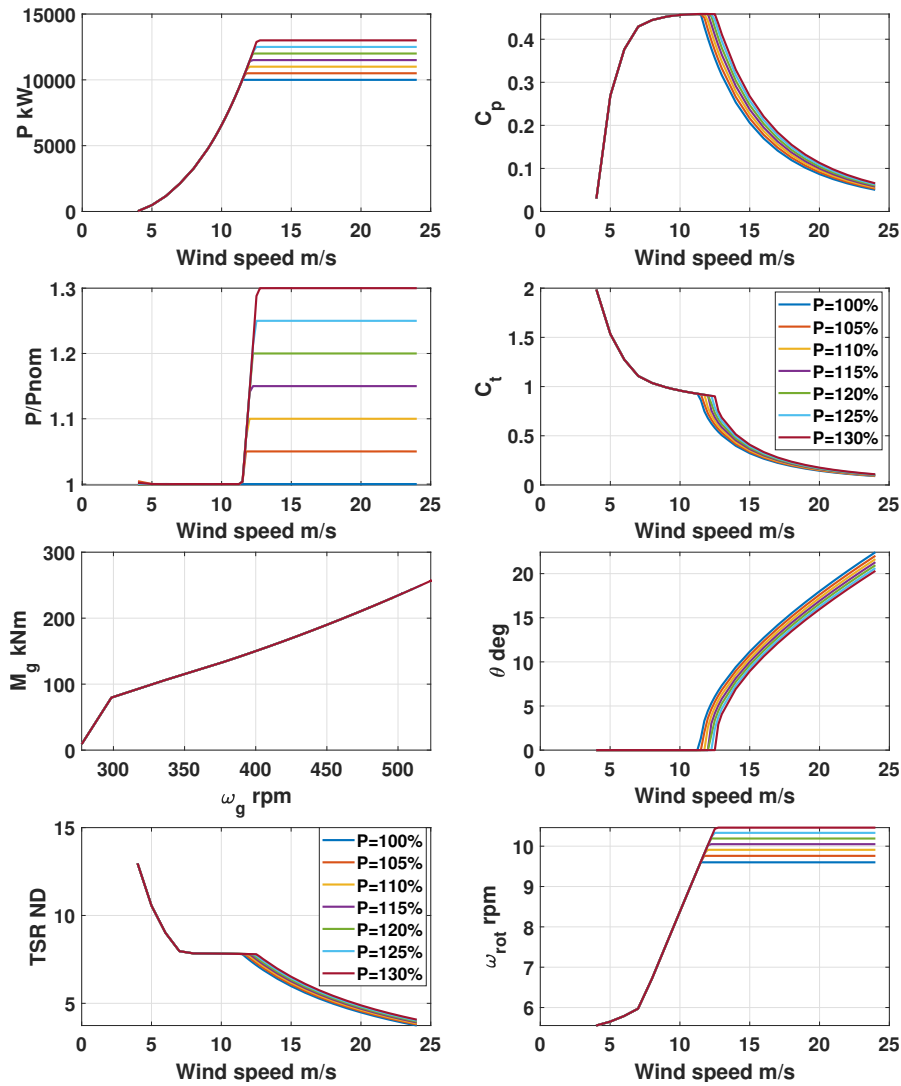


Figure 3.8: Steady state operational characteristics for the power boosting mode

### 3.4 Individual blade control

An individual pitch control loop is integrated into the controller as a structural load reduction method complementing down-regulation. The approach selected was the IBC approach described in section 2.4. The objective of the controller design is to create a simple and robust IBC loop completely decoupled from the main CPC loop, which is responsible for speed regulation in the full load region. The only requirement for its implementation, apart from software modifications, is the installation of load sensors at the blade roots.

For this, an IBC loop is created based on three independent controllers feedbacking directly the measured flapwise bending moments at the root of each blade, as explained in section 2.4. The method is based on [80, 77, 78] and was initially presented and evaluated in [87]. The IBC approach, compared to the traditional Coleman transformation [73], commonly used in IPC, allows more freedom to controller design both in terms of inputs and outputs. Transforming

the moments from the rotating to the inertial frame inherently rejects the higher frequencies than 1P, giving a low-frequency measure of the rotor unbalance in the form of yaw and tilt collective rotor moments along with the 0P component. The output of such an implementation is then a cyclic, azimuth-dependent pitch command canceling out the rotor imbalance. The main benefit of this transformation is the removal of the periodical component, making the derivation and tuning of the controller easier. The drawback is the limitation in targeting a wider spectrum of frequencies, and it can be seen as a loss of information about the blade state. The rotating frame input, considered within the IBC approach, provides all the frequencies affecting the blade response and allows it to act instantaneously and independently on the different conditions that each blade experiences with the cost of higher pitch actuation. The control system can target different frequencies, which in turn can focus on the load alleviation of different components. The main challenges in this approach are identifying such a system with periodical characteristics and limiting pitch actuation to the meaningful bandwidth for load alleviation of different components. Nevertheless, it is shown in [70] that the IBC and the Coleman-based IPC approaches have fundamental similarities, and given the tuning and their structure, they can have similar performance.

The initial task for creating the IBC loop is linear system identification. The rotor's properties, weight, coning, tilting, and overhang produce a deterministic loading, while the temporal and spatial discretization of turbulent wind, including shear effects, produce stochastic loading. Their coupling depends on the turbine's non-linear structural and aerodynamic response at the operating point. In literature, different simplified modeling concepts for controller design have been suggested based on physical second-order mass spring damper systems, such as in [110] or gray models introducing fictitious forces [77]. In the present work, the blade model is completely decoupled from the rest of the turbine. The flapwise bending moment was selected as the reference signal instead of out-of-plane or other combinations of flapwise and edgewise moments as it is considered more sensitive to fatigue load due to their higher magnitude and the blades' shape. Nevertheless, the same method can be applied with any input. Using black box identification methods, more precisely the *n4sid* algorithm for subspace state space system identification [111] using the Canonical Variable Algorithm (CVA) [112] as implemented in Matlab, an LTI state-space model is obtained per operating point. This approach with a non-physical model was preferred in an attempt to capture higher harmonics with the identified model.

The transfer function from inputs, pitch, and blade effective wind speed to output flapwise bending moment is identified based on closed-loop, full flexible model and rotor geometry, non-linear simulations with low TI wind fields. The required TI was identified by a sensitivity analysis since it had to be high enough to excite the relevant frequencies and low enough to stay as close as possible to the required operating point. This approach has the benefit of capturing

the non-linear structural behavior of the blade, including also the actuator and baseline PI pitch controller implicitly, as their effects are included in the identification dataset. The calculation of blade effective wind speed, modeling the rotational sampling of turbulence by the blades, uses azimuth discretized and spanwise averaged wind speeds, taking into account instantaneous blade azimuth and tower top structural motion. The number of points and the weighting average along the blade were obtained by parametric tests, with the metric being the agreement with the non-linear model in terms of input-to-output comparisons. The whole procedure was executed iteratively where a 3600s wind field with 5% TI was used for identification, and another one with the same TI but a different seed was used for validation. The models for every wind speed were assessed based on time and frequency domain convergence. In this manner, a linear model around each operating point presenting excitation to the relevant blade frequencies, as well as capturing the coupling of wind and pitch to bending root moment, is obtained. The resulting fifth-order LTI systems fit the FAST simulations up to 3P (0.48 Hz), as shown in 3.9. The resulting Variance Accounted For (VAF) was calculated at a level of 65% for all speeds.

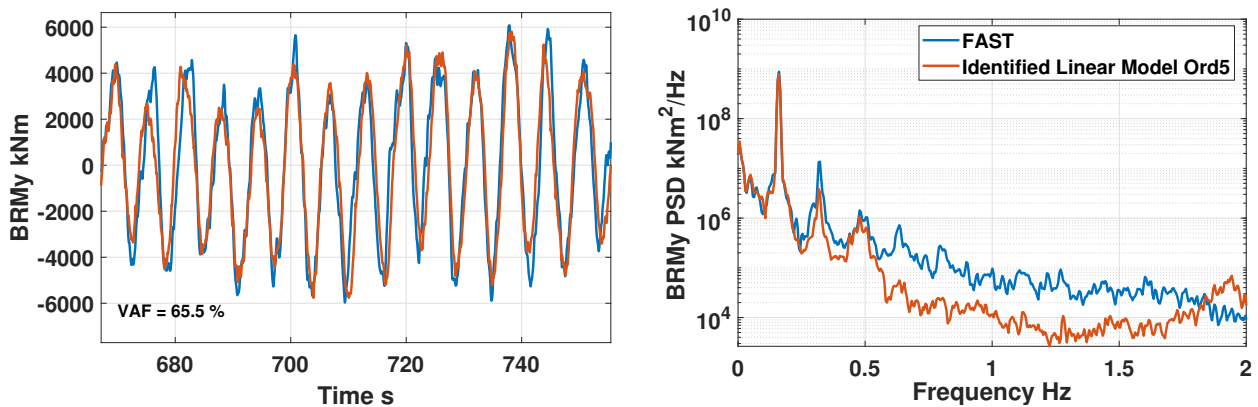


**Figure 3.9:** Identified linear model and FAST simulation response around 16 m/s with 5% turbulence intensity

The IBC controller is used as an add-on to the existing baseline PI CPC controller which is not re-tuned or otherwise changed. Therefore, the differential  $\Delta\theta_{IBC}$  contribution in pitch demand of each SISO controller is summed with the commanded pitch of the baseline CPC controller. IBC is active only in above-rated conditions and the switching between regions is done based on the generator power signal where the IBC outputs are scaled with a factor varying linearly between 0 and 1 for power between 90% and 100% of rated. This strategy ensures smooth transitioning while minimizing power losses and enhancing load alleviation. The parameters of the scaling were assessed by manual testing in terms of power and loads through simulations around rated wind speed. For this region-switching approach, the minimum acceptable pitch angle was set to -3 deg, lower than the theta fine of 0 defined for regions 1.5 and 2.

Moreover, the gains of the controller, similar to the traditional CPC controllers, are scheduled based on the collective pitch values in order to compensate for the non-linear dynamics and different sensitivity of pitching at different wind speeds. This was done for three wind speeds 16, 20 and 24 m/s (and the corresponding mean pitch angle) and linearly interpolated for the rest of the operational points. The control scheme itself is a traditional linear feedback PI structure due to its simplicity and robustness. A simple, although maybe not optimal, control design is more likely to be adopted by the industry while making it easier to apply online adaptive techniques for periodical re-tuning following the changes in the turbine's operational characteristics over time. Another important part of the controller design is the combination of the filters used for the input blade root bending moment and for the output pitch command, regulating the effective bandwidth of the controller. Hence, the parameters defining the controller's behavior are the frequencies of the high pass (HP) and band stop (BS) filters, as well as the tuning of the gains. The schematic diagram of the control system is presented in figure 3.10.

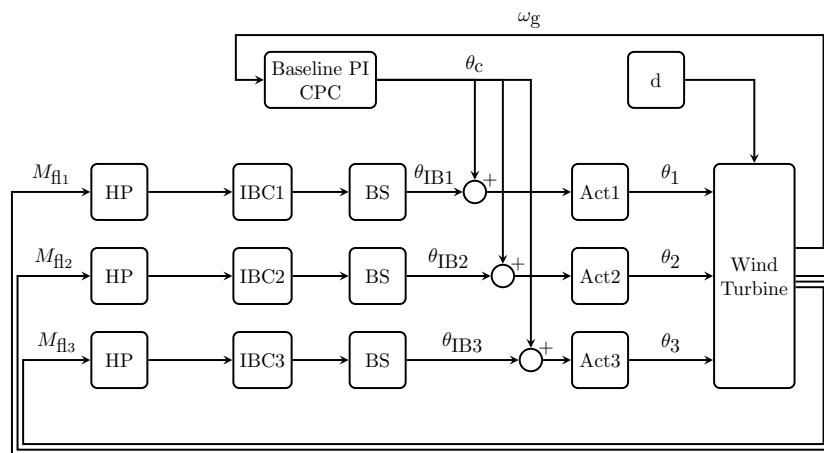


**Figure 3.10:** Block diagram of the IBC controller

The input to the controller is the high pass (HP) filtered flapwise moment, in order to avoid the compensation of frequencies close to 0P and part of the deterministic loading. A first-order HP filter is used and the corner frequency was identified together with the gains since they are coupled. The value used was 0.05 Hz. The output of the controller is BS-filtered limiting the targeting frequencies. Since there is a coupling between control bandwidth and load alleviation and pitch actuation, the purpose of the filters is to exclude specific frequency ranges with the minimum effect on the rest of the bandwidth. Several setups were tested with the implementation of different order low pass and Butterworth notch filters, but the inherent delays and ripple showed to be detrimental for load reduction. In order to avoid these effects, 3-DOF notch filters were implemented in series. This way, specific frequencies can be targeted while regulating the phase response close to these frequencies. Notch filters with parameters

$Q_{width}$ ,  $Q_{depth}$  and  $\omega_n$  regulating the width, depth, and natural frequency, respectively, were implemented with the transfer function shown in equation 3.4.

$$Notch_{3DOF} = \frac{s^2 + sQ_{width}Q_{depth} + \omega_n^2}{s^2 + sQ_{width} + \omega_n^2} \quad (3.4)$$

These 3DOF notch filters were designed separately from the controller according to the targeted frequencies. The goal was to be able to optionally exclude the region of 2P and 3P. Moreover, the attenuation of higher frequencies was considered, which did not contribute significantly to load alleviation but increased the pitch actuation. Multiple in-series filters were chosen over one, combining-all, due to the aforementioned delays. The parameters of the filters were manually tuned for each case with targeted frequencies of 0.32 Hz (2P), 0.48 Hz (3P), 0.9 Hz, and 1.5 Hz. Bandwidth higher than 2Hz is out of the system's response envelope and was not considered. The bode plots of the implemented filters are shown in figure 3.11.

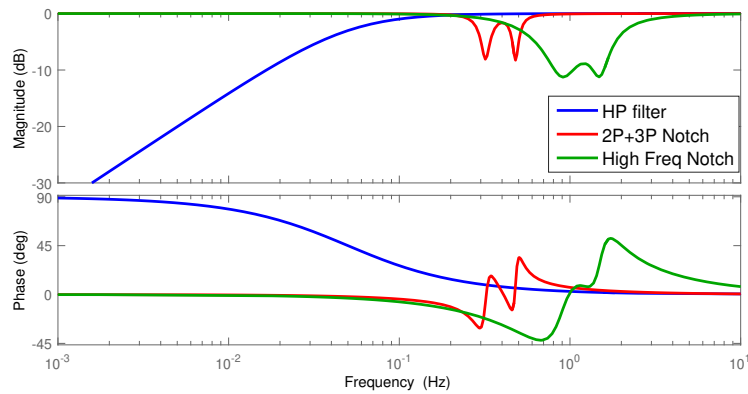


**Figure 3.11:** Filter design for the IBC loop

The feedback control for this system has some unique characteristics. The input values are zero mean due to the HP filter, and the set point is always zero. This means that the measured process variable is always the error. Moreover, the possible contribution of the IBC should be small, typically a few degrees, since the aim is to maintain the operating point without interfering with the CPC controller. Moreover, the effective bandwidth is bounded by the system's relevant frequencies, which in the present case are below 2Hz. Thus, an integral part is not useful as it creates an offset and counteracts the HP filtering. Moreover, a possible derivative term is partially substituted by the HP filter and is also commonly avoided on measured signals with noise in order to avoid amplification. Hence, the tuning problem is reduced to identifying an optimal proportional gain for each operating point. This is done with open loop shaping, where the identified linear state space model from pitch to blade moment is used. The gain is pushed until the phase and gain margins reach a certain threshold (5 dB and 40 deg), which is a measure of the robustness of the linear controller. Starting with these as initial values, further gain tuning was investigated manually with aeroelastic simulations based

on metrics of load reduction, pitch travel, pitch rate, and the magnitude of the differential command in order to obtain the gain per operating point. This process makes sure that pitch rate saturation is not reached, blade load alleviation is maximized, and speed regulation is intact. Finally, it is noted that the filter parameters were kept constant for all operating points since no added benefit was found by scheduling both gains and filter parameters.

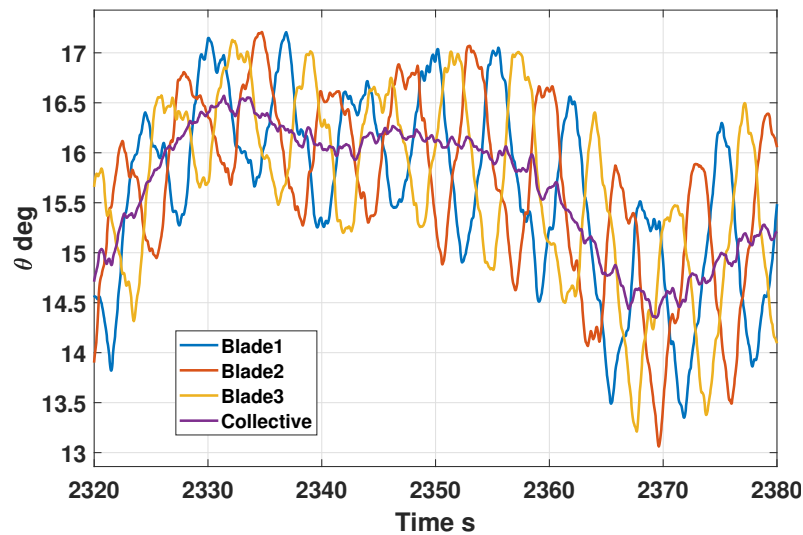


**Figure 3.12:** Indicative time series of the pitch angle of each blade along with the mean pitch value for a simulation with mean wind speed 18 m/s

The only control input is the flapwise bending root moment signal, which means that the other loads can only be implicitly affected by the complex dynamic structural coupling of the wind turbine system. By identifying an effective, or even optimal, control setup for blade load reduction, acting only on the spectrum excited by the blades, the only tunable parameter correlated to the other components is the control bandwidth limitation. Therefore, three different controllers were created with different setups in the output filters to examine the possible benefits of increasing bandwidth beyond 1P. The first, denoted as 'IBC 1P,' includes all the filters combined in series, focusing the IBC bandwidth up to 1P. The second, 'IBC 1P+2P+3P', uses the two higher frequency notch filters targeting frequencies up to 3P. The third controller, denoted 'IBC all', has no active filter, and no frequency is attenuated. An example time series of the blade pitch angles from a simulation at 18 m/s with 8% TI using the 'IBC 1P' controller is shown in figure 3.12.

In figure 3.13, the power spectral density (PSD) of  $\dot{\theta}$  and blade root moment from a simulation at 16 m/s are plotted to show the different behavior of the three controllers. A linear-linear plot is used for  $\dot{\theta}$  since the area in this type of plot is the variance of the quantity. It is shown that the higher the control bandwidth, the higher the pitch actuation. Especially when the higher frequencies are not attenuated, the increase is substantial, as seen from the 'IBC all' case. Moreover, the blade root spectra show that the most energy is concentrated around 1P

and, secondarily, at 2P and 3P peaks, which contribute the most to blade loading. It is also observed that IBC increases the energy slightly in higher frequencies. The latter is attributed to the non-ideal filters affecting more frequencies than intended.

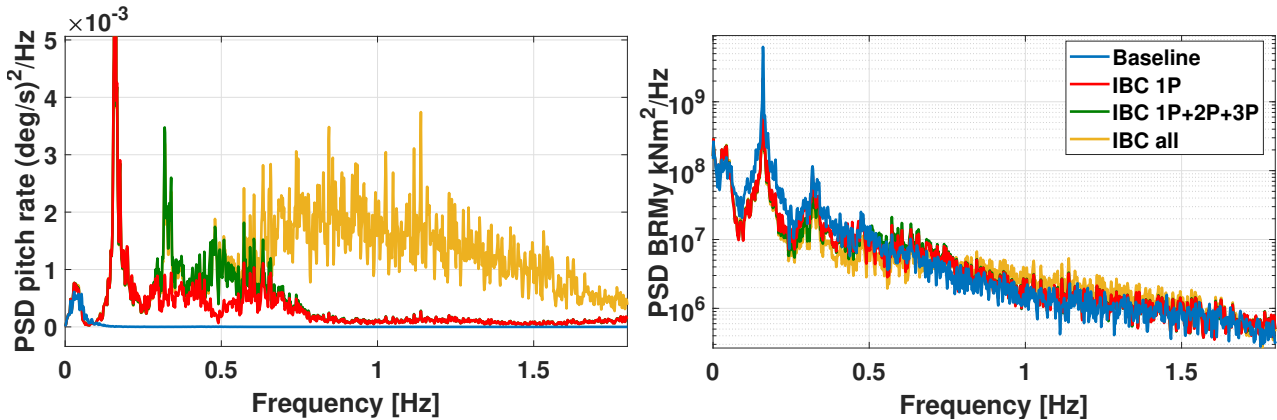


**Figure 3.13:** Blade root flapwise moment and pitch rate PSD at 16 m/s

The effect on the loads for each controller setting over the full operational range can be found in [87]. The study showed that there are some benefits in using the higher bandwidth up to 3P in terms of load reduction magnitude but not a significant improvement in targeting more components. Nevertheless, the tradeoff of a high increase in pitch actuation led to the decision to use only the 'IBC 1P' version in this work. The load reductions achieved for the different power levels and wind conditions are discussed in chapter 4.

To adapt the IBC loop to the different power levels, some parameter changes are required. The HP filter was kept the same for every power level, while the frequency of the in-series BS filters was changed on the adjusted rated rotational speed for each mode. As the manual fine-tuning of the gain is a time-intensive procedure, it was decided to simplify the process by only tuning the gains for the other power levels in one wind speed and performing a linear regression to derive a linear function of the gain over power levels. The gain scheduling over wind speeds per power level was simply done by offsetting the schedule derived for 100% power level and adjusting according to the mean speed corresponding to the mean CPC blade angle. This process was done for power levels in the range of 50-130% with a step of 5% and formulated as a look-up table. The gains and corresponding scheduling were calculated with linear interpolation for any power level between the tabulated values.

### 3.5 Summary-Conclusions

This chapter presented the wind turbine controller structure and tuning methods for all the modes and their combinations. The decision-making for the operational mode is done externally

by the wind farm operator. In the context of this work, the decision-making is done for a specific time block, and the required power level and IBC activation options are fed to the controller. There, the relevant parameters are calculated from the look-up tables or direct calculations, and the relevant values are updated. A high-level overview of this process is shown in figure 3.14. The dashed lines denote the software implementation on the individual turbine, and the outer layer represents the external decision-making process updating the operational mode in regular time intervals. In this work, the transition between the modes is not investigated in terms of numerical simulations in the time domain. It is expected that a few seconds, depending on the operating conditions, will be required from the moment the signal is given to the turbine controller until the turbine adapts to the new power level and the IBC loop is switched on or off.

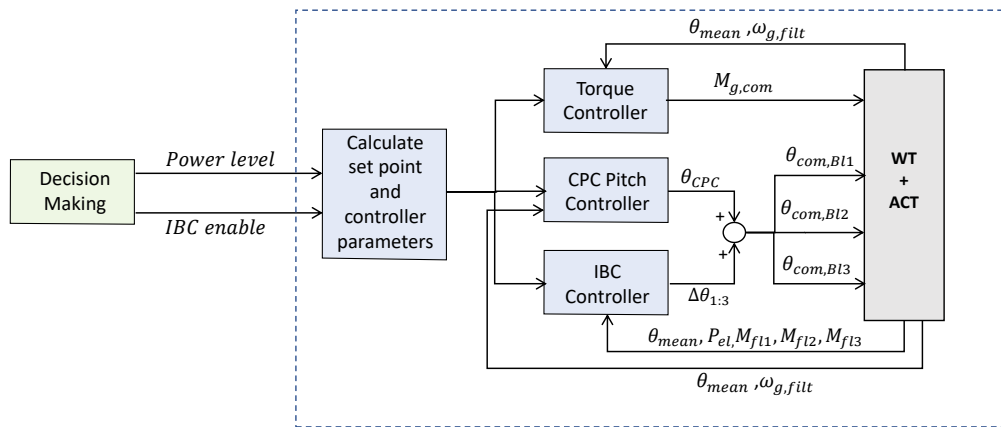


**Figure 3.14:** Overview of the controller structure, including the switching between modes cascaded in the decision-making loop

The presented controller for the DTU 10 MW rwt is able to change the power reference to any value between 50% and 130% with 100% denoting the baseline operation (10MW rated power). The IBC loop based on 3 SISO controllers feedbacking the measured flapwise blade root bending moment can be switched on or off. For the down-regulation, two methods have been implemented. The first changes the power output by additional pitching and keeping the TSR the same as the baseline operation (*constTSR*), and the second is a combination of reducing TSR by reducing the rotational speed and additional pitching (*lin70*).

The controller under consideration is specifically designed for normal operation scenarios, excluding provisions for managing start-up, shutdown procedures, or any integrated safety system. This design assumes the technical feasibility of accommodating a maximum 8.3% increase in rotational speed, a necessity for the power-boosting mode, while ensuring mechanical and aerodynamic integrity. Moreover, the design assumes that increasing the generator torque by up to 18.8%, for the maximum power level considered, is within the permissible limits regarding thermal, mechanical, and electrical considerations.

The controller structure presented here consists of simple and robust approaches that serve the scope of the work. More sophisticated controller design and tuning techniques, as well as more extensive fine-tuning, could be applied to achieve e.g.: optimal load reduction per down-regulation level, optimal power extraction, and reduced loading at regions 1.5 and 2.5 using the approaches discussed briefly in section 2.4. In an actual implementation, this would be beneficial. In this case, the aim is simplicity and a unified approach that will not drive the optimization procedure to specific points due to controller design choices. This could be an extension of this work on the topic of controller co-design optimization. After performing the full operational management optimization, the most crucial loads and operational points can be identified, and the controller structure and tuning can be modified to the specific requirements.

This chapter included only the controller design and the operational characteristics of the different control modes. The resulting aeroelastic response (including the tradeoffs between loads, power, and actuator metrics) for the full range of operating conditions is discussed in section 4.3.

# Chapter 4

## Surrogate modelling and aero-servo-elastic analysis

In this chapter, the focus is on discussing the surrogate modeling and the aero-servo-elastic behavior of the turbine in different control modes. Given the computational constraints of conducting individual aeroelastic simulations for each instance in the context of long-term optimization, an efficient model is needed to accurately capture the turbine response based on a dataset of comprehensive aeroelastic simulations. The choices of input/output variables and the sampling process for creating the training and validation sets are discussed. The two approaches used in this work, spline-based interpolation and Gaussian Process Regression (GPR), are specifically examined, highlighting their differences. Furthermore, the uncertainty of the surrogate models is quantified for the various quantities of interest across the range of considered input dimensions. Lastly, an aero-servo-elastic analysis is performed to explore the tradeoffs between loads and power associated across the different controller modes for the entire spectrum of considered environmental conditions.

### 4.1 Surrogate modelling methodology

The overview of the surrogate modeling process used in this work is shown in figure 4.1. The yellow blocks denote the creation of the training set based on some design of experiment (DOE) approach. The range of the input variable space has to be defined first according to the scope of application. Then, the appropriate sampling method and size for the training set have to be determined based on the computational cost constraints. Having the training set, a regression

method has to be applied, allowing to request for any arbitrary value within the range of the input space to obtain the output prediction. This is the core of the surrogate model, shown in the dashed lines in the plot, that will be used for the rest of the work. Additionally, the regression model can be compared to a validation set to quantify the expected uncertainty, as shown by the blue blocks in the figure.

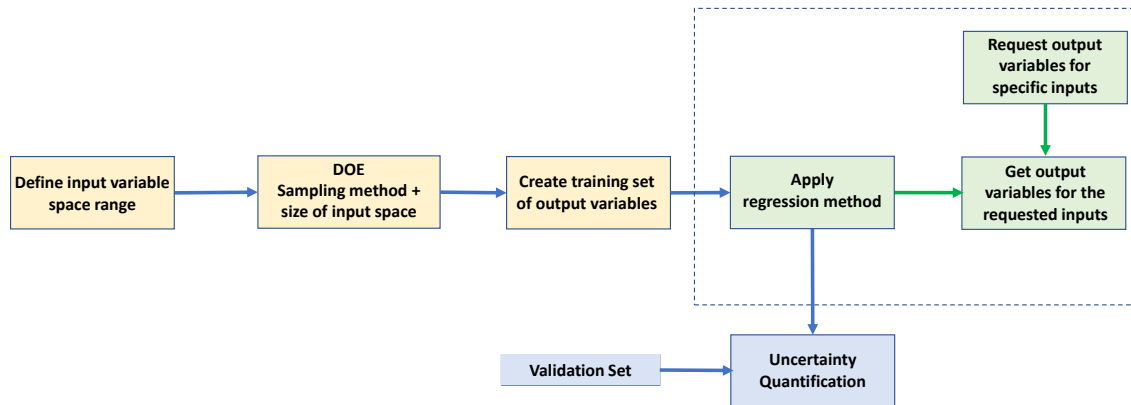


**Figure 4.1:** Overview of the procedure to create, apply and validate a surrogate model. The dashed rectangular indicates the actual surrogate model. The yellow blocks show the steps to create the training sample, and the blue blocks show the uncertainty quantification.

### 4.1.1 Input and output variable space

The first step in creating the training set is to define the input variables and their range, which is application-specific and constrained by the available computational power. In most of the applications discussed in the literature (see section 2.5), the goal is to have a full environmental contour including all operational conditions (e.g., shear, veer, air density, yaw misalignment, etc.) with the goal to have a full environmental contour for a single turbine or even a wind farm. This approach leads to a high dimensional input space, with more than  $n=7$  input variables in most cases, which makes a dense factorial sampling infeasible due to the computational cost as the sample size scales with the power of  $n$ .

The present application aims to capture the response of a single onshore turbine operating with different control modes. Hence, no wind farm flow effects are considered. Furthermore, it is assumed that the turbine operates with no yaw misalignment (intentional or not). This assumption is considered since it would not be possible to define the specific magnitude and time intervals when the turbine is misaligned, while applying it in a stochastic manner could bias the optimization results. According to the IEC standard 61400-1 for wind turbine design [113], the main inflow conditions that need to be considered for load assessment are the mean hub height wind speed, the turbulence intensity, the wind shear, the air density, and the vertical flow angle. The vertical flow angle is site-specific, which means it can be accounted for

as a fixed independent input variable. In this work, it is considered to be 0 degrees. The air density could be measured on-site using temperature, pressure, and humidity gauges and be fed as an input to the digital twin. Nevertheless, studies have shown that its much less influential on the loads compared to the other parameters, and its variability is highly site-dependent. Hence, for the specific application, it was decided to keep it constant at the standard value of  $1.225 \text{ kg/m}^3$ . As previous studies have shown (see e.g., [95, 99, 96]), the most influential characteristics are the mean wind speed and the turbulence intensity, with the wind shear following. To reduce dimensionality but also due to the fact that shear measurements are commonly not available in the operational stage, it was decided to keep it constant to the conservative value of 0.2 as suggested by the IEC standard.

With these considerations, the input variable space is three-dimensional, including mean wind speed, TI, and controller mode. Additionally, to account for the seed-to-seed variability, it was decided to use three stochastic wind field realizations for each combination of wind conditions. The simulation duration is set to 3600s as the optimization is performed based on hourly time blocks. An additional 100s interval is included at the beginning of each simulation that is removed in post-processing to exclude transient numerical effects. The longer time duration, compared to the 600s commonly used, reduces the seed-to-seed variability and also includes more low-frequency components that may influence loads.

The limited input variable space used in this work, in contrast to the literature discussed previously, allows for a full factorial sampling DOE. For the available computational setup, the simulation time is approximately three times the real-time, making a dense sampling feasible. The wind speeds are discretized with a step of  $1 \text{ m/s}$  from cut-in to cut-out. TI space ranges from 2% to 24% with a 2% step. The power level is discretized from 50% to 130% with a step of 5% with both down-regulation strategies (constTSR and lin70) considered. Power boosting and IBC modes are simulated for wind speeds  $> 10 \text{ m/s}$ . The resulting amount of unique wind fields generated is 756, and the total simulations performed are 24912. An overview of the variable space and simulation parameters is given in table 4.1. The simulation setup and turbine properties are discussed in section 2.3. The quantities of interest and metrics considered are summarized in table 2.1

The time series outputs for the quantities of interest are post-processed to derive the target metrics. The three turbulence seeds considered for each wind condition are used to derive the mean value and standard deviation for each metric. The processed metrics are then tabulated in 3D matrices having dimensions: wind speed, TI, and power level. In total, four independent matrices, per metric considered, are created for the different control modes and their combinations: constTSR, constTSR\_IPC, lin70, and lin70\_IPC. These four matrices are the training datasets on which the regression methods will be applied.

Additionally to the training dataset, a validation dataset was created following the same

**Table 4.1:** Variables and parameters for the simulations used to create the training set

Variable/Parameter	Values
Wind speed	4:1:24 <i>m/s</i>
TI	2:2:24 %
Shear PL exponent	0.2 ND
Air density	1.225 <i>kg/m<sup>3</sup></i>
Inflow angle	0 deg
Yaw misalignment	0 deg
Power level	50:5:130 %
IBC	On/Off (for <i>wsp</i> >10 <i>m/s</i> )
Turbulence model	IEC Kaimal
Surface roughness	0.03 m
Simulation duration	3600 s
Simulation time step	0.025 s
Turbulence seeds	3

process. The scope of the validation set is to assess the performance of the surrogate model in terms of predictive accuracy by comparing the surrogate response to unseen data. For this process, only one control mode was considered, the constTSR without IPC. This was done to reduce the required sampling size to effectively cover the input space, as the general trends are similar for the different controller modes. The validation set consists of 200 unique points derived using the Latin Hypercube Method (LHM) [114, 115] and is presented in figure 4.2. The whole space was sampled for the wind speed and power level input variables. For TI, the interval considered was 2%-18%. This was chosen as 18% is the maximum value of TI in the datasets used later for the optimization.

LHM is a sampling technique used in scientific and engineering studies to efficiently explore the parameter space of a mathematical model or simulation. It is particularly useful when evaluating models with multiple input parameters. LHM aims to ensure an even and representative parameter space coverage by dividing each parameter range into equally spaced intervals. Unlike simple random sampling, LHM ensures that each interval of every parameter is represented exactly once in the sample. This improves the robustness and accuracy of the analysis by reducing sampling bias and providing a more comprehensive exploration of the parameter space. LHM is widely employed in various fields, including optimization, uncertainty analysis, and sensitivity analysis, to improve complex systems' understanding and decision-making processes.

### 4.1.2 Regression approaches

Having the training and validation datasets, the next step is to perform the regression. Before applying the regression methods, an additional step of smoothing the training dataset is

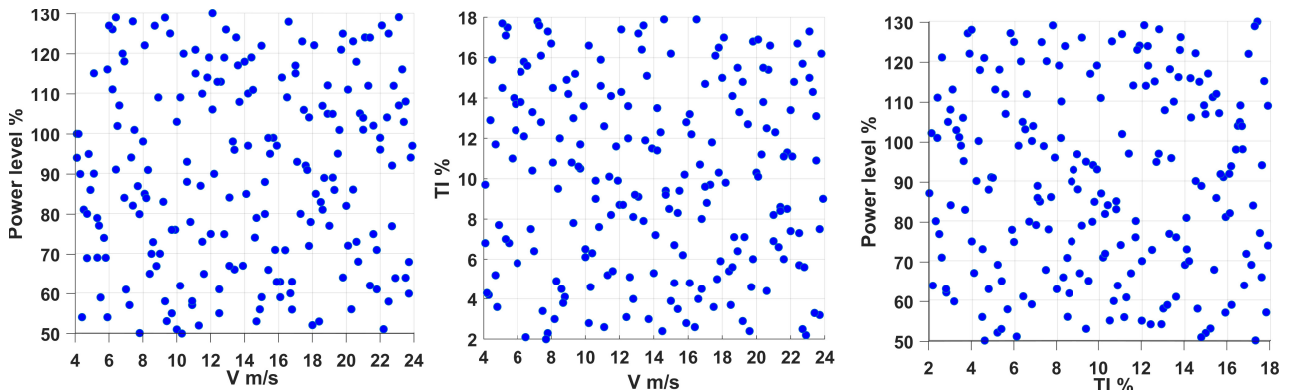


**Figure 4.2:** Sampling of validation set based on the latin hypercube method

performed. This was done retrospectively since it was observed that, in some cases, local extrema could drive the optimization process consistently to specific values. These extrema could be attributed to the variability of the specific seeds in combination with the controller tuning. The four matrices were filtered using a 3D Gaussian filter with a convolution kernel size of  $3 \times 3 \times 3$  points and a standard deviation of 0.6. These values were derived iteratively, aiming for a filter that smoothens these local peaks but does not change the general trends or increase the uncertainty metrics considered.

This work uses two regression methods: a spline-based interpolation and a GPR model. The spline-based interpolation is a straightforward and efficient regression technique selected for its simplicity, ease of implementation, and fast prediction capabilities. It serves as a baseline method to compare against the more computationally demanding GPR model, identified in the literature as one of the best-performing methods for the application. The objective is to assess whether the increased computational cost associated with GPR yields any advantages for the specific task under consideration.

Spline-based interpolation involves fitting a smooth curve or surface, called a spline, through the given data points. The spline is composed of piecewise-defined polynomial functions that ensure continuity and smoothness across the entire interpolation region. This technique is used to generate continuous and differentiable approximations of the underlying data, enabling accurate representations. It is often preferred to pure polynomial interpolation using a single polynomial to fit the whole dataset. Spline interpolation produces similar results, even when using lower-degree piecewise polynomials, while avoiding the issues with using single higher-degree polynomials that can lead to rippling near the edges of the interpolation interval. In this work, cubic splines are used with not-a-knot end conditions. Thus, even the third derivative is continuous at the first and last interior break.

GPR (also referred to as Kriging) is a statistical modeling technique used to estimate and predict values in a continuous domain. It is based on the concept of Gaussian processes, which

are collections of random variables that jointly follow a multivariate Gaussian distribution. In GPR, a Gaussian process is used to model the underlying relationship between input variables and corresponding output values [116, 92]. By leveraging the assumption of smoothness and incorporating prior knowledge, GPR provides a flexible framework for interpolation and extrapolation. It estimates not only the mean prediction but also the uncertainty associated with each prediction. GPR is widely used in various fields, including machine learning, geostatistics, and optimization, to handle non-linear relationships, make data-driven predictions, and quantify uncertainty in the predictions.

GPR uses a Gaussian process to model the relationship between input variables ( $X$ ) and output variables ( $y$ ). A Gaussian process is characterized by its mean function  $\mu(x)$  and a covariance function  $k(x, x')$ . The mean function represents the expected value of the output variable at any given input point, while the covariance function quantifies the similarity between output variables at different input points.

The output variable is assumed to follow a Gaussian distribution:  $y = f(x) + \epsilon$ , where  $\epsilon$  is Gaussian noise with mean zero and variance  $\sigma^2$ . The goal is to predict the output variable  $y^*$  for a new input  $x^*$  given a training dataset with input-output pairs  $(X, y)$ . The predictive distribution of  $y^*$  given the training data is also Gaussian:  $p(y^*|x^*, X, y) \sim N(\mu^*, \sigma^{*2})$ . The predictive distribution's mean  $\mu^*$  and variance  $\sigma^{*2}$  can be computed using the training data and covariance function. Specifically, the mean and variance are given by:

$$\mu^* = k(x^*, X)(K + \sigma^2 I)^{-1}y \quad (4.1)$$

$$\sigma^{*2} = k(x, x^*) - k(x^*, X)(K + \sigma^2 I)^{-1}k(X, x^*) \quad (4.2)$$

where  $k$  is the covariance function (kernel function),  $K = k(X, X')$  is the covariance kernel matrix where its entries correspond to the covariance function evaluated at the observations.

The choice of covariance function, such as the squared exponential, Matérn, or rational quadratic, along with the choice of hyperparameters, determines the smoothness and complexity of the resulting regression model. These hyperparameters can be learned from the data using maximum likelihood estimation or other methods. Model selection and evaluation in Gaussian process regression can be performed using techniques like cross-validation or Bayesian model comparison. More details on the mathematical implementation of GPR can be found in [116].

In this work, GPR is implemented using the native Matlab implementation framework included in the machine learning toolbox. For each quantity of interest, a separate GPR model is trained using the response data from the training set for the three input variables. This approach allows for fine-tuning the parameters individually for each response and ensures accuracy by accommodating different scales and smoothness characteristics of the response

signals. For each quantity of interest, hyperparameter optimization was performed using the Matlab framework provided with the *fitrgp* library using the random search optimization method. The chosen kernel and radial basis functions for the GPR models are presented in table 4.2. The noise standard deviation input was set close to zero since, in this work, the regression results are treated in a deterministic manner. However, for probabilistic assessment, the noise can be adjusted point-wise based on the standard deviation of the three seeds.

**Table 4.2:** Kernel functions and basis functions used in GPR for the different quantities of interest

Quantity	Kernel function	Basis function
BRMx	Matern32	Linear
BRMy	Matern32	Constant
BRMz	Matern52	Linear
BROop	Matern32	Quadratic
BRIp	Matern32	Linear
TBMx	Matern32	None
TBMy	Matern32	Linear
TBMz	Matern32	Linear
TTMx	Matern32	Linear
TTMy	Matern52	None
TTMz	Matern32	Linear
LSSMy	Matern32	Linear
LSSMz	Matern32	Linear
LSSTq	RationalQuadratic	None
Power	Matern32	Constant
Energy	Exponential	Quadratic
PitchTr	Matern32	None

## 4.2 Uncertainty quantification

The surrogate models are evaluated by comparing them to the validation set to assess the prediction performance of the two regression methods. Additionally, the uncertainty associated with each quantity of interest is quantified. The objective is to determine the overall level of uncertainty for each quantity and identify the specific conditions where the highest uncertainty is observed. In this analysis, only the constTSR down-regulation trajectory is considered, as it exhibits similar behavior to the lin70 trajectory, and the focus is on comparing the regression models.

The box plots of the relative error and relative absolute error, expressed in percentages, are shown in figure 4.3 for both methods. The central mark indicates the median, and the bottom and top edges of the box indicate the 25<sup>th</sup> and 75<sup>th</sup> percentiles, respectively. The whiskers

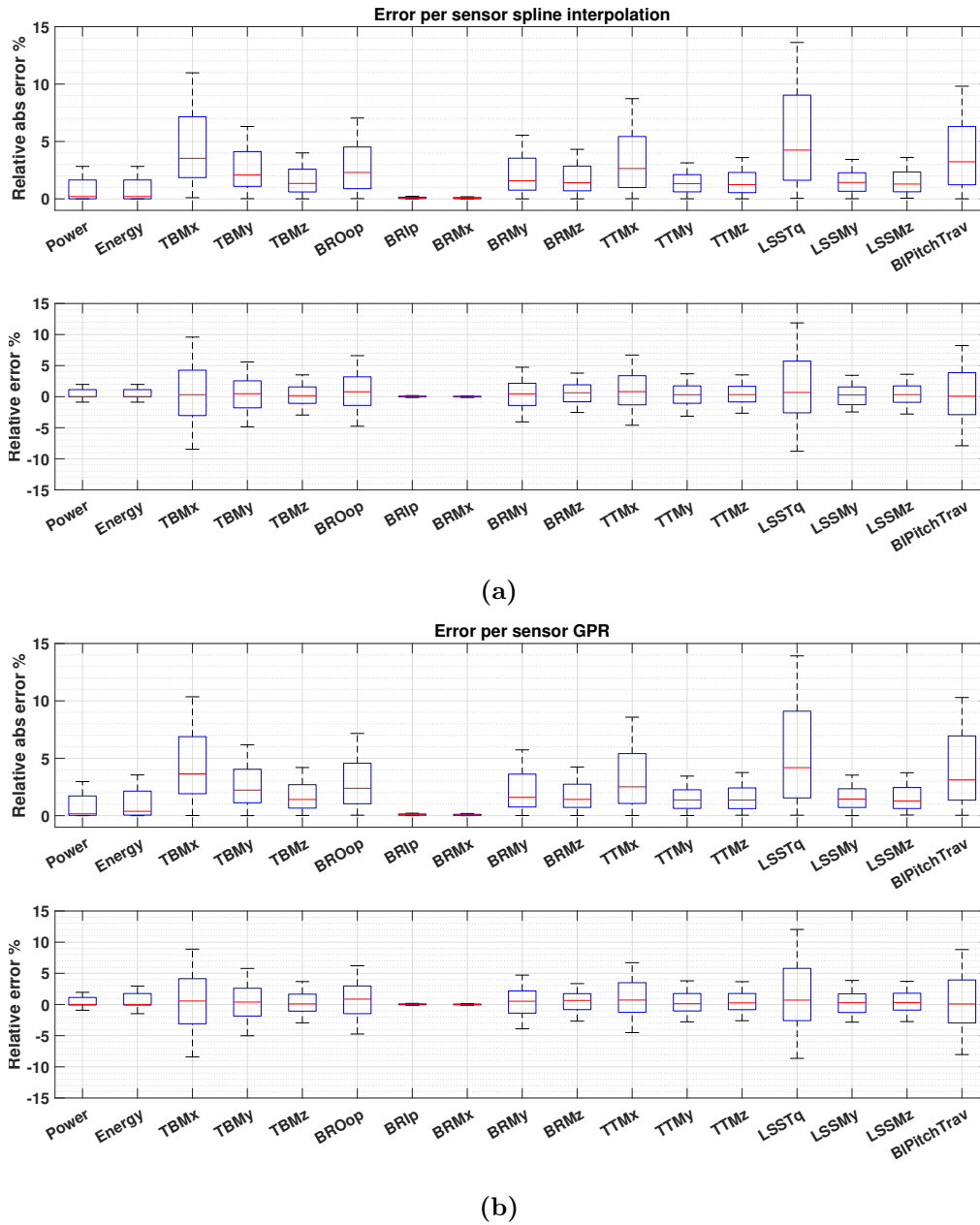


**Figure 4.3:** Box plots of the relative error and relative absolute error for the spline interpolation (a) and the GPR model (b) to the validation set per sensor. The central mark indicates the median, and the bottom and top edges of the box indicate the 25<sup>th</sup> and 75<sup>th</sup> percentiles, respectively. The whiskers extend to the maximum and minimum values not considered outliers

extend to the maximum and minimum values not considered outliers. An overview of all the mean errors, mean absolute errors, median absolute errors, and coefficients of determination for all quantities of interest for both regression methods are shown in table 4.3.

Both regression methods exhibit similar results in terms of uncertainty, accurately capturing the response of the output variables. The mean error for most loads is less than 1%, except for LSSTq, which is around 2%. The mean absolute error is below 4% for most loads, except for LSSTq and TBMx, which reach 7% and 5%, respectively. The median absolute error is below

**Table 4.3:** Evaluation metrics of the GPR and spline-based surrogate models compared to the validation set. ME: mean error %, MAE: mean absolute error %, MedAE: Median absolute error %,  $R^2$ : coefficient of determination. s denotes the spline-based interpolation and g the GPR model

Quantity	ME s	ME g	MAE s	MAE g	MedAE s	MedAE g	$R^2$ s	$R^2$ g
BRMx	0.0	0.0	0.1	0.1	0.1	0.1	0.9981	0.9981
BRMy	0.6	0.6	2.4	2.5	1.6	1.6	0.9966	0.9966
BRMz	0.6	0.6	2.1	2.1	1.4	1.4	0.9936	0.9937
BROop	0.8	0.8	3.0	3.0	2.3	2.4	0.9950	0.9951
BRIp	0.0	0.0	0.1	0.1	0.1	0.1	0.9987	0.9987
TBMx	0.6	0.6	4.9	4.9	3.5	3.6	0.9915	0.9916
TBMy	0.5	0.6	3.2	3.2	2.1	2.2	0.9914	0.9913
TBMz	-0.6	-0.5	2.6	2.7	1.3	1.4	0.9987	0.9987
TTMx	1.3	1.3	4.0	4.1	2.6	2.5	0.9933	0.9934
TTMy	0.7	0.7	1.8	1.9	1.3	1.4	0.9990	0.9990
TTMz	0.6	0.6	1.7	1.8	1.2	1.3	0.9990	0.9990
LSSMy	0.6	0.7	1.8	1.9	1.4	1.5	0.9990	0.9990
LSSMz	0.6	0.8	1.8	2.0	1.3	1.3	0.9990	0.9990
LSSTq	1.8	1.9	6.7	6.8	4.2	4.2	0.9584	0.9580
Power	1.8	2.0	3.3	3.6	0.2	0.1	0.9998	0.9998
Energy	2.0	1.9	2.8	4.4	0.2	0.4	0.9998	0.9997
PitchTr	1.9	2.1	11.6	11.2	3.2	3.1	0.9927	0.9928

3% for most loads, except for LSSTq and TBMx, which reach 4% and 3.5%, respectively. Power, energy, and pitch travel are influenced by specific wind speed regimes, resulting in higher error statistics, although they exhibit very low uncertainty in the majority of the variable space. The impact of specific conditions on uncertainty will be further discussed later in this section.

Comparing the two methods and their uncertainty metrics shows that they have practically the same level of accuracy with small discrepancies in the level of decimals in percentage. This shows that for the present application and the dense factorial sampling used, there is no significant benefit in accuracy by using the GPR model. The main benefit of using the model would be its ability to give uncertainty estimates for each prediction that can be used for uncertainty quantification in the overall optimization process. The disadvantages of the GPR model compared to the spline-based interpolation are the computational time for training, the size of the model, and the longer time to produce the predictions. The first one is not crucial as it has to be done only once in the initial stage of the process. The other two are important when considering an optimization process where the repetitive model calls can be in the order of  $10^3 - 10^6$ . Then, the slower response can have a high computational overhead while the large size of the model slows down the parallelization process significantly as large chunks of data need to be moved to the parallel workers frequently.

In order to understand the uncertainties of the surrogate model better, the different quantities

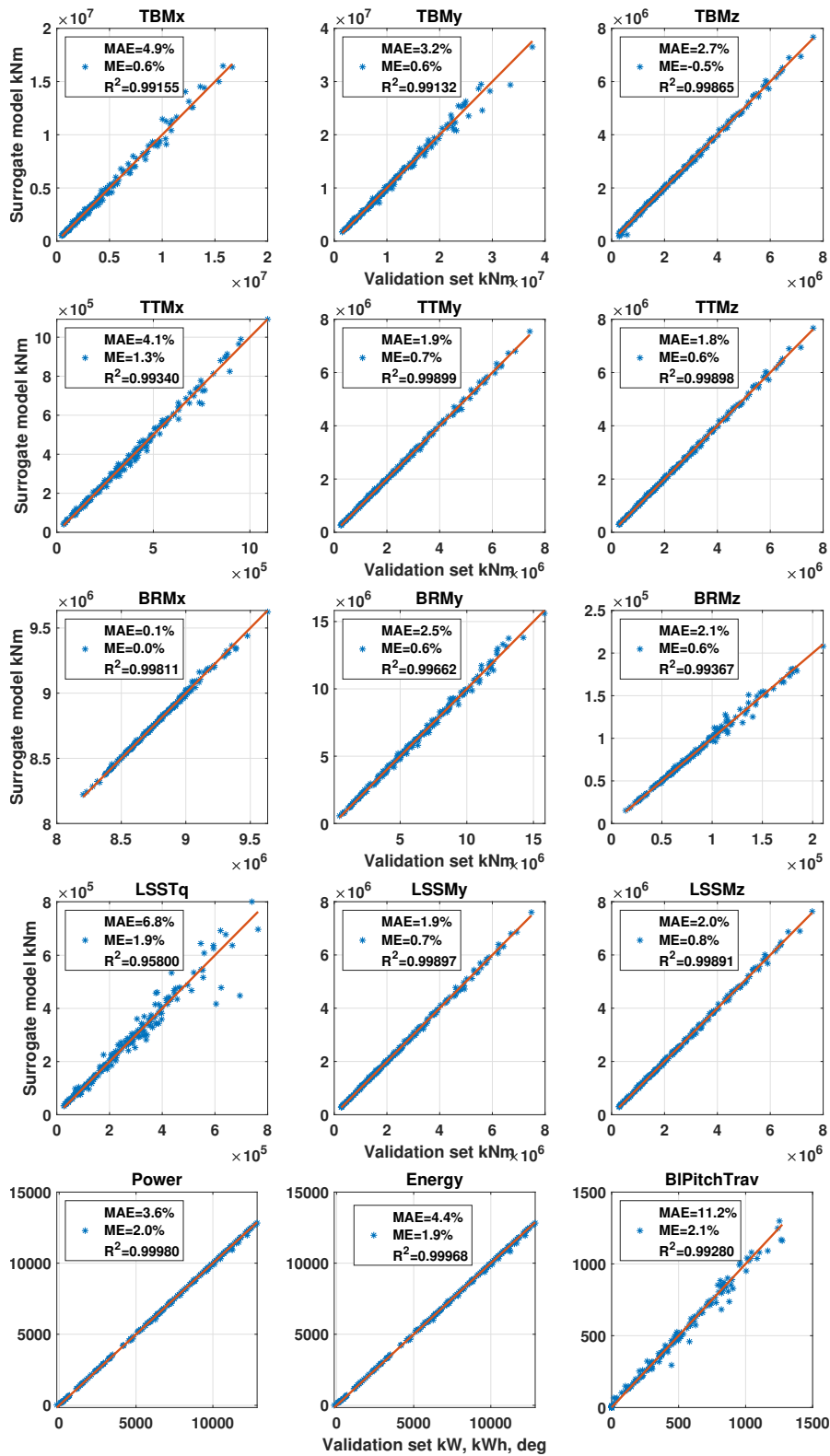


**Figure 4.4:** Comparison between the surrogate response and the validation set per quantity of interest using the GPR regression and the constTSR trajectory for down-regulation. Legends include the coefficient of determination  $R^2$ , the mean error (ME), and mean absolute error (MAE)

of interest are analyzed individually. Since both surrogate approaches behave similarly, only the GPR model is used for this analysis. The comparison of the surrogate response to the validation set is shown for all quantities in figure 4.4.

The blade loads, BRMx and BRIp, are captured with very high accuracy with an MAE of less than 0.2%. This is expected as these loads are mainly driven by the rotational speed and gravity and don't vary as much with the thrust. The BRMy and BRMz loads have an MAE smaller than 2.5%. Figure 4.5 shows the error sorted per input variable for these loads. TI influences the uncertainty in both cases the most as the error scatter increases with increasing TI. Moreover, BRMz uncertainty is higher for above-rated wind speeds, which can be attributed to pitch control activation as torsional blade loads are increased with pitching and the exact pitching behavior depends on the stochastic behavior of the wind. At low wind speeds  $< 5\text{ m/s}$ , higher error values can be seen in both cases. Here the controller is in region 1.5, and depending on the turbulence, the wind speed can go below cut-in or operate in region 2 for different periods making the results sensitive to these changes. Additionally, the lower power levels change the length of these regions as well as the cut-in wind speed, which also increases the uncertainty. Finally, the absolute values are very small in this regime, which has a magnifying effect on the errors. Small changes in the absolute value lead to high changes in the relative error. This observation can be generalized for most of the output quantities considered.

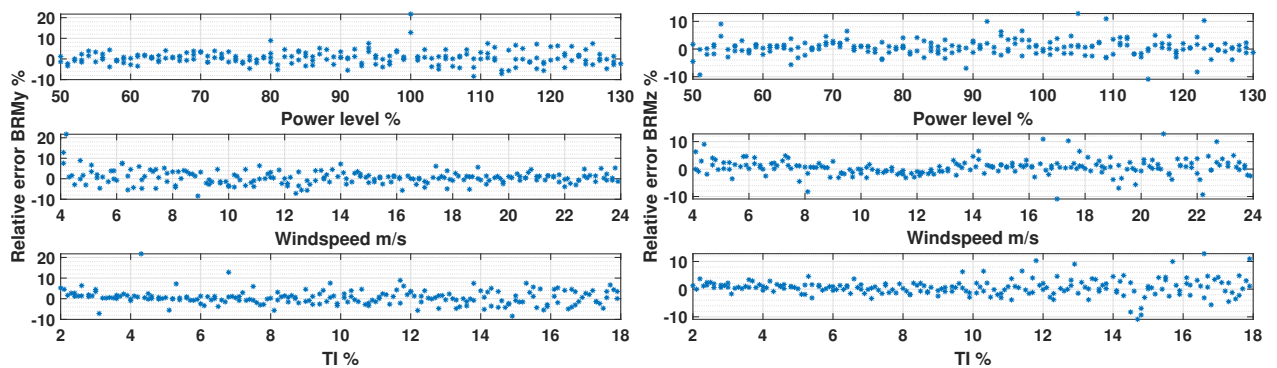


**Figure 4.5:** Relative error between the surrogate predictions and the validation dataset sorted per input variable. Left: blade root flapwise moment DEL, Right: blade root torsion DEL

The tower bottom load with the least uncertainty is the torsion TBMz. The MAE is 2.7% with the highest errors in the very low wind speeds  $< 5\text{ m/s}$ . The MAE for TBMx and TBMz loads is 4.9% and 3.2%, respectively. The relative error sorted by the input variables for these loads is shown in figure 4.6. TBMx has the second-highest error values from all the loads considered. As the side-side component is less damped by the aerodynamic forces, it presents a more stochastic loading behavior over wind speeds. It has a higher dependency on the turbulence seed realization, which leads to higher uncertainty for the surrogate model. For the TBMz load, higher uncertainty is observed for low TI ( $< 4\%$ ), with the surrogate consistently

overestimating the output. Moreover, a weaker correlation between increased uncertainty with increased load magnitudes (seen in figure 4.4) is observed. The highest fore-aft loads are observed around the rated wind speed, a region of higher uncertainty for TBM<sub>y</sub>.

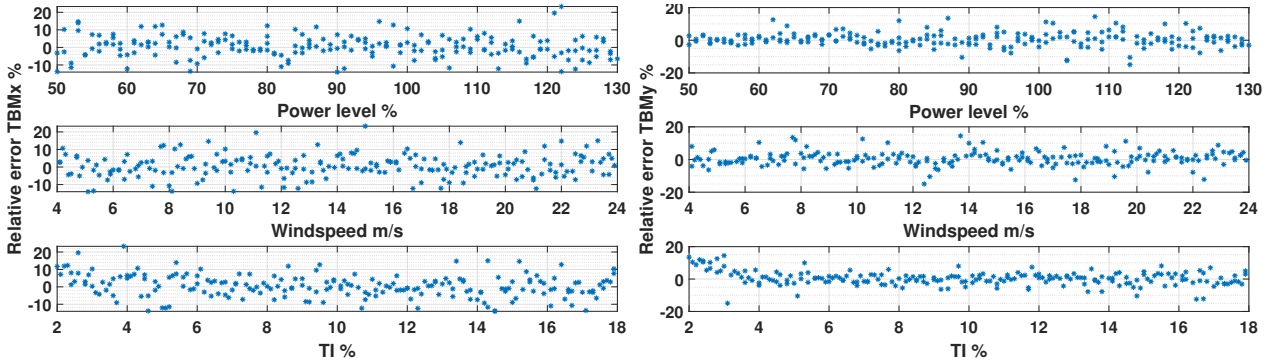


**Figure 4.6:** Relative error between the surrogate predictions and the validation dataset sorted per input variable for the tower bottom loads. Left: tower bottom side-side moment DEL, Right: tower bottom fore-aft moment DEL

The tower top loads TTM<sub>y</sub> and TTM<sub>z</sub> exhibit very similar patterns in terms of error magnitudes and uncertainty distribution. The relative error sorted by the input variables for TTM<sub>x</sub> and TTM<sub>z</sub> is shown in figure 4.7. For these loads, the MAE is 4.1% and 1.9%, respectively. In the case of TTM<sub>x</sub>, the uncertainty is primarily driven by wind speeds, with the highest values observed in below-rated wind speeds and the uncertainty increasing as wind speeds decrease. As the roll moments correlate with the variation in rotational speed and generator torque, the DELs in below-rated regions, especially in region 1.5, have the highest variation leading to high sensitivity of loads to conditions. This translates to higher prediction uncertainty for the surrogate model. For TTM<sub>y</sub> and TTM<sub>z</sub>, there is no clear trend of correlation of uncertainty to input variables. In most cases, increased uncertainty is observed for very low wind speeds ( $< 5m/s$ ).

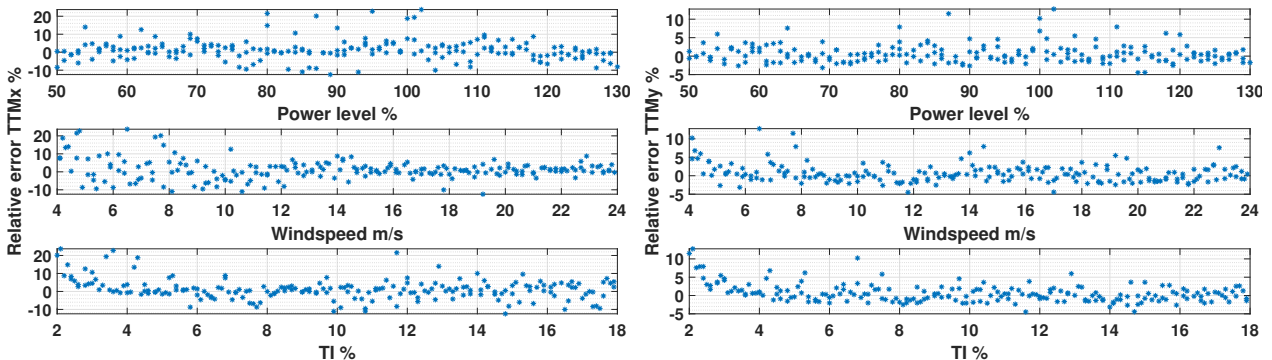


**Figure 4.7:** Relative error between the surrogate predictions and the validation dataset sorted per input variable for the tower top loads. Left: tower top roll moment TTM<sub>x</sub> DEL, Right: tower top pitch moment TTM<sub>y</sub> DEL

Low-speed shaft bending moment loads, LSSM<sub>y</sub> and LSSM<sub>z</sub>, present very similar patterns in terms of error magnitudes and uncertainty distribution. The relative error sorted by the

input variables for LSSMy and LSSTq is shown in figure 4.8. For LSSMy and LSSMz the MAE is 2%. There is no clear pattern of dependency of uncertainty to input variables. The LSSTq load has the highest uncertainty from all loads considered, with an MAE of 6.8% and the lowest coefficient of determination. As seen from the one-to-one comparison in figure 4.4, the highest uncertainty is correlated with the highest magnitudes, which in turn occur in the transition region around rated. This is also confirmed in figure 4.7, where higher errors are seen in this region.

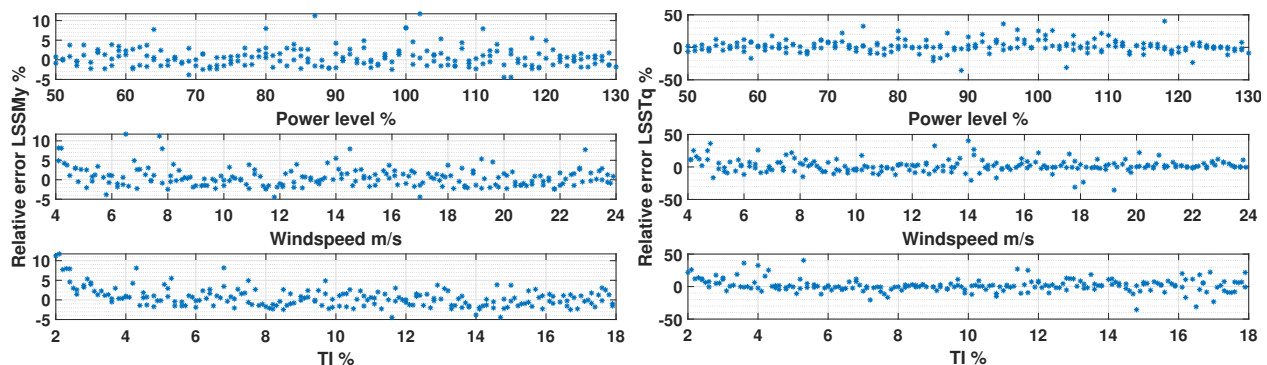


**Figure 4.8:** Relative error between the surrogate predictions and the validation dataset sorted per input variable for the low-speed shaft loads. Left: low-speed shaft moment around y-axis LSSMy DEL, Right: low-speed shaft torque LSSTq DEL

Power, energy, and blade pitch are also captured by the surrogate. The relative error sorted by the input variables for these is shown in figure 4.9. Power and energy are highly correlated in terms of error magnitudes and uncertainty distribution. The reported MAE values close to 4% can be misleading as the high error values are primarily observed at very low wind speeds below 5 m/s. In this region, even small changes in wind speed can lead to larger errors, although the absolute difference in power is only a few kW. If only speeds above 5 m/s are considered for the calculation of MAE, the value becomes 0.4%, and the highest uncertainty is observed in the transition region around rated wind speed. The blade pitch travel output has an MAE of 11.2%. The figure shows larger errors are observed in the rated and slightly below-rated wind speeds. Since the transition to region 3 depends on the variation of wind speeds, the pitch travel magnitude depends highly on the specific turbulent realization leading to higher uncertainty for the surrogate model in this region. This is confirmed if only samples with wind speed  $> 12\text{m/s}$  are considered for the error calculation. Then, the MAE becomes 4% (not shown here).

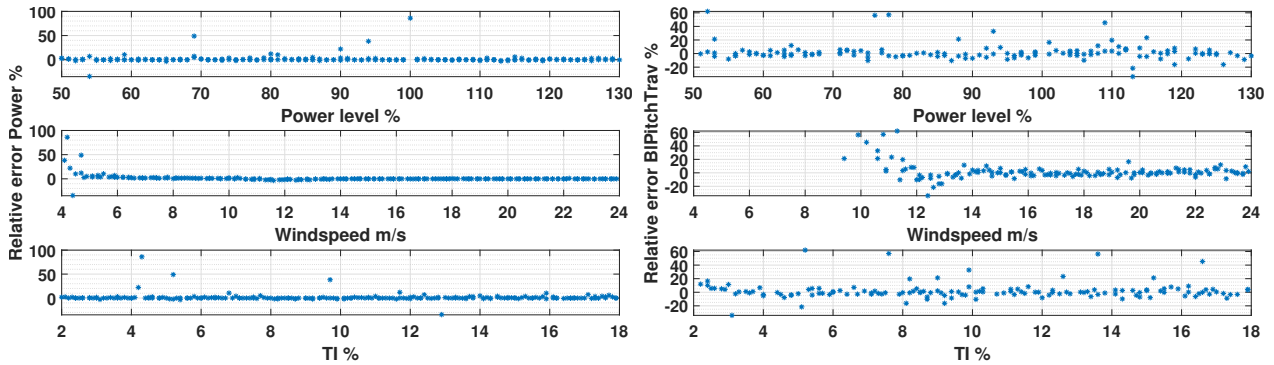


**Figure 4.9:** Relative error between the surrogate predictions and the validation dataset sorted per input variable for mean power and blade pitch travel. Left: mean electrical power, Right: blade pitch travel

### 4.3 Aero-servo-elastic analysis

In this section, the response of the wind turbine is analyzed using the surrogate response for the different control models and input conditions. Only the GPR surrogate is used, as the response between the two regression methods is similar. The goal is to identify the trends of loads, power, and pitch travel for the considered range of input variables, as well as the effect of the IBC loop and the two down-regulation trajectories. This analysis provides a better insight into the dependency of the loads on different conditions and controller modes. Moreover, the tradeoff between power and loads for the different power levels is discussed, which is the core element for the optimization. The sensitivity of the quantities of interest to the input variables is discussed in groups of relevant quantities (blade loads, tower bottom loads, etc.), and the visualization is based on parametric swipes of the surrogate response for the range of each input variable.

Figure 4.10 shows the tower bottom load response under varying input conditions for all controller modes. The side-side load,  $TBM_x$ , magnitude is highest in higher wind speeds showing an almost linear increase with increasing wind speeds in the above-rated region. Varying the power level in above-rated conditions has a minor effect on loads ( $<7\%$  variation). The  $TBM_x$  load is slightly damped aerodynamically and depends mainly on rotational speed, gravity, and aerodynamic torque. In the case of down-regulation using the constTSR trajectory, the lower torque leads to lower loads. In power boosting mode, the higher rotational speed leads to higher 3P frequencies, which move further away from possible tower crossing frequencies, leading to slight DEL reductions. Using the lin70 trajectory for down-regulation has the opposite effect, increasing the  $TBM_x$  load up to 30% in the partial load region and up to 11% in the full load region. This increase is attributed to the decrease in rotational speed, which brings it closer to the tower's natural frequencies. The sensitivity of the DTU 10 MW rwt with respect to resonances leading to increased  $TBM_x$  loads has also been documented in literature [46, 67].

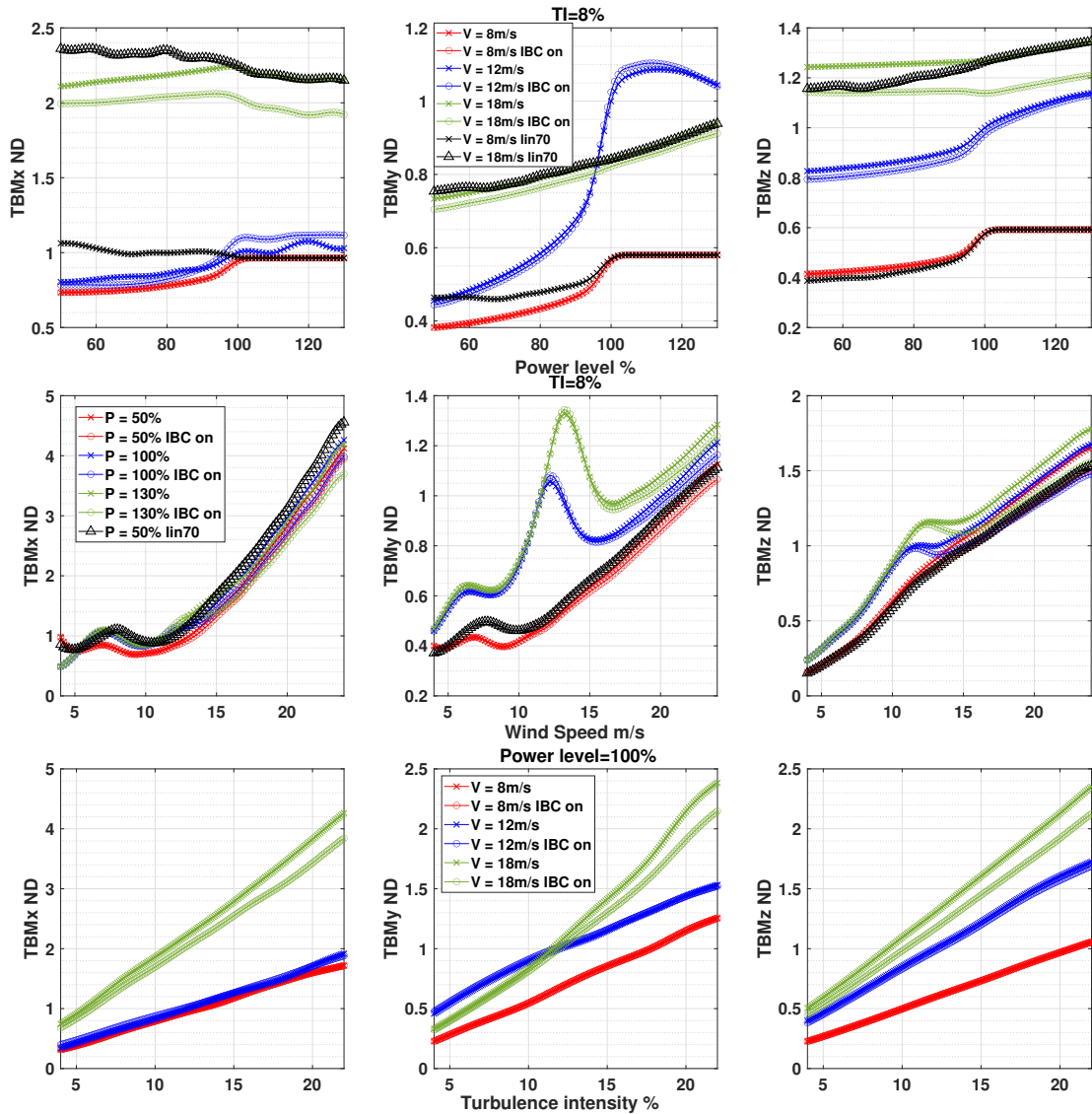


**Figure 4.10:** GPR surrogate response for the tower bottom DELs. For the power level and wind speed sensitivity plots, values are normalized with the power level of 100% at 12 m/s without IBC. For the sensitivity to TI, values are normalized with the output for 12% TI at 100% power level without IBC

Activating the IBC loop leads to TBMx load reduction in the order of 10-15% for all power levels, while in the rated region, it marginally increases it. In rated and below-rated conditions, down-regulation using the constTSR trajectory leads to load reduction up to  $\sim 20\%$  for the minimum power level. The rate of reduction is higher until about 90% power level, where a 15% reduction is already reached. Conversely, the lin70 trajectory exhibits the opposite behavior, with the loads increasing with decreasing power levels. The impact of TI is similar to all tower bottom loads, which exhibit a nearly linear increase with increasing TI. The effect is more pronounced in above-rated conditions, where the rate of increase is higher. Additionally, the effectiveness of the IBC is dependent on TI for all tower bottom loads. Increasing TI increases IBC load reductions proportionally to the power level.

The fore-aft tower bottom DEL,  $TBM_y$ , is higher at wind speeds in the transition region and at the highest wind speeds. In the full load region,  $TBM_y$  varies almost linearly with the power level. The maximum decrease observed is in the order of 15% for the minimum power level, while the maximum load increase is around 10% for the maximum power level. The loads in the transition region are the most sensitive to changes in power level due to the maximum thrust in this region and the transition between control regions. For maximum power boosting,  $TBM_y$  load increase in this region reaches 25% and is proportional to the power level. Down-regulation, with both trajectories, in the transition region effectively reduces the loads by up to 50%. In the partial load region, down-regulation with constTSR reduces the loads by up to 35% while the lin70 trajectory reduces them by up to 25%. For both transition and below-rated regions and both down-regulation trajectories, more than 50% of the  $TBM_y$  load reduction occurs until 90% power level. The IBC loop has a small effect on  $TBM_y$  loads with a maximum load reduction of 4% for all power levels and wind speeds.

The magnitude of the torsional load at the tower bottom,  $TBM_z$ , is proportional to the wind speed with a small local peak in the transition region. Power boosting increases DELs in the transition region up to 20% for the maximum power level. In the full load region, less than 5% increase is observed for all wind speed and power levels. Down-regulation in the full load region using the constTSR trajectory has practically no effect, while the lin70 trajectory reduces the  $TBM_z$  load up to 7%. In the partial load and transition regions, down-regulation can lead to load reductions up to 30% for the minimum power level. More than 50% of these reductions are achieved at 90% down-regulation. This shows that the most effective power level range, in terms of the tradeoff between power and loads in the partial and transition operating regions, is 90-100%. The application of IBC leads to  $TBM_z$  load reductions to a level of 10%, with the effectiveness increasing with increasing TI levels.

The tower top loads response is shown in figure 4.11. The roll moment load,  $TTM_x$ , is higher for the higher wind speeds and has a significant peak in the transition region. This peak is proportional to the power level, increasing with power boosting and reducing with down-regulation. Power boosting increases the peak loads in the transition region up to 20% for maximum power level proportionally to the boosting level. For higher wind speeds, it has a marginal impact on the  $TTM_z$  loads. Down-regulation, with both trajectories, is able to reduce  $TBM_z$  in all operating regions. In the full-load region, the load reduction is proportional to the wind speeds reaching a maximum reduction of 10-15% for the minimum power level for both trajectories. The largest reductions by down-regulation, up to 80%, are observed in the transition region. The reduction is proportional to the power level with a higher reduction rate until 90% power level. In the partial load region,  $TTM_x$  load reduction is linearly correlated to power level. The constTSR trajectory is more effective, achieving a maximum reduction of 45% for the minimum power level. With the lin70 trajectory, these reductions are found up to

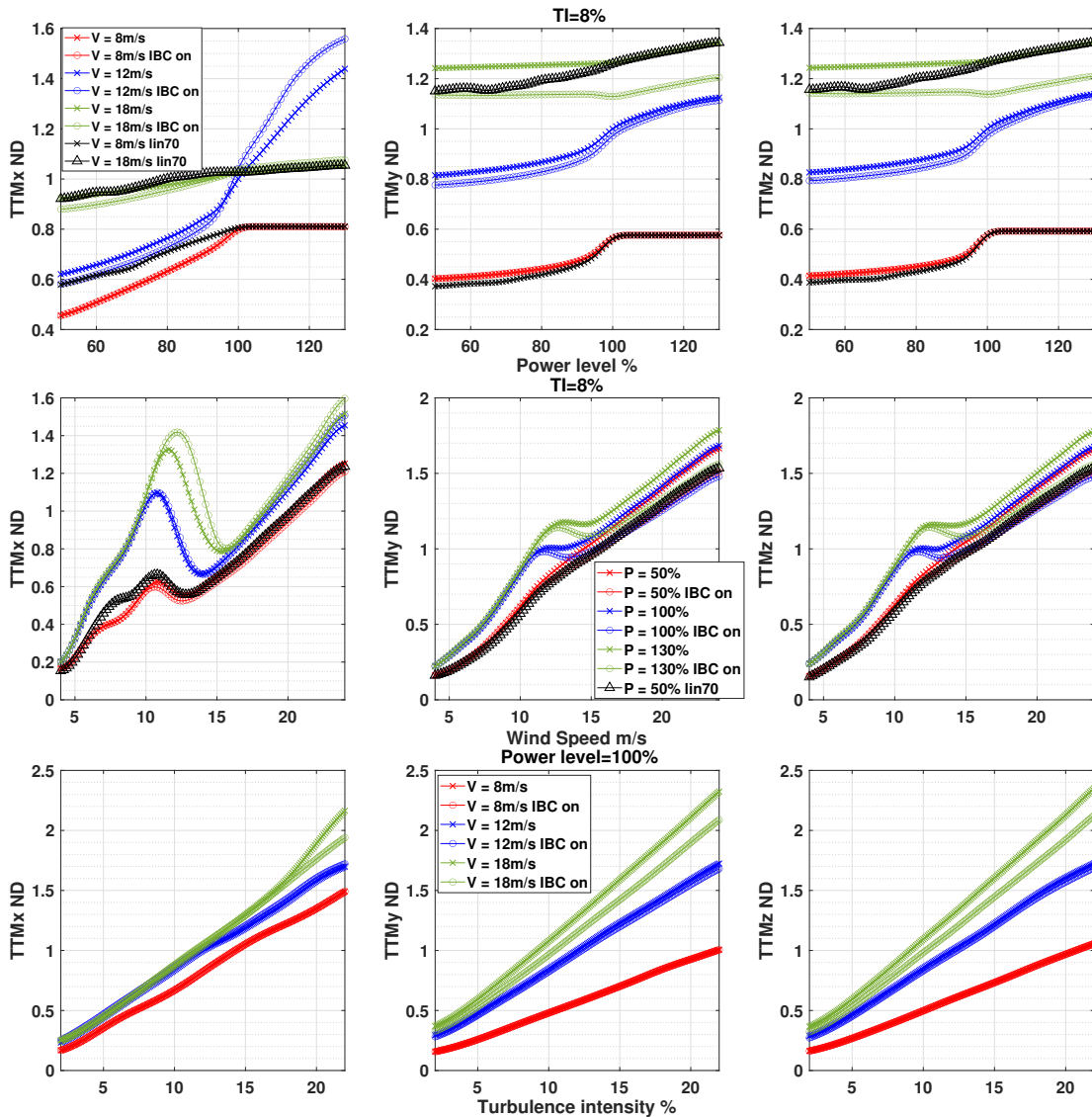


**Figure 4.11:** GPR surrogate response for the tower top/nacelle loads. For the power level and wind speed sensitivity plots, values are normalized with the power level of 100% at 12 m/s without IBC. For the sensitivity to TI, values are normalized with the output for 12% TI at 100% power level without IBC

~30%. The application of IBC does not influence TTMx loads significantly. When applied with power-boosting, IBC slightly increases the loads proportionally to the boosting level, while in power levels below 80% it slightly decreases the loads. In all cases, the maximum load difference is less than 5%. All tower top loads exhibit similar trends regarding sensitivity to TI, increasing linearly with TI. The loads are about 10 times higher for above-rated conditions and 5 times higher for rated and below-rated conditions between the minimum and maximum TI levels considered.

The tower top roll and pitch moment loads, TTM<sub>y</sub> and TTM<sub>z</sub>, have a very similar response to the input variables and are discussed together. The load distribution over wind speeds follows the same trends with the tower bottom torsion TBM<sub>z</sub>. The DEL magnitude is proportional

to the wind speed for the whole wind speed range with a small peak in the transition region. Power boosting increases these loads the most in the transition region up to  $\sim 20\%$  for the maximum power level. In higher wind speeds, the maximum increase for any power level is lower than  $8\%$ . These increases are linearly correlated with the power level. Down-regulation in the full-load region using the constTSR trajectory has no effect on these loads. Conversely, employing the lin70 trajectory shows a reduction of up to  $10\%$  depending on the power level. In the transition and partial load regions, down-regulation can reduce the loads up to  $30\%$  and  $35\%$  considering the constTSR and lin70 trajectories, respectively. Most of the load reduction is achieved until a power level of  $90\%$ . For lower levels, the load reduction rate is significantly smaller. The IBC controller is able to reduce TTM<sub>y</sub> and TTM<sub>z</sub> loads up to  $10\text{-}15\%$  for all power levels.

The sensitivity of blade root loads to the input variables is shown in figure 4.12. The edgewise bending moment load BRM<sub>x</sub>, which is mainly influenced by gravity and rotational speed, displays a small sensitivity ( $<10\%$  in total) to all the input variables. The DEL magnitude is higher in the transition region, and it is reducing in the partial and full load regions. Power boosting has a small effect on increasing the BRM<sub>x</sub> loads up to  $2\%$  for the maximum power level. Similarly, down-regulation with the constTSR trajectory shows a small load reduction ( $<2\%$ ) for all regions and power levels. Applying the lin70 trajectory reduces BRM<sub>x</sub> loads more in all operating regions, up to  $4\%$ , due to the reduced rotational speed. The IBC controller has practically no effect on the BRM<sub>x</sub> loads, showing a reduction of up to  $1\%$  for all cases. TI does not significantly influence BRM<sub>x</sub>, with differences of less than  $8\%$  between all TI levels considered. Overall, BRM<sub>x</sub> is the least sensitive load to the input variables, and it is not expected to significantly influence the optimization.

The magnitude of the blade root flapwise bending moment load, BRM<sub>y</sub>, is correlated with wind speed. The highest DELs are observed at the highest wind speeds. Moreover, a significant peak exists in the transition region around the rated wind speed. Power boosting has the greatest impact on increasing the loads in the transition region, with the maximum increase reaching  $20\%$  for the maximum power level. In higher wind speeds, the maximum load increase with power boosting is  $8\%$ . In both regions, BRM<sub>y</sub> load increase is linearly correlated with the power level increase. In the full-load region, down-regulation using the constTSR trajectory does not significantly reduce the loads ( $<3\%$ ). In contrast, the lin70 trajectory shows a load reduction of up to  $10\%$ , with the reduction being directly proportional to the power level. The highest load reductions with down-regulation are observed in the transition region. The lin70 trajectory reaches a maximum reduction of about  $30\%$  and the constTSR  $25\%$ . In the partial load region, both trajectories show similar load reductions up to  $20\%$  for the minimum power level. For both trajectories, most of the load reduction is already achieved at the  $90\%$  power level in rated and below-rated regions. Further reduction in power level has a small effect on

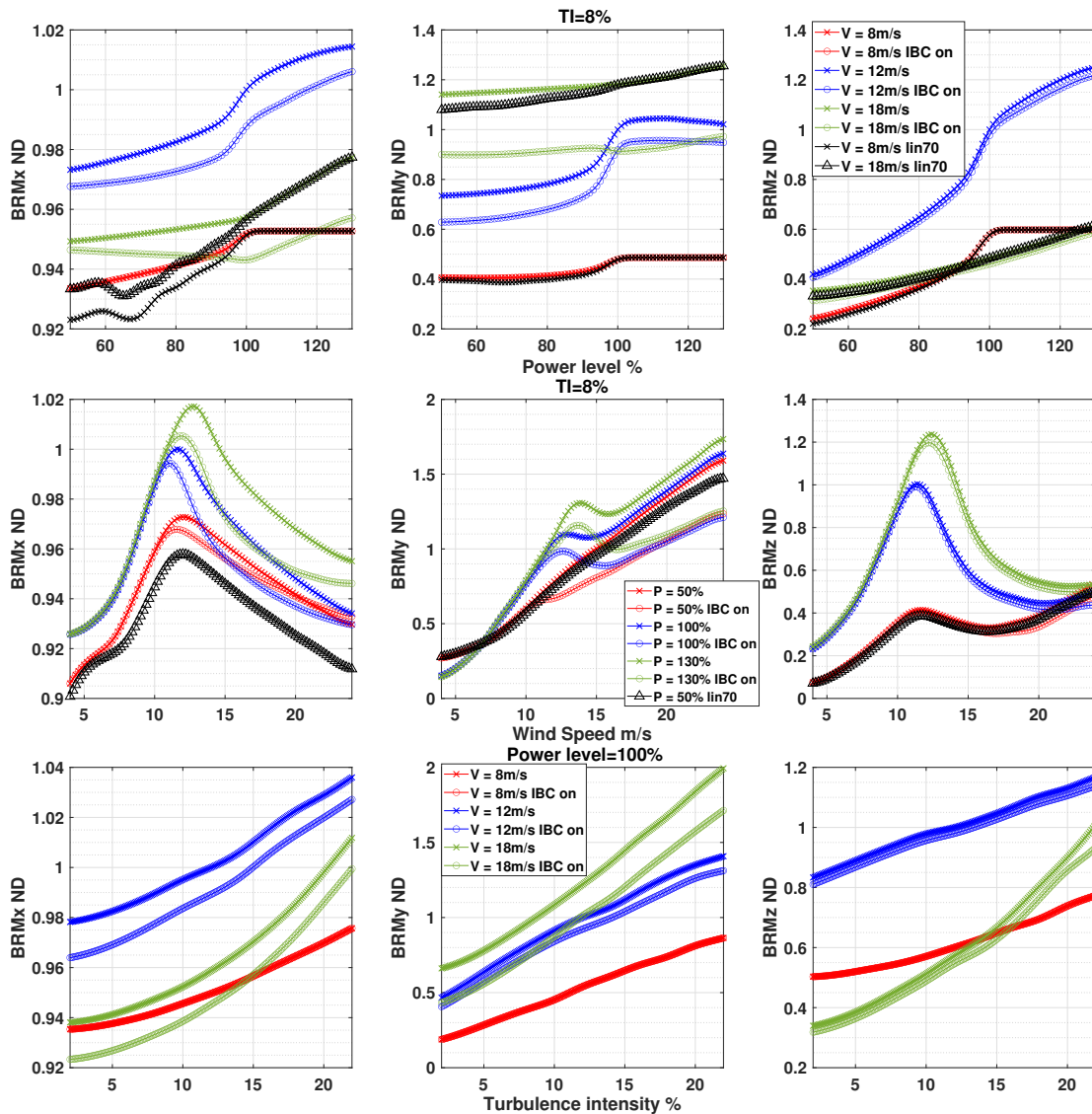


**Figure 4.12:** GPR surrogate response for the blade root loads. For the power level and wind speed sensitivity plots, values are normalized with the power level of 100% at 12 m/s without IBC. For the sensitivity to TI values are normalized with the output for 12% TI at 100% power level without IBC

load reduction.

It is worth noting that for very low wind speeds  $< 6.5$  m/s and low power levels ( $< 65\%$ ), considering both down-regulation trajectories, BRMy DELs are increased compared to the baseline level. This effect was also observed for the TBMx load but for wind speeds below 5 m/s. This shows the limits of down-regulation in terms of power levels for very low wind speeds in control region 1.5, as explained in section 3.2. As expected, the IBC controller is highly effective in reducing BRMy loads since it is the controller’s target load. In the higher wind speed regime, IBC can reduce the loads to a level of 20-25% for all power levels, while in the transition region, the load reduction is in the order of 10-15%. TBMx DELs show a linear correlation to TI, with the maximum difference between the bounds of the considered

TI range being in the order of approximately three times higher. Furthermore, in contrast to other loads discussed, the results show that the effectiveness of IBC in BRMy load reductions does not increase with TI.

The blade torsion load, BRMz, is higher in the transition region and decreases in the partial and full load. This trend changes with decreasing power levels. For lower power levels, the region with the highest DELs is shifted towards the highest wind speeds. The BRMz load is sensitive to power boosting, exhibiting an almost linear dependency on power level. For the highest power level considered, the load increase at the transition region is found in the order of 25% and at the full load region in the order of 20%. Down-regulation effectively reduced loads in all operating regions, with the two trajectories showing no significant differences. In the full-load region, the load reduction with down-regulation reaches 30% for the lowest power level, with the reduction being proportional to the down-regulation level. In the partial load and transition regions, the maximum load reduction reaches 60%, with half of it reached at the 90% power level, after which the load reduction-to-power level ratio reduces. The IBC controller has a negligible effect on BRMz loads. TI has a greater impact on BRMz loads in the full load region. A linear correlation between DEL increase and TI is observed, with the load being three times higher between the minimum and maximum TI levels considered.

The low-speed shaft loads response is shown in figure 4.13. The low-speed shaft torque load, LSSTq, shows similar trends with the TTMx load in terms of the distribution of loads over wind speeds for the nominal power level. The highest loads are found in the transition region and in the highest wind speed region. The significant peak in the transition region increases further with power boosting and decreases substantially with down-regulation. Power boosting increases the LSSTq load only in the transition region, where the magnitude of the increase displays a linear correlation to the power level. The maximum increase in the peak load in the transition region is  $\sim 20\%$ , and increases up to 40% are observed for different wind speeds in this region. This increase is the highest increased observed across all loads considered.

Down-regulation can reduce the LSSTq load in all operational regions. In the partial load, the reduction is linearly correlated to the power level, with a maximum reduction of 45% observed for the constTSR trajectory and 30% for the lin70 trajectory at the lowest power level. The highest load reduction is observed in the transition region, with both trajectories behaving similarly, exhibiting a maximum load reduction of about 55%. The rate of reduction is higher for higher power levels, with 25% load reduction reached already at the 90% power level. In above-rated conditions, load reduction is linearly proportional to power level with a maximum reduction of up to 25% for the constTSR trajectory and 20% for the lin70. Applying IBC has adverse effects on the LSSTq load, leading to increased DELs, especially when combined with power boosting. The maximum increase is found in the transition region, with a proportional correlation to the power level and a maximum value of around 20%. At higher wind speeds,

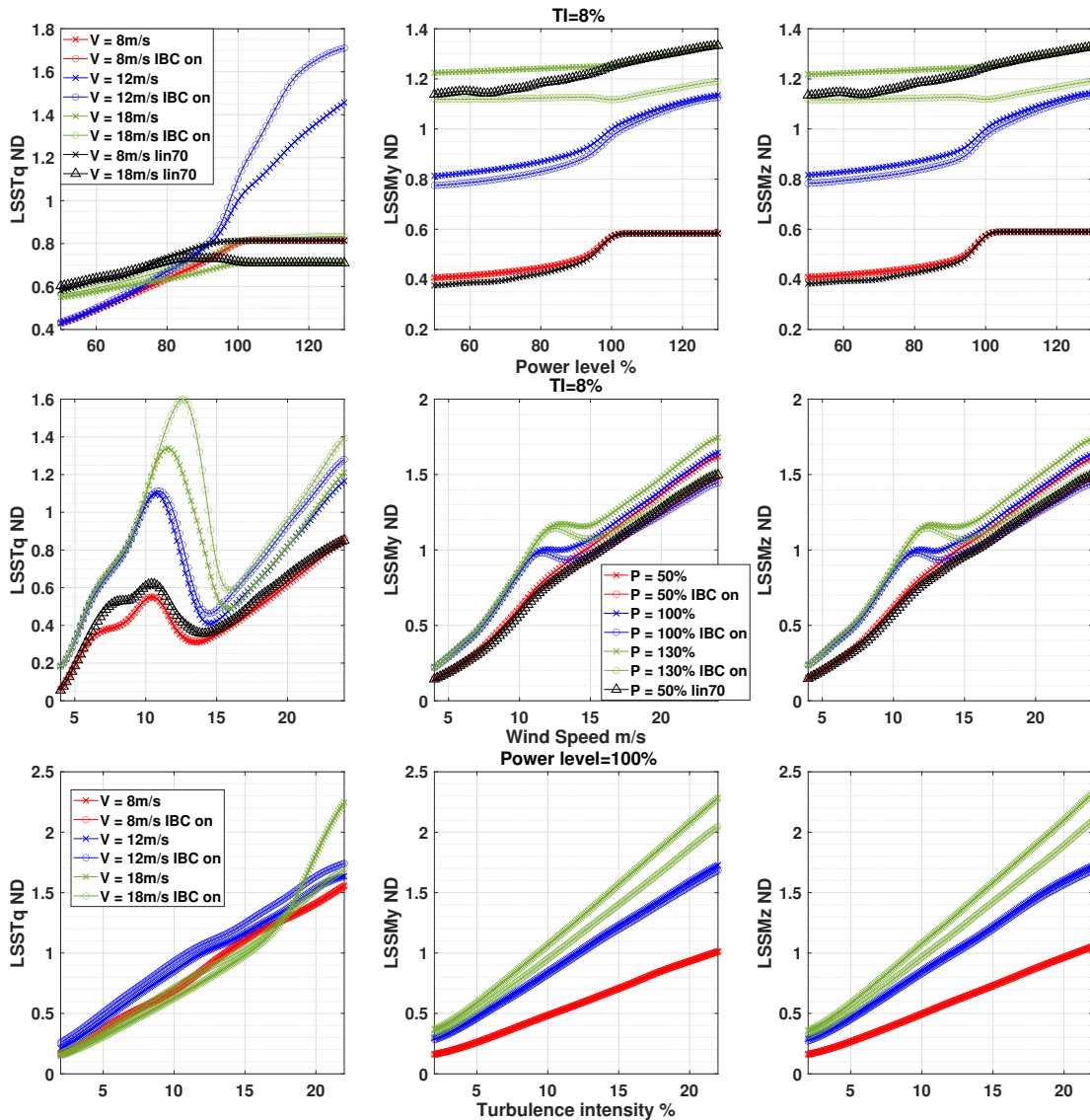


**Figure 4.13:** GPR surrogate response for the low-speed shaft loads. For the power level and wind speed sensitivity plots, values are normalized with the power level of 100% at 12 m/s without IBC. For the sensitivity to TI values are normalized with the output for 12% TI at 100% power level without IBC

the load increase due to IBC is smaller, up to 15%, and proportional to the power level. The LSSTq load is linearly correlated to TI with the load increasing approximately seven times within the considered TI range.

The low-speed shaft moment loads around the y and z axes, LSSMy and LSSMz, demonstrate very similar trends and, therefore, are discussed together. These loads show a similar pattern to the TTM<sub>y</sub> and TTM<sub>z</sub> loads. The simplified drive train modeling in FAST assumes a rigid shaft, while the bearings are not modeled. Hence, loads are transferred directly from the shaft to the tower top node, with the difference being the small offset between the tower top and the shaft without any damping component in between. Power boosting increases the LSSMy

and LSSMz loads, primarily in the transition region. Down-regulation is effective in reducing these loads, particularly in the transition and below-rated regions. The lin70 trajectory is more effective compared to the constTSR in load reduction. The IBC controller effectively reduces these loads at higher wind speeds by 15-20% across all power levels.

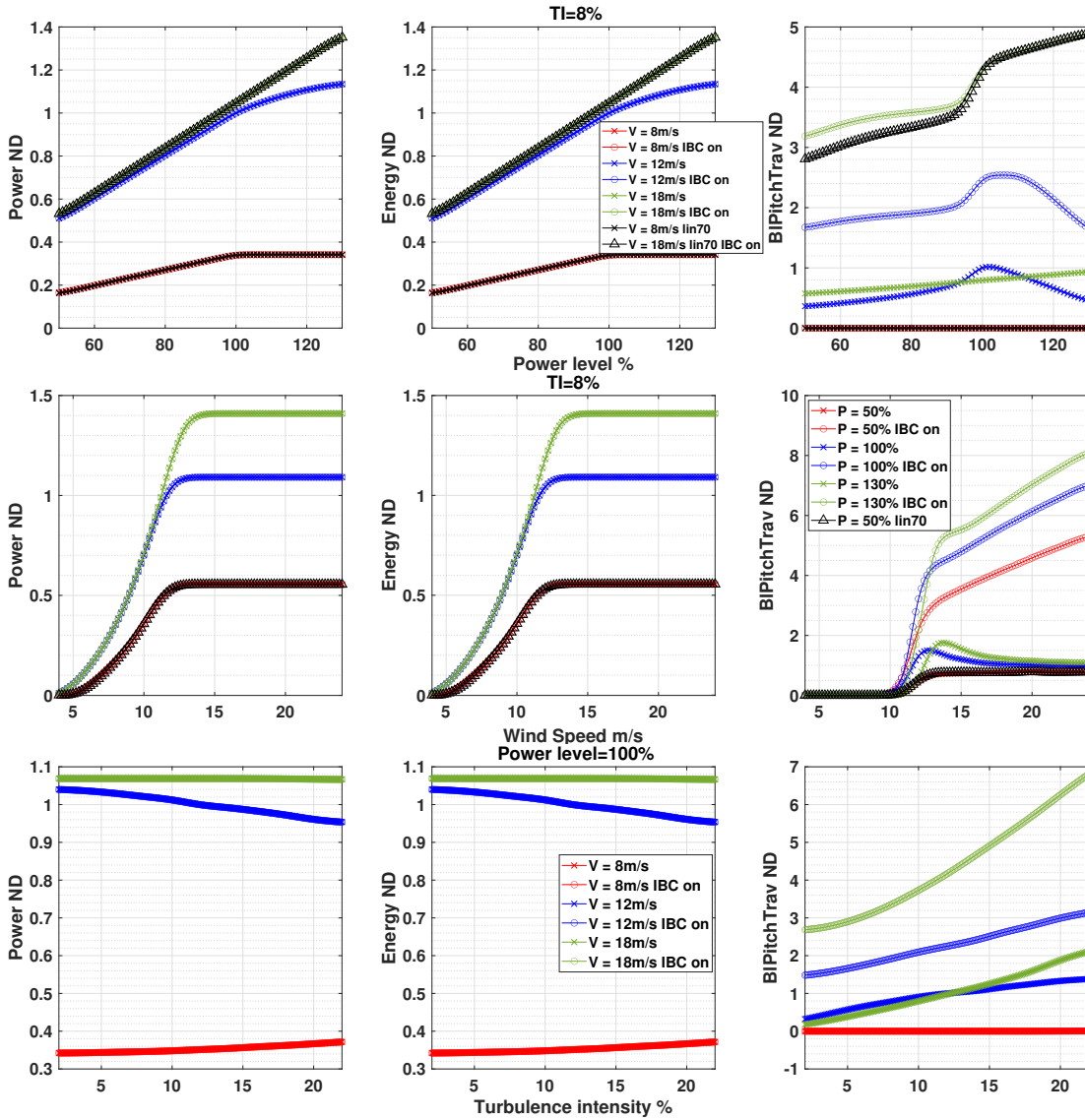


**Figure 4.14:** GPR surrogate response for electric power, energy, and blade pitch travel. For the power level and wind speed sensitivity plots, values are normalized with the power level of 100% at 12 m/s without IBC. For the sensitivity to TI values are normalized with the output for 12% TI at 100% power level without IBC

Figure 4.14 shows the surrogate response for mean power, energy production, and blade pitch travel over the input variable space. Power and energy are fully correlated, exhibiting the same response as the simulations have a duration of one hour, and kWh units are used for energy. The response of power and energy over wind speeds and power levels verifies that the controller modes perform as intended in dynamic simulations. Both down-regulation trajectories and the power-boosting mode are able to track the power reference as intended. Furthermore, it is

verified that IBC is not affecting power production. Additionally, the minimum mean wind speed required for the turbine to generate energy is observed to shift with the power level. For the minimum down-regulation level, this value is approximately 5 m/s. Power is sensitive to TI with a linear correlation. Increasing TI decreases the mean power produced in the partial load with a  $\sim 10\%$  difference between the lowest and highest TI values considered. In the transition region, increasing TI has the opposite effect, reducing power production. The reduction is linearly correlated to TI, with a maximum reduction of  $\sim 10\%$  for the highest TI level.

The blade pitch travel is a simplified metric to account for pitch actuator usage. The aim of the metric is to quantify the effect of the IBC loop and different power levels on the actuator usage over different wind conditions. Pitch travel is correlated to the power level in a linear manner. For the maximum power level, the increase is in the order of 20% for all wind speeds. For the minimum power level and for both down-regulation trajectories, the decrease in the full load reaches  $\sim 25\%$ . In the transition region, the difference is higher, in the order of  $\sim 50\%$ , as reducing the power levels smoothens out the turbine response in control region 2.5. The application of IBC leads to a substantial increase in blade pitch travel. The magnitude of this increase is directly proportional to wind speed for each power level. For the 100% power level, the increase varies linearly with wind speeds between 500% and 700%. Changing the power level has a smaller effect on the pitch travel increase due to IBC. For the minimum power level, the maximum increase by activating the IBC loop is found in the order of  $\sim 660\%$ , while for the maximum power level  $\sim 740\%$ . As also observed in many loads, the rate of decrease is higher until a down-regulation level of 90%. The increase in pitch travel due to the IBC application does not exhibit a correlation with TI. The high increases observed in blade pitch travel explain the choice to constrain IBC to the 1P frequency, even though including higher harmonics could result in slightly higher load reduction, as discussed in section 3.4.

### 4.3.1 Discussion on tradeoffs and optimization potential

The sensitivity of all quantities with respect to input conditions and control mode are discussed individually in the previous section. The present section provides a qualitative summary of these findings, along with a discussion of their implications in the context of potential tradeoffs that can be leveraged in the longer-term optimization process.

The metric of blade pitch travel cannot be practically used to establish a definitive maximum acceptable limit. The assessment of reliability and estimation of the remaining useful lifetime of the pitch system and its subcomponents require a complex analysis that relies on detailed knowledge of the specific design and components, including motor type and bearing design. Since such information is unavailable within the scope of the present thesis, the optimization objective would be to minimize the increase in blade pitch travel, which serves as an indicator

of the pitch system's state, by minimizing the application of IBC as much as possible.

The objective of the optimization is to enhance the wind turbine's operation by increasing revenue and either decreasing or maintaining the fatigue damage level compared to the baseline operation, which corresponds to 100% power level and no individual blade control (IBC). To accomplish this, power boosting mode is employed as a means to increase power, while down-regulation and/or activation of the IBC loop are utilized to reduce loads. Therefore, it is crucial to understand which loads are sensitive to these control modes and in which operating regions.

Table 4.4 summarizes qualitatively these effects. Down-regulation is more effective in reducing loads in the partial load and transition regions. On the other hand, it is less effective in the full load region, especially when considering the constTSR trajectory. This shows that IBC and down-regulation complement each other as load reduction methods, and their combination fits the purpose.

**Table 4.4:** Qualitative summary of DELs' sensitivity to the controller modes and wind conditions. PB: power boosting, DRb: down-regulation in the partial load, DRt: down-regulation in the transition region, DRa: down-regulation in the full load region, IBC: individual blade control loop activated. o: no significant change, + and ++: moderate and higher increase, - and -- moderate and higher reduction. TSR: constTSR down-regulation trajectory, lin: lin70 trajectory

Load	DRb TSR	DRb lin	DRt TSR	DRt lin	DRa TSR	DRa lin	PB	IBC
TBMx	-	+	-	+	o	+	o	-
TBMy	--	-	--	-	-	-	+	o
TBMz	--	--	--	--	o	-	+	-
TTMx	--	-	--	-	-	o	++	+
TTMy	--	--	--	--	o	-	+	-
TTMz	--	--	--	--	o	-	+	-
BRMx	o	-	o	-	o	o	o	o
BRMy	--	--	--	--	o	o	+	--
BRMz	--	--	--	--	-	-	++	o
BR0op	--	--	--	--	o	-	+	--
BR1p	o	-	o	-	o	o	o	o
LSSTq	--	o	--	--	-	-	++	++
LSSMy	--	--	--	--	o	-	+	-
LSSMz	--	--	--	--	o	-	+	-

The TBMx, BRMx, and BR1p loads exhibit the least sensitivity across all control modes, indicating that they are unlikely to significantly impact the optimization process. Moreover, TBMy, TTMx, BRMz, and LSSTq loads are found to be influenced the most by power boosting.

Activating the IBC loop has either no effect (TBM<sub>y</sub> and BRM<sub>z</sub>) or increases the load in the same region where power boosting has the greatest impact (TTM<sub>x</sub>, LSST<sub>q</sub>). In such cases, the only viable approach to counterbalance load increases caused by power boosting is through down-regulation, and it is suggested that performing this down-regulation in the transition region would be more efficient based on load trends. Additionally, the findings suggest that activating IBC at higher wind speeds than the transition region would be advantageous, as it prevents the negatively affected loads from increasing. Moreover, for the positively influenced loads, IBC proves to be equally effective across the entire applicable wind speed range. For the majority of loads, the IBC effectiveness increases with increasing TI.

A significant portion of the expected load reduction achieved through down-regulation is associated with a small decrease in power level. This can be attributed to the steep  $C_p$  peak in the  $\lambda - \theta$  space, as discussed in chapter 3. The analysis conducted previously revealed that, for the DTU 10 MW rwt aerodynamic design, over 50% of the maximum load reduction can be accomplished with a down-regulation level of 90%. Conversely, at lower down-regulation levels, the rate of load reduction per power level diminishes significantly. This indicates that the tradeoff between power and loads is more favorable in this particular region. Further reductions in power yield diminishing effects, as a small load reduction is accompanied by greater losses in power production (and subsequently revenue). This effect was primarily observed when down-regulating in the transition and below-rated regions for the TBM<sub>x</sub>, TBM<sub>y</sub>, TBM<sub>z</sub>, TTM<sub>y</sub>, TTM<sub>z</sub>, BRM<sub>y</sub>, BRM<sub>z</sub>, LSSM<sub>y</sub>, and LSSM<sub>z</sub> loads.

The transition region, between partial and full load, is a highly sensitive region in terms of loads, regardless of the controller design. In most cases, implementing down-regulation within this region has a smoothening effect on the transition, resulting in load reduction. This observation is further supported by measurement data, as shown in [86]. Leveraging this insight in the optimization process suggests that a small decrease in power level within the transition region can yield overall positive effects on loads, with a relatively minor energy loss.

Another factor that can be utilized in the optimization process is grouping loads that exhibit similar responses to the control modes. Defining a load ensemble for the load evaluation function is essential for optimization. Loads that demonstrate similar behavior can be grouped together, or one load from the group can be selected as a representative. This approach reduces the number of optimization variables and enhances the efficiency of the process. The analysis conducted in the previous section revealed that TBM<sub>z</sub>, TTM<sub>y</sub>, TTM<sub>z</sub>, LSSM<sub>y</sub>, and LSSM<sub>z</sub> exhibit very similar responses and can be effectively used for this purpose. LSST<sub>q</sub> and TTM<sub>x</sub> also display similar responses, particularly in the transition and partial load regions, although the correlation is weaker compared to the previous group.

Comparing the two trajectories considered for down-regulation set-point derivation, it was observed that the trajectory choice impacts the loads. By maintaining constant rotational

speed and performing down-regulation using the generator torque, the constTSR trajectory exhibited higher load reduction per power level for the TBMX, TBMy, TTMx, and LSSTq loads. On the other hand, combining both torque and rotational speed in the lin70 trajectory resulted in higher load reduction for TBMz, BRMy, TTMy, TTMz, LSSMY, and LSSMz loads. This effect was particularly prominent in the full load region, suggesting that further rotational speed reduction may be beneficial for load reduction in that region.

Especially for trajectories involving rotational speed reduction, it was found that there is a limit to the minimum assignable power level due to the impact of reduced rotational speed on region 1.5, cut-in wind speed, and loads. In this region, the turbine operates off-design and can exhibit unpredictable behavior, particularly at lower power levels where accurate power tracking becomes challenging and load dependence on power level diminishes. Moreover, reducing rotational speed alters the effective cut-in wind speed, and this effect becomes more prominent for lower power levels in trajectories relying on rotational speed reduction. A different controller design approach, employing a PI feedback loop in region 1.5, could be advantageous as it eliminates the ramp and ensures turbine operation at a constant speed within this region. This information holds greater significance when considering down-regulation for optimal power tracking, such as in scenarios where significant curtailment is required by the grid operator. However, in cases where load reduction is the objective, as in this study, or in wind farm control scenarios targeting thrust reduction, such low levels of down-regulation may not yield meaningful outcomes. Furthermore, considering the stiff-stiff tower design combined with low structural damping, it is crucial to prevent the excitation of tower frequencies. Resonances, particularly in the low-damped tower side-side loads, can occur with a lower TSR.

It is important to mention that the quantities discussed in the previous sections refer to DELs. As explained in Section 2.2, DELs are converted to damage values to facilitate linear summation and track the progression of damage over time. It is important to consider the impact of the Wöhler exponent in this conversion process, as it is dependent on its value. Consequently, loads associated with a higher exponent will exhibit larger changes in damage with smaller changes in DELs. As a result, the sensitivity of these loads is expected to amplify and influence the optimization process accordingly.

## 4.4 Summary

The derivation of a surrogate model for the turbine response used as a basis for the evaluation/optimization framework was discussed in this chapter. The chosen input variable space, fitting the purpose, is limited to three, including mean wind speed, TI, and controller mode (power level and IBC activation). The low dimensionality allowed for a dense factorial sampling to be used as a DOE approach. Two regression methods were applied and compared. A

spline-based interpolation and a Gaussian Process Regression model. The results in terms of uncertainty were found to be very similar between the two methods, which can be attributed to the dense sampling. The benefit of using spline-based interpolation is that it is much faster to apply for the same level of uncertainty in predictions compared to the high computational cost of GPR. The GPR approach has the benefit that it can provide direct uncertainty estimates of the prediction that can be potentially used for further uncertainty propagation studies into the overall optimization process.

The overall uncertainty was found to be low, with a mean error below 1% for most cases and a mean absolute error below 3%. The quantities with the highest uncertainty were found to be the tower bottom side-side load, the low-speed shaft torque load, and the blade pitch travel. The error per input condition was analyzed with the results showing that the very low wind speed region  $<6$  m/s and the higher TI present the highest uncertainty in most cases. The mean error close to 0 and the low absolute error, as well as the comparison with a validation set, showed that the surrogate model fits the purpose and can be used for the optimization without introducing bias.

Using the surrogate model, an analysis of all quantities of interest with respect to the inputs was performed, identifying trends and tradeoffs. Down-regulation and IBC complement each other as load reduction methods as they target different loads in different regimes, allowing for a load-power balancing optimization. The two controller trajectories considered for the down-regulation were compared, showing how choosing different set points changes the response of the loads. This suggests that depending on the considered objectives and the focus on specific loads, different trajectories might be optimal. Finally, the response was discussed in terms of tradeoffs between loads and power that can be leveraged for optimization.



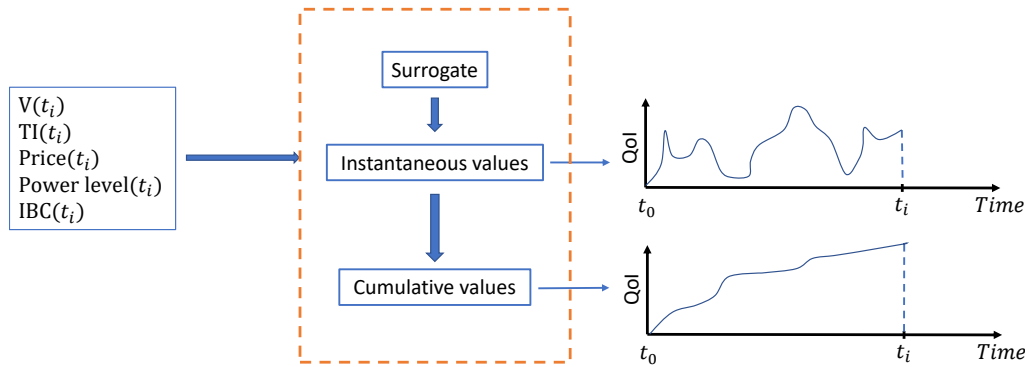
## Chapter 5

# Evaluation-optimization framework

This chapter introduces the computational framework for the accumulation of values over time and optimization. The framework utilizes as inputs the surrogate models, wind conditions, and controller mode to evaluate the response of the wind turbine and accumulate metrics over time, effectively creating a data-driven digital twin. The methods and metrics employed in this process are discussed, followed by a detailed discussion on the formulation of the optimization problem and the optimization methods. This includes the formulation of the objective function and the utilization of relevant optimization techniques. Furthermore, the chapter addresses the assumptions and limitations associated with the overall optimization process and considers potential alternative applications of the framework beyond its current scope.

### 5.1 Accumulation and evaluation framework

In order to keep track of the accumulation of quantities of interest over time and also to evaluate the effects of different operational approaches, a computational framework based on the surrogate model is created. The time step is considered to be one hour since the day ahead price signals by the electricity markets are given in these intervals and the surrogate is created with this application in mind. The inputs at each time step are the mean hub-height wind speed, TI, electricity price, and control mode in terms of power level and IBC activation. The surrogate is used to predict the turbine response based on the wind conditions and chosen controller mode, providing the instantaneous (hourly intervals) values of all the quantities of interest. The instantaneous values are accumulated at each time step, keeping track of the cumulative values over time. The overview of this process is illustrated in figure 5.1.



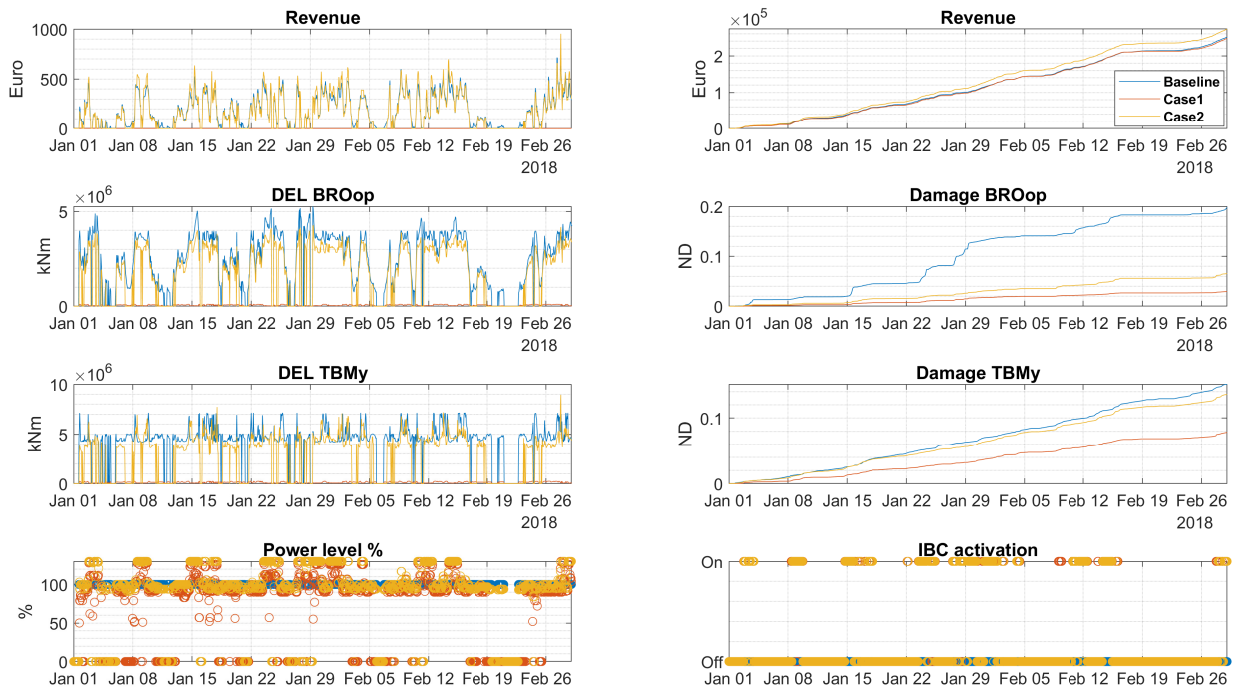
**Figure 5.1:** Overview of the accumulation process

Table 5.1 shows the instantaneous and cumulative quantities considered. The accumulation of the values besides fatigue loading is straightforward, with linear addition of the values over time. For the loads, the instantaneous 1Hz DELs, calculated based on equation 2.7, are obtained by the surrogate and converted to damage using equation 2.8. The instantaneous damage values are added linearly to account for the accumulated damage per load at each point in time. As explained in chapter 2, damage can only be considered as a relative measure for comparison when the exact component design and materials are unknown. Hence, in the scope of this work, the critical damage ( $D=1$ ) for each load is considered to be the damage accumulated by operating the turbine in the baseline control mode, i.e., 100% power level without IBC, for the total period considered. This is a conservative assumption, as some extra fatigue margins possibly exist due to a mismatch between the actual site conditions and the turbine class used for the type certification. Moreover, it is possible that not all component design is fatigue-driven but also driven by other factors such as extreme loads, buckling, etc., leading to further design fatigue margins. In an actual application of the framework, the fatigue state limits could be either provided by the manufacturer or roughly reverse-engineered based on the procedure described in the relevant standards.

**Table 5.1:** Instantaneous and cumulative quantities included in the output of the evaluation framework

Instantaneous values	Cumulative values
DEL	Damage
Energy	Energy
Revenue	Revenue
Pitch travel	Pitch travel
Power level	IBC activation %
IBC status	Shut down %

To utilize the framework for evaluation and optimization, a reference case is necessary as a basis for comparisons. For the scope of the thesis, historical data sets are used for the evaluation. Thus, it is possible to fully simulate the baseline operation for the whole period considered, which in turn defines the limit for the long-term accumulated values for all metrics considered. This way, the effect of any optimized operational strategy can be evaluated at any given point in time. An example output of the framework to evaluate different strategies is shown in figure 5.2.



**Figure 5.2:** Example output of the framework applied to evaluate different operational strategies

However, in real-time applications, this would not be possible. In this case, the total damage budget of each component would be defined, as explained previously. Then, at each point in time, the effect of any applied operational strategy can be compared up to this instance with the simulation of the baseline case to evaluate the effects of the strategy, while the long-term accumulation of damage can be compared to the design loads. Similarly, for optimization purposes using forecasts, the optimization can be performed by targeting a specific revenue and damage objective for the forecast period in comparison with a hypothetical baseline operation. Additionally, at this stage, the uncertainty of the surrogate could be considered. Using the probabilistic output of the surrogate at each time step, the accumulation could be accounted for as a probability distribution instead of the deterministic approach considered in this work.

The proposed framework is used in this work as a platform to apply and test the long-term optimization approaches. Apart from this use case, further applications can be envisioned. It can be directly used as a real-time data-driven digital twin for O&M purposes. The crucial

aspect of such an application would be the quality of the aeroelastic model and the accuracy of measuring the input wind conditions. If the aeroelastic model and the fatigue limits are not provided by the manufacturer, a rough approximation could be obtained by tuning a reference wind turbine model, like the DTU 10 MW rwt used here. Additionally, any available measurements, especially for loads, could be used to augment the model-based surrogate and improve its accuracy over time. The wind speed and TI can be retrieved in various ways and different levels of accuracy, such as the onboard nacelle anemometers, the SCADA data using estimators based on the system's observability, additional lidar devices within a wind farm combined with a farm flow model, etc. Finally, the framework can be extended by increasing the dimensions of the surrogate to account for operational conditions such as yaw misalignment and changes in the turbine's behavior over time, such as changes in the aerodynamic performance due to the deterioration of the blade's surface.

## 5.2 Optimization problem formulation

In broad terms, mathematical optimization is the process of selecting the best input values from within an allowed feasible space to maximize or minimize an objective function. The input variables are called decision variables and can be either continuous or discrete. The decision variables can be bounded in a feasible space defined by constraints. When the objective function's output is a scalar, the process is called single-objective optimization and when it is a vector, it is called multi-objective optimization. In the case of multi-objective optimization, optimal decisions need to be taken in the presence of trade-offs between two or more conflicting objectives as, for a nontrivial multi-objective problem, no single solution exists that optimizes all objectives simultaneously.

In this work, the aim is to optimize the operation of the wind turbine over time by selecting the most appropriate controller mode to minimize accumulated fatigue damage and/or maximize accumulated revenue, compared to the baseline case, at the end of a specified time period. The optimization process considers two key factors that vary during this finite period: wind speed and electricity prices. The objective function is designed to assess the impact of different control modes on the turbine's performance over time. To achieve this, two discrete cases of optimization are explored in this study:

- **Optimize based on wind speeds only considering the site-specific long-term wind speed distribution.** The prices are not considered in this approach. The goal of the optimization is to assign the decision variables for each wind speed bin considered.
- **Optimize based on a forecast of wind speed and prices.** The goal of the optimization is to assign the decision variables for each wind speed - electricity price pair at each timestep or wind speed - electricity price bin for the forecasting period.

The first case assumes a constant price for the whole period and considers only the statistical distribution of wind speeds, characterized by the Weibull distribution. The Weibull distribution is site-specific and derived from the entire historical dataset available for each site considered. The goal of the optimization is to assign control modes for each wind speed, such as the total revenue and fatigue damage accumulation reach the requested objectives. Within this approach, the optimization is done offline once per site and can be repeated in cases where the local wind speed distribution changes over time, such as cases where new wind farms are built in the vicinity of the site (as shown in [117]).

In the second case, the optimization is done independently for the different forecast horizons. It is assumed that hourly wind speeds and prices can both be previewed perfectly within this horizon. The optimization goal is to determine the optimal controller mode for each time step, meaning each speed-price pair, or for each speed-price bin if the values are grouped, thereby optimizing revenue and damage accumulation for the given forecast horizon. The optimization process is repeated as time progresses for the consecutive forecasting horizons. Both optimization approaches can be applied to both fluctuating and constant price scenarios.

For both cases, the decision variables are the power level (or shut down) and IBC activation that should be assigned to the turbine at each point in time. The power level is a continuous variable that is bounded, due to the controller design constraints, to 50-130% for wind speeds above 11 m/s and to 50-100% for wind speeds below 11 m/s. The IBC activation and shutting down are discrete on/off variables. However, as using discrete and continuous variables together in the same optimization problem is not feasible, these two variables are mapped to continuous ones. For the IBC activation variable, the goal of the optimized solution is to reduce the IBC activation in order to reduce the pitch actuator load. To address the IBC activation, which is most effective at higher wind speeds and turbulence intensities, a minimum wind speed threshold is introduced, converting the discrete variable to a continuous one within the bounds of 11 to 24 m/s. On the other hand, the option of shutting down implies that all instantaneous quantities are reduced to 0, leading to maximum load and revenue reduction compared to the baseline. Keeping this in mind, and since the power level cannot go below 50%, the discrete shutdown variable is replaced with a continuous threshold of projected revenue below which the turbine is shut down. This way, all three decision variables are continuous with specified bounds, enabling the optimization process.

In order to formulate the optimization problem, the objective function must be defined. The objective function has a black-box structure and is multi-objective in nature. It uses as inputs the control modes suggested by the optimizer for each condition (be it wind speeds or speed-price pairs), and the accumulated damage (per load) and revenue values produced with the baseline operation. Subsequently, the cumulative values produced using the inputs requested by the optimizer are calculated internally, leveraging the evaluation framework. The

output provided by the objective function includes the relative differences between the new control strategy and the baseline cumulative values. This process is repeated for each function evaluation required by the optimizer, with the computational cost for each evaluation being dependent mainly on the surrogate prediction costs.

This work aims to optimize the loads considering all the major components of the wind turbine as defined in chapter 4. In total, 15 objectives, including loads and revenue, can be defined as outputs for the objective function. Many of these objectives are conflicting. For example, power boosting increases revenue but also increases loads, or one load is reduced significantly in a specific wind speed with down-regulation while another is not sensitive. The amount of objectives and the complexity of their correlations make it infeasible to perform multi-objective optimization and apply methods such as Pareto optimality to choose between the solutions. Hence, it was decided to transform the problem into a single objective problem using the Weighted Sum method [118]. The method involves scalarizing the set of objectives into a single objective by multiplying each individual objective with a user-defined weight and summing the weighted objectives. One of the main advantages of this method is its ease of use, enabling finding diverse solutions close to or on the Pareto-optimal front. The disadvantages include not being able to find all solutions in a non-convex solution space and not having a straightforward way of assigning weights to objectives.

Based on the nature of the problem, it makes sense to separate the objectives initially into two: relative accumulated fatigue damage and relative accumulated revenue. The second one is straightforward, as it is a scalar value by default. In order to transform the entire load ensemble into a scalar value, the newly calculated accumulated damage relative to the baseline accumulated damage per load is added linearly with weights using equation 5.1. Note that the value is expressed as a relative difference in percentage and the sum of all weights is equal to one. This approach allows assigning weights to loads according to criteria such as their sensitivity to the controller modes or excluding some of the loads due to low sensitivity or due to similarity with other loads allowing versatility in the exploration of the potentially optimal combinations for the overall optimization.

$$\Delta D_{tot} = \sum_{i=1}^N w_{D,i} \left[ 100 \left( \frac{D_{i,new}}{D_{i,base}} - 1 \right) \right] = \sum_{i=1}^N w_{D,i} \Delta D_i \quad (5.1)$$

where  $N$  is the amount of loads considered.

Furthermore, to merge the accumulated revenue and damage objectives, they are linearly added with respective weights to form the final single objective output of the function as shown in equation 5.2. Both variables are represented as relative differences in percentage to allow for equal scaling and to capture each quantity's relative increase or decrease. Since the two objectives are in conflict – seeking a decrease in accumulated damage while aiming

for an increase in accumulated revenue – the negative value of relative revenue is employed, formulating a minimization problem. This enables the optimization process to appropriately balance the trade-offs between the two objectives.

$$f(x) = w_{dam}\Delta D_{tot} - w_{rev} \left[ 100 \left( \frac{Rev_{new}}{Rev_{base}} - 1 \right) \right] = w_{dam}\Delta D_{tot} - w_{rev}\Delta Rev \quad (5.2)$$

These weights are used to steer the optimization to either objective. By applying a higher weight to one objective, the optimizer is directed toward solutions that favor this objective. The issue with this approach is that the optimizer does not have information about the other objective since it is converted to a single objective problem and will tend to favor dominated solutions that minimize one objective but increase the other. To tackle this issue, penalties are applied to the output of the objective function. When a threshold is exceeded for any of the individual objectives, then an additional penalty is added to the objective. The penalty formulation can be expressed as shown in equation 5.3. The alternative route to tackle this issue would be to include the evaluation of the other objective in a separate black box function and passed to the optimizer as a non-linear constraint. This approach was dismissed due to the additional computational cost introduced by probing the surrogate a second time at each function evaluation.

$$P(Q) = \sum_{i=1}^m (\max\{0, g_i(Q_i)\}) \quad (5.3)$$

where  $m$  is the total amount of objectives ( $Q_i$ ) considered including  $\Delta Rev$  and  $\Delta D_1 \dots \Delta D_N$ .  $g_i(Q)$  is a function for each objective  $Q_i$  that checks whether the threshold is exceeded:

$$g_i(Q_i) = Q_i - k_i \quad (5.4)$$

where  $k_i$  is a user-defined threshold for each objective.

Then the output of the objective function becomes:

$$F(x) = f(x) + c_{pen}P(Q) = w_{dam}\Delta D_{tot} - w_{rev}\Delta Rev + c_{pen}P(Q) \quad (5.5)$$

where  $c_{pen}$  is a user-defined gain that defines the overall magnitude of the penalty applied to the final objective.

Moreover, it was observed that the varying magnitudes of each objective's response, combined with the weighting approach used to transform the multi-objective problem into a single-objective problem, influenced the optimizer towards solutions dominated by certain objectives. For instance, the accumulated damage at the blade root exhibited high sensitivity to load reductions through IBC and down-regulation, causing the optimizer to prioritize maximizing

reductions in these loads even when assigning low weights to the blade loads. To address this challenge, an additional step was incorporated in the calculation of the initial objectives to bound each objective within specific value ranges, as shown in Equation 5.6. This step helped balance the optimization process and avoid overemphasis on particular objectives.

$$Q_i = \min\{Q_i, u_i\} \quad \text{and} \quad Q_i = \max\{Q_i, l_i\} \quad (5.6)$$

where  $u_i$  and  $l_i$  are user-defined constants defining the upper and lower bounds of the allowed range of each objective.

The determination of appropriate values for the weights between the damage and revenue objective ( $w_{dam}$  and  $w_{rev}$ ), the penalty thresholds ( $k_i$ ), the bound thresholds ( $u_i$  and  $l_i$ ) and the gain for the total penalty term ( $c_{pen}$ ) is required to effectively drive the optimizer towards different objectives. This task is complex, problem-specific, and lacks a standardized methodology in the existing literature. As a result, an iterative process of trial and error was employed to fine-tune these parameters individually for each optimization scenario. Through this iterative approach, the most suitable combination of values was identified to strike a balance between the competing objectives and ensure a satisfactory optimization outcome.

Having explained the formulation of the black-box objective function and the relevant manipulation techniques applied, the overall optimization problem can then be expressed as a continuous minimization problem with a bounded decision variable space as shown in equation 5.7.

$$\begin{aligned} & \text{minimize} && F(x) \\ & \text{subject to} && x \in X \end{aligned} \quad (5.7)$$

where  $X$  is defined by the bounds applied to the decision variables.

The objective function setup, discussed previously, is common for the two optimization cases considered. The two approaches differ in the quantities used internally by the objective function. In the first case, where the optimization is based on wind speed distribution, the probability of occurrence per wind speed bin and a constant value for the prices are considered for the calculations of the baseline values and the relative cumulative differences. The decision variables are the power level per wind speed bin, the IBC wind speed activation threshold, and the projected revenue threshold for shutdown according to the user-defined bin discretization. Their amount is equal to  $B + 2$ , where  $B$  is the total amount of wind speed bins considered. The resulting optimized values are then used by the evaluation framework to calculate the instantaneous and cumulative values of the quantities of interest over time, assigning control modes per time step according to the mean wind speed.

The long-term optimization process is based on discrete optimizations for consecutive forecasting horizons in the second case. In order to calculate the baseline values and evaluate the objective for a given horizon, the wind speed and electricity price per time step are utilized. In this case, the number of decision variables is equal to  $T_h + 2$  where  $T_h$  is the number of time steps included in the horizon. In cases where longer horizon periods are considered, the problem can become infeasible to solve as the amount of variables increases. For these cases, a preprocessing step is applied where the wind speeds and prices are binned together. The bivariate probability of occurrence per bin is then used to calculate the baseline values and the relative differences for each objective, similar to the case based on wind speed distributions. The optimized variables per bin assigned by the optimizer are then fed to the evaluation framework, which calculates the instantaneous and cumulative values of the quantities of interest over time, assigning control modes per time step based on instantaneous wind speed and price. Figure 5.3 presents an illustrative overview of all optimization approaches.

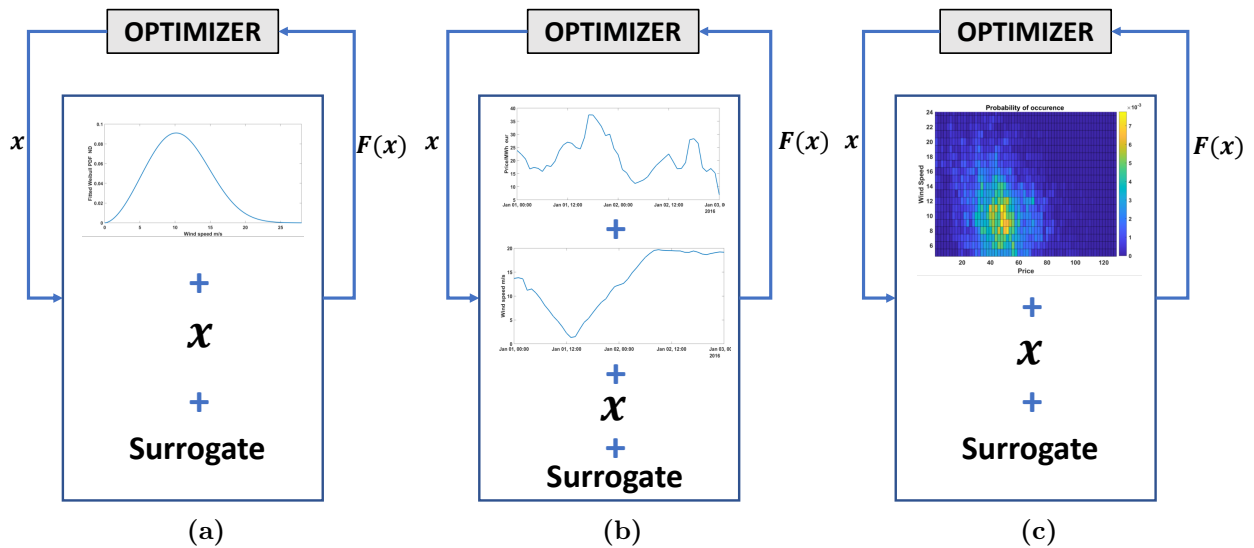


**Figure 5.3:** Schematic overview of the optimization process for all cases considered. a: Optimization based on wind speeds only using the wind speed distributions and a constant price. b: Optimization using hourly price and wind speed value pairs based on forecasted time series. c: Optimization using price and wind speed bivariate probability of occurrence based on forecasted time series.

Once the optimization problem is formulated, the appropriate optimization algorithms need to be selected. These algorithms fall into two main categories: gradient-based and gradient-free. Gradient-based algorithms rely on mathematical principles and utilize the derivatives of the objective and constraint functions to find the optimal solution. They are particularly effective at finding optimal local solutions and perform well for problems with differentiable, convex, and smooth objective functions. On the other hand, gradient-free algorithms do not require the use of derivatives and can be either based on mathematical principles or heuristics. In the first case, mathematical principles guide the iterative exploration process and the optimality criteria. In the second case, heuristics, usually inspired by natural processes, are used to

efficiently search the solution space. Gradient-free algorithms are well-suited for black-box functions that may not be smooth or continuous and are more robust for global optimization as they are not easily drawn towards local extrema. However, they cannot guarantee finding the optimal solution, tend to become less efficient as the number of dimensions and variable space increases, and often require a higher number of function evaluations to converge to the optimized solution. A detailed analysis of optimization algorithms and their applicability to engineering design problems can be found in [119].

Finding the appropriate algorithm is highly application-dependent. In this work, the objective function is a black box, making it impossible to calculate analytical derivatives. It also exhibits multimodality with multiple local extrema, as assigning different control mode combinations for different conditions can produce similar results. The objective function's smoothness and continuity cannot be directly assessed, but understanding the nature of the problem, it is assumed to be continuous and not smooth, particularly in regions of the solution space affected by penalty terms. The dimensionality of the decision variables can vary between 20 to around 150, depending on the horizon size and discretization. Additionally, the computational cost of evaluating the objective function is relatively low.

Among the optimization methods considered, gradient-based algorithms exhibited limitations, often converging towards local minima and being sensitive to initial starting points. To overcome this issue, algorithms like Global Search and Multi Start [120, 119, 121] were tested. These algorithms use gradient-based solvers but introduce some logic to distribute the starting points of the optimization across the entire decision variable space, attempting to overcome the issue with the local minima. Although they performed better than single starting point gradient-based algorithms, the performance was still worse in terms of objective minimization compared to gradient-free algorithms. Moreover, the computational time was higher for these methods to reach similar results compared to the gradient-free algorithms tested. Consequently, it was found that, for the present application, gradient-free heuristic algorithms are better suited for the problem due to the nature and structure of the objective function.

Opting for gradient-free optimizers indeed leads to increased computational costs due to the necessity for a larger number of evaluations. Moreover, it requires accepting that the solutions obtained are improved compared to the baseline case but may not be globally optimal. After extensive testing of various algorithms, the Genetic Algorithm (GA) and the Particle Swarm Optimization (PSO) algorithm emerged as the top-performing options.

The genetic algorithm, inspired by the principles of natural selection and evolution, was first introduced in the 1970s and has been adapted and improved since then [122]. It has become a widely used optimization technique due to its versatility and ability to solve complex problems. The algorithm mimics the process of natural selection, where fitter individuals are more likely to survive and reproduce, while less fit individuals gradually decline. The genetic algorithm

commences by generating an initial population of random solutions. Subsequently, it iterates through a series of new populations, employing individuals from the current generation to generate the next one. During this process, the algorithm follows specific steps: it assesses each member's fitness by computing raw fitness scores, which are then scaled to more practical values called expectation values. Based on these expectations, certain members (parents) are selected. Some individuals with lower fitness in the current population are designated as elite and carried over to the next generation. Children are produced from these parents through mutation (random changes to a single parent) or crossover (combining vector entries from a pair of parents). These children replace the current population, forming the next generation. The algorithm continues until one of the stopping criteria (such as total time spent, maximum amount of generations, objective value, etc.) is met, signifying the completion of the optimization process. More details on GA and its algorithmic implementation can be found in [123, 119].

Particle swarm optimization is a nature-inspired optimization algorithm developed in the 1990s [124, 125]. It is based on the collective behavior of particles in a swarm, where each particle represents a potential solution to the optimization problem. The main idea behind PSO is to iteratively update the position of each particle based on its own experience and the experiences of its neighboring particles, aiming to find the optimal solution through collaboration. PSO initiates by generating an initial random set of particles and assigning them random initial velocities. Each particle's objective function is evaluated at its location, determining both the best function value and the corresponding location. Next, new velocities are calculated based on the current velocity, each particle's individual best location, and the best locations of its neighboring particles. The algorithm iteratively updates the particle locations, adjusting them according to their velocities while ensuring they remain within the defined bounds. The process continues through iterations until a stopping criterion, such as the maximum number of iterations, objective value target, maximum time elapsed, etc., is met. More details on PSO and its algorithmic implementation can be found in [119, 126, 127].

Both algorithms were utilized for all optimization cases, and the best results are presented in the results chapter 7. Multiple optimization runs were performed with each algorithm for each case to ensure reliable outcomes, aiming for convergence to near-optimal solutions within the available computational resources and time limitations. Nevertheless, it is important to acknowledge that the global optimality of the solutions cannot be guaranteed. Both algorithms are implemented in the optimization framework using Matlab's native libraries *GA* and *particleswarm* provided in the optimization toolbox. Values for the key hyperparameters were determined through iterative experimentation and maintained consistent across all optimization runs, as summarized in table 5.2. Additionally, default values were retained for other tunable hyperparameters not specified in the table. Customized settings, such as initial population

sizes and optimization stopping criteria, were tailored for each case, considering the number of variables and available computational capacity. As a general guideline, an initial population of approximately 10 times the number of decision variables proved to be a reasonable starting point, although its feasibility depended on computational resources in certain cases.

**Table 5.2:** Hyperparameters used for the GA and PSO algorithms as implemented in the Matlab optimization toolbox. The parameters not mentioned are kept to default, except the initial sizes and the optimization stopping criteria that were customized per application

GA hyperparameters	GA values	PSO hyperparameters	PSO values
FunctionTolerance	$10^{-4}$	FunctionTolerance	$10^{-4}$
CrossoverFraction	0.85	SelfAdjustmentWeight	1.3
EliteCount	0.075 x population size	SocialAdjustmentWeight	1.4

For all cases, the optimization was parallelized up to 36 cores using the local cluster of the Stuttgart Wind Energy (SWE) institute. The optimization time varied depending on the complexity of each case, ranging from minutes for cases with fewer variables and optimization loops (e.g., wind distribution-based optimization) to days for cases involving rolling horizons and a larger number of decision variables. As discussed in chapter 4, the size of the GPR objects and the computational costs to generate the predictions compared to the spline-based interpolation slowed down the optimization. On one hand, moving the GPR objects to the parallel workers introduced a significant overhead restricting the number of parallel workers that could be effectively utilized. On the other hand, each individual objective function evaluation was slower due to the increased prediction times of GPR, resulting in a further increase in the total optimization time. Given that both surrogate models exhibited similar accuracy, the decision was made to exclusively use the more efficient spline-based surrogate for the optimization tasks.

### 5.3 Assumptions and considerations about the method

The overall optimization process described in the present chapter is applied to evaluate the long-term operational management approach proposed in this work by evaluating various scenarios. As this is a study for the proof of concept, several assumptions have been made. This section provides a comprehensive summary of all these assumptions and critically examines their potential implications, along with possible solutions to address them in future applications. Moreover, the chosen approach to the formulation of the optimization problem poses some limitations that are summarized and discussed in this section.

The estimation of fatigue damage consumption and its development over time is a core

element of the optimization process. To calculate the fatigue loads, Miner's linear damage accumulation rule is employed, along with the rainflow counting algorithm, considering only load ranges and not mean values. However, it is important to note that power boosting can lead to an increase in both mean loads and load ranges. Therefore, it is recommended to conduct further analysis that includes the mean load level to obtain a more comprehensive understanding of the loading behavior. Additionally, the buckling failure mode, particularly relevant for the tower and blade structures, is not taken into account. As buckling is sensitive to increased mean loads, the influence of power boosting should be further examined.

Another assumption in the fatigue damage accumulation is that only normal operation is considered. According to the design standards, the operational conditions of start-up, normal shutdown, and parked operation with idling or locked rotor should also be considered. Loads and power are considered zero for the periods when the turbine is not operating, and no additional loading is accounted for during time steps when the turbine is starting up or shutting down. In the scope of the optimization, the optimized operation is compared to the baseline. The accumulated loads from idling are expected to be similar in both cases and not significantly impact the results, as the total downtime is similar and the magnitude of loads is low. The amount of start-ups and shutdowns actively changes with the optimization as it is a parameter considered in the process. To provide a rough measure of these changes, the amount of shutdown time of the baseline and optimized cases are tracked and reported by the framework. Nevertheless, these cases should be evaluated with aeroelastic simulations and incorporated into the surrogate model in a practical application. An example of such an approach is demonstrated in [108].

Furthermore, the fatigue damage budget of each load considered is defined by the baseline operation as explained in section 5.1. This is a conservative assumption fitting the scope of this work, as the potential fatigue margins produced by the method are only influenced by the operational mode. Nevertheless, to assess the full potential, the actual design loads have to be considered as discussed.

The entire wind turbine structure is considered with the optimization targeting the loads' ensemble as described in section 5.2. Furthermore, specific negative margins on the revenue or total damage objectives can be assigned, a feature that will be explored in some of the scenarios discussed in the upcoming chapters. Beyond the proof of concept, this capability can be extended to allow for tailored negative margins based on a comprehensive techno-economic evaluation, taking into account factors such as replacement costs and maintenance expenses, ultimately enhancing the overall profitability of the project.

Another critical consideration is the evaluation of ultimate loads. This study exclusively focuses on managing fatigue consumption, assuming that the increased loading due to power boosting does not exceed the structural strength limits of the turbine components. However,

this is a significant assumption that must be validated through simulations in a real-world implementation. The results of these simulations can be the deciding factor in determining the maximum power level that can be safely assigned to a specific wind turbine design.

The availability of the turbine is assumed to be 100% for this work. This means that the turbine is not operating only when the wind speeds are outside of the operational range or in cases dictated by the optimization. There is no straightforward way to implement down-time due to O&M when evaluating historical data. Nevertheless, downtime due to O&M operations, especially planned maintenance activities, has to be considered in such optimization and possibly be part of the optimization itself, shifting the scheduled maintenance downtime as it fits better to the long-term objectives. A possible way to do it would be to consider historical seasonal variations of wind and prices to identify optimal windows. Additionally, down-regulation due to preventive maintenance reasons (as shown in [86]) or due to request by the grid operator is not considered in this work. The turbine is operating in down-regulation mode only in optimized cases according to the optimized operational plan. In all other cases, it operates at the 100% baseline power level.

In scenarios considering fluctuating market prices, the wind turbine is considered to be shut down in cases of negative prices for both baseline and optimization cases. Hence, in the scope of this work, the wind turbine is considered to be shut down when negative prices occur, or the mean wind speed is outside the operational envelope. When considering fixed prices through premiums or subsidies, the operator of the wind farm might shut it down depending on the subsidy system. Since this depends on the specific contract, it is not taken into account. For this work, it is assumed that in fixed price scenarios, the turbine never shuts down due to pricing. In a real-world implementation, the specific pricing mechanism has to be considered.

In the optimization process based on forecasting horizons, accurate predictions of hourly mean wind speeds and spot electricity prices are essential. This study examines horizons ranging from 24 hours to a full year, assuming perfect forecasts for both variables at each horizon period. However, it is important to acknowledge that forecasting uncertainty increases with the length of the horizon. Realistically, accurate forecasting at an hourly level, for both electricity prices and wind speeds, is limited to a maximum of a few days [128, 129]. A variety of methods exist for short- to medium-range time series wind speed forecasting horizons up to approximately 10 days, with the results varying significantly depending on the methods and the sites considered [130]. Approximately a mean absolute error of up to 15% can be expected for a horizon of up to three days with a steep increase beyond this horizon [131, 132]. The prediction of the spot electricity prices involves modeling and simulation of both expected demand and expected production in combination with statistical data-driven methods with historical data. The accuracy reported in the literature varies highly according to location/market, time of the year, energy mix of the system, and possible interconnections [128, 133] with values of mean

absolute error reported in the ranges of 5-80%.

Despite this limitation, this work considers longer horizons to evaluate the theoretical potential of the optimization method, even if their practical applicability may be limited. A small sensitivity study on the topic, introducing noise on the forecasts used for the optimization, is performed in chapter 7. However, given the crucial role of these forecasts in the method, a more comprehensive understanding of the modeling and quantification of uncertainty would be necessary for further implementation.

As discussed in the previous section, the structure of the objective function, which involves combining weights, penalties, and bounds, along with the use of heuristic algorithms, presents certain limitations. Specifically, calculating a Pareto front of the revenue and damage objectives is not feasible, and determining the appropriate weighting of objectives requires manual experimentation with the combination of parameters. To address these constraints, the analysis is conducted through the examination of various scenarios that represent different business cases with distinct overall objectives. The results presented in chapter 7 are derived from the best outcomes obtained with manual tuning and multiple optimization runs using the two algorithms considered. Despite these limitations, this analysis offers valuable insights into the potential of the optimization method for wind turbine operational management.

## 5.4 Summary

This chapter introduced the computational framework used for wind turbine operational management analysis. The framework tracks the turbine's state over time. Moreover, it is used for performing the optimization and comparing the various cases based on the accumulated values achieved. Key assumptions in calculating and accumulating quantities of interest over time are discussed, and potential further use cases of the evaluation framework as an online digital twin are explored.

The optimization problem is formulated as a continuous, single-objective problem with a black box objective function that employs the surrogate model to calculate the relative differences of the accumulated metrics between the optimized and baseline case at each function evaluation. The approach of combining multiple objectives into a single one using the weighting sum method is explained, along with applying penalties and bounds to guide the optimizer towards specific objectives. Limitations arising from these methods are discussed.

Two methods for performing the optimization are presented: The first is based on wind speeds only, utilizing the site-specific wind speed distributions, and the optimization assigning a control mode for each wind speed bin considered. The second is based on wind speed and electricity price forecast rolling horizons, with the optimizer assigning a control mode at each

time step of the horizon. The choice of heuristic optimization algorithms, specifically the genetic algorithm and the particle swarm optimization, is motivated, and their optimal settings found through experimentation are presented. Challenges related to computational feasibility and directing the optimizer towards a specific combination of objectives due to the problem formulation are discussed.

Finally, the chapter critically examines the assumptions and limitations of the methods used and proposes potential strategies to address these. The discussion aims to provide a clear understanding of the framework's capabilities and offer insights into future developments and applications.

# Chapter 6

## Data sets and definition of scenarios

This chapter focuses on the data sets selected for assessing the proposed method and the various scenarios explored within the optimization process. The boundary conditions of the local wind conditions and the electricity market in which the wind turbine operates are crucial parameters for the optimization method. The rationale behind the choice of datasets is explained, considering the objectives of this study. Detailed analyses of the datasets are conducted, including statistical evaluations and comparisons between different locations, time periods, and electricity markets under consideration. The influence of the different boundary conditions on the wind turbine operation and the potential for optimization are also discussed.

Furthermore, a set of scenarios is defined to demonstrate the diverse applications of the optimization method for various objectives, representing a fundamental collection of potential business cases. The motivation and assumptions behind each scenario are discussed, and further possibilities for applying the optimization approach in scenarios beyond this study are explored.

### 6.1 Presentation and analysis of data sets

The optimization of the long-term operation of a wind turbine heavily relies on the boundary conditions of the wind conditions, the electricity prices, and their combination, which are external and beyond direct influence. These boundary conditions play a significant role in determining the efficacy and feasibility of the proposed optimization methods. The variability of wind speeds and prices, as well as the variability of their combination, enables the optimizer to assign adaptively control modes allowing for optimizing the long-term objectives. For

instance, at a site with less frequent wind speeds in the above-rated range, there would be fewer opportunities to apply power boosting. Similarly, in market environments where the prices are highly correlated to wind speeds due to high wind penetration, there will be fewer favorable instances with high prices in conditions where power boosting can be applied.

The wind climate is mostly site-dependent but also period-dependent, as the wind speed patterns can vary over years at the same location [134, 117]. Hence, in order to effectively assess the optimization method, it is crucial to consider data from various locations spanning several years. Additionally, the pricing behavior is influenced by the electricity market structure, local policies, and the power generation mix, which can vary significantly from one country to another. The magnitude and variability of electricity prices can also change over time due to factors like policy shifts, fuel availability, and alterations in the energy production mix. Consequently, to thoroughly examine the proposed method, it is essential to incorporate data from different market environments over multiple years. By considering these site- and period-dependent aspects, the optimization approach can be tested and its effectiveness demonstrated across a range of scenarios.

Based on the considerations outlined, this work incorporates historical data from two different locations in distinct countries. The first location is situated in Germany, specifically at the North Sea's Alpha Ventus offshore wind farm. The choice of country and location is motivated by North Sea being one of the most common locations for offshore wind installations in North Europe. Moreover, Germany is one of the biggest European energy markets in terms of volume and has a relatively low percentage of wind in its energy mix, with a substantial portion of energy production coming from coal, lignite, and nuclear power plants. The second site is also located offshore, close to the west coast of Denmark, near the Horns Rev wind farm. Denmark's electricity market is chosen due to its high penetration of wind energy, making it the leading country in Europe in this regard. Additionally, Denmark's electricity market is connected to the Scandinavian market, which is also significantly influenced by renewables. The choice of these two sites addresses the requirement for considering different wind conditions at locations commonly used for wind farm installations and also the consideration of different electricity markets with different regulations and energy mixes. For both locations, data spanning multiple years including wind speeds, TI, and DA electricity prices are utilized.

The wind data for the German site were acquired from the New Wind European Atlas (NEWA). NEWA is an EU project combining different numerical tools from mesoscale to microscale with historical datasets to improve resource assessment for wind energy applications [135, 136]. One of the outputs of the project was the validated wind atlas offering microscale and mesoscale historical data for Europe and Turkey [135]. The data don't consider the presence of the wind farms and their possible effects on the local microclimate and can be considered as representative of the free-stream conditions at the site. The data used are

microscale data for the location 54°00'40.0"N 6°36'28.0"E coinciding with the Alpha Ventus wind farm. The period considered is from 1.1.2016 to 31.12.2018. The data, including mean wind speed and turbulent kinetic energy (TKE), were obtained in a 30-minute resolution and subsequently resampled to hourly values. TI is not provided by the NEWA directly. Hence it was indirectly approximated using the turbulent kinetic energy using equation 6.1.

$$TI = \frac{\sqrt{2TKE}}{u_{mean}} \quad (6.1)$$

The price dataset for the German electricity market was obtained by SMARD [137], the Federal Network Agency's (Bundesnetzagentur) electricity market information platform. The dataset includes the settled DA prices from 2016 to 2018 in an hourly resolution. Until 30.9.2018, the data corresponded to the Germany/Austria/Luxembourg and, after that, to the Germany/Luxembourg bidding zone. Additionally, the DA price dataset for 2022 was obtained to form an additional case.

The inclusion of the 2022 dataset is significant as it represents a period of fuel shortages triggered by geopolitical events, resulting in radical changes in wholesale pricing and market behavior. This led to increased magnitude and variability of electricity prices. This particular case is explored in this work to assess the suggested operational optimization in a destabilized market environment with considerably different behavior compared to the previous years. It aims to examine the potential of the proposed optimization under such conditions, as similar scenarios may arise in the future due to changes in market structures, the phase-out of conventional generation sources (nuclear, coal, etc.), and energy security concerns, among other factors. Hence, this special case combines the 2022 electricity prices with the 2018 German wind data to evaluate the optimization's performance under such challenging conditions.

The selected Danish site is the one considered by the TotalControl [138] and FarmConnors [139] EU projects for their reference wind plant located close to the existing Horns Rev offshore wind farm as described in [140]. The wind time series were provided by the project partners and were created using the Correlations in Renewable Energy Sources (CorRES) tool by DTU [141, 142]. The tool combines meteorological reanalysis data with stochastic simulations to provide generation and forecast time series for wind and solar with temporal resolution down to a minute scale. The weather time series are correlated with the DA price time series, as they are an output of the same underlying data. Nevertheless, it should be mentioned that the wind variations may be smoothed due to spatial and temporal averaging effects in mesoscale models. The weather data represent the mean value for the central point of the reference wind plant without the presence of the turbines (i.e. no wake effects included). The obtained data were provided in an hourly resolution for the period 1.1.2013 to 31.12.2020. The relevant data include the mean wind speed and the surface stress parameter ( $u_*$ ). The turbulence intensity

was approximated based on the  $u_*$  values at each time step using equation 6.2.

$$TI = \frac{2.5u_*}{u_{mean}} \quad (6.2)$$

The time series for 2013-2020 of the settled DA prices for the DK1 (west Denmark) bidding zone were obtained in hourly resolution by the Danish transmission system operator Energinet [143]. An illustrative time series containing all three considered variables for an entire year is presented in figure 6.1. An overview of all datasets and their sources is provided in table 6.1.

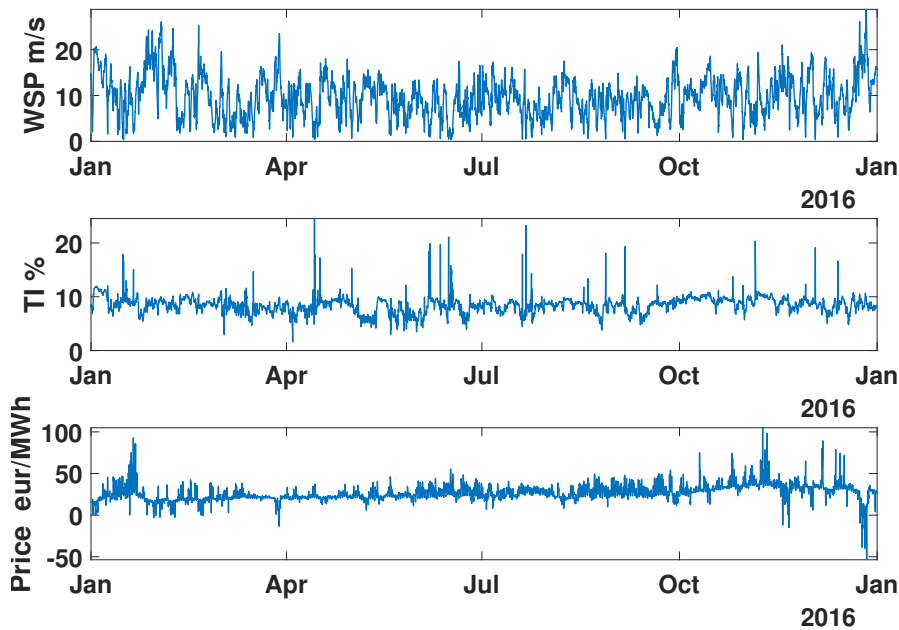


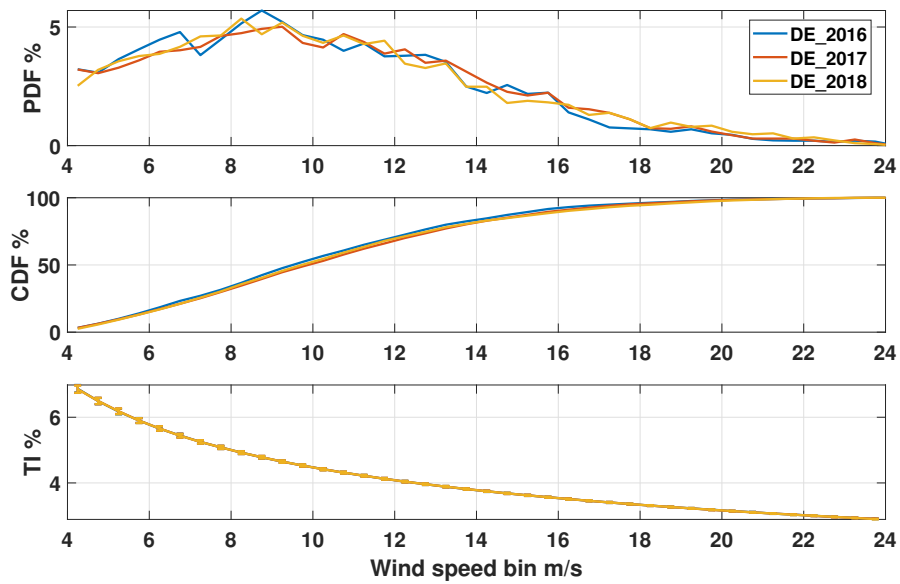
**Figure 6.1:** Example time series of the data used. Mean wind speed, turbulence intensity, and settled DA electricity prices in hourly resolution for 2016 at the DK site.

**Table 6.1:** Overview of datasets used

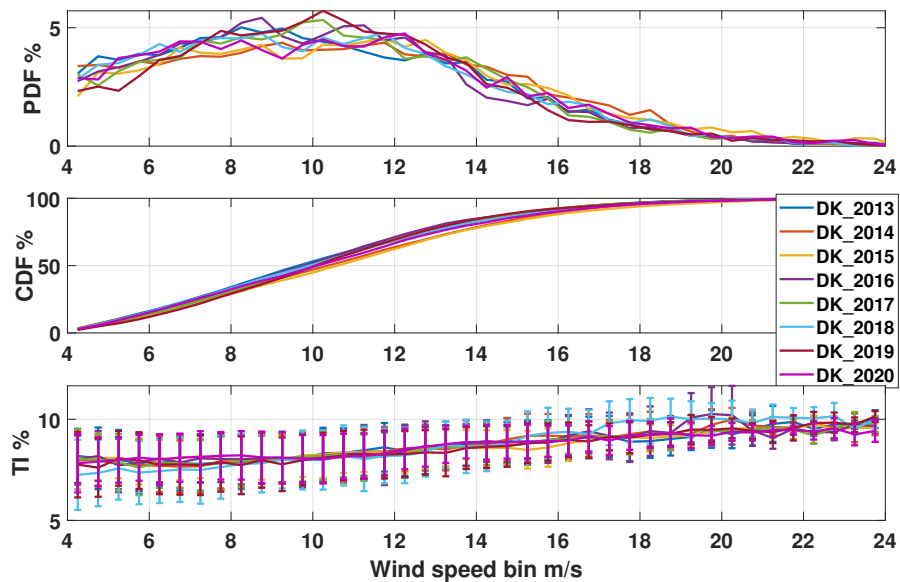
	Case 1	Case 2	Case 3
Location	DK Horns Rev	DE Alpha Ventus	DE Alpha Ventus
Years	2013-2020	2016-2018	2022
Wind data	CorRES	NEWA	NEWA 2018
DA prices	Energinet	SMARD	SMARD
Bidding zone	DK1	DE/LU	DE/LU
Naming	DK_all	DE_all	DE_2022

Figure 6.2 displays the PDF and cumulative density function (CDF) of wind speeds, along with the mean and standard deviation of TI for each wind speed bin per calendar year and

per location. Wind speeds at the DK site tend to be higher compared to the DE site for most years. Additionally, the variability in wind speed distributions across different years is more pronounced at the DK site. The TI values for the DE site are fairly constant per wind speed and almost the same for all years. In contrast, the DK site exhibits substantial variability in TI per wind speed bin and per year. This divergence can be attributed to distinct modeling approaches, with the NEWA data relying solely on mesoscale data and presenting a deterministic wind speed-to-TI relation. In contrast, the CorRES modeling approach generates



(a)



(b)

**Figure 6.2:** Wind speed PDFs and CDFs, and TI distributions over wind speeds for all years and locations considered. The error bars in the TI plots denote one standard deviation. (a) DE site, (b) DK site

more diverse time series that better mirror real-world correlations between wind speed and TI. This leads to a more realistic and more challenging case for the DK site since, as shown in chapter 4, TI levels have a high influence on the loading level.

The long-term wind distribution of each site was defined by fitting the Weibull PDF to all the available data. The resulting distribution and the corresponding parameters for each location are depicted in Figure 6.3. To derive these values, only data points with wind speed within the operational ranges of the wind turbine and positive prices were considered. The derived distributions verify that, in general, higher wind speeds occur at the DK site. These distributions serve as the baseline reference for each respective site in the optimization cases where only wind speed distributions are taken into account.

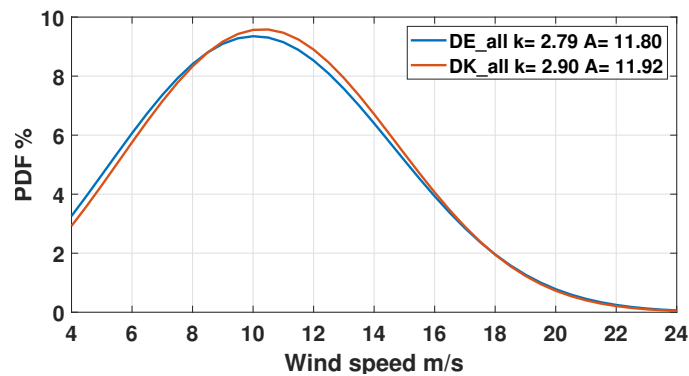


**Figure 6.3:** Fitted Weibull distributions for the wind speeds at both sites using all the available data. Data are filtered, excluding wind speeds outside the operational range and prices  $\leq 0$  eur/MWh.

The PDF and CDF of DA prices, along with their mean and standard deviation for both electricity markets considered are shown in figure 6.4. The DE prices until 2018 show a pattern of increase with time and show a similar distribution over the different years. In contrast, DK prices display a substantial year-to-year variation both in terms of magnitude and distribution. In most cases, DE prices tend to demonstrate greater intra-year variation compared to DK, with 2018 being the year with the highest variability. For the DK market, the years 2018, 2019, and 2020 are characterized by the highest variability in prices. On the other hand, the years 2013, 2014, and 2017 show the lowest variability. This is important to consider for the optimization as the lower variability of prices is expected to make the optimization less efficient. The probability distribution for the prices in 2022 showcases the relevance of considering this special case. The prices are 5-10 times higher than all the other years considered, also showing a much higher variability.

In order to understand the impact of the boundary conditions on the wind turbine operation, the percentages of time were calculated, per year and location, for when the turbine is: (a) not operating, (b) the wind speed is above the rated baseline value, and (c) the wind speed is above rated while the price is above the mean of each year. The results are summarized in

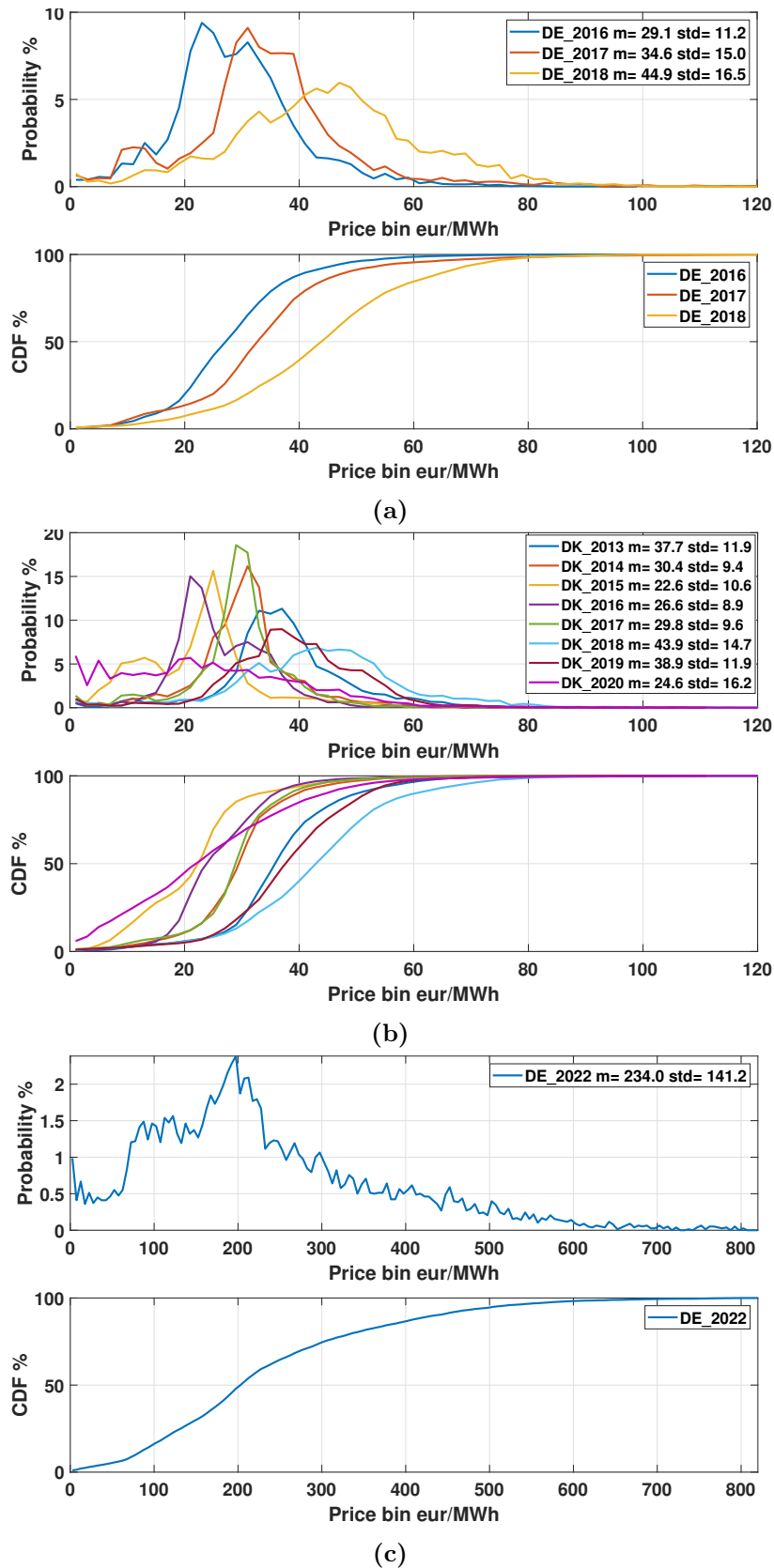


**Figure 6.4:** Electricity price PDFs and CDFs for all years and markets considered. The mean (m) and standard deviation (std) values are provided in the legends. (a) DE 2016-2018, (b) DK1 2013-2020, (c) DE 2022

figure 6.5.

For the DE site, the turbine is not operating, due to negative prices or wind speeds out of the operational range, for 11-12% of the time for all years considered. For the DK site, this value is slightly lower between 9% and 11% for all years. The amount of time the turbine is not operating is mainly driven by the wind conditions. Since wind conditions have similar trends over the years for a specific location, the low variation between the years and the similarity between the years at the same site is expected. The low variation of the value for all cases suggests that this aspect will not have a significant influence on the optimization. Years with less downtime are expected to have slightly higher potential for optimization due to more instances available for optimization.

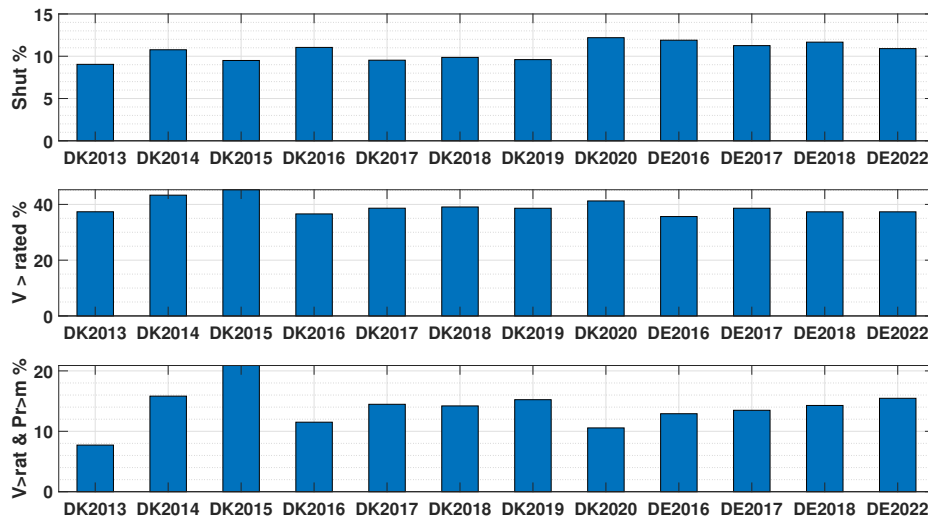


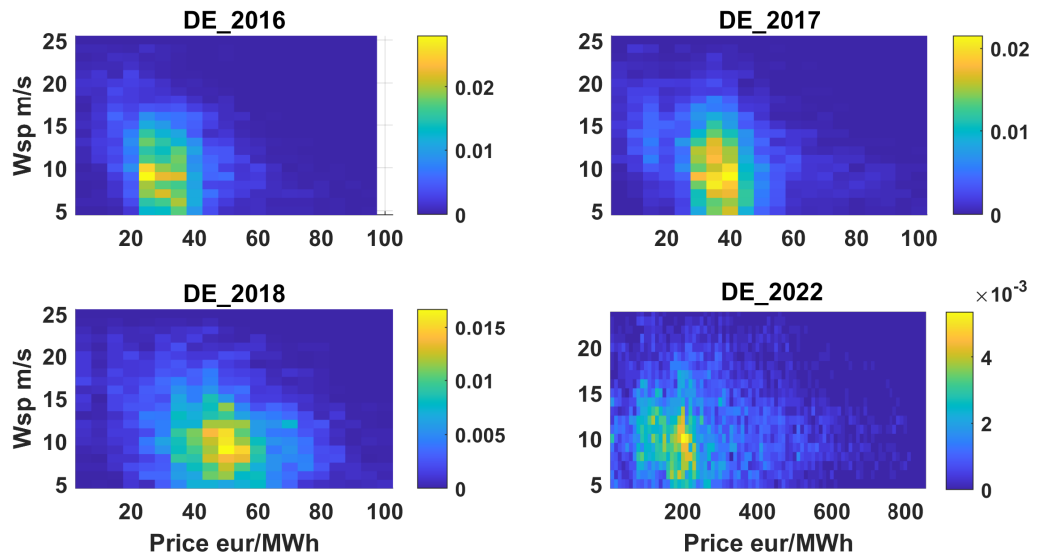
**Figure 6.5:** Percentage of time when the turbine: is not operating (upper), the mean wind speed is above baseline rated (middle), the mean wind speed is above rated and the price higher than the mean of the year (lower) for all years and sites.

To leverage the potential tradeoffs of power boosting, it is relevant for the optimization to quantify the percentage of time when the turbine is able to operate in the full load region. At the DE site, the data consistently indicate a moderate variation, with the percentage of time spent in the full load region ranging from 36% to 39% across all three meteorological years. In contrast, the DK site exhibits a more significant year-to-year variation, presenting higher values overall. The values were identified in the 35-45% range. The higher variation suggests that, on one hand, there is more potential for optimization for the Danish site due to the broader time windows where power boosting can be applied. On the other hand, when optimizing based on the mean wind speed distribution of the site, the higher variation over the years can potentially reduce the efficiency of the optimization process. It should also be noted that these percentages indicate the maximum fraction of time that the IBC can be potentially applied and can be used for comparison with the optimization results, providing a measure of the IBC activity for each case.

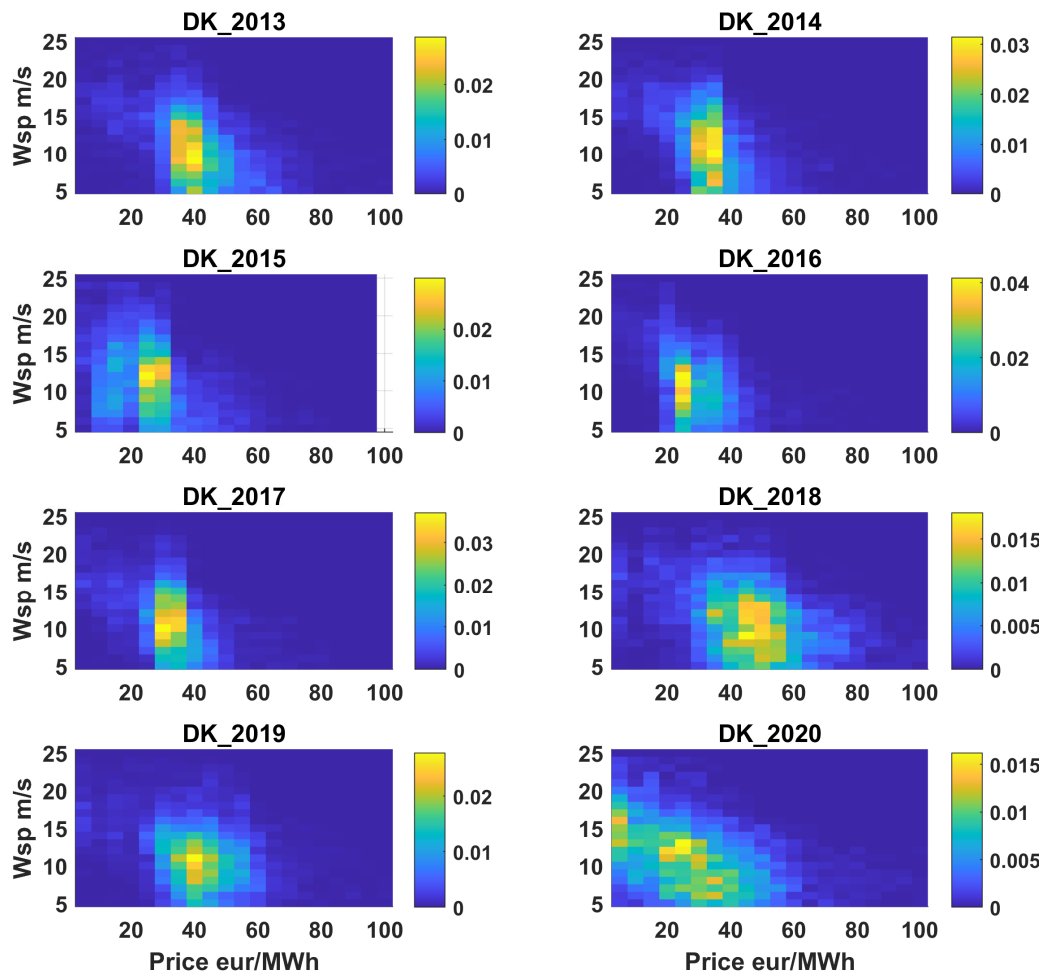
Moreover, it is relevant for the optimization to quantify the amount of time when the turbine operates in the full load region with high prices. These are the instances where power boosting can be applied more efficiently as the revenue is maximized the most. This dynamic is influenced by a combination of both wind conditions and price boundary conditions. A simplistic measure to quantify this is calculating the amount of time, per year and location, that the turbine operates in full load and the price is above the mean of the year. At the DE site, this percentage spans the range of 13% to 15% for the years 2016 to 2018, while it reaches 17% for the year 2022. Notably, the distinction in 2022 arises solely from differing market conditions, as the wind conditions are the same as those of 2018. The variation is much higher at the DK site, with values ranging from 7% in 2013 to 21% in 2015. This divergence in behavior between the two sites underscores how distinct market environments and energy generation compositions can significantly influence system dynamics and optimization potential. Years characterized by a higher frequency of above-rated wind speeds coupled with elevated prices are anticipated to hold greater optimization potential, particularly in scenarios involving fluctuating prices.

To further explore the correlation of the boundary conditions, the bivariate probability of wind speeds and DA prices for each year and location is presented in figure 6.6. Comparing the probability distributions between the two sites, the higher dispersion of the distributions at the DE site for years 2016-2018 compared to the DK site is evident. At the DK site for the years 2013-2017, a pattern of lower dispersion of prices is observed, which changes for the later years. In the years 2018-2020, the distribution is closer to the DE site, with the bins with higher probability distributed over more wind speed-price bins. In the case of DE 2022 the distribution changes significantly both in terms of higher ranges of values and larger spread of the scatter.

Leveraging the scatter of the bivariate probability is central to optimizing wind turbine operation for long-term objectives amidst fluctuating prices. Power boosting can be strategically applied to maximize revenue under high price - high wind speed conditions, while accumulated load can be minimized through down-regulation in low-revenue cases or via the application of IBC during high wind speed instances. As previously demonstrated in chapter 4, the most effective load reductions through down-regulation typically occur around the rated wind speed range. Therefore, from an optimization perspective, a distribution with higher probabilities of both elevated wind speeds coupled with higher prices, along with lower prices paired with wind speeds around the rated value, would be more favorable. Additionally, instances characterized by low prices and low wind speeds provide opportunities for selective turbine shutdown, reducing fatigue damage accumulation with a minimal impact on revenue.



(a)



(b)

**Figure 6.6:** Bivariate probability of wind speed and electricity prices for all years and sites considered  
(a) DE, (b) DK

## 6.2 Definition and discussion of optimization scenarios

As elaborated in chapter 5, the formulation of the optimization problem and the computational costs require that the optimization analysis is done based on scenarios. The scope of the scenarios is to investigate different use cases of the proposed operational management method stemming from different overarching operational goals. As this study is a proof of concept, the aim is to define some basic scenarios representing potential business cases from the perspective of a wind farm operator. Each scenario is evaluated utilizing both data sets to investigate the efficiency and efficacy of the optimization to the specific objectives across varying wind and market pricing boundary conditions.

All scenarios considered will be evaluated considering two pricing mechanisms applicable to the electricity producer. The first considers fixed prices, assuming a fixed subsidy or PPA is in place. In this case, all the time series for the DA prices are replaced with a constant value. For this purpose, a value of 80 eur/MWh is selected, which reflects the current magnitude of existing subsidized schemes. It is worth noting that, for comparison purposes only and in the absence of an underlying cost model, the specific price level does not exert any influence on the results. In the second case, the electricity producer is assumed to operate without any subsidy or PPA arrangement. In this case, the producer places the entire electricity production on the DA market of the relevant bidding zone. No further participation in other markets, such as intraday or balancing, is considered focusing solely on the DA market for revenue generation. In addition, the producer is assumed to be an exclusive price taker without the ability to influence the prices by modifying the dispatch strategy. Moreover, the study does not account for coordination among multiple assets within a larger portfolio owned by the same developer, thereby isolating the impact of the optimization process on the individual wind turbine.

For all scenarios and pricing mechanisms, the optimization will be performed using both developed approaches: the first involving only the wind speed distributions as input, and the second incorporating a forecast horizon of wind speeds and prices. The optimization relying solely on long-term wind speed distributions demands fewer inputs and generally entails lower uncertainty compared to forecasts, especially for horizons extending beyond a few days. Moreover, it exhibits computational efficiency and demands less knowledge and infrastructure for implementation (as it is executed once per site and objective).

In contrast, the optimization involving forecast horizons, encompassing both wind speeds and price inputs, has the potential to yield enhanced results as it can capture the intermediate-term and short-term fluctuations of both conditions. Furthermore, it provides the opportunity for adjusting objectives over time to adapt to evolving requirements. Additionally, it enables experimentation with cases featuring extended horizon previews, which, though unrealistic, offer insights into the upper bounds of potential outcomes. The examination and comparison of these

approaches within the context of diverse scenarios and varying boundary conditions can yield comprehensive insights into the practicability and efficacy of the optimization methodology.

Furthermore, the scenarios are employed to assess the effect of the control modes, presented in chapter 3, on the optimization. The impact of the different loading profiles between the two down-regulation strategies on the optimization will also be investigated. The required frequency of application of the IBC loop is another focus of the study. The impact of the maximum allowed power boosting level on the optimization is examined through the analysis, along with the possible benefits of selective shut-down according to the operating conditions.

In total, two scenarios are defined:

### **1. Maximization of accumulated revenue**

The operational goal is to maximize the accumulated revenue within a predefined period compared to the baseline operation. Additionally, the cumulative fatigue damage for each load considered should not exceed the baseline value. This scenario focuses on identifying the maximum revenue with the constraint of not exceeding the damage budget. This approach reflects a business case where the primary aim is to increase income over a given period without the anticipation of extending the operational lifetime.

Moreover, within this scenario, cases are where the accumulated damage for each of the considered loads is allowed to increase, compared to the baseline case, up to a specific percentage defined by a cap. This would represent a business case where the highest revenue is sought for a specific period, accepting a possible reduction in the lifetime of some components. This could be relevant, for example, in business cases where a PPA or subsidy is in place for a limited period with higher prices compared to projected future rates or during exceptional market conditions characterized by unusually high prices.

### **2. Minimization of accumulated fatigue damage**

The operational goal is to minimize the accumulated fatigue damage within a predefined period compared to the baseline operation. Moreover, the cumulative revenue at the end of the period should not be lower than the achieved revenue with the baseline operation. This scenario focuses on the maximum load reduction while ensuring that the projected baseline income is not influenced for this period. This scenario represents a business case where the focus would be to increase the lifetime of the components as much as possible without undermining the financial inflow. The accumulated fatigue damage in the optimization process is calculated based on a weighted sum of all loads. Thus, different weight combinations can lead to varying distributions of load reductions among the components. The decision-making for choosing these weights has to be application-specific. For the results presented in this work, an effort to explore different combinations of weights was made, although not exhaustively or systematically.

Hence the results shown in the next chapter only indicate the potential of optimization in such a scenario.

Furthermore, within this scenario, additional cases are examined where the cumulative revenue at the end of the period is allowed to decrease down to a specific percentage defined by a cap. This scenario represents business cases where the expected financial benefit by extending the lifetime of the turbine (or specific subcomponents) is higher than the projected income loss. Such a business case could occur, for example, if a longer than the design lifetime favorable PPA or subsidy can be achieved in combination with regulatory or other issues not allowing for repowering at the considered site. Similar considerations for load weightings, as discussed in the second scenario, hold relevance here as well.

All optimization cases for all scenarios are evaluated based on the same KPIs as defined in section 2.2. The KPIs regarding loads and revenue are utilized to evaluate the optimization efficiency with respect to the primary objectives. The energy metric is used to examine the effect of the optimization on the total energy production since the revenue increase does not necessarily translate to an energy production increase for the cases considering fluctuating prices. The KPI related to downtime is used to evaluate the optimization results in terms of the frequency of selective shutdowns. The KPI regarding the IBC activation is used to assess the utilization of the IBC loop, as minimizing the usage of the IBC loop is desirable to prolong the longevity of the pitch actuator system.

## Discussion

The evaluation of the optimization results regarding the loads is focused only on the difference in accumulated fatigue damage. These changes in fatigue damage can be roughly translated to lifetime extension duration by assuming an average yearly fatigue damage consumption. Subsequently, the anticipated number of years required to reach the predefined threshold can be calculated. Similar methodologies have been discussed in existing literature (e.g., [79, 87, 38]). However, extending the operational lifetime involves various complexities beyond only considering fatigue margins. These complexities encompass factors such as permits, maintenance agreements, insurance policies, replacing components, material conditions, certification processes, warranties, and more. As a result, it was decided for this study to conclude the analysis at the level of reduced cumulative damage. This measure can be practically assessed by industry professionals while taking into account the specific costs and constraints applicable to specific business scenarios.

Similarly, the assessment primarily concentrates on revenue evaluation, rather than delving into metrics such as profitability or LCOE. This approach is motivated by the substantial variation in standard costs (CapEx and OpEx), alongside the additional costs incurred from

the implementation of operational management strategies, which can significantly differ from one project to another. Imposing specific values for these parameters during optimization runs could potentially yield outcomes that are either unrealistic or biased. Therefore, the technical focus is centered on revenue management objectives, while a comprehensive financial evaluation of the proposed methodologies is beyond the scope of this study. Nevertheless, it is important to emphasize that conducting such a comprehensive financial assessment represents a crucial next step in the practical application of the method.

Moreover, the assumption that the wind energy producer is not influencing the market prices by participating in the DA market is important to be discussed. In practice, especially in systems characterized by significant wind energy penetration, the adoption of such a strategy by a substantial portion of wind producers could introduce feedback into the market price levels. This dynamic has the potential to provide a stabilizing effect on the prices, as high prices might decrease while low prices could rise due to the adjustment of dispatch volumes based on operational strategies that respond to price signals. However, a comprehensive analysis of these potential impacts lies beyond the scope of this current work. To thoroughly assess these dynamics, it would be necessary to conduct further investigations, potentially involving simulations of future energy systems and market structures.

Beyond the scenarios introduced for the proof of concept in this work, there exists a wide range of potential business cases that can be addressed using the proposed optimization framework. These optimization objectives can evolve over time to accommodate changing conditions. The scenarios outlined in this study focus on specific objectives for the entire operational period, and the optimization is carried out without utilizing feedback from past outcomes.

A potential avenue for further enhancement is to establish an automated method, possibly integrating an inertia term analogous to the integrator in a PID control loop. This mechanism could gradually reevaluate the achievement of goals over time, taking historical data into account and adjusting the optimization strategy to enhance overall performance. Moreover, the incorporation of human or AI-driven decision-making could be explored to dynamically adapt objectives based on anticipated market or meteorological conditions. This adaptive approach has the potential to provide a more flexible and responsive optimization framework in real-world scenarios.

An alternative option could involve implementing the proposed operational strategy as a retrofit solution for an existing wind energy project. As demonstrated in [79], this approach can have an impact on establishing damage margins and influencing revenue outcomes. Given that some information about the damage accumulation can be derived for the period until the retrofit application, a tailored business case could be formulated. For instance, the strategy could be devised to extend the project's operational lifetime and enhance profitability by prolonged

operation or increase short-term profitability by expediting project duration. An example of such a scenario might involve an operational wind farm transitioning from a beneficial subsidy contract to a significantly lower PPA arrangement or directly into the spot market.

The proposed method can potentially optimize scenarios including participation in markets beyond the DA market. Markets like intraday, balancing, or reserve markets can be strategically integrated into the optimization process. Such a method could entail allocating a portion of the forecasted dispatchable energy for these markets, while the remainder is optimized for the spot market. These energy reserves can then be managed based on price thresholds, either for intra-day trading, utilization in reserve markets, or even not used to enhance damage margins. Implementing such scenarios introduces greater complexity, and obtaining publicly available historical data with the necessary temporal discretization is challenging. To address this, tools like CorRES [141, 142] could be employed to generate realistic energy market data, enabling an initial assessment of the potential advantages associated with integrating these additional objectives into the optimization. Furthermore, exploring other potential revenue streams, such as synergies with energy storage, power-to-X applications, and more, could also be integrated into the optimization scenarios, offering the prospect of further enhancing overall profitability.

The optimization scenarios can also incorporate scheduled maintenance planning, which holds particular relevance, especially for offshore installations. This approach would involve identifying time frames during which environmental conditions permit maintenance activities without adversely impacting the optimization objectives. This strategy could potentially make use of seasonal trends observed in historical environmental data, adjusting the optimization objectives to align with these periods in a strategic manner.

## 6.3 Summary

The dataset employed for the application of optimization across diverse scenarios was presented in this chapter. Long-term wind and DA price time series, encompassing multiple years, were acquired for two offshore sites: one situated in Germany at the North Sea and the other located near the western coast of Denmark. The data are analyzed statistically and discussed comparatively. Furthermore, recognizing that distinct market and wind conditions, in conjunction, define the optimization's boundary conditions, a comprehensive analysis of these factors was conducted to unveil possible effects on the overall potential for optimization.

Additionally, this chapter introduced two scenarios, each representing a potential application of the method within a business context. For the purposes of assessing the proof of concept, these scenarios reflect cases where revenue accumulation increase is prioritized while fatigue objectives target specific constraints, alongside scenarios prioritizing fatigue accumulation reduction while constraints are applied to the revenue objective. The rationale underpinning

the selection of these scenarios was explained. The assumptions and limitations related to the scenario formulation were also critically discussed. Moreover, the chapter discussed the possibilities of additional scenarios that could capture broader business cases, thereby touching upon a spectrum of potential applications achievable through the proposed operational management approach.

## Chapter 7

# Optimization results and discussion

In this chapter, the results of the optimization for the different scenarios are presented and discussed. In the first section, the baseline response is presented, and the damage and revenue contributions per wind and price condition are discussed in the context of the optimization. Additionally, this section assesses the potential of the different methods employed in the optimization, i.e., applying the IBC loop, down-regulation, power boosting, and selective shutdown, in terms of their effects on loads and revenue in order to identify the possible optimization bounds.

The optimization results are divided into two main sections, considering fixed electricity pricing and fluctuating market spot prices. In both cases, all the scenarios outlined in section 6.2 are evaluated using both optimization approaches presented in section 5.2. The goal is to quantify the effectiveness of the method for the different scenarios in various market and weather conditions, as well as to evaluate the effect of the different control methods on achieving the objective. In the final section, the results are discussed comparatively, and overall conclusions are drawn regarding the effectiveness of the methods.

As mentioned in chapter 5 an automated tuning of the objective function parameters in terms of weights, penalties, bounds, etc., could not be achieved. The heuristic algorithms used, combined with the available computational power constraints, don't guarantee optimal solutions. Hence, the results presented here are created by iterative manual tuning of the parameters and serve only as a proof of concept on the potential of the method. The best settings found were used for the entire duration of each case, i.e., all years for the same location, optimization scenario, down-regulation trajectory, and maximum power level, in order to ensure consistency over the results. As these settings are specific to the exact implementation of the

code, the specific datasets, and the turbine model, they cannot be generalized. Therefore, they are not reported here, and the reader is referred to the code repository provided in the appendix A.1, where a subset of the presented cases are included as examples for these settings.

## 7.1 Potential

### 7.1.1 Baseline response

The baseline case considers the response of the turbine using the baseline DTU 10MW rwt controller with a rated power of 10 MW without activating the IBC loop and without any selective shutdowns. The availability is considered 100%, and the turbine shuts down only when the wind speeds are outside of the operating range or when the electricity price is less than or equal to 0 eur/MWh.

Using the evaluation framework, the baseline response of the turbine is evaluated for the various datasets for the DE and DK sites. All results are presented as relative differences in comparison to these baseline results based on the KPIs defined in section 2.2. To facilitate the understanding and interpretation of these relative values, the absolute baseline values of the KPIs are provided here. In terms of accumulated damage, the baseline response is normalized to 1 for each load considered at the end of the considered period. The optimization results are then normalized with the same factor to obtain the resulting value. The absolute values of the metrics regarding accumulated revenue, total produced energy, blade pitch travel, and capacity factor are summarized in table 7.1.

**Table 7.1:** Absolute performance metrics for the baseline operation for all periods and sites considered. Fixed refers to fixed prices, and fluc to fluctuating market prices

	DK_all	DE_all	DE_2022
Revenue fixed M. eur	31.73	11.42	3.83
Revenue fluc M. eur	11.51	4.77	11.03
Energy GWh	390.46	139.50	47.54
Pitch travel 10 <sup>6</sup> deg	16.19	2.51	0.85
Capacity factor ND	0.56	0.53	0.54

The results confirm the observation that the DK site experiences higher wind speeds with about 5% higher energy production on average per year. Regarding the revenue, the higher prices of the German market translate to a higher revenue per year compared to the Danish site when considering fluctuating prices. Notably, the substantial increase in market prices for the DE\_2022 case leads to revenue approximately seven times higher than in DE\_2018, despite identical wind conditions.

Comparing the revenue under fluctuating and fixed prices, the fixed pricing leads to significantly higher revenue even with the conservative value of 80 eur/MWh used here. This highlights the challenges of the current electricity market structures to accommodate the non-subsidized operation of wind farms at the current cost levels. Additionally, this observation underscores the importance of enhancing the flexibility and profitability of wind turbines, particularly when operating within electricity market price dynamics.

To gain a deeper insight into how the boundary conditions impact revenue and identify the potential for managing revenue levels through optimization, the contribution of each price-wind speed bin to the annual revenue for the baseline operation is presented in figure 7.1. These contributions are influenced by both the probability of occurrence of each bin and the wind turbine's power production at each time step, considering the exact wind speed and TI. In comparison to figure 6.6 that showed the probability of occurrence of each bin, the revenue contribution is shifted towards higher wind speeds where the power production is higher (albeit the lower frequency) and towards higher prices.

For the considered optimizations, regions with above-rated wind speeds and high contributions to revenue are important, as this is where power boosting can be employed to increase revenue. Similarly, regions with low contributions to revenue but high occurrence can be used to reduce loads by reducing the power level with a low impact on overall revenue. Additionally, a higher spread of revenue can potentially lead to higher gains by allowing more effective distribution of set points, leading to more effective balancing of revenue and fatigue objectives over time. These observations are more relevant for cases where the optimization is based on the wind speed distributions or in cases where longer forecast horizons are considered. In cases with shorter forecast horizons, the optimizer operates with limited foresight, focusing solely on the immediate time steps and their corresponding power-load tradeoffs.

The higher inter-annual differences in wind conditions and even more in market prices at the DK site are reflected in the annual revenue distributions that vary significantly from year to year compared to the DE site. This suggests that optimization based on wind speed distributions can potentially be less effective due to the higher variability. Additionally, at the DK site there is less contribution to revenue in higher wind speeds. This can be attributed to the different electricity generation profiles between the two countries. In DK, the greater integration of wind energy into the energy mix exerts downward pressure on prices during periods of high wind speeds, a dynamic that aligns with the prevailing merit order used to prioritize energy sources within the current market structures.

The significant effect of the market behavior becomes even more evident by examining the DE\_2022 distribution, where the revenue is highly spread over the whole wind speed range and in a higher price range. During this period, electricity prices were primarily influenced by fuel costs, resulting in a reduced correlation with wind speeds. Consequently, the prospect for

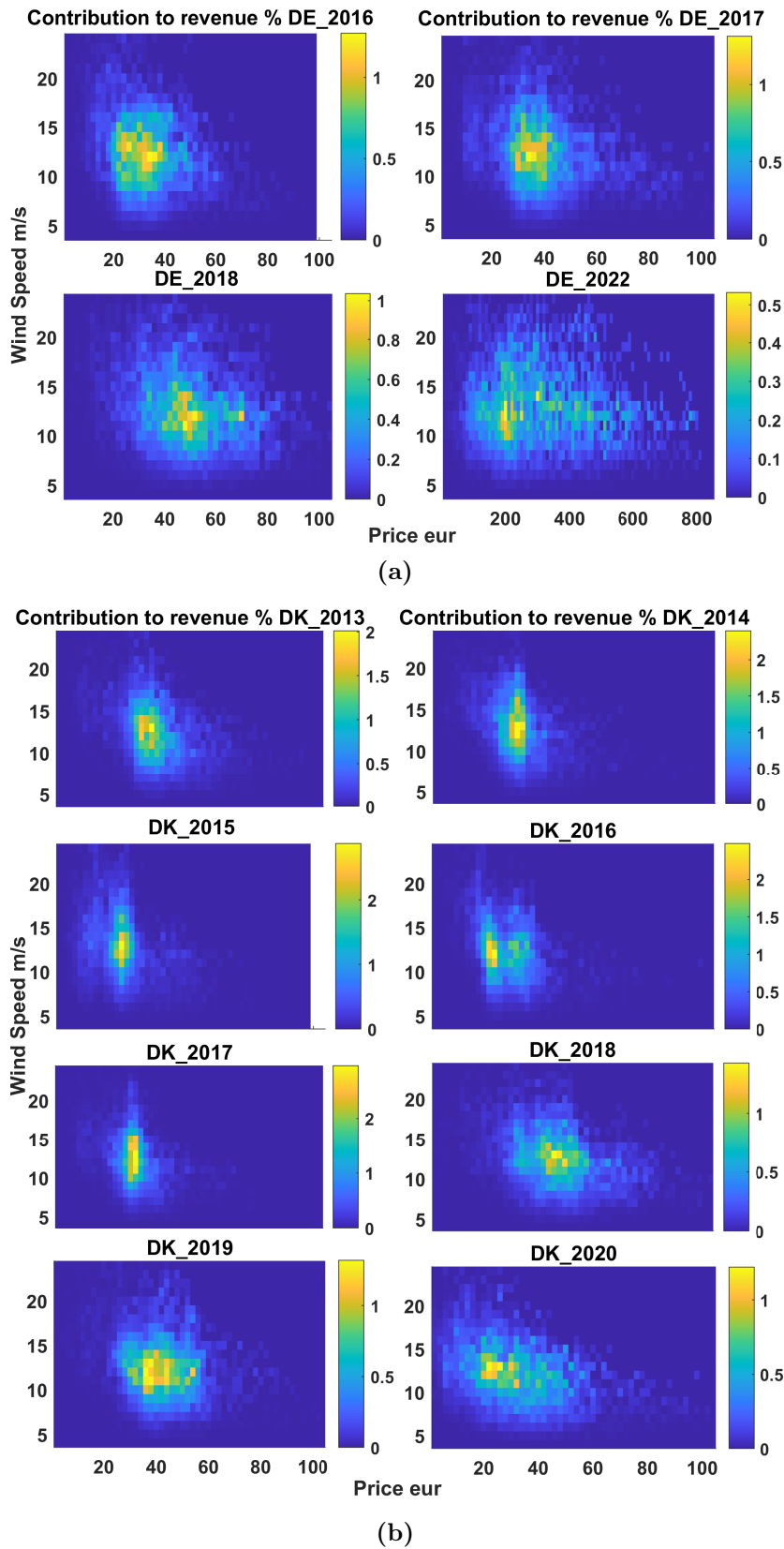


**Figure 7.1:** Contribution of wind speed and electricity prices bins to the total revenue for all years and sites considered using the baseline control mode in fluctuating market prices. (a) DE, (b) DK

optimization is more promising when addressing scenarios within the context of fluctuating prices.

Figure 7.2 shows the revenue contribution of the entire analyzed period at each site. Comparing the two locations, it is seen that the revenue contribution is more widespread in terms of prices and wind speeds at the DE site. Furthermore, for both locations, the major contribution to revenue comes in wind speeds between 9-15 m/s, which coincide with the extended transition region. These cumulative distributions over multiple years show a higher spread in terms of prices than what can actually be used in finite horizon optimizations. Nevertheless, the general trends show that at the DE site, the combination of wind conditions and the electricity market structure is more favorable from a revenue management perspective.

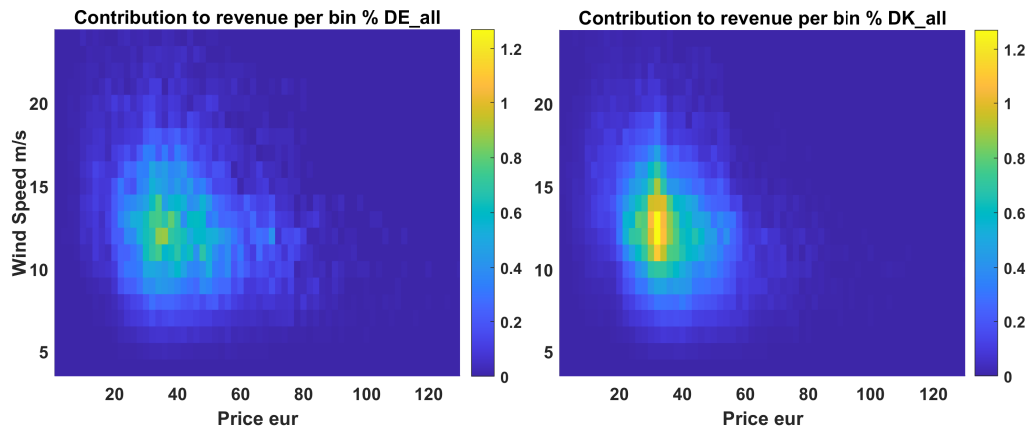


**Figure 7.2:** Contribution of wind speed and electricity prices bins to the total revenue for all years combined. (a) DE years 2016-2018, (b) DK 2013-2020 using the baseline controller in fluctuating market prices

In addition to assessing revenue contribution, it is of equal significance to evaluate the damage contributions associated with each price-wind speed bin, contributing to the overall cumulative damage. In order to balance loads and revenue, the conditions with higher contribution to accumulated damage can be leveraged to reduce loads by down-regulation and activating the IBC when applicable. Moreover, the fatigue loading behavior of each component is dependent on the interplay between turbine design, controller design, and wind conditions, as elaborated in section 4.3. This behavior varies substantially across the spectrum of considered loads, underscoring the intricacies inherent in the multi-objective optimization problem. Within the optimization process, the optimizer is tasked with identifying the opportune conditions for prioritizing each objective to optimize the cumulative fatigue accumulation of each load alongside revenue accumulation.

Figure 7.3 shows the contribution of each bin to the total accumulated damage of tower bottom, tower top, and low-speed shaft loads for all datasets considered. The fore-aft tower bottom load, TBM<sub>y</sub>, has the highest damage contribution in wind speeds around rated as expected. At the DE site, the subsequent most contributing region is the below-rated region,

while for the DK site is the above-rated region. This difference stems from the different wind speed distributions between the two sites but also from the different TI levels. Given that the TBMy load can be reduced mainly with down-regulation and not by applying IBC, this difference suggests that it can be more challenging to balance this load at the DK site. This challenge is emphasized by the fact that the most impactful reductions can be achieved in the above-rated wind speed region where the load reduction from down-regulation is less pronounced, revenue impact is higher, and there exists an overlap with the region where power boosting can be applied effectively. This is valid for both optimization approaches: wind speed-based and forecast-based. The DE\_2022 has similar behavior with the DE\_all case with a much wider spread of the prices.

The tower bottom side-side load, TBMx, shows the highest contributions in the higher wind speed range, above 15 m/s, for both locations. This load is one of the least sensitive to all control modes and can be reduced mainly by the application of IBC at higher wind speeds. This suggests that the behavior in terms of optimization is expected to be similar in both locations. For the tower top roll moment load, TTMx, fatigue damage is mainly contributed by the wind speeds close to rated and slightly below for both sites. However, owing to differences in local wind conditions, in the DE cases, the region of high influence extends to lower wind speeds, while in the DK site, it is more confined within the range of 9-12 m/s. As the activation of IBC increases the TTMx load in the transition region, the most effective approach for load reduction in this context is primarily through down-regulation in the rated and below-rated wind speed regions.

For the low-speed shaft torque load, LSSTq, most of the damage is concentrated within a narrow band of wind speeds around the rated speed between 9-12 m/s for the DK site and 8-12 m/s for the DE site. Moreover, the LSSTq load is negatively influenced by IBC. Thus, the main fatigue reductions are expected by down-regulation at the rated region, which, as shown earlier, coincides with the region where most of the revenue is generated. These observations suggest that managing the LSSTq load along with the revenue is more challenging in the context of optimization for both locations.

Figure 7.4 presents the damage contribution of the speed-price bins for the analyzed blade loads. For the blade root out of plane moment load, BROop, most of the fatigue damage is contributed in wind speeds around the rated and in the higher above-rated wind speeds close to cut out. At the DK site, there is more concentration of damage in the rated region compared to the DE site. This can be attributed to wind speeds close to the rated being more frequent at the DK site. The blade root out of plane load, BRMy, displays a very similar distribution. The only difference is that most of the contribution is shifted towards the highest wind speeds for both sites. Since these two loads are the most positively influenced by IBC and given that the Wöhler exponent of 10 used for the damage calculations leads to higher damage reduction

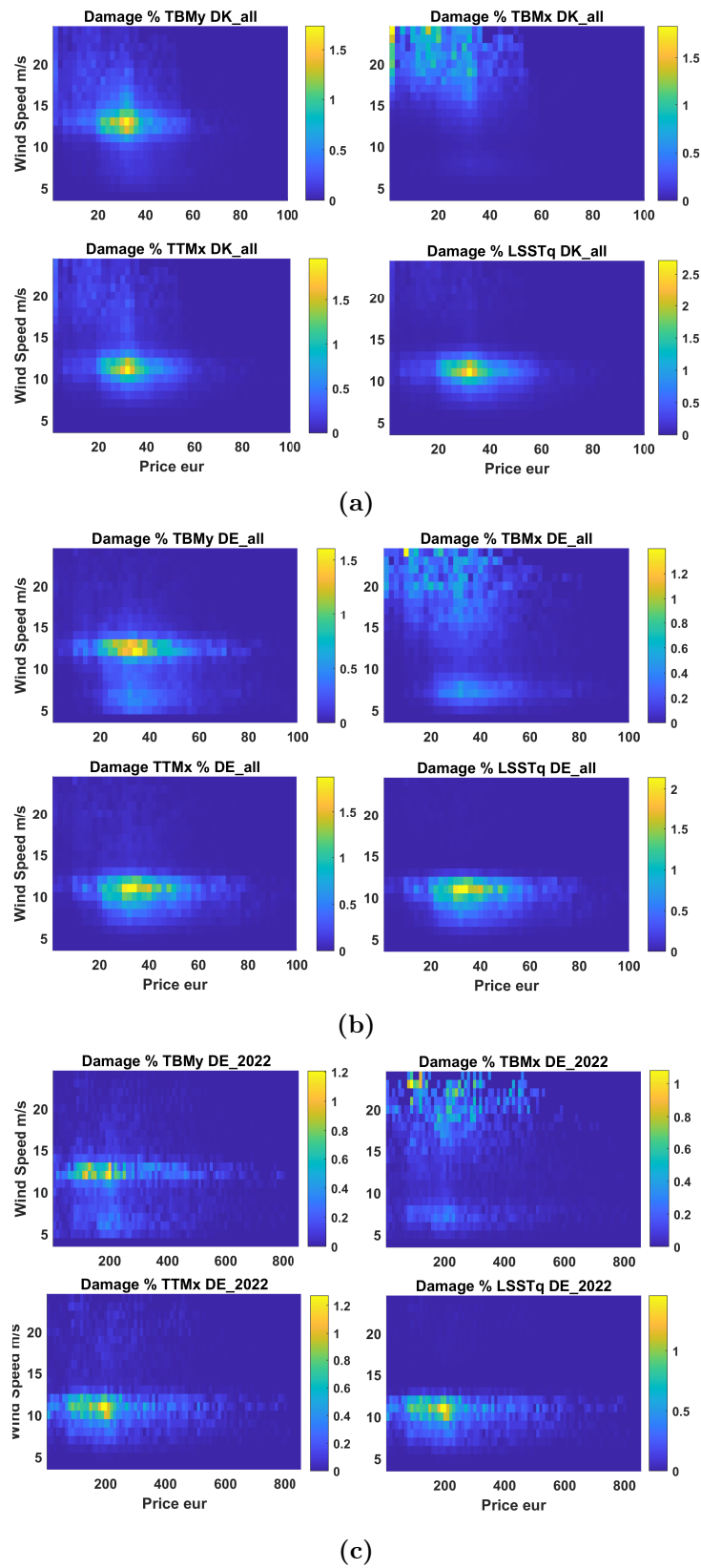


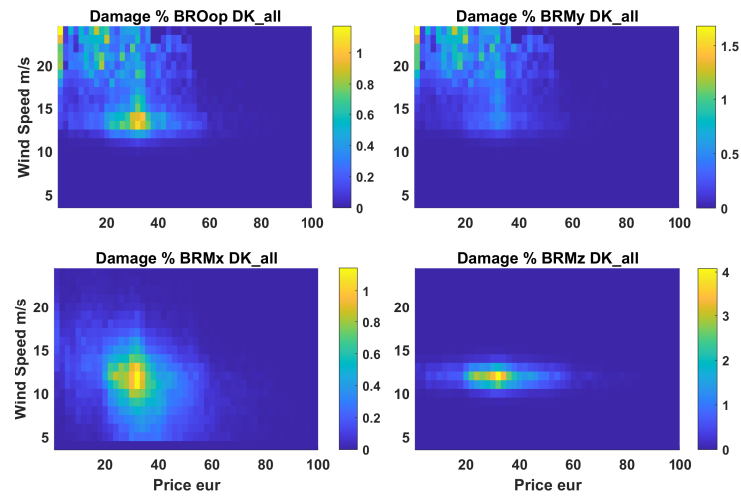
**Figure 7.3:** Contribution of wind speed and electricity prices bins to the total accumulated damage for the tower, nacelle, and low-speed shaft loads using the baseline controller in fluctuating market prices (a) DK\_all, (b) DE\_all (c) DE\_2022

from smaller DEL reductions, it can be expected that balancing them with the revenue should be straightforward. This can be primarily accomplished through the application of IBC, which can counterbalance potential load increases arising from applying power boosting.

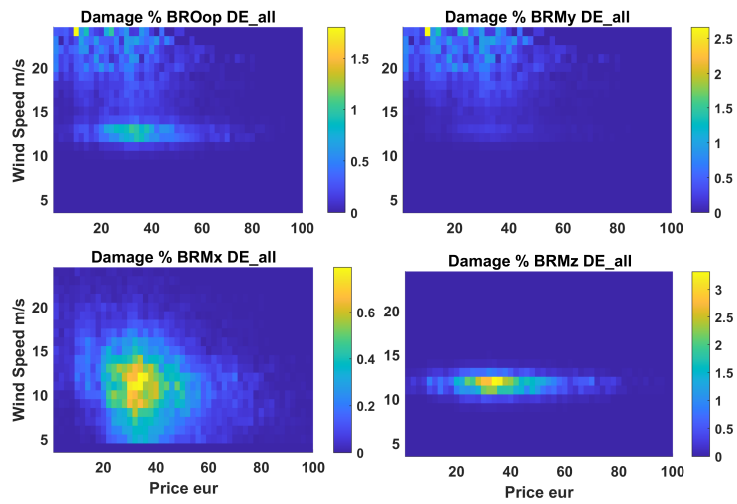
The highest damage accumulation for the blade root edgewise load, BRMx, is concentrated at the rated region. For the DE wind conditions, the load contribution is more spread to wind speeds from 5 to 18 m/s, while for the DK site is narrower. Given that the BRMx load is one of the least sensitive to all the controller modes, it is expected not to play a significant role in balancing loads and revenue. Furthermore, it is one of the loads that, given the response to the controller modes and to the wind conditions, is not expected to be able to be targeted for minimization. The blade root in-plane load, BRIp (not shown in the figure), has a similar response.

The blade root torsional load, BRMz, shows a similar pattern to the LSSTq load, with the damage contribution being concentrated within a narrow band of wind speeds between 10 and 13 m/s for both locations. Additionally, the BRMz was shown not to be affected by the application of IBC, and the highest potential load reductions can be achieved by down-regulation around the rated region. Thus, similarly to the LSSTq load, BRMz is a load that is expected to be more challenging to balance within the optimization.

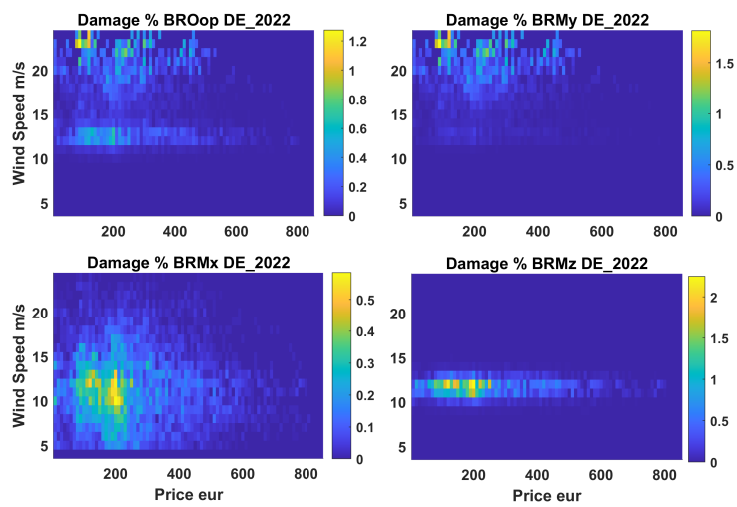
The TBMz, LSSMY, LSSMz, TTM<sub>y</sub>, and TTM<sub>z</sub> all have a similar response in terms of fatigue loading over the entire spectrum of wind conditions as discussed in 4.3. They are less influenced by the application of power boosting, while they can be effectively reduced with the application of IBC. Furthermore, a significant portion of their damage contribution originates from wind speeds above rated, implying that the strategic use of IBC could effectively counterbalance potential load increases resulting from the application of power boosting.



(a)



(b)



(c)

**Figure 7.4:** Contribution of wind speed and prices bins to the total accumulated damage for the blade loads using the baseline controller in fluctuating market prices. (a) DK\_all, (b) DE\_all (c) DE\_2022

## 7.1.2 Potential by applying IBC

In this section, the effect of the application of IBC is quantified in terms of load reductions and actuator usage. In order to understand the potential of the IBC application, it is examined individually by simulating the available datasets with the evaluation framework with a constant power level of 100% and no selective shutdowns.

Figure 7.5 presents the KPIs for each year in both locations by applying IBC in all applicable wind speeds. This configuration assumes the IBC functions as a standard feature of the controller, thereby capturing its maximum potential.

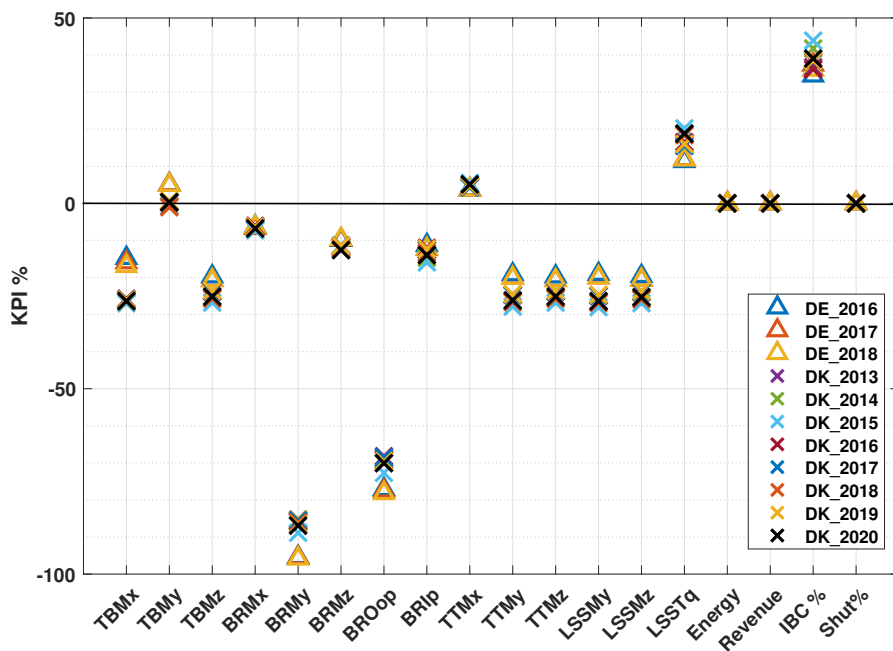


**Figure 7.5:** KPIs by applying the IBC loop per year and location considered

The results show minor variations among different years at the same location. Due to the generally higher speeds at the DK site, the application of IBC has a higher impact compared to the DE site. The cumulative fatigue damage is, as expected, reduced the most for the blade BRMy and BROop loads, by 80% and 70%, respectively, for both sites. The rest of the considered blade loads, BRMx, BRIP, and BRMz, are less influenced by IBC, resulting in damage reductions of approximately 10-15%.

The tower fore-aft load TBMz is not affected by the application of IBC for the DK site. However, at the DE site, it's increased by approximately 5%. This divergence can be attributed to the increased probability of wind speeds around the rated region at the DE site since this is the only region where the IBC loop marginally increases the TBMz loads. The highest discrepancy between the two sites is observed in the side-side tower bottom load TBMx. At the DE site, cumulative fatigue damage reduction for TBMx stands at approximately 15%, whereas for the DK site, it is around 25%. Additionally, the cumulative damage reduction for

tower bottom torsion, TBMz, ranges between 15-20% for both sites.

The tower top and low-speed shaft loads TTM<sub>y</sub>, TTM<sub>z</sub>, LSSM<sub>y</sub>, and LSSM<sub>z</sub> display reductions of about 20% for the DE and 25% for the DK site. The tower top roll moment TTM<sub>x</sub> cumulative damage is increased in both cases to a level of 5%. The load with the highest negative impact by applying the IBC is the low-speed shaft torque load LSST<sub>q</sub>, with the increase in cumulative damage reaching levels between 10% and 20% in both cases.

The optimization outputs include the choice of the minimum wind speed threshold to activate the IBC loop as an optimization variable aiming to reduce unnecessary overuse of the pitch actuator and to limit the adverse effects of the IBC loop. The KPIs for varying activation thresholds for the DE\_all and DK\_all datasets are presented in figure 7.6. This allows for quantifying the effect of the threshold on loads and assessing how the different thresholds translate into pitch travel and percentage of time while IBC is activated. Furthermore, the differences in terms of blade pitch travel and percentage of time the IBC loop is active, for various wind speed thresholds, are summarized in table 7.2.

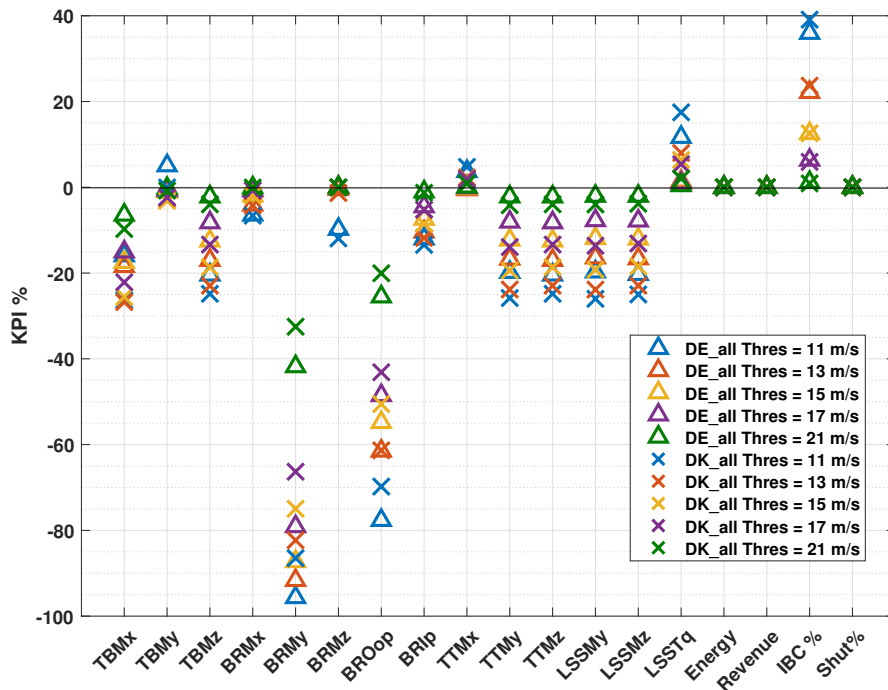


**Figure 7.6:** KPIs by applying the IBC for wind speeds above the threshold considering all years for both locations

The cumulative fatigue damage reductions for the TBM<sub>z</sub>, TTM<sub>y</sub>, TTM<sub>z</sub>, LSSM<sub>y</sub>, and LSSM<sub>z</sub> loads, which show similar responses, have a nearly linear correlation to the threshold, with the level of reduction decreasing as the threshold increases. The TBM<sub>x</sub> load shows small differences for thresholds between 11 and 17 m/s, with the decrease in the effectiveness of IBC in cumulative damage reductions being significantly reduced at the highest threshold only. The blade loads, BRO<sub>op</sub> and BRM<sub>y</sub>, are the most sensitive to the different thresholds. The

Period	V thres 11 m/s		V thres 13 m/s		V thres 15 m/s		V thres 17 m/s	
	Time %	$\Delta$ Ptr %						
DE2016	34.5	456.1	20.7	347.1	11.2	213.8	5.1	110.0
DE2017	37.4	469.6	23.4	367.8	13.1	233.5	6.5	127.7
DE2018	36.1	479.6	22.4	377.2	13.4	254.1	7.4	154.2
DE_all	35.9	468.5	22.2	364.2	12.6	233.9	6.4	130.7
DK2013	36.7	227.2	22.9	178.0	11.4	103.1	5.0	50.1
DK2014	41.8	235.9	27.2	190.8	15.0	119.9	6.9	61.3
DK2015	43.9	242.8	28.0	193.8	16.2	127.8	8.2	73.4
DK2016	36.1	219.3	20.0	162.1	10.8	100.9	4.9	51.6
DK2017	38.3	225.5	23.4	175.4	11.2	98.5	4.9	48.7
DK2018	38.4	228.3	22.8	176.0	12.6	112.3	5.8	58.2
DK2019	38.5	220.7	21.7	163.6	10.5	93.8	5.4	53.5
DK2020	39.1	231.5	23.7	179.2	13.0	112.6	6.3	60.6
DK_all	39.1	229.2	23.7	177.9	12.6	109.1	5.9	57.6

**Table 7.2:** Relative increase in blade pitch travel ( $\Delta$ Ptr %) by applying IBC and percentage of time IBC is active for various activation thresholds considering all years for both locations

effectiveness of IBC in reducing the accumulated damage in these loads is highlighted by the fact that even for the 21 m/s threshold, there is a substantial reduction to a level higher than 20% and 30%, respectively. Blade loads correlated more to edgewise directions, BRMx and BRIp, are also correlated to the threshold, but due to the smaller magnitude of reductions, the changes are relatively small between different thresholds.

For the adversely affected loads, results indicate that the TBMy cumulative damage for the DE site is increased only when the lowest threshold is applied. For higher thresholds, there is a slight decrease or no influence compared to the baseline. The cumulative damage for TTMx is increased for the DE site only for the lowest wind speed threshold. Under the DK conditions, TTMx shows lower increases for lower wind speed thresholds but is, in every case, increased. This suggests that under these conditions, the TTMx load is increased by both power boosting and IBC, and reducing the power level is the only means to counterbalance these increases.

The increase in fatigue damage for the LSSTq load is reduced in both sites by increasing the IBC activation threshold. At the DE site, the damage increase with any threshold above 13 m/s remains below 2%. In contrast, at the DK site, the damage increase for LSSTq remains above 5% until the threshold of 17 m/s. These findings suggest that, within the DK conditions, restricting the LSSTq and TTMx loads in the context of optimization is more challenging, especially for scenarios aiming for revenue increase where power boosting is more pronounced. This shows the dependency of the efficiency of the methods on the local wind conditions and highlights the fact that any possible operational plan aiming for revenue and loads optimization cannot be generalized and has to be site-specific.

Regarding the impact of applying the IBC loop on the blade pitch travel for different wind

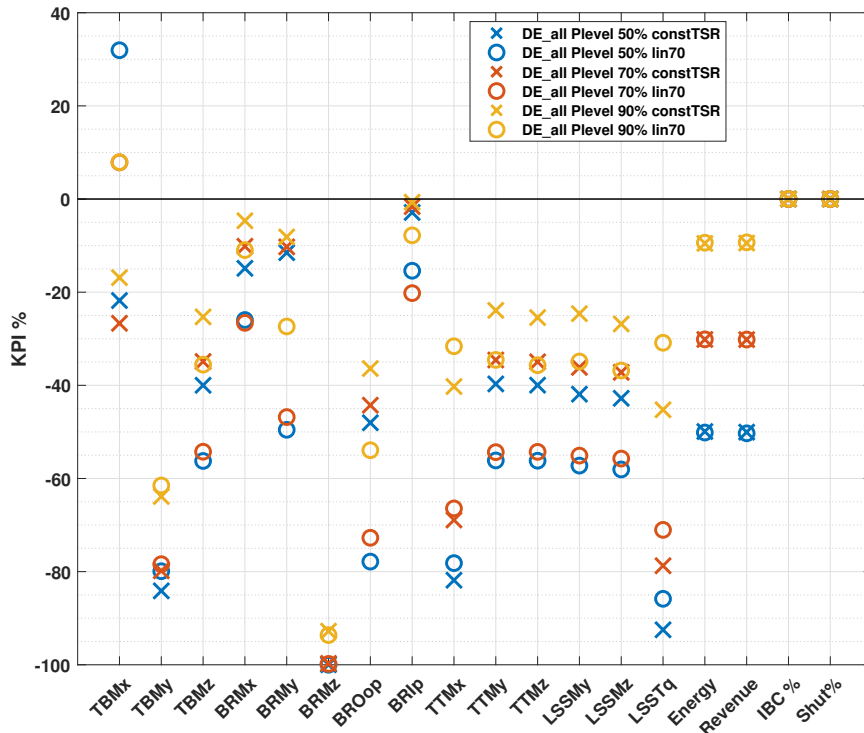
speed thresholds, the results show that despite the higher wind speeds and turbulence intensity at the DK site, the blade pitch travel increase is considerably lower compared to the DE site. Focusing on the entire period for each site for the lower wind speed threshold, IBC is active for 36% of the time and for the DK site for 39%, reflecting the differences in wind speed distributions. However, the relative increase in pitch travel at the DE site is found at a level of about 470%, while for the DK site, it is about half at 230%. This counterintuitive difference could be possibly attributed to differences in the probability of occurrence of wind speeds close to rated in correlation with local turbulence variations. This result shows the need for a detailed, site-specific, analysis when considering the effect of IBC application on the blade pitch actuator.

Moreover, a significant reduction in the increase of blade pitch travel with increasing activation thresholds is observed, with both locations exhibiting similar trends. Increasing the wind speed threshold to 13 m/s shows a decrease in pitch travel increase by 25%, while for the highest threshold, this decrease reaches 75%. These findings highlight the sensitivity of the actuator usage to the IBC activation which, combined with the load alleviation capabilities at different thresholds, can be leveraged to optimize the IBC usage to the necessary for the application. As the results in the following sections don't directly include the relative difference in pitch travel, the reader is referred to table 7.2 in order to quantify the increase in blade pitch travel based on the percentage of time provided with each result. Although the application of power boosting and down-regulation can affect these values, as demonstrated in section 4.3, the difference is small, and the duration of IBC activation can be implicitly used to approximate the blade pitch travel.

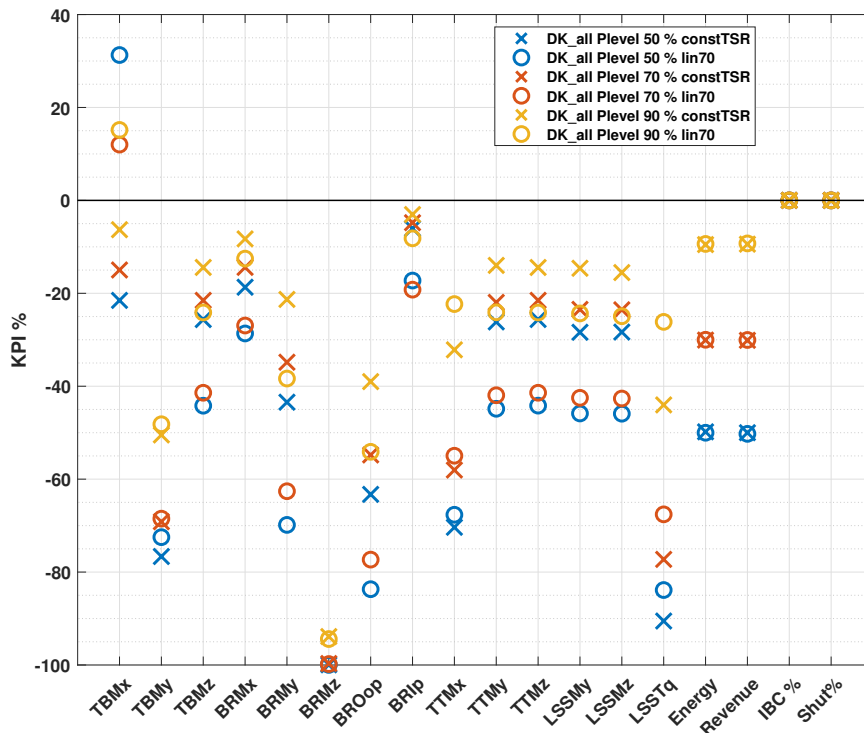
### 7.1.3 Potential by applying down-regulation

To quantify the effect of reducing the power level on loads at the two locations, the response of the turbine was simulated using the evaluation framework considering operation in constant power levels below the baseline. Figure 7.7 presents the relative differences in cumulative KPIs compared to the baseline for the entire period considered in both locations, incorporating both down-regulation trajectories for power levels in the range of 50-90%.

The cumulative fatigue damage for the TBMx load decreases for both datasets when considering the constTSR trajectory. For the DE dataset, TBMx damage is reduced by approximately 15-30%, and this reduction increases as the power level decreases. More than 50% of the maximum possible reduction is achieved already with the 90% power level. For the DK dataset, the reductions are in the level of 5-25%, while the damage reduction is directly proportional to the down-regulation level. As explained in chapter 4, the lin70 trajectory increases the TBMx load due to tower resonances. This leads to a damage increase of up to



(a)



(b)

**Figure 7.7:** KPIs by operating the turbine constantly in different power levels below the baseline for the whole period in both locations considered. Colors indicate the power level and markers indicate the chosen down-regulation trajectory. IBC is not active. (a) DE\_all, (b) DK\_all

30%, with the level increasing as the power level decreases for both datasets.

Regarding TBM<sub>y</sub>, the cumulative damage decreases significantly with both trajectories. For both datasets and trajectories, the majority of the reduction is achieved until the 90% power level, with a lower rate of decrease as power levels further reduce. The two trajectories show similar performance in damage reductions. For the DE site, the calculated damage reductions are between 60% and 85% for all power levels. The reductions for the DK site are lower at a level of 50-75%. The same trend is observed for the TBM<sub>z</sub> load, with the cumulative damage reduced more for the DE site, at a level of 25-55%, compared to the DK site, where reduction ranges between 15% and 45%. In both cases, the lin70 trajectory is more effective in reducing the TBM<sub>z</sub> damage. For both trajectories, most of the reduction is achieved already at the 90% power level.

For the blade loads, the blade root torsion BRM<sub>z</sub> cumulative fatigue damage is reduced the most by down-regulation. These reductions surpass 90% for all considered power levels, primarily due to the significant load reductions in the rated region. For the BRM<sub>x</sub> and BRIP loads, cumulative damage is reduced to levels of 0-25% for the DE site and 5-30% for the DK site. The lin70 trajectory is more effective in reducing the damage for both loads due to the reduced rotor speed, while for the BRIP load, the constTSR trajectory has no effect.

The BRM<sub>y</sub> cumulative damage is reduced more with the lin70 trajectory compared to the constTSR. At the DE site, the reductions are nearly identical for all power levels at about 10% with the constTSR trajectory. In contrast with the lin70 trajectory, reductions range from 25 to 50%. Under the DK conditions, the BRM<sub>y</sub> cumulative damage decreases by 20-45% with the constTSR and 35-70% with the lin70 trajectory. For both trajectories, the fatigue reduction to down-regulation ratio is higher until 90% power levels and reduces below that. These trends are similar for the BROop load, which exhibits a larger magnitude of reductions compared to BRM<sub>y</sub> for both datasets and trajectories.

The cumulative damage of the tower top TTM<sub>x</sub> reduces significantly with down-regulation for both sites. The two trajectories show similar behavior both in terms of trends and magnitudes. For the DE dataset, the achievable reductions range between 30% and 80%, and for the DK dataset, within the range of 20-70%. Additionally, the cumulative fatigue damage of the shaft torque load LSST<sub>q</sub> is also significantly reduced by down-regulation, with the constTSR trajectory performing better for both datasets. The observed reductions range from 25 to 90% for both sites. The cumulative damage reduction of both TTM<sub>x</sub> and LSST<sub>q</sub> exhibit similar behavior in both sites with respect to the power levels. In contrast to the rest of the considered loads, the rate of reduction is relatively constant until 70% and diminishes for lower power levels.

The response of the TTM<sub>y</sub>, TTM<sub>z</sub>, LSSM<sub>y</sub>, and LSSM<sub>z</sub> loads is similar in terms of cumulative damage reductions by applying down-regulation. The reductions are relatively higher when

applying the lin70 trajectory, reaching levels of 35-55% for the DE dataset and lower levels of 25-45% for the DK one. Employing the constTSR trajectory, reductions reach levels between 25% and 45% for the DE dataset and 15-30% for DK. For both trajectories and locations, the rate of damage reduction is higher for power levels down to 90% and declines for lower levels.

These results demonstrate that IBC and down-regulation can be complementary methods for reducing the cumulative damage across the loads ensemble for both datasets. The cumulative damage of the TBMy, LSSTq, TTMx, and BRMz loads is highly influenced by down-regulation, while IBC has either adverse or no effects. The cumulative damage of BRMx and BRIp is affected to a smaller extent by down-regulation, while applying IBC has a lower but still positive influence. For the BRMy and BROop loads, both methods significantly reduce cumulative damage, with IBC having the greater influence. For the TTMy, TTMz, LSSMy, and LSSMz loads, cumulative damage is moderately reduced by both methods, with down-regulation showing higher decreases.

Moreover, the effects of applying IBC showed to be similar across the different loads in the two sites, while down-regulation showed differences between the two sites. This suggests that the impact of down-regulation, as a fatigue reduction method, is more dependent on the specific wind conditions compared to IBC, with both wind speed distributions and TI levels contributing to these variations.

Finally, it is worth noting that the load response behavior in down-regulation, as discussed in section 4.3, regarding the power levels, carries over to the cumulative damage analysis presented here. The cumulative damage of the TBMy, TBMz, BRMy, BRMz, BROop, LSSTq, TTMy, TTMz, LSSMy, and LSSMz loads decreases at a higher rate with down-regulation levels until 90% while for lower levels, the rate of decrease diminishes. This signifies that low levels of down-regulation can effectively influence damage accumulation with a lesser impact on revenue.

#### 7.1.4 Potential by applying selective shutdown

Selective shut-down based on a projected revenue threshold is the third load reduction method considered in the context of the operational management optimization method suggested in this work. As explained in section 5.3, the effect on fatigue of shutting down and starting up the wind turbine is not considered in this work. Hence, selective shut-down is used in the optimization to reduce the added damage of the time step to zero while no revenue is generated in the time step.

The effect of different thresholds under the various wind and market conditions is examined here, as one of the optimization variables involves the threshold for selective shut-down. The results in terms of KPIs for different revenue thresholds are presented in figure 7.8, considering the entire period in all cases. The thresholds selected for this analysis were chosen in order

to ensure that cumulative revenue decreases by less than 10%, and additional shutdown time does not exceed 30% of the total period.

As shutting down has a drastic effect on revenue and the definition of thresholds is sensitive to the temporal variations of the electricity market prices, assigning a general threshold for a period covering multiple years is not useful in practice. This approach is used solely to examine the general trends of the potential fatigue damage reductions.

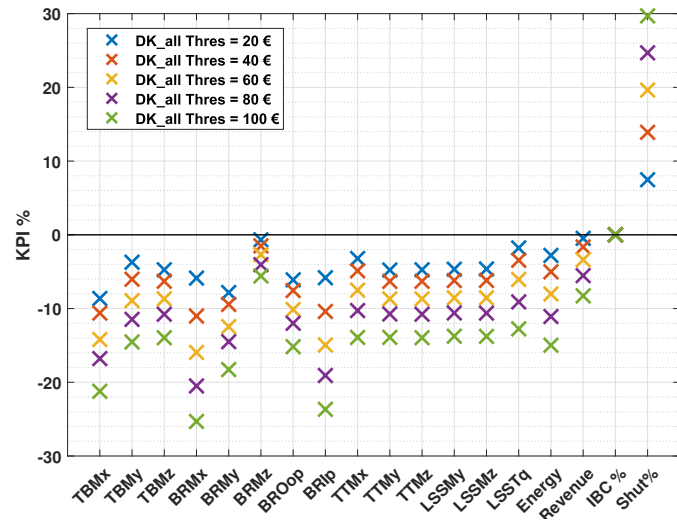
Revenue magnitude is influenced by the electricity price as well as the wind speed, which in turn defines the power production. Consequently, a low price and/or a low wind speed can lead to low revenue. From a fatigue alleviation perspective, this means that the most effective cases are the ones when low prices occur in combination with rated or above-rated wind conditions, depending on the aeroelastic response of each load. This implies that the method will be most effective in markets where electricity prices are more correlated with wind energy production. This observation is indeed verified by comparing the results of loads with a high correlation to the wind speed, such as TBMx, TTMy, or LSSMY, between the DK\_all and DE\_all cases. Fatigue damage reduction is higher for the DK site for similar thresholds and percentages of downtime.

In all cases, the most influenced loads are the blade root BRMx and BRIp loads. This can be attributed to the fact that these loads are the ones varying the least over wind speeds. Thus, shutting down at any wind speed is equally effective, resulting in higher overall cumulative damage reductions compared to the other loads.

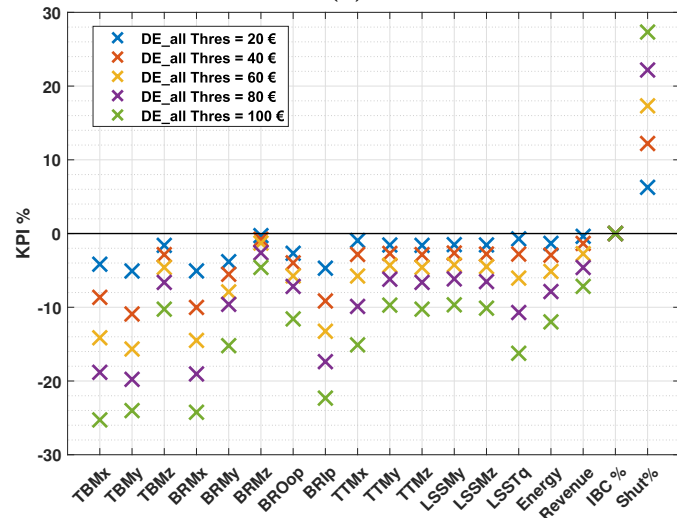
For the DK\_all dataset, the lowest threshold leads to a revenue reduction of less than 0.5%, which translates to a reduction of energy production of approximately 3%. The total additional downtime for this threshold is 8%. For the highest threshold, revenue reduction reaches 8% with a 15% reduction in energy production, corresponding to 30% additional downtime.

Moreover, for the lowest threshold, the cumulative damage reduction is fairly constant for the TBMz, BRMx, BROop, BRIp, TTMy, TTMz, LSSMy, and LSSMz to a level of 5-6%. For the highest threshold, the reduction reaches a level of approximately 15%. The most significant fatigue reductions are observed for the TBMx and BRMy loads, reaching 8% for the lowest threshold and nearly 20% for the highest. For the BRMx and BRIp loads, the expected range of damage reductions falls between 6% and 25%. The least affected loads are LSSTq and BRMz, with a reduction of less than 2% for the lower threshold and up to 13% and 6%, respectively, for the highest threshold. This is due to the damage distribution of these loads being highly concentrated on the rated wind speeds, which are less probable to be affected by shutdowns since, as shown earlier for both sites, this is the region where the probability of very low prices is lower.

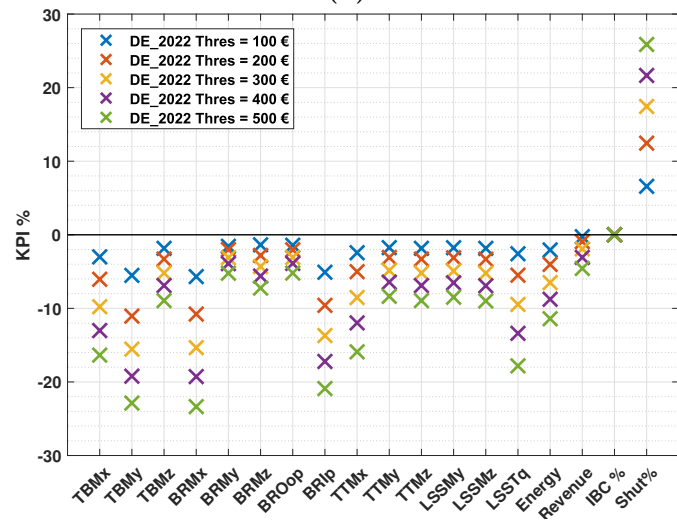
Regarding the DE\_all dataset, applying the lower threshold leads to a 0.4% reduction in



(a)



(b)



(c)

Figure 7.8: KPIs by applying selective shut-down based on projected revenue thresholds. (a) DK\_all, (b) DE\_all, (c) DE\_2022

revenue and a 1.5% decrease in energy production, with an additional downtime of approximately 6%. When considering the highest threshold, revenue reduction is found at 7%, and the energy reduction is 12% for an additional downtime of 28%. The influence of the market conditions can be observed by comparing with the DE\_2022 case, where the downtime and energy envelopes are similar, but the revenue reduction envelope is narrower, ranging from 0.3% to 4.5%.

Examining the cumulative damage response for the DE\_all and DE\_2022 datasets, the TBMz, TTM<sub>y</sub>, TTM<sub>z</sub>, LSSM<sub>y</sub>, and LSSM<sub>z</sub> loads have a similar response for the lowest and highest thresholds with reductions varying between 2% and 12%. Likewise, the TBM<sub>y</sub>, BRM<sub>x</sub>, and BRIP loads have similar responses for the two cases with a reduction envelope ranging from 4% to 24%. The BRM<sub>z</sub> load shows the least sensitivity to the method, similar to the DK\_all dataset, with reductions in the range of 0-8% for both cases.

The LSST<sub>q</sub> and TTM<sub>x</sub> loads display similar trends with a cumulative damage reduction envelope of 1-16%. The blade root loads BRM<sub>y</sub> and BROop show a reduction envelope of 4-16% for the DE\_all dataset while for the DE\_2022, this range narrows to 1-4%, showing the highest discrepancy resulting from the different market conditions. Moreover, the cumulative damage reduction envelope for the TBM<sub>x</sub> load is 4-26% for DE\_all and 2-16% for the DE\_2022. These findings suggest that for the DE\_2022 market environment, potential load reductions by selective shutdown can be lower but also come with a smaller impact on revenue.

The analysis of the expected fatigue and revenue envelopes shows the high sensitivity of revenue and energy production to the selective shutdown approach, indicating that it has to be cautiously applied. The analysis suggests that selective shutdown can be effectively used for small load reductions and peak shaving but may not be suitable for substantial load reductions. This is due to the significant influence on both revenue and energy production, resulting in a substantial tradeoff between fatigue damage reduction and revenue.

### 7.1.5 Potential by applying power boosting

To assess the potential for increasing revenue through power boosting, the turbine response was simulated using the evaluation framework while considering constant power levels. The results, in terms of relative differences to the baseline in cumulative revenue under fluctuating market prices, are presented in figure 7.9.

The maximum increase in revenue for the 130% power level is approximately 14% for both locations when considering the entire dataset. The DK dataset exhibits higher inter-annual variability with values ranging between 13 and 16%. In contrast, the DE\_all dataset shows less variation, with the maximum difference being 0.5% between all years. However, when considering the 2022 prices, the maximum potential revenue increase reaches 15.5%. As anticipated, the revenue increase is almost linearly correlated with the power level, with minor

deviations stemming from the increase in rated speed as power levels increase.

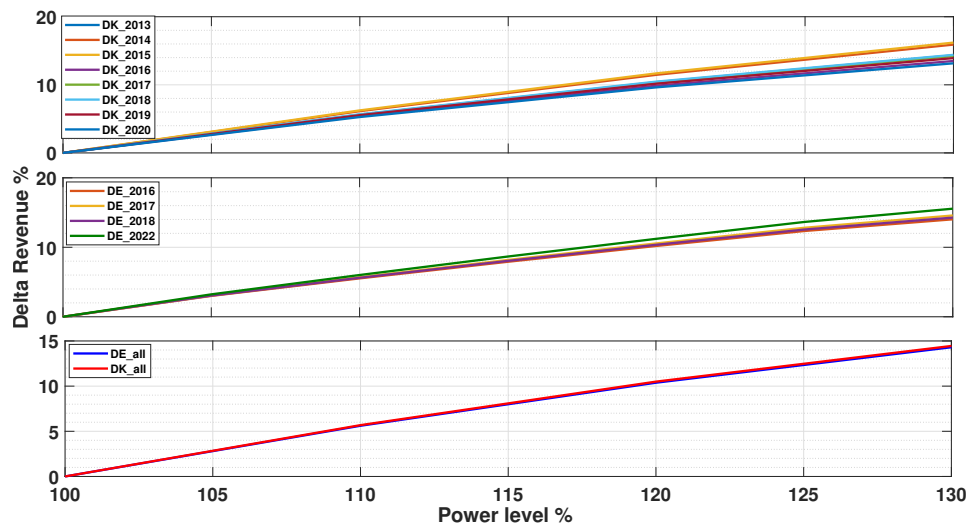


**Figure 7.9:** Expected relative increase in revenue compared to the baseline operation by constantly applying different levels of power boosting under fluctuating prices

The impact of constant power boosting on loads is quantified in figure 7.10, which presents the results for constant down regulation under fixed prices. In all cases, revenue is increased by 1-2% compared to fluctuating prices for both market conditions considered.

The trends in load increases are similar for both datasets, with the magnitudes diverging due to the different wind distributions and correlated TI levels. The BRMz load shows the highest sensitivity to power-boosting levels, reaching relative damage increases up to 700% for DK and 600% for DE. The second most affected load is also at the blade root, BROop, showing maximum increases of 240% for DK and 200% for DE. Moreover, the BRMy and LSSTq loads show similar responses with an increase of up to 80% for DE and 140% for DK.

The TBMy and TTMx loads display similar responses to power-boosting, showing an increase of up to 70% for the DE and 85% for the DK site. The TBMz, TTMy, TTMz, LSSMy, and LSSMz loads exhibit similar responses to power-boosting with relatively low increases up to 40-45% for both cases. The least influenced loads across all cases are the TBMx, BRMx, and BRIp loads, indicating that loads related to side-side and edgewise directions are, in general, less affected by both power boosting and down-regulation. It is worth noting that for all loads, cumulative damage increases proportionally with increasing power level, in contrast to down-regulation, where it was shown that decreases are higher for power levels down to 90%.

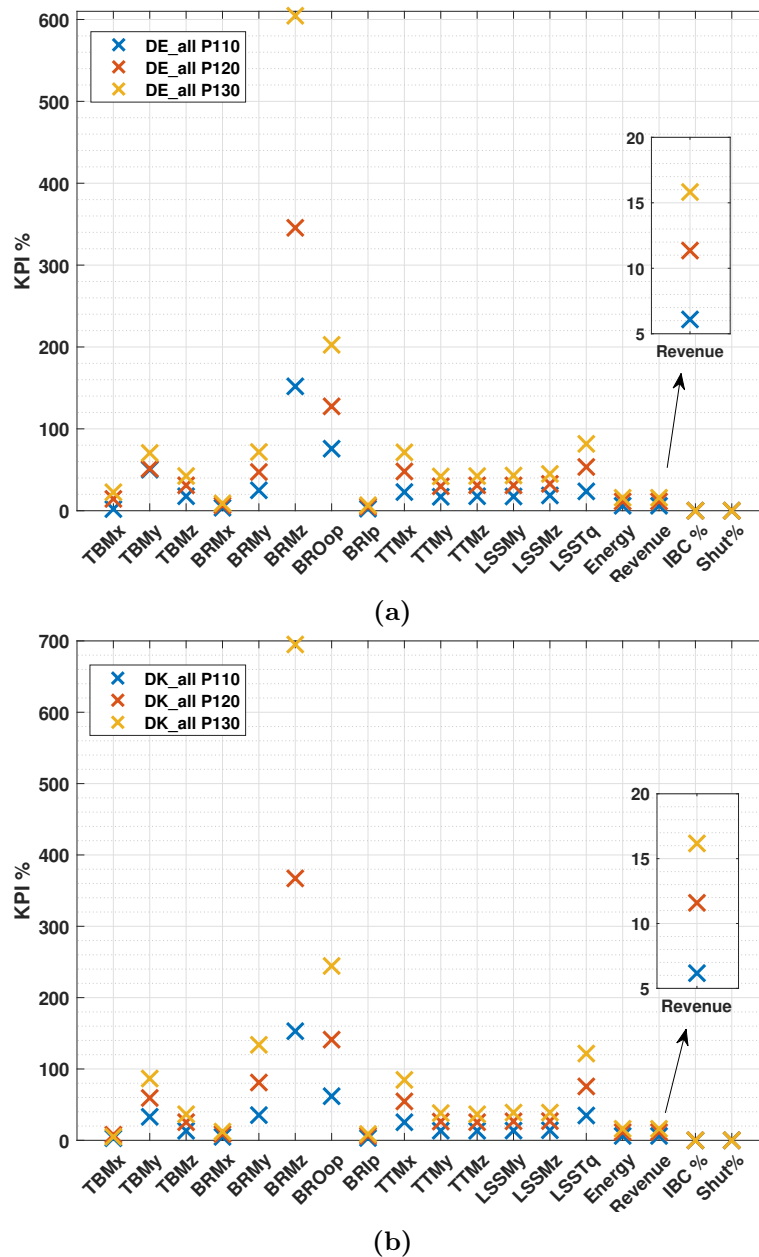


**Figure 7.10:** KPIs by applying constant power boosting for the whole period considered and both locations under fixed prices (a) DE\_all, (b) DK\_all

## 7.2 Optimization under fixed prices

This section presents and discusses the results of optimizing cumulative revenue and fatigue under fixed prices. Both optimization approaches, based on the mean wind speed distributions and based on forecast horizons, are used and compared. The results are divided into two cases; the first prioritizes fatigue damage minimization as the main objective, and the second focuses on revenue maximization according to the scenarios outlined in section 6.2. Additionally, a sensitivity study is conducted to explore the effects of mean wind speed distribution uncertainty on the optimization process.

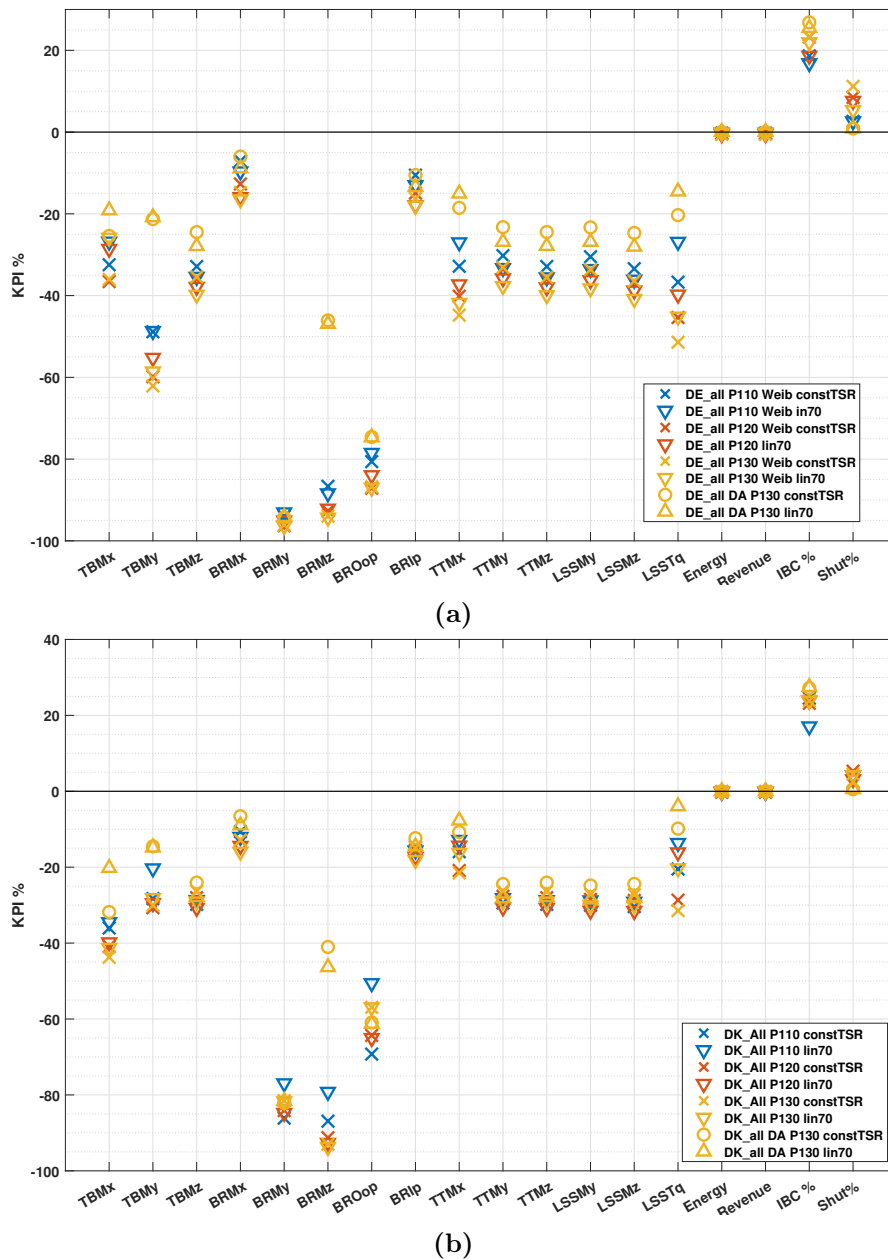
### 7.2.1 Fatigue damage minimization under fixed prices

Figure 7.11 presents the results for the scenario of revenue-neutral load minimization under fixed prices. The results include varying maximum power levels from 110% to 130% and employ both down-regulation datasets for the DE\_all and DK\_all datasets. Higher cumulative fatigue damage reductions are achieved across the entire load ensemble, along with reduced IBC activation, compared to the constant application of IBC as a standard feature discussed in section 7.1.2. Moreover, the cumulative revenue and energy production are maintained at the baseline level.

The optimization based on wind speed distributions performs better than the DA forecast-based approach. This is expected as the optimizer considers the long-term distribution and can assign control modes more effectively. In contrast, the DA approach is limited to independent consecutive short-term optimizations without awareness of the long-term effects. This is more pronounced in the DE dataset, possibly due to less variability in wind conditions. The BRMz load, in both datasets, shows the highest discrepancy between the two approaches. As BRMz is only reduced by down-regulation while it is significantly increased by power boosting, it can be more effectively reduced when the whole distribution is considered, while the intraday variations don't allow for effective power and load balancing. Specifically, the BRMz damage is reduced by 40-45% with the DA approach and by more than 80% with the Weibull-based approach for both sites.

The results for the TBMy load exhibit high sensitivity to the optimization approach, as well as site-specific conditions. Considering the DE\_all dataset, the DA-based optimization shows fatigue damage reductions around the 20% level while the distribution-based approach achieves reductions of 50-60%. However, considering the DK\_all dataset, the difference between the two approaches is much smaller. The DA-based results show reductions of 15%, and the Weibull-based approach yields reductions of 20-30% for all power levels. This difference can be explained by the distinct distributions of damage over wind speeds in the two sites, as shown in figure 7.3. For the DE site, more damage is contributed within the above-rated wind speed range, while for the DK site, this damage is shifted towards lower wind speeds. This highlights the importance of thoroughly considering site-specific conditions when evaluating potential fatigue reductions.

Regarding power levels, increasing the maximum power boosting level leads to greater accumulated fatigue reductions. This is explained by the higher margin for down-regulation allowed by the higher power boosting level, which compensates more for the revenue decrease. Nevertheless, in all cases the differences are relatively small, indicating that the majority of the potential fatigue reduction can be achieved with a maximum power level of 110%. The variations between power levels are more pronounced for the DE site, where the lower variation



**Figure 7.11:** KPIs for revenue-neutral load minimization cases under fixed prices using both trajectories for the entire period considered for both locations and different maximum power levels. Optimization cases based on wind speed distribution are denoted as Weib, and cases based on day-ahead forecasts of wind speeds are denoted as DA. P110, P120, and P130 denote the maximum power level allowed for each case. (a) DK\_all, (b) DE\_all

of wind conditions over time enables the optimizer to adjust the control modes more accurately for different maximum power levels. This different behavior between the two sites is more evident in the TBMz, TTMz, TTMz, LSSMy, and LSSMz loads, which show similar responses. For the DE dataset, the cumulative fatigue reductions vary between 25% and 40%, while for the DK site, the range of variation is less than 3% with a reduction of approximately 30% for all power levels.

The load influenced the most by IBC, BRMy, exhibits low sensitivity to the maximum power level. The BRMy load shows a decrease in cumulative damage of 80-85% for the DK site and 93-95% for the DE site across all power levels. The similarly behaving BROop load shows a relatively lower sensitivity to power levels, while the magnitude of reductions is lower than the BRMy. Although both loads are significantly influenced by IBC, the higher concentration of damage contribution in the rated wind speed region for the BROop load leads to lower overall cumulative damage reductions and a higher dependency on down-regulation for load management. It is worth noting that the BROop results for DK\_all are the only case where the reductions are increasing with decreasing maximum power level.

The LSSTq load shows the most variations across the different power levels for both datasets. Since this load is increased by IBC and is less sensitive to low levels of down-regulation while the major damage contributions come from a small range of wind speeds, it is of particular interest for fatigue minimization scenarios. The fatigue reduction for the different power levels, using the wind speed distribution-based method, varies within 25-55% for the DE site and 13-30% for the DK site.

The least influenced loads overall are BRIp and BRMx, showing low sensitivity to the different datasets, trajectories, and power levels with decreases of 5-20% for every case. As the blades are an expensive component of the structure and the impact of the different directions of loading on lifetime is highly dependent on the specific design, these loads can potentially be the decisive factor for the duration of possible lifetime extension. Nevertheless, this has to be evaluated taking into account the specific design and costs and cannot be determined with the present depth of analysis.

The fatigue reductions for the TTMx load show a sensitivity to the maximum power level for the DE site varying between 25% and 45%, while for the DK site, the reductions are smaller and less sensitive to power levels ranging within 10-20%. This is explained by the fact that TTMx can only be reduced with down-regulation while above-rated wind speeds have higher damage contributions for the DK site.

Regarding the differences between the two down-regulation trajectories, they show overall similar performance when considering revenue-neutral load minimization. The highest discrepancies are found for LSSTq, which can be more effectively reduced using the constTSR trajectory, which showed 5-10% higher reductions compared to the lin70 for all power levels and methods. Moreover, the differences between the two trajectories are more pronounced for the DE site while for the DK site, except for the LSSTq and TBMx loads, all other loads are practically unaffected by the trajectory choice. Interestingly, the TBMx load, which was shown to be negatively affected by down-regulation using the lin70 trajectory, shows similar reductions with both trajectories. For the DE site, these reductions are found at levels of 25-35%, and for the DK site, 35-45%. This example shows the effectiveness of the proposed

optimization approach to leverage and combine the advantages of each individual control mode to achieve the objectives.

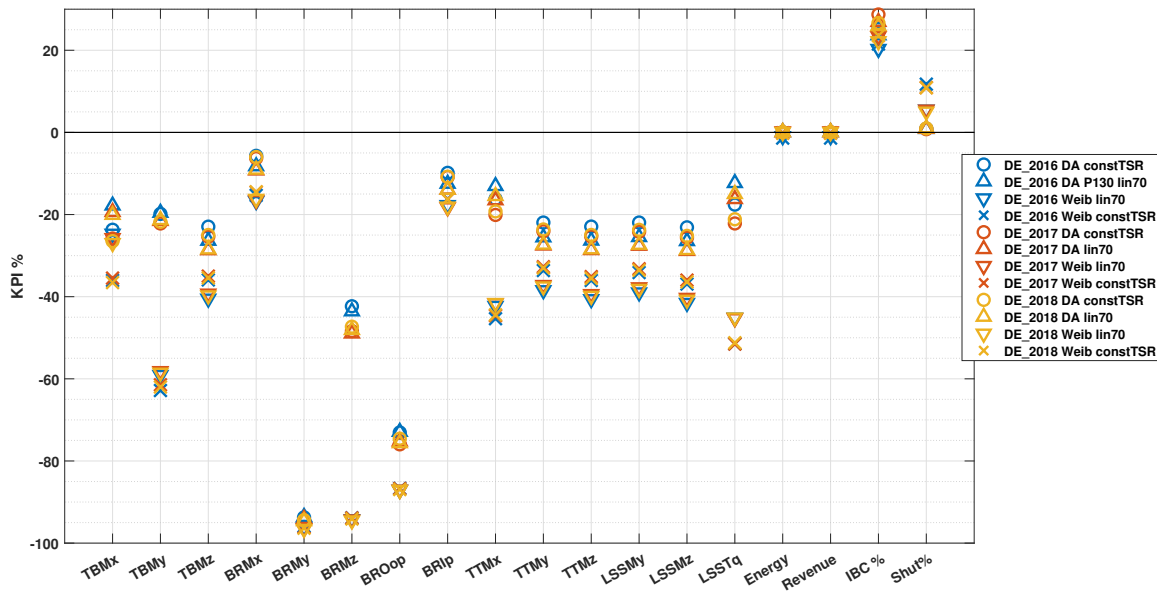
Regarding IBC activation, the results indicate that for the DK dataset, for most of the wind distribution-based cases, IBC is active for approximately 20% of the time. Beyond this point, further increases in IBC activation seem to yield diminishing results and have adverse effects on some loads. This level of activation translates to an increase in blade pitch travel of 150-190% across all power levels and trajectories. For the forecast-based optimization, this is slightly increased to 210%. For the DE dataset, the IBC activation duration falls within the range of 15-25% of the total time and slightly increases with increasing power levels. This increase in activation corresponds to an increase in blade pitch travel of 350-430%.

The downtime due to the application of selective shutdown for the DE dataset increases with the power level and is slightly higher for the constTSR cases. The additional downtime ranges between 3 and 12% for all cases, with values increasing proportionally with the maximum power level. For the DK site, the results suggest an upper limit of about 4% of additional downtime applicable for all cases. When considering the DA-based optimization approach, the downtime is nearly zero for both datasets, since the limited horizon windows do not allow for effective revenue balancing when selective shutdown is applied frequently.

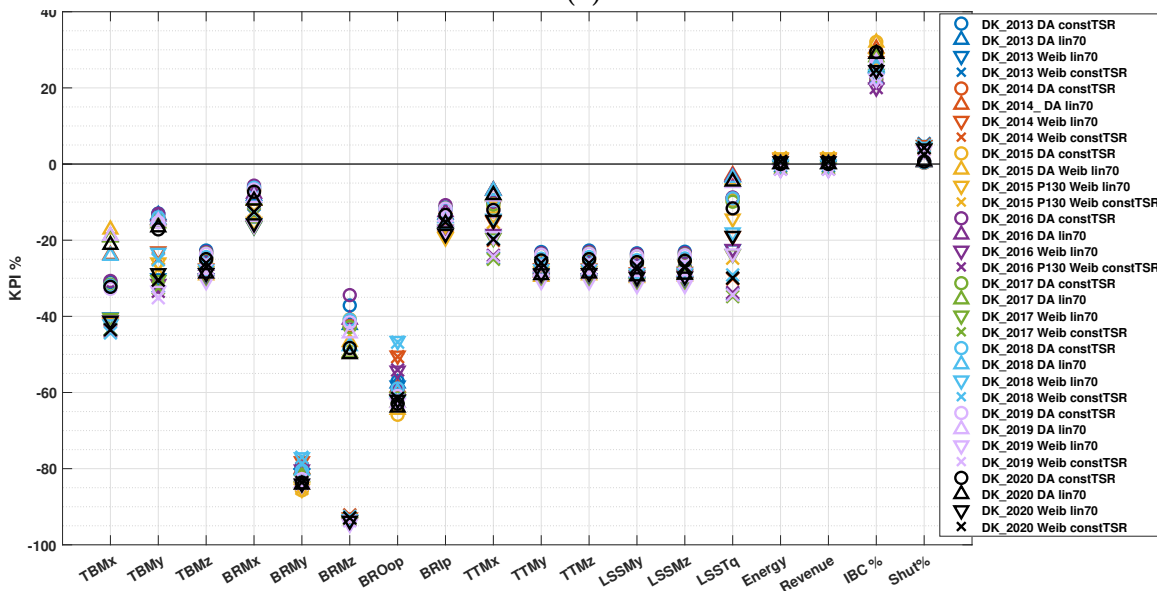
Figure 7.12 presents the KPIs for revenue-neutral load minimization and a maximum power level of 130% per year. This analysis allows examining the inter-annual variability in the response to optimization for each site. For the DE site, which exhibits lower variability in conditions over time, the results remain relatively constant from year to year when the optimization based on wind speed distribution is considered, while variations up to 5% are observed for the forecast-based approach. Conversely, at the DK site, variations of up to 20% are evident across different years when employing the same optimization approach. The highest variations are observed for the BROop, LSSTq, and TBMy loads. These findings suggest that the efficiency of the long-term optimization strategy has to be evaluated using sufficiently large historical data. The necessity for a larger dataset becomes more pronounced as wind conditions exhibit greater variability, both intra- and inter-annually.

The optimization outputs in terms of power level assignment per wind speed bin for revenue-neutral load minimization considering wind speed distributions for both down-regulation trajectories and varying maximum power levels are presented in figure 7.13.

The general trend remains consistent across all cases, with power levels varying between 90-100% for below-rated wind speeds with a peak close to 8 m/s. Within the rated wind speed range of 9-13 m/s, power levels decrease further with a valley at the rated speed. For higher wind speeds, power levels increase continuously until the maximum power level is reached and thereafter remains constant. Additionally, in some cases for the DE site, the power is again reduced in the highest speed range close to the cut-off. This aligns with previous findings



(a)



(b)

**Figure 7.12:** KPIs for revenue-neutral load minimization under fixed prices using both trajectories per year and per location. Optimization cases based on wind speed distribution are denoted as Weib. Cases based on day-ahead forecasts of wind speeds are denoted as DA. The maximum power level allowed is 130% for all cases. (a) DE results per year, (b) DK results per year

regarding the aeroelastic response for the different control modes (see section 4.3), where it was shown that power levels down to 90% yield a higher load reduction-to-revenue loss ratio. Furthermore, as demonstrated earlier, the rated region is crucial for most loads, offering the highest potential for load reductions, thus justifying the assignment of lower power levels within this region.

The main difference between the results for different maximum power levels is that in the

below-rated and rated regions, the assigned power levels decrease as the maximum power level increases. Additionally, the point at which the maximum power level is reached is shifted towards higher wind speeds with increasing maximum power levels. This suggests that a large part of the load reductions is achieved by down-regulation. Simultaneously, the increased power levels in high wind speeds, in combination with the IBC activation, compensate for the revenue reductions caused by down-regulation while also restricting the increase in loads due to power-boosting.

Comparing the results with regards to the down-regulation trajectory, it can be seen that when considering the lin70 approach, the peak in power in the below-rated region and the valley at the rated region are both increased compared to the constTSR. This highlights the impact of the set point choice on the resulting operational schedule.

Finally, it is worth noting that this scheduling of power levels over wind speeds becomes smoother as the amount of allowed iterations in the optimization increases. Due to the nature of the heuristic optimization algorithms used, this cannot be avoided. Therefore, it is advisable

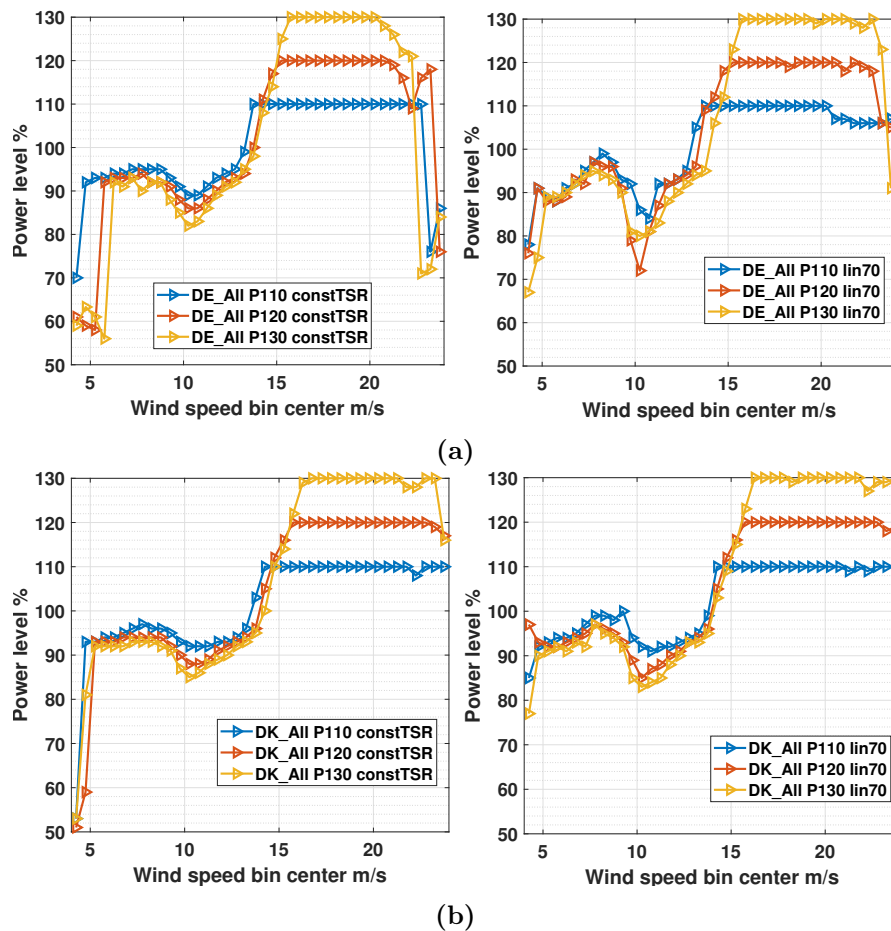


**Figure 7.13:** Power level per wind speed bin resulting from revenue-neutral load minimization for all locations and trajectories. Maximum power levels denoted as P110, P120, and P130. (a) DE\_all, (b) DK\_all

to allow the optimizer to run longer despite the additional computational cost. Additionally, exploring the potential for manual smoothing may be considered for further fine-tuning.

### **Fatigue damage minimization with a revenue reduction cap under fixed prices**

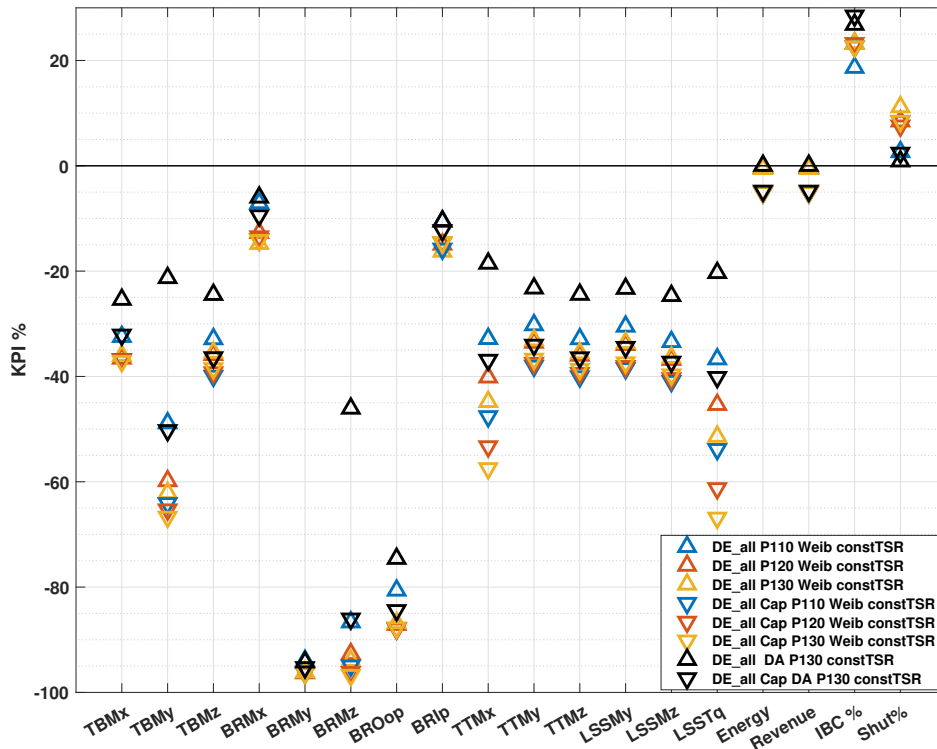
The scenario of fatigue load minimization is further explored with additional cases where the revenue is allowed to decrease, as explained in chapter 6. In these cases, a revenue reduction cap of 5% is applied to examine the potential of further fatigue load reductions compared to the revenue-neutral case.

The results for the DE\_all dataset considering varying power levels and both down-regulation trajectories are shown in figure 7.14 where they are plotted against the results for the revenue-neutral cases. For all cases, the tracking of the revenue objective is accurate, with the reduction in accumulated revenue deviating less than 0.1% from the target value.

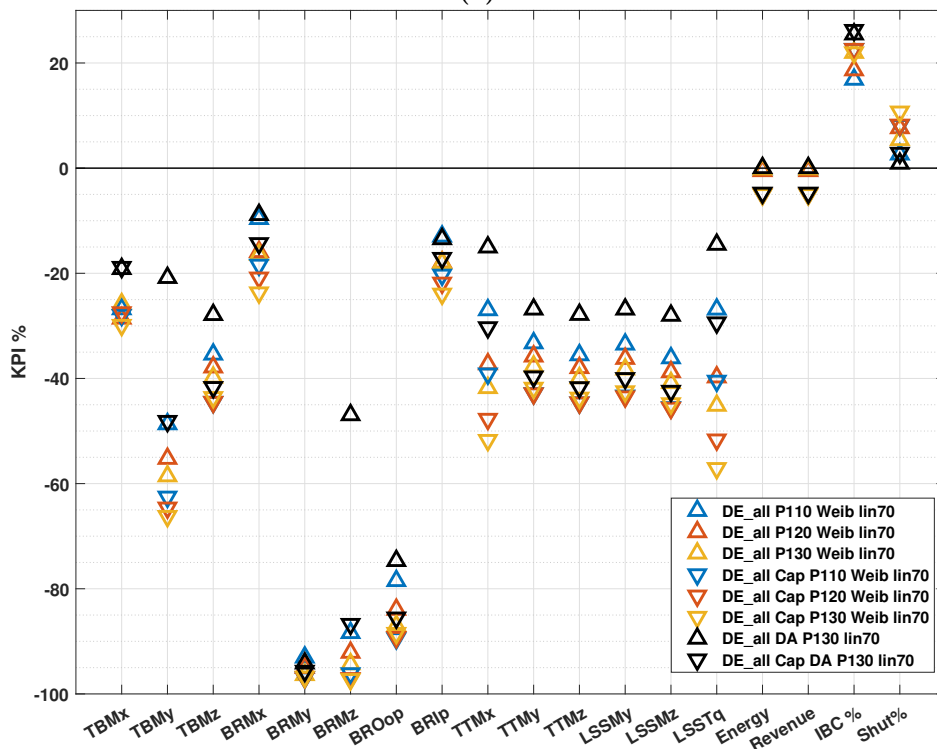
The introduction of the revenue cap is more effective in further reducing the cumulative fatigue when the DA forecast-based optimization approach is used compared to the wind speed distribution approach for both down-regulation trajectories. This can be attributed to the higher versatility provided by the revenue cap, allowing for more effective optimization in the short time interval while leveraging the day-to-day variability. In contrast, the distribution-based approach has less flexibility in this regard. Furthermore, the metrics in terms of IBC activation and downtime are not significantly affected by the revenue cap, with differences of less than 2% observed in most cases.

Considering the Weibull distribution-based optimization approach, the additional cumulative fatigue reductions with the revenue cap are minimal when considering the constTSR trajectory. For all loads, except TTMx and LSSTq, the additional reductions remain below 5%. The only exception is for the TBMy load for a maximum power level of 110%, where a significant additional fatigue reduction of 25% is observed. For the TTMx and LSSTq loads, the additional reductions for all power levels fall within the range of 10-15% when considering the revenue cap. Concerning the lin70 trajectory, the trends are similar, with slightly higher additional fatigue reductions observed for the less impacted loads. In contrast, the more impacted TTMx and LSSTq loads show slightly lower additional reductions up to 10%.

With respect to the DA optimization, substantial additional fatigue reductions can be achieved when employing the revenue cap. Apart from the BRMx and BRIp loads, which are practically unaffected, and the TBMx load, which displays slightly higher reductions, all other loads show significant additional reductions compared to the revenue-neutral case. The most influenced loads include TBMy, BRMz, TTMx, and LSSTq, with additional reductions roughly doubling those observed for the no-cap case. The highest differences are found for the TBMy and BRMz loads, where reductions compared to the baseline increase by 25% for the TBMy



(a)



(b)

Figure 7.14: KPIs for load minimization cases including a revenue reduction cap of 5% for the DE site. Both trajectories for the entire period considered and different maximum power levels 110%-130%.

(a) constTSR, (b) lin70

load and 40% for BRMz. The rest of the considered loads show additional fatigue reductions in the range of 10-15% for both trajectories and all power levels. It's worth noting that despite these considerable additional reductions achieved with the DA optimization approach under the revenue cap, the attained reductions are either lower or equal to the distribution-based reductions achieved without the revenue cap for the DE\_all dataset.

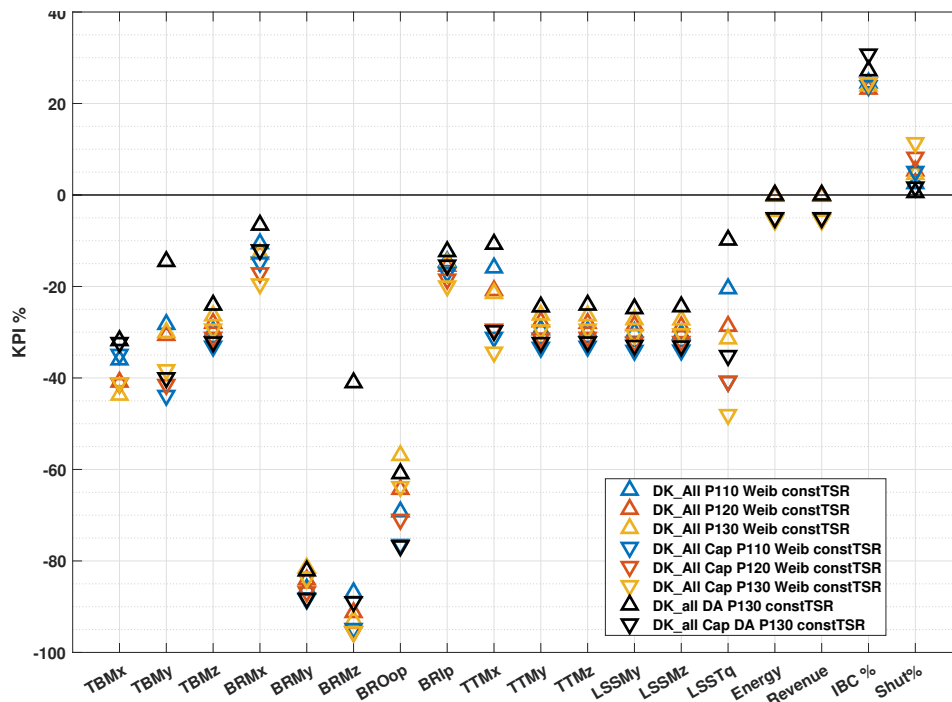
The relevant results for the DK\_all dataset are presented in figure 7.15. The results for the DA-based optimization with the lin70 trajectory are not included due to limitations in available computational power. Nevertheless, the limited obtained results (not shown here) exhibit similar trends to the constTSR trajectory.

The general trends in the DK\_all results are similar to those in the DE\_all results. The revenue reduction cap target was also reached accurately in the DK\_all case. This shows that revenue caps can be robustly tracked under a variety of wind conditions when considering operation under fixed prices. For the distribution-based optimization, the highest additional fatigue reductions of 10-15% are found for the LSSTq and TTMx loads. Besides these loads, for the DK dataset, the TBMy and BROop loads also show additional reductions of 5-13%. For the remaining loads considered, including the 5% revenue cap increases the fatigue reductions by less than 5% compared to the no-cap case.

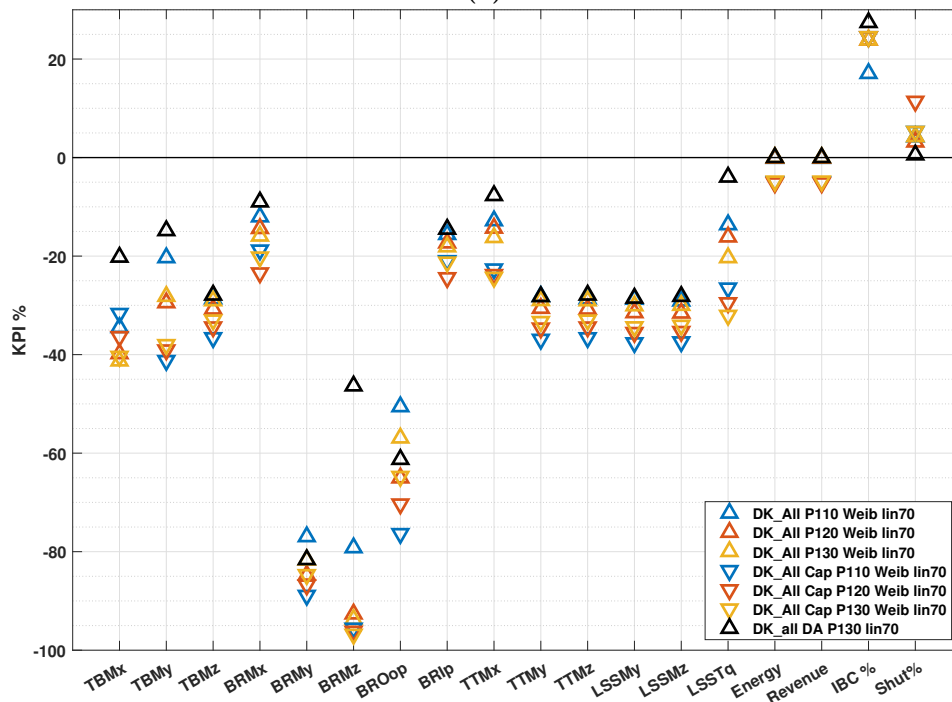
The forecast-based approach also shows similar trends for the DK\_all dataset, with the revenue cap leading to significant load reductions. The most significant additional reductions are observed for the TBMy, BRMz, TTMx, and LSSTq loads at 25%, 45%, 20%, and 25%, which correspond to values higher than double the no-cap case. For the remaining loads, except for TBMx, BRMx, and BRIp, which are practically unaffected by the revenue cap, the rest are additionally reduced by 5-8% with the cap. In contrast to the DE dataset, the additional reductions achieved by the DA approach with the revenue cap result in lower reductions compared to the Weibull-based approach without the cap. In some instances, these reductions even fall below the levels observed for the Weibull-based approach with the cap. This is due to the different wind conditions at the DK site, which already allow the DA-based optimization results to be close to the Weibull-based. This is the major difference observed in the behavior of the load minimization with a revenue cap case regarding the effect of the boundary wind conditions.

The results in terms of power level assignment per wind speed bin for load minimization with a revenue cap considering wind speed distributions for both down-regulation trajectories and varying maximum power levels are presented and compared to the revenue-neutral results in figure 7.16.

The main differences between the results when implementing the revenue cap compared to the revenue-neutral cases are the further reduction of power levels within the rated wind speed region reaching 80% and below as well as the increase of the wind speed where the maximum



(a)



(b)

**Figure 7.15:** KPIs for load minimization cases including a revenue reduction cap of 5% for the DK site. Both trajectories for the entire period considered and different maximum power levels 110%-130%.

(a) constTSR, (b) lin70

power level is reached in the above-rated region. This explains the low efficiency of this method to reduce the fatigue loads as, for most loads, the rate of reduction for power levels below 90% decreases, and the revenue-load reduction tradeoffs become more prominent. This effect is amplified by the fact that, for both sites (and typically for most wind farm locations), the rated wind speed region has the highest probability of occurrence, making it challenging to reduce the loads further without significant revenue loss.

Overall, applying a revenue reduction cap in load minimization cases under fixed prices with the distribution-based optimization approach does not yield significant additional benefits. The incremental additional reductions achieved are relatively modest compared to the revenue-neutral case and may not adequately offset the revenue tradeoff. Conversely, significant additional fatigue reductions can be achieved when considering a revenue cap within the DA approach, where it was shown that for some loads, the achieved reductions are doubled compared to the revenue-neutral DA case. Nevertheless, for the DE site, these did not reach the revenue-neutral reductions achieved by the wind speed-based optimization, while for the DK site, they marginally exceeded them. This suggests that applying a revenue reduction cap can hold potential value primarily within business cases employing the DA optimization approach under constant prices. To this extent, project-specific requirements can be accommodated by considering various levels of revenue reduction caps, significantly influencing the resulting cumulative fatigue. Moreover, although the results differ in magnitude between the two datasets, in general, accumulated fatigue minimization in constant prices is found to be effective and robust across different wind conditions.

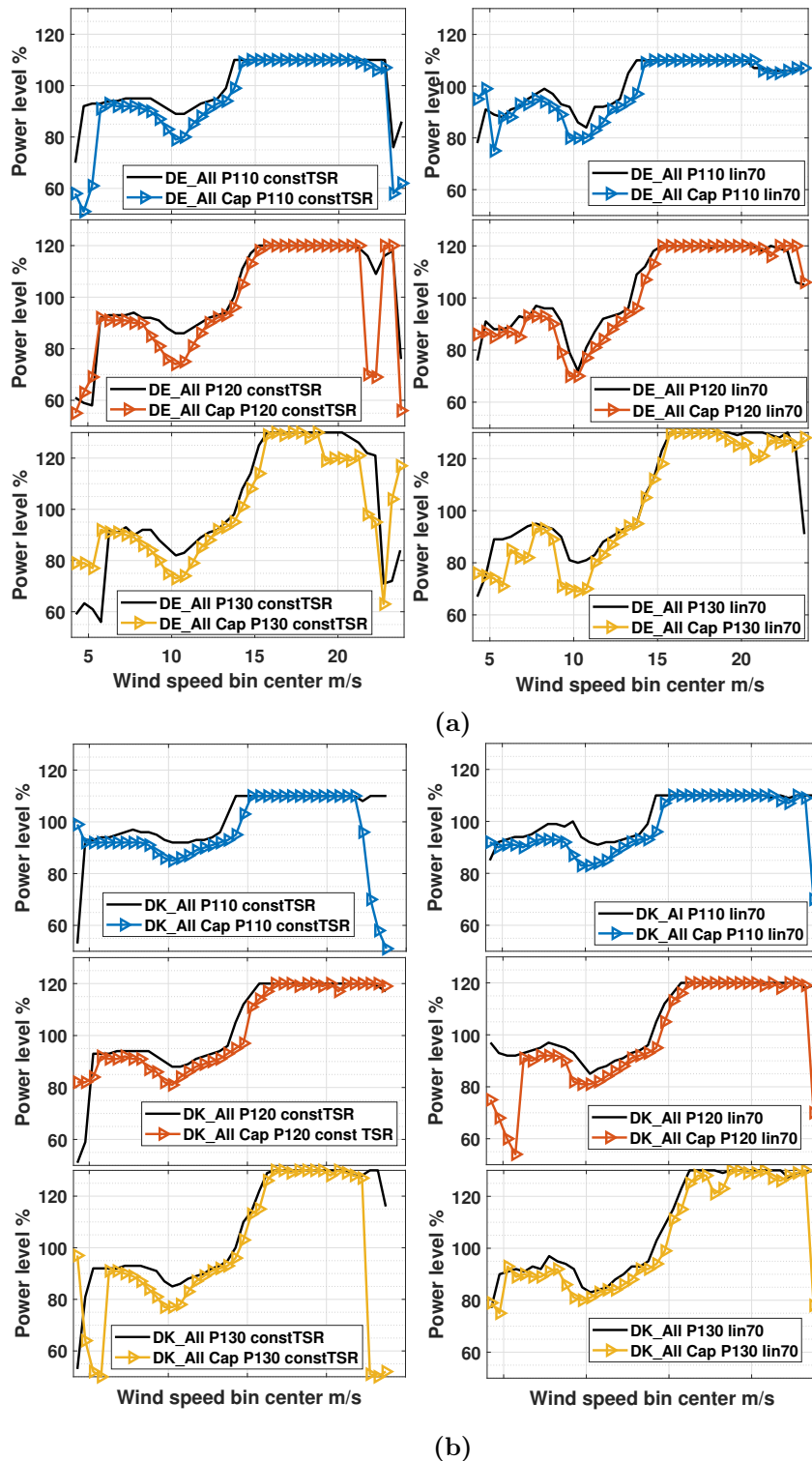


**Figure 7.16:** Power level per wind speed bin resulting from optimization using wind speed distributions for load minimization with a revenue reduction cap of 5% for all locations and trajectories. The black solid lines show the optimized power level identified without the cap. Maximum power levels are denoted as P110, P120 and P130. (a) DE\_all, (b) DK\_all

## 7.2.2 Revenue maximization under fixed prices

The results for load-neutral cumulative revenue maximization under fixed prices are shown in figure 7.17. The results include varying maximum power boosting levels from 110 to 130% using both down-regulation trajectories for the DE\_all and DK\_all datasets. The goal of restricting the cumulative fatigue damage for all components equal to or below the baseline levels is achieved for both sites and trajectories. The only exception is noted for the DK\_all case when considering the lin70 trajectory. In this instance, the LSSTq load consistently surpasses the baseline value across all maximum power levels considered.

The wind distribution-based optimization approach is more effective in revenue maximization under fixed prices compared to the forecast-based approach for both datasets. For the DE\_all dataset, the increase in revenue is found to be around 4% for a 110% maximum power level, 7% for 120%, and 10% for 130%, considering the distribution-based approach. Conversely, with the DA approach, the revenue increase approaches 6% for the 130% power level. The difference between the trajectories in terms of revenue increase is small, with a maximum discrepancy of 0.5% across all cases. Taking into account that the maximum possible revenue increase with the considered methods was found to be about 14%, the achieved values demonstrate the efficiency of the proposed method under the DE wind conditions.

For the DK\_all dataset, the achieved revenue increases are approximately 3.5% for a maximum power level of 110%, 5% for 120%, and 6.5% for 130% when the distribution-based approach is considered. With the DA-based approach, the revenue increase approaches 3% for the 130% maximum power level. The discrepancies, in terms of revenue, between the two trajectories are less pronounced for the DK\_site, with differences lower than 0.2%.

In terms of resulting cumulative fatigue, at the DE site, the constraint of not exceeding the baseline values is satisfied. The only exception is the DA-based approach with the constTSR trajectory, where the accumulated fatigue of the LSSTq load is increased by 2%. As the loads have different responses to the control modes and the optimization approach targets the fatigue loading of all major components, many loads show fatigue reductions. This is more evident for loads influenced by IBC.

The forecast-based optimization approach generally yields lower fatigue reductions, except for loads significantly impacted by IBC. The BRMy load shows reductions above 85% for all cases and the BROop above 40% for most cases. Similarly, the TBMz, TTMMy, TTMz, LSSMy, and LSSMz loads show fatigue damage reductions of 5-15% for all cases. The TBMx load also decreases across all cases by 15-25%. The BRMz load demonstrates the highest variation between the cases with reductions between 10% and 50%. Notably, the reductions for the TBMMy, BRMz, and BROop loads are found to be increasing with increasing maximum power level. As the IBC activation is similar for most cases and TBMMy and BRMz are not influenced

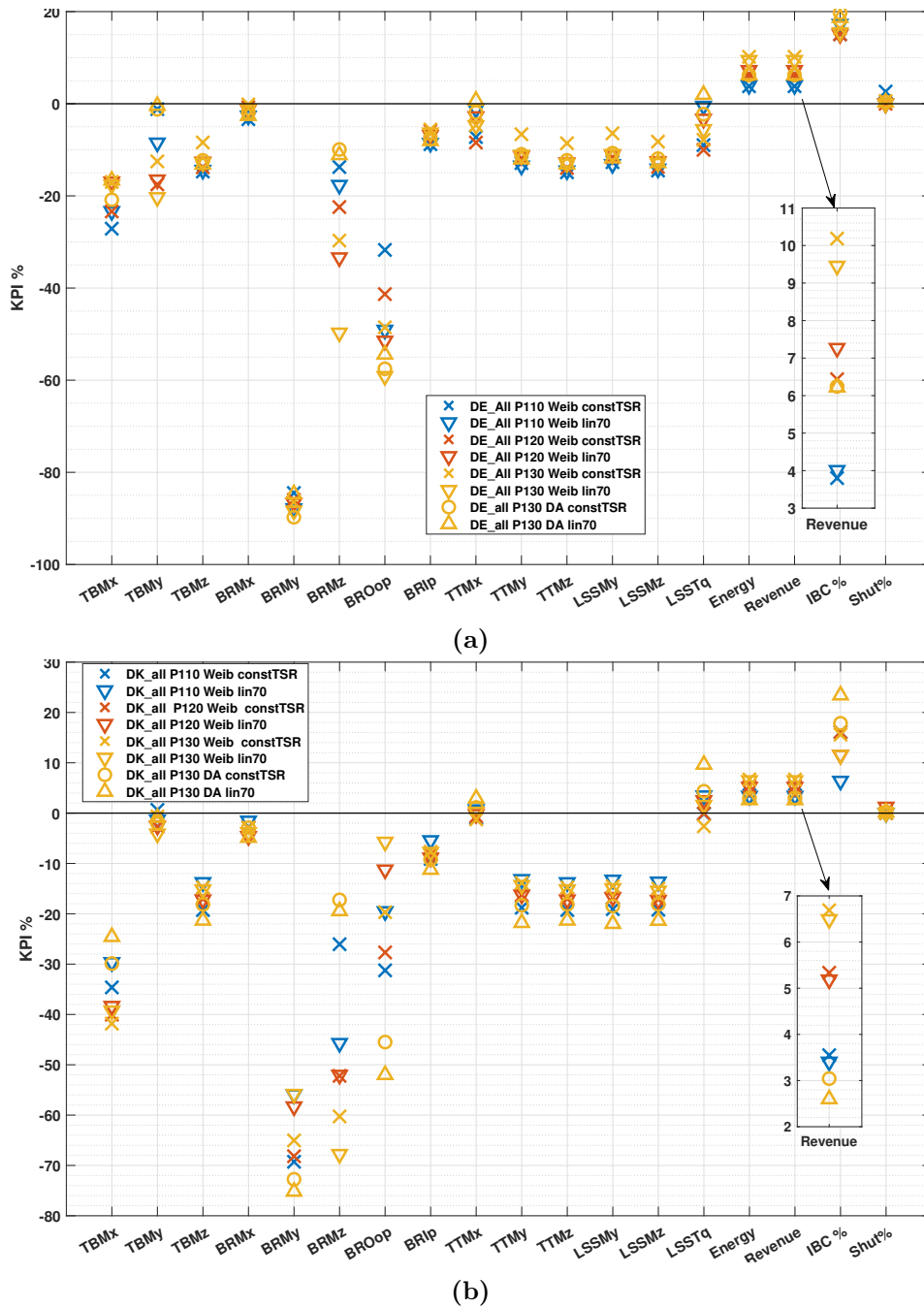


**Figure 7.17:** KPIs for load-neutral revenue maximization cases under fixed prices using both trajectories for the entire period considered for both locations and different maximum power levels. Optimization cases based on wind speed distribution are denoted as Weib, and cases based on day-ahead forecasts of wind speeds are denoted as DA. P110, P120, and P130 denote the maximum power level allowed for each case. (a) DK\_all, (b) DE\_all

by IBC, this can be attributed to the lower power levels assigned at the rated wind speed region as the maximum power boosting level increases.

The TBM<sub>y</sub>, BRM<sub>x</sub>, TTM<sub>x</sub>, and LSST<sub>q</sub> loads draw the limit for revenue maximization as they approach the baseline value. BRM<sub>x</sub> is generally less influenced by the control modes and

demonstrates low variability with reductions in the range of 0-4%. The TBMy load reaches the limit only with the DA approach and the forecast-based approach employing the constTSR trajectory with a 110% power level. In all other cases, it is decreased by 10-20% compared to the baseline. LSSTq and TTMx loads are closer to the limit across all cases with maximum reductions of 10%.

The differences between the trajectories are small in terms of resulting fatigue damage margins. The most notable variations within the DE\_all dataset occur for the BROop and BRMz loads, where the lin70 trajectory consistently yields higher load reductions for all cases. For the rest of the loads, these differences remain below 3%.

For the DK site, where revenue increases are lower compared to the DE, the load response is different, with the baseline limit being exceeded for some cases. Specifically, the TBMz, TTMy, TTMz, LSSMY, and LSSMz loads are reduced in the range of 10-20% for all cases. The TBMx load is reduced by 25-40%. The BRMy and BROop loads are less reduced compared to the DE site for all cases, with the BROop load displaying fatigue reductions of less than 10% for some cases. This difference between the two sites is explained by the lower IBC activation at the DK site. The wind conditions at the DK site lead to the optimizer reducing the IBC application in order to restrict the cumulative fatigue increase of the TTMx and LSSTq loads, which are two of the loads setting the limits of the revenue maximization also for the DK site. The LSSTq load is increased when the lin70 trajectory is considered for the DK site up to 4% with the distribution-based approach. With the forecast-based optimization, it increases up to 10% with the lin70 trajectory and up to 4% with the constTSR. Cumulative fatigue for the TTMx load is near the limit for all cases and marginally exceeds the baseline value by 3% for the DA approach with the lin70 trajectory. The TBMy load is also critical for the DK dataset, exhibiting slight reductions up to 4% but remaining below the baseline threshold in all cases.

In general, for the DK conditions, the choice of down-regulation set points has a higher impact compared to the DE conditions. This highlights the significant effect of boundary conditions on the presented method and underscores the necessity of tailoring the control strategy to the specific characteristics of each site.

The results, broken down by year, for load-neutral revenue maximization considering a maximum power boosting level of 130% are presented in figure 7.18. The higher variability over the years at the DK site is evident for revenue and fatigue damage KPIs. The revenue increase between all years considering the same optimization approach varies by 1% for the DE site and by 3% for the DK site. This is also observed for the BRMy and BROop loads and the IBC application percentage, which vary highly depending on the trajectory and optimization approach considered for the DK site in contrast to the DE site.

Moreover, these findings highlight the differences between the DA- and Weibull distribution-based approaches. The flexibility of adapting the optimization daily to the conditions is more

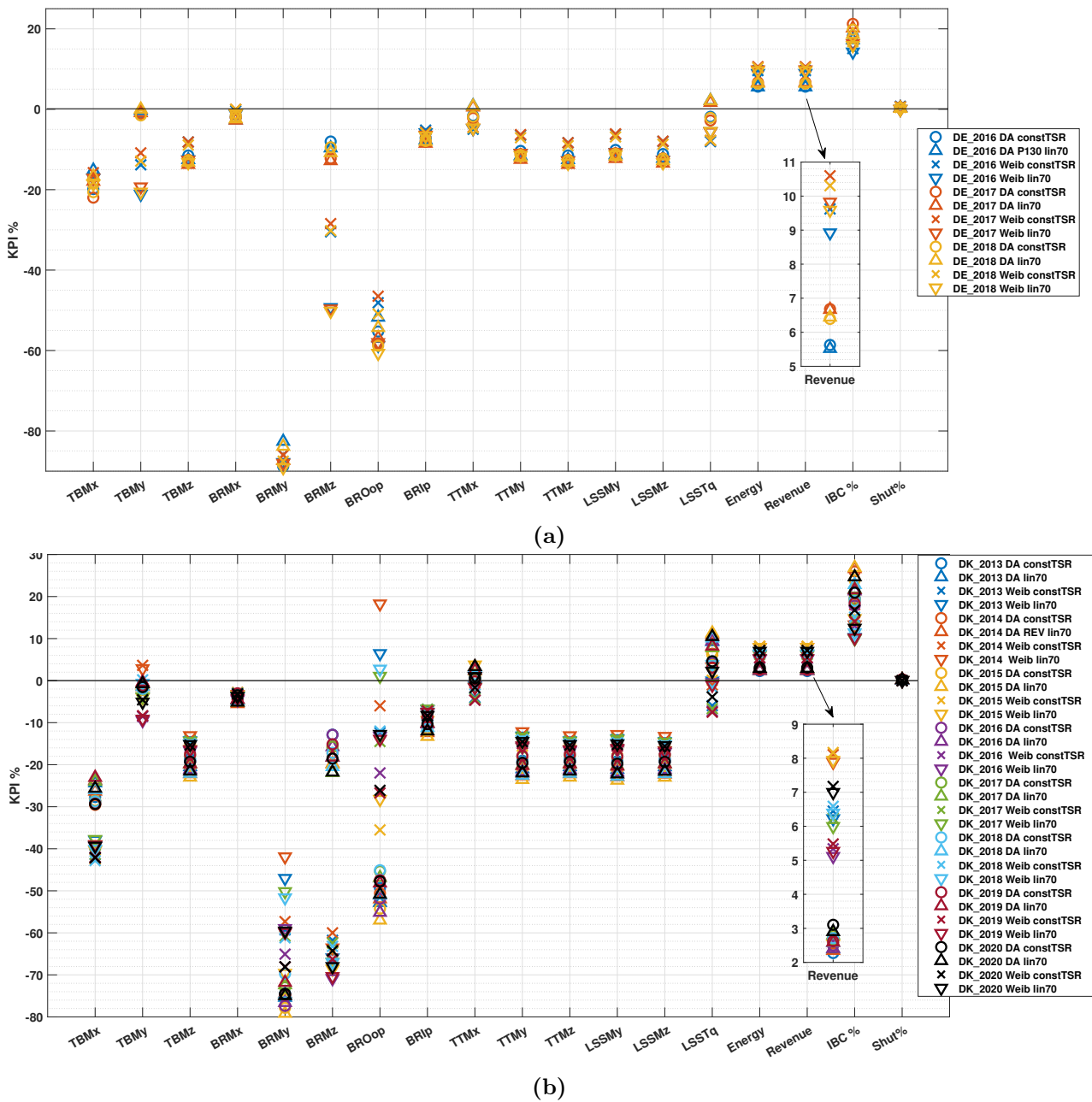


**Figure 7.18:** KPIs for load neutral revenue maximization under fixed prices using both trajectories per year and per location. Optimization cases based on wind speed distribution are denoted as Weib. Cases based on day-ahead forecasts of wind speeds are denoted as DA. The maximum power level allowed is 130% for all cases. (a) DE, (b) DK

efficient in restricting the loads to not exceed the baseline thresholds, which in turn comes with the cost of less efficiency to increasing the long-term revenue. This can be seen, for instance, by the variations of the TBM<sub>y</sub> load, which never exceeds the limit for the DA cases, but for the Weibull-based cases, it shows both reductions and increases. This behavior has the opposite effect on the loads negatively affected by IBC, such as TTM<sub>x</sub> and LSST<sub>q</sub>. The lack of long-term information leads to higher IBC activation, resulting in greater increases in

cumulative fatigue for these loads. This discussion shows that both approaches have benefits and shortcomings. Deciding which approach is more favorable would depend on the specific application and requirements.

The optimization results in terms of scheduling power levels per wind speed for revenue maximization with the Weibull-based approach are presented in figure 7.19. The trends for both datasets and trajectories are similar. Power levels are reduced the most at the lowest wind speed with a monotonic increase until approximately the beginning of control region 2, where the power level reaches 100%. The power level stays constant at 100% until the rated region, where it decreases again with a local minimum at the rated speed. Subsequently, it increases again until reaching the maximum allowed level at some wind speed between 14 and 16 m/s.

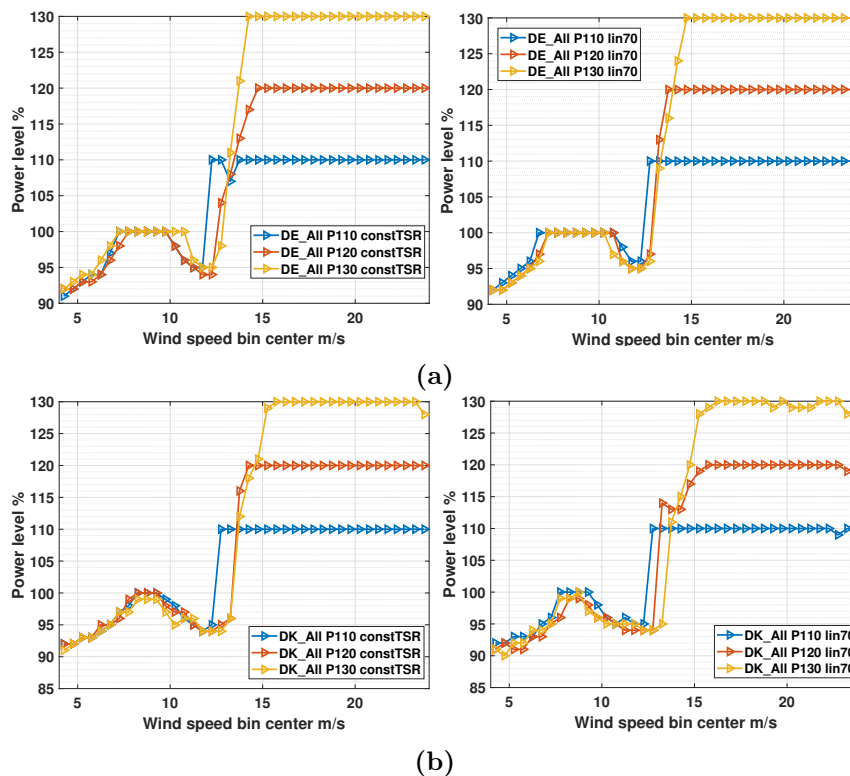


**Figure 7.19:** Power level per wind speed bin resulting from optimization for load-neutral revenue maximization for all locations and trajectories. Maximum power levels denoted as P110, P120 and P130 (a) DE\_all, (b) DK\_all

The reduced power levels never drop below 90% in all cases. The extent of the wind speed range characterized by a constant 100% power level in the below-rated region varies depending on the site's wind conditions, with a narrower range observed for the DK site. The revenue gains are achieved by power boosting at higher wind speeds, while the increases in load are offset by down-regulation at the lowest wind speeds and within the transition region. The main difference between the various maximum power boosting levels lies in the shift of the point at which the maximum power level is reached, moving towards higher wind speeds as

the maximum power level increases.

These findings demonstrate that cumulative revenue can be significantly increased under fixed prices with the operational management method proposed in this work. The maximum power boosting level plays a pivotal role in revenue maximization cases where the revenue increase is directly proportional to the maximum allowable level, in contrast to the load minimization scenarios. While the down-regulation trajectories behave similarly with regard to revenue, they diverge in terms of their impact on loads. However, the most pronounced differences arise from boundary conditions, where variations in wind conditions exert substantial influence on the potential for revenue increase and the associated fatigue damage margins. Furthermore, these results shed light on the intricacies of targeting precise damage margins across the entire load ensemble. Achieving such precision is not as straightforward as in the case of revenue objectives. This stems from the objective function setup and the complex interaction of the weights, penalties, and limits within the optimization framework.

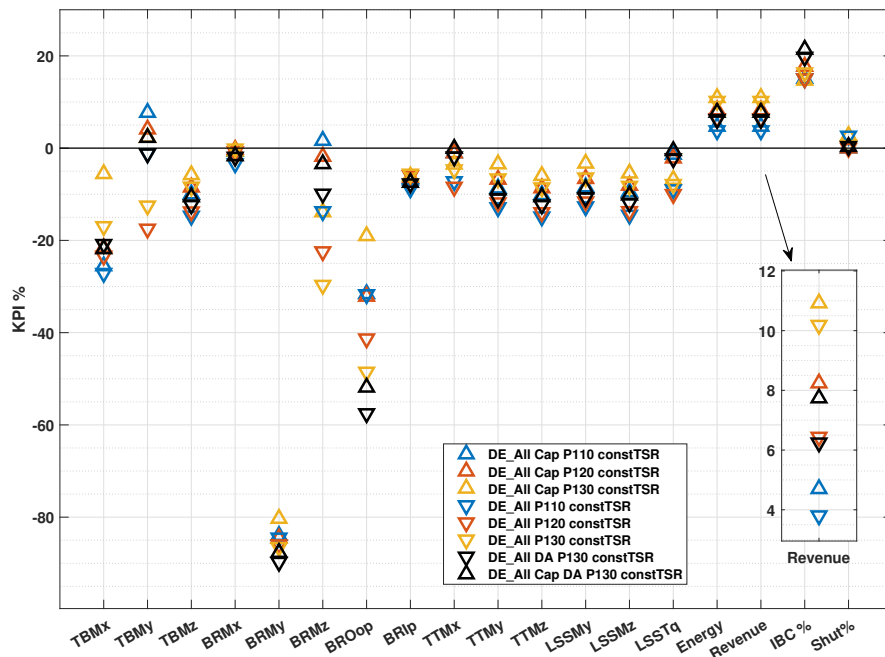
### Revenue maximization with a load increase cap under fixed prices

The possibility to further increase revenue by incorporating a load increase cap in the objective function is also assessed within the revenue maximization scenario. The allowed cumulative fatigue increase cap is set to 5% for all considered loads. The results, in terms of KPIs for both the cap and load-neutral cases, are presented for the DE\_all dataset in figure 7.20.

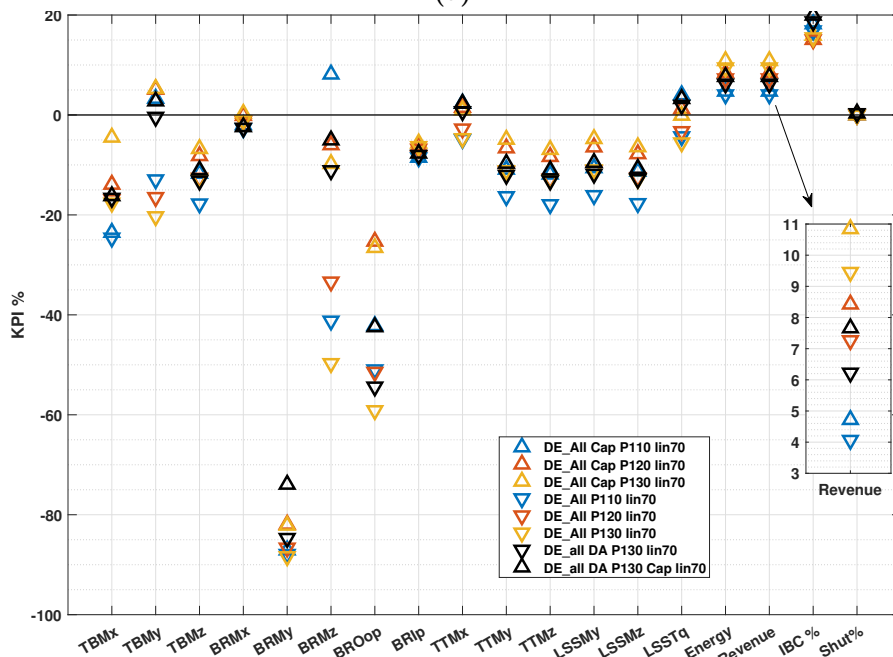
In all cases, the revenue increases compared to the load-neutral scenario. Specifically, for the constTSR trajectory and power levels of 110% and 130%, employing the Weibull-based approach, results in an additional revenue increase of 0.5%. Meanwhile, for the 120% power level, the increase is 1.5%, and for the DA approach with 130% power level, it is 1%. For the lin70 trajectory, the additional increase in revenue is in the order of 1% for all cases except for the 110% power level, where the additional increase is approximately 0.5%. The metrics regarding IBC activation and selective shutdown have not changed significantly compared to the load-neutral case. This shows that the inclusion of the load increase cap is leveraged by the optimizer mainly by redistributing the power levels in order to further increase revenue.

Regarding the loads, the 5% maximum increase constraint is met in most cases. Considering the constTSR down-regulation trajectory, the only load that exceeds the baseline level is TBMy, which sets the limit for revenue maximization. The 5% increase cap is exceeded only for the 110% maximum power level, with the increase reaching 8%. For the rest of the loads, there are still observed reductions compared to the baseline but lower than the load-neutral case. The level of reduction is in the range of 0-10% for these loads, except for BRMy and BROop, which, due to the high impact of IBC, still show significant reductions.

When the lin70 trajectory is considered, the TBMy, TTMx, and LSSTq loads exceed the



(a)



(b)

**Figure 7.20:** KPIs for revenue maximization cases including a load increase cap of 5% cases under fixed prices for the DE site. The entire period is considered using both down-regulation trajectories and different maximum power levels 110%-130% (a) constTSR, (b) lin70

baseline value and draw the limits for revenue maximization in most cases. In all cases, the 5% increase limit is not surpassed. The only exception is for the 110% power level, where the highest increase is found for the BRMz load at 9%. For the rest, the trends are similar to the constTSR trajectory, with cumulative fatigue reductions up to 10% for most loads.

The relevant results for the DK\_all dataset are presented in figure 7.21. In most cases

employing the wind distribution-based optimization approach, revenue is increased compared to the load-neutral case. However, for the DA-based approach employing the constTSR trajectory as well as the Weibull-based approach employing the lin70 trajectory with a maximum power

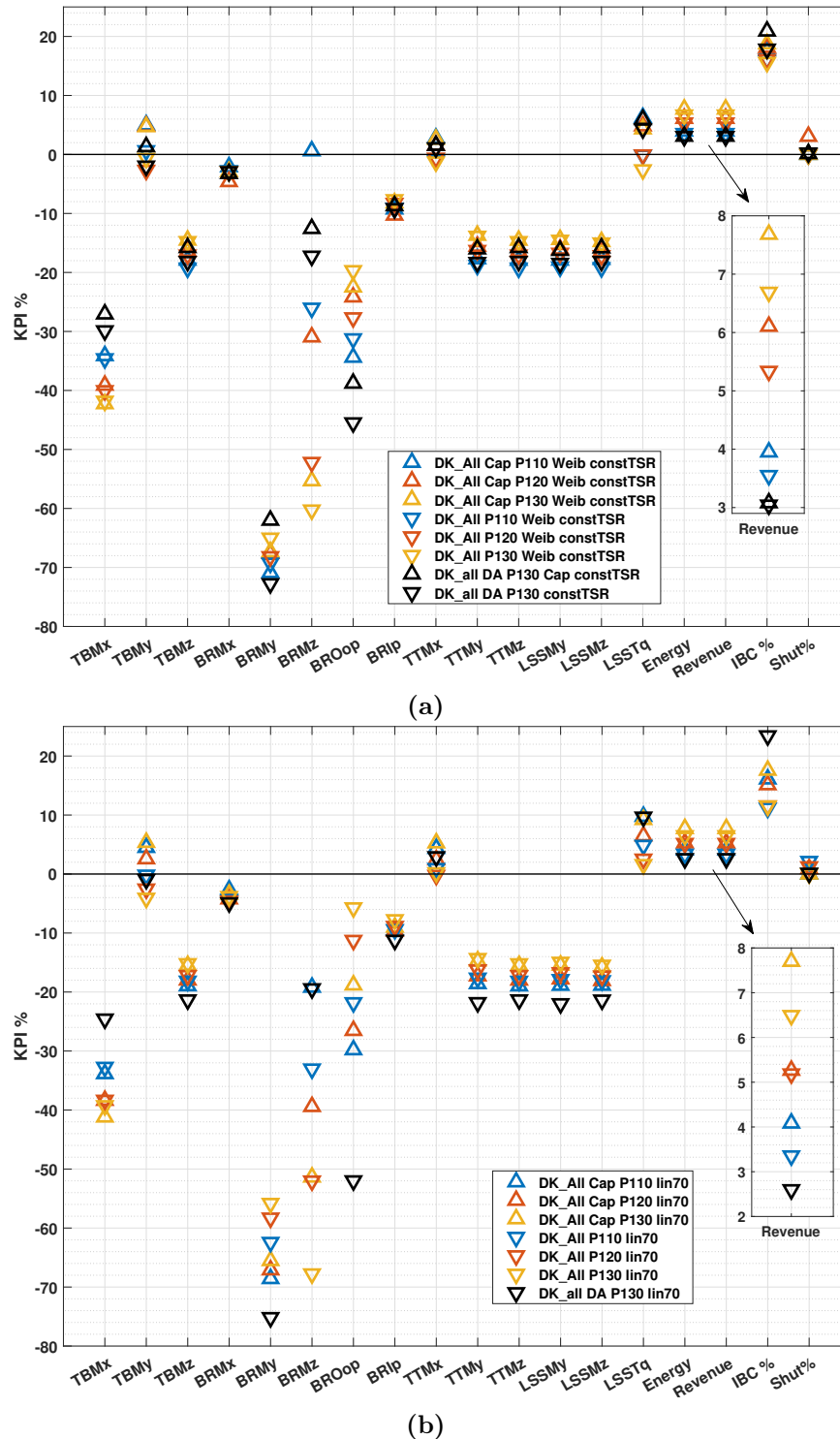


**Figure 7.21:** KPIs for revenue maximization cases including a load increase cap of 5% cases under fixed prices for the DK site. The entire period is considered using both down-regulation trajectories and different maximum power levels 110%-130% (a) constTSR, (b) lin70

level of 120%, the inclusion of the load increase cap does not result in additional revenue. Using the constTSR trajectory with the Weibull-based optimization approach, the additional increase in revenue is 0.3%, 0.7%, and 1% for the 110%, 120%, and 130% power levels. For the lin70 trajectory, the revenue increase is found to be 0.6%, 0%, and 1.1% for maximum power boosting levels of 110%, 120%, and 130%. The DA case results for the lin70 trajectory are not available due to computational constraints, but, the limited results obtained showed similar behavior to the results obtained with the constTSR. These findings suggest that the DA optimization approach, in combination with the DK conditions, does not yield any additional benefits by including a load increase cap in revenue maximization scenarios.

The results for the constTSR trajectory reveal that the loads reaching the cap limit include TBMy, TTMx, and LSSTq, with LSSTq exhibiting the maximum increase of 6% compared to the baseline. The BRMz load shows the highest increases compared to the load-neutral case but still maintains one of the highest damage margins. These trends remain consistent when considering the lin70 trajectory. In this case, the LSSTq load exceeds the 5% increase cap, reaching a maximum increase of 10% for the 110% and 130% power levels.

The optimization outputs, concerning the power level allocation across wind speeds for revenue maximization with a load increase cap, are presented in figure 7.22. For both sites, a consistent trend emerges. Additional revenue gains are achieved by moderately increasing power levels for the wind speed region of 13-15 m/s, just above the rated region. Additionally, the power levels are slightly increased at the limits of the flat region around the control region 2. In this region, the turbine is still in down-regulation but at higher power levels compared to the load-neutral case.

This also explains the higher increase in the LSSTq load observed for the DK dataset. As demonstrated in section 7.1.1, most of the fatigue damage for LSSTq is contributed within the wind speed range of 9 to 13 m/s. This range coincides with the area where additional revenue can be generated. Additionally, as discussed in section 4.3, the LSSTq load is less reduced when using the lin70 trajectory compared to the constTSR. Furthermore, as seen from the results, e.g. for the lin70 trajectory with 120% maximum power level, when the wind conditions drive loads close to the cap limit, the optimizer seeks to compensate by reducing power levels in other regions. However, the challenge arises from the high sensitivity of revenue to down-regulation, limiting the potential for substantial overall revenue increase beyond a certain point, as seen from the results for DE\_all with the constTSR trajectory and the 130% power level.

In summary, implementing a load increase cap under fixed prices resulted in moderate revenue increases for most cases across both sites. These findings suggest that revenue is sensitive to the cap, which could be advantageous in certain business case contexts. Comparing the two optimization approaches, the wind distribution-based approach consistently outperformed the

forecast-based approach for all cases. The forecast-based approach shows a high dependency on wind conditions in terms of both efficacy and efficiency. The load increase cap constraint cannot be tracked as accurately as the revenue decrease cap for the fatigue minimization cases

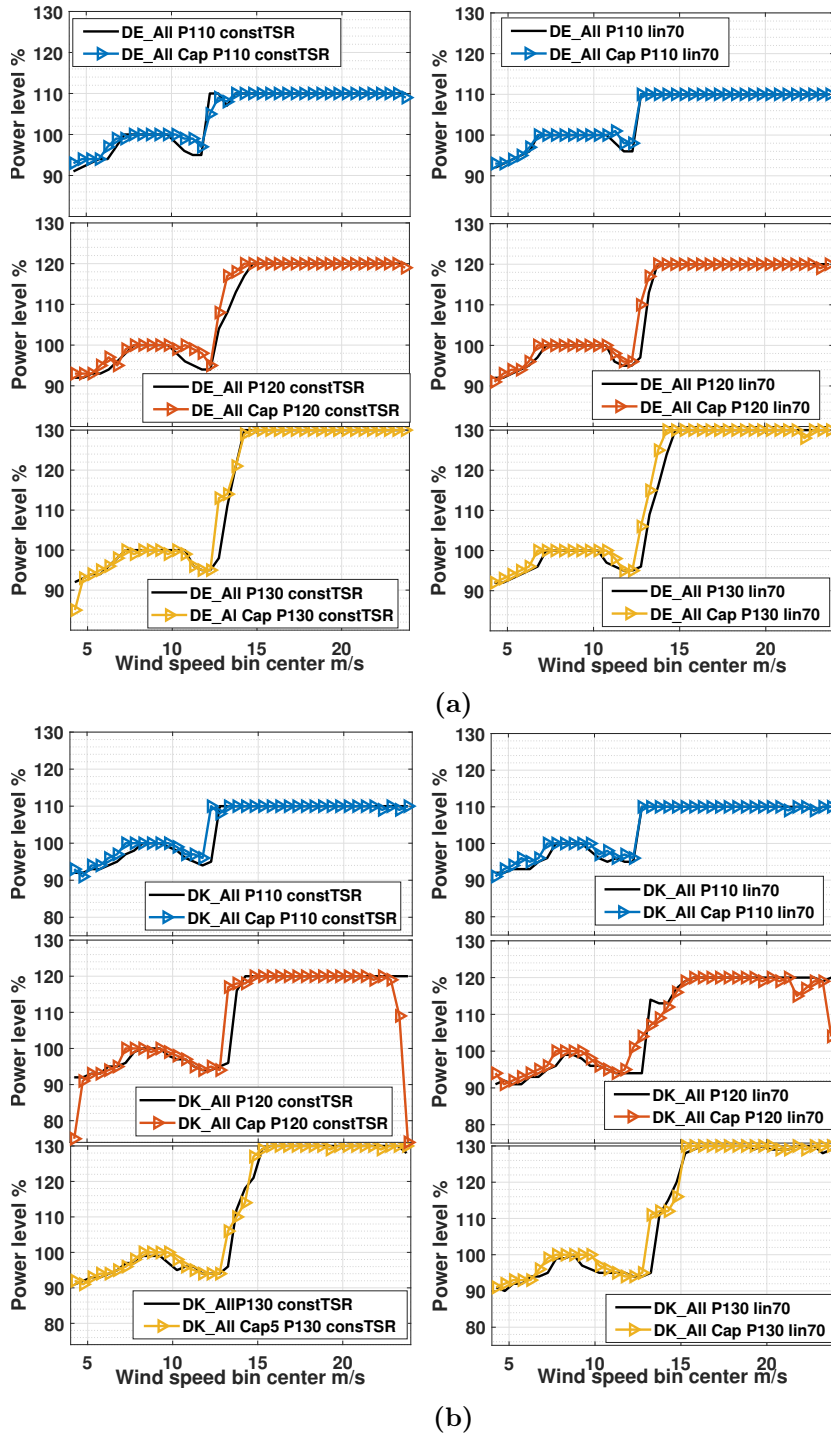


**Figure 7.22:** Power level per wind speed bin resulting from optimization using wind speed distributions for revenue maximization with a load increase cap of 5% for all locations and trajectories. The black solid lines show the optimized power level identified without the cap. Maximum power levels are denoted as P110, P120 and P130. (a) DE\_all, (b) DK\_all

and showed higher sensitivity to the wind conditions, the down-regulation trajectories, and the maximum power boosting levels. The effect of the wind conditions is prominent as it was shown that for the same turbine, with the same controller settings, and the same optimization approach based on forecasts, in one site, the optimization produced revenue gains with the cap while having no effect at the other.

### 7.2.3 Sensitivity to wind distribution uncertainty under fixed prices

The wind distribution-based optimization approach was shown to perform better in all scenarios examined under fixed prices. A core element of this method is the long-term wind speed Weibull distribution, which is the primary input to the optimizer. In order to evaluate the robustness of the method in the face of input distribution uncertainty, a sensitivity analysis is conducted. The derived distributions for each site are systematically modified and used as inputs to the optimizer. Subsequently, the resulting output variables, in terms of power levels per wind speed bin, IBC activation thresholds, and selective shutdown thresholds, are applied to the full dataset using the evaluation framework. This analysis allows for comparing all the results to the baseline and quantifying the effect of uncertain wind speed distribution inputs on the proposed operational management method.

The scale ( $A$ ) and shape ( $k$ ) parameters of the originally derived Weibull distributions are both systematically adjusted in the range of  $-10\%$  to  $10\%$  with a step size of  $5\%$ . This comprehensive exploration involves considering all potential combinations of these modified parameters, resulting in a total of 24 modified Weibull distributions. The modified wind speed distributions, along with the unmodified distribution for each site, are presented in figure 7.23.

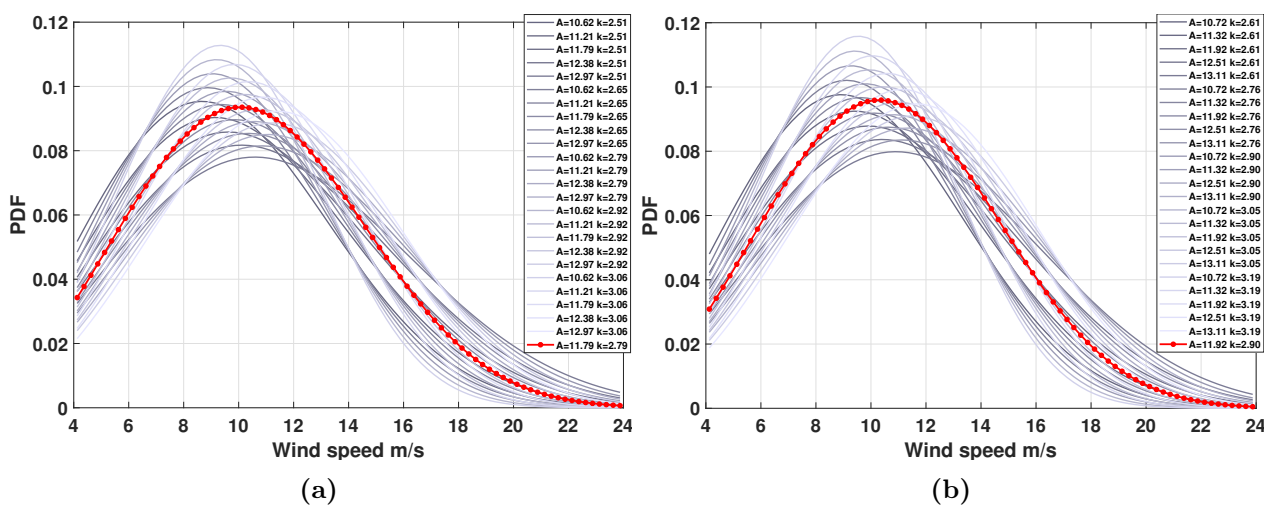


**Figure 7.23:** Resulting Weibull wind speed distributions by varying the originally derived coefficients  $\pm 10\%$ . The value of the Weibull coefficients varies from  $-10\%$  to  $+10\%$  with a step of  $5\%$  and is reported in the legend. The red line indicates the unmodified Weibull distribution derived by the entire dataset. (a) DE\_all, (b) DK\_all

Given that revenue-focused scenarios exhibited higher sensitivity, two specific cases are examined: one for load-neutral revenue maximization using the DE\_all dataset, and another for revenue maximization with a 5% load increase cap for the DK\_all dataset. Both scenarios employ the constTSR trajectory with a 130% maximum power boosting level. The outcomes of the sensitivity analysis are presented in figure 7.24.

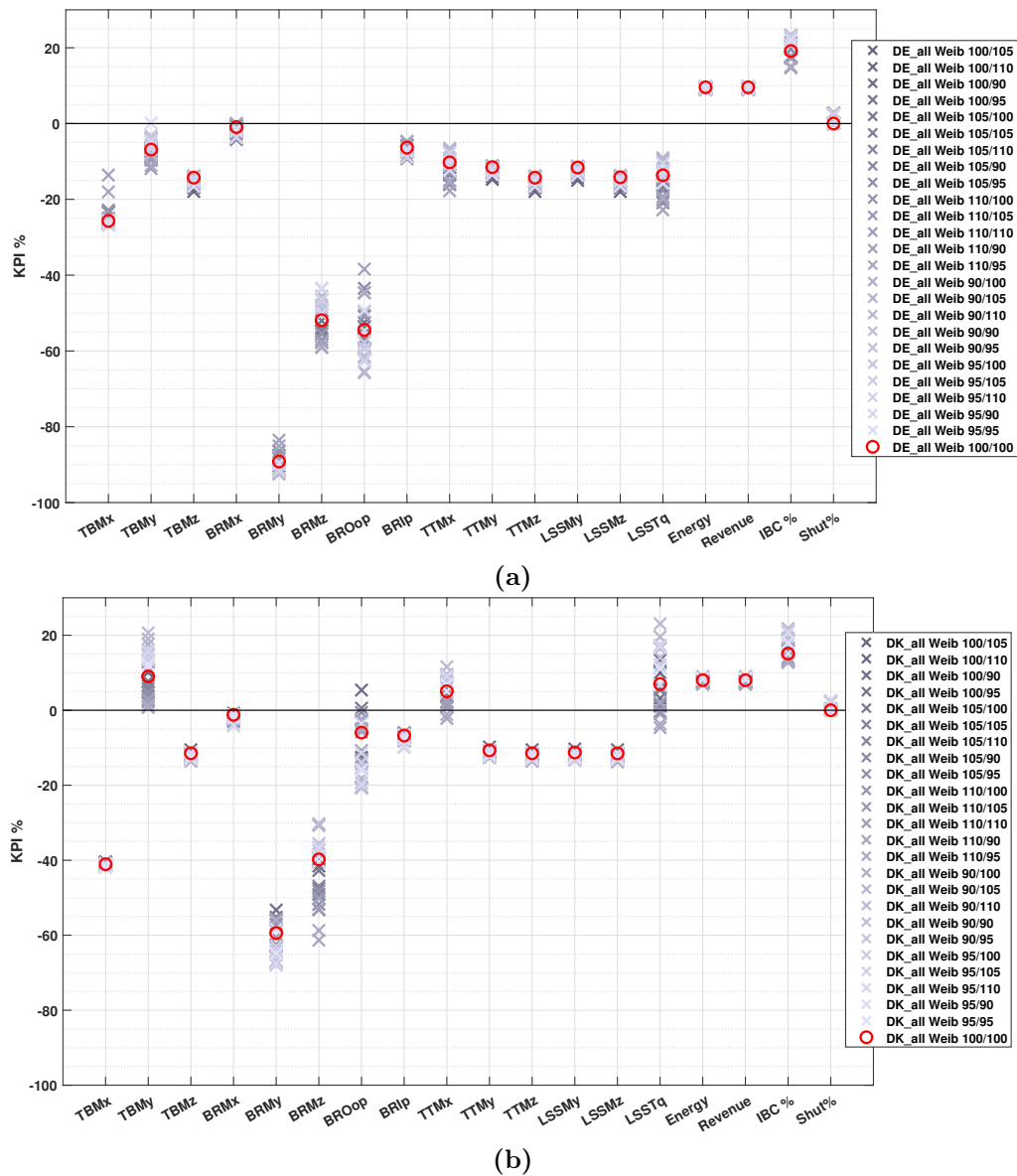


**Figure 7.24:** Results of optimization cases compared to baseline operation under fixed prices using the modified Weibull distribution. Values in the legend report the percentages of the unmodified parameters. The first value refers to the scale (A) and the second to the shape (k) parameter. The cases with red denote results obtained using the unmodified Weibull distributions. (a) DE\_all results for a case with revenue maximization objective, (b) DK\_all results for a case with revenue maximization objective with a load cap

In both datasets, the resulting revenue increase remains largely unaffected, with variations across all cases staying below 0.5%. However, the uncertainty in the wind distribution does

impact certain load-related metrics. Specifically, the TBMy, BRMy, BRMz, BROop, TTMx, and LSSTq loads exhibit the highest variations, along with the duration of IBC activation. On the other hand, all other loads and metrics show minimal influence, with variations below 5% for all cases.

The influenced loads exhibit a considerably wider range of variation for the DK site compared to the DE site. This discrepancy can be attributed to the higher variability in wind conditions at the DK site. Additionally, as the DE results for the unmodified wind distribution showed fatigue damage reductions compared to the baseline, none of the cases resulted in fatigue damage exceeding the baseline level.

The TBMy and BRMy results show variations compared to the unmodified distribution cases in relative differences to the baseline, in the range of  $\pm 5\%$  for the DE dataset and  $\pm 10\%$  for the DK dataset. For the BRMz load, this range is approximately  $\pm 7\%$  for the DE dataset and  $-20\%:10\%$  for the DK dataset. The BROop load shows variations within the range of  $\pm 10\%$  for the DE and  $-15\%:10\%$  for the DK site. For the TTMx load, the range is found  $-10\%:5\%$  for the DE case, and around  $\pm 5\%$  for the DK case. Finally, for the LSSTq load, the variation falls within the range of  $-10\%:5\%$  for DE and  $-10\%:15\%$  for DK.

Regarding the effect of the Weibull parameter variation, the general trends are similar for both sites. The TBMy, BRMz, TTMx, and LSSTq loads show higher increases as the scale parameter decreases and the shape parameter increases compared to the unmodified values. Conversely, they show higher reductions as the scale parameter increases and the shape parameter decreases. This suggests a correlation between the cumulative fatigue for these loads and the type of uncertainty. The cumulative fatigue increases when the wind conditions are underestimated and decreases when they are overestimated. In contrast, the BRMy and BROop loads exhibit the exact opposite behavior, which can be attributed to their high correlation with IBC activation.

More extensive and systematic analysis is required to comprehensively understand the impact of uncertainty and quantify the potential implications of applying the distribution-based optimization approach with uncertain inputs. The present findings suggest that the effects of the uncertainty are contingent on the specific turbine model and controller design, in terms of which loads are affected by the uncertain input. Moreover, the magnitude of the variation depends on the wind conditions, with greater variability in wind conditions leading to larger deviations.

## 7.3 Optimization under fluctuating market prices

This section presents the results related to optimization in fluctuating market prices for all considered scenarios. The efficiency of both optimization approaches is discussed individually and comparatively. Similar to the preceding section, the results are categorized based on the defined scenarios of revenue maximization and fatigue minimization. Additionally, sensitivity analyses are included for day-ahead forecast uncertainty, forecast horizon length, and mean wind speed distribution uncertainty.

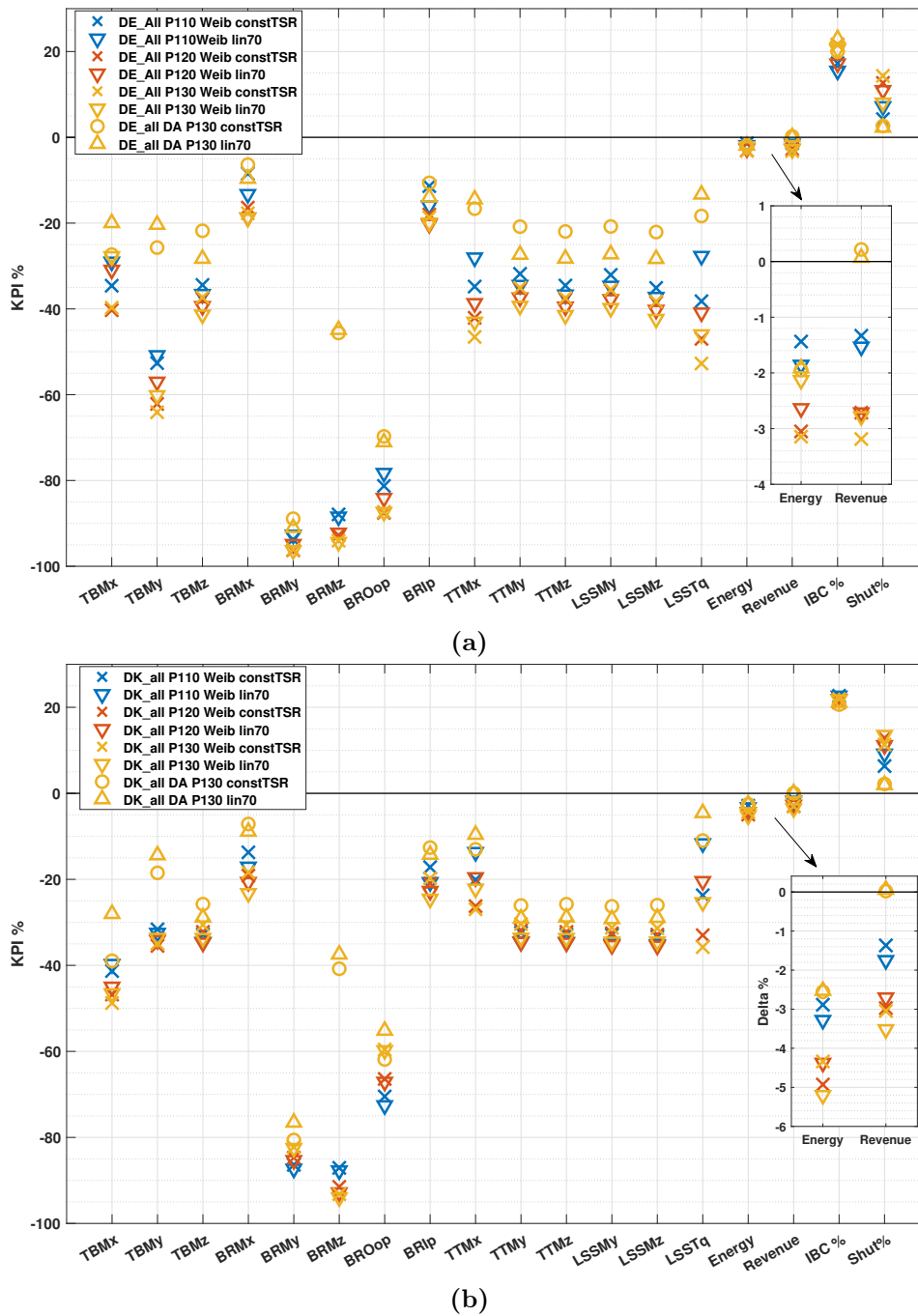
### 7.3.1 Fatigue damage minimization under fluctuating market prices

Figure 7.25 presents the results for revenue-neutral cumulative fatigue minimization under fluctuating prices. This analysis encompasses both optimization approaches, both down-regulation trajectories, and varying power levels for the DE\_all and DK\_all datasets.

The wind distribution-based optimization approach yields similar levels of fatigue reductions and IBC activation across all cases, consistent with the results discussed for fatigue minimization under fixed prices in section 7.2.1. This is expected as the wind conditions and the power level scheduling are identical. The small variations stem from the different shutdown behavior due to negative prices and also the effect of the threshold for selective shutdown under fluctuating prices. The load reductions with the DA-based approach, considering both wind speeds and price forecasts, are also similar to the results under fixed prices. This indicates that, for load minimization objectives, the optimization's efficiency in terms of load reduction magnitudes is more reliant on wind conditions and controller design rather than on price fluctuations.

The main distinction between the optimization approaches is that only the forecast-based approach is able to achieve the revenue-neutral objective. The efficacy of the Weibull-based approach, which was shown to perform best under fixed prices, does not carry over to fluctuating price scenarios. The variability of the prices leads to revenue and energy reductions, showing the limitation of relying solely on wind speed as an input to the optimization process. Conversely, the forecast-based approach, while less effective in minimizing cumulative fatigue, consistently accomplishes the load-neutral objective due to the inclusion of price information and also the higher adaptability to changing conditions. However, this approach also leads to a reduction in energy production, with decreases of up to 3% observed across all cases. This shows that when the electricity pricing is not fixed, power production and revenue objectives are not necessarily aligned.

For both datasets, the results suggest that a cumulative fatigue reduction in the order of 15-30% can be expected for the TBMx, TBM<sub>y</sub>, TBM<sub>z</sub>, TTM<sub>z</sub>, TTM<sub>z</sub>, LSSM<sub>y</sub>, LSSM<sub>z</sub> loads considering both trajectories with the forecast-based optimization approach. The BRM<sub>x</sub>, BRIP,



**Figure 7.25:** KPIs for revenue-neutral load minimization cases under fluctuating prices using both trajectories for the entire period considered for both locations and different maximum power levels. Cases employing the Weibull-based approach are denoted as Weib, and cases based on day-ahead forecasts as DA. P110, P120, and P130 refer to the maximum power level. (a) DK\_all, (b) DE\_all

TTMx, and LSSTq are the least reduced loads, with reductions up to 15% for all cases. The BRMz load shows a reduction of 40-45% for both datasets. The loads highly influenced by IBC, BROOp and BRMy, exhibit the highest fatigue damage reductions in the range of 60-90%. Higher fatigue reductions can be achieved with the Weibull-based approach, although this comes at the cost of revenue reductions of 1-3% for the DE conditions and 1-4% for the DK

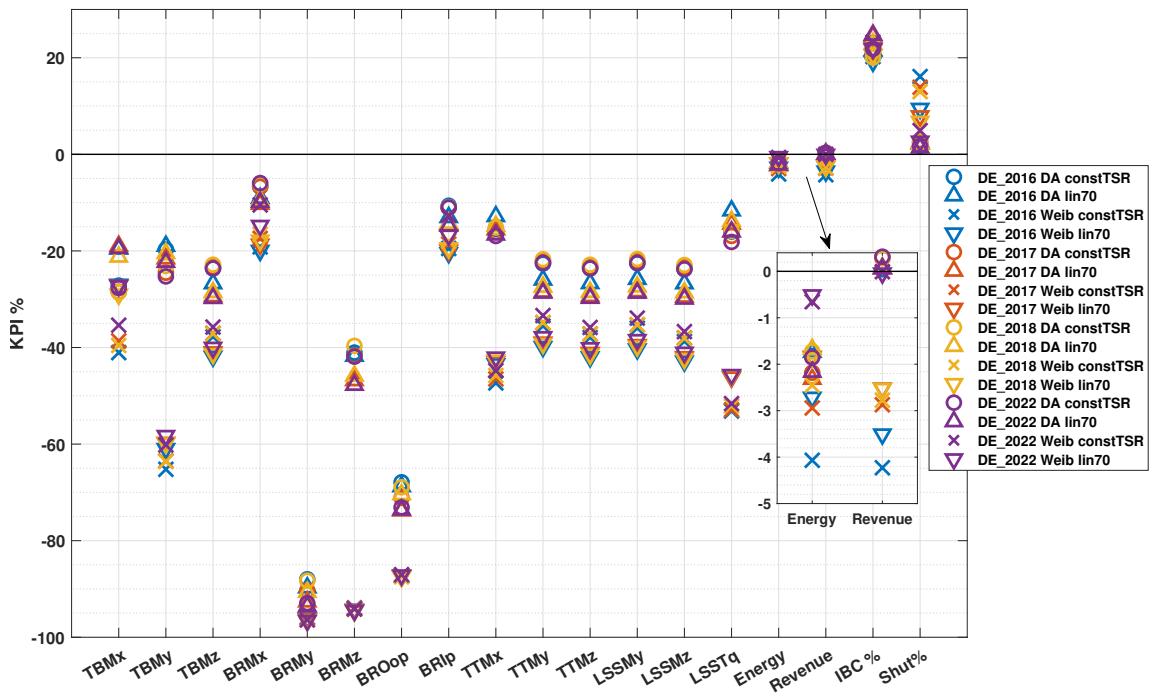
conditions. The corresponding energy production reductions are found in the range of 1-3% for DE\_all and 2-5% for the DK\_all dataset. For both datasets, optimization approaches and down-regulation trajectories, the reductions in energy and revenue (when applicable), increase proportionally to the maximum power level.

Another difference between the two sites is the selective shutdown duration. With the forecast-based approach, the selective shutdown duration is found to be approximately 3% of the total time for both cases. However, with the distribution-based approach, the DK prices result in shutdown durations approximately double to triple those observed in the fixed price case. Conversely, with the DE prices, the durations are similar for both constant and fixed prices. This is correlated to the overall lower prices and the generally higher variability of prices overtime at the DK site. These findings suggest that the choice of the fixed price magnitude, serving as input for the wind distribution-based optimization, can affect the method's efficiency under fluctuating prices. Adjusting the input to align with expected price levels may offer potential benefits.

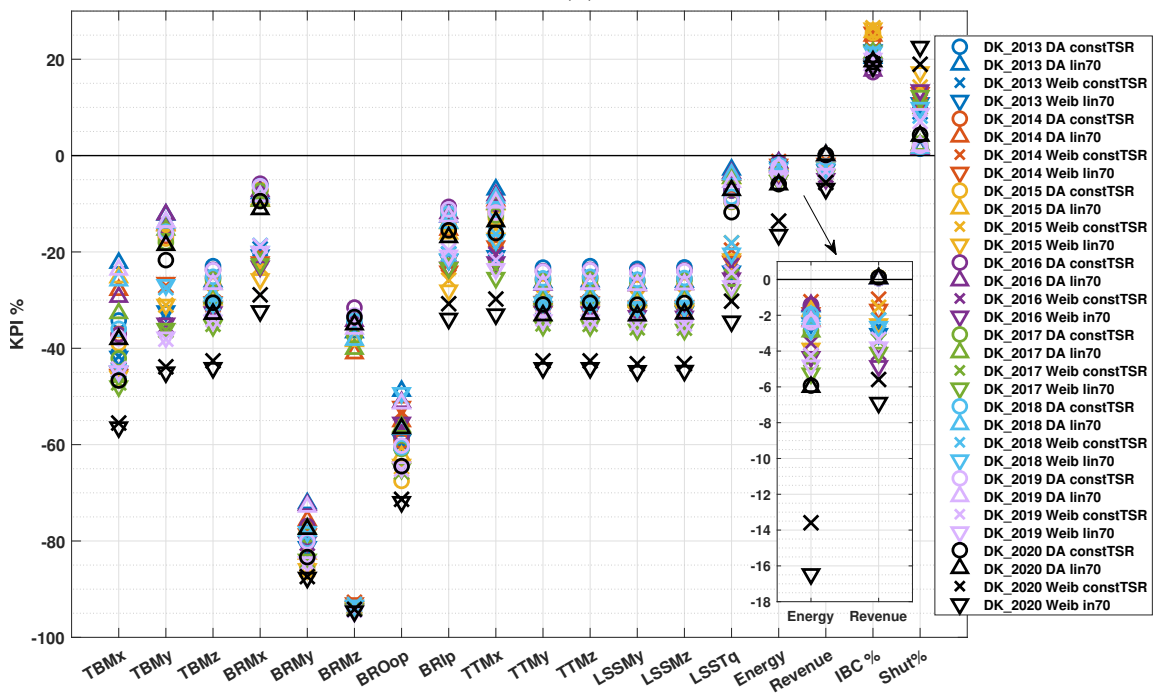
The results on a yearly basis, including the DE\_2022 dataset, are presented in figure 7.26. The results show that the increased variability of wind and prices at the DK site translates to higher variability in the efficiency of the optimization for fatigue minimization in fluctuating prices.

An illustrative example of the effect of the boundary conditions on the optimization efficiency can be observed in the DK\_2020 results. As discussed in section 6.1, the prices during this year were generally lower with a higher dispersion compared to the other DK years. Applying the optimization based on the site's mean wind distribution and a constant fixed price as inputs results in high discrepancies for this year. This leads to revenue reductions of approximately 6% and energy reduction of about 15%, along with a high shutdown percentage of 20%. Nevertheless, DK\_2015, which is the year with the second lowest prices of the DK dataset, shows relatively low revenue and energy reductions, albeit the second-highest shutdown percentage.

For the DE\_2022 dataset, which has the same wind conditions as the DE\_2018, the results show that using the distribution-based approach remains effective in fluctuating prices. The fatigue reductions are similar to the DE\_2018 levels showing that the magnitude is bounded by the wind conditions and the controller design. However, the very high overall prices, along with a lower correlation between wind speeds and prices, lead to revenue-neutral outcomes. Additionally, energy production is reduced the least compared to all cases at a level of 0.5%. Regarding the DA-based optimization approach employed for the DE\_2022 dataset, there is no improvement compared to the DE\_2018 case. This implies that, within the DA-based approach, the short forecast horizons don't allow for leveraging the higher optimization potential presented by the DE\_2022 boundary conditions.



(a)



(b)

**Figure 7.26:** KPIs for revenue-neutral load minimization under fluctuating prices using both down-regulation trajectories per year. Cases employing the Weibull-based approach are denoted as Weib, and cases based on day-ahead forecasts as DA. The maximum power level is 130% for all cases. (a) DE, (b) DK

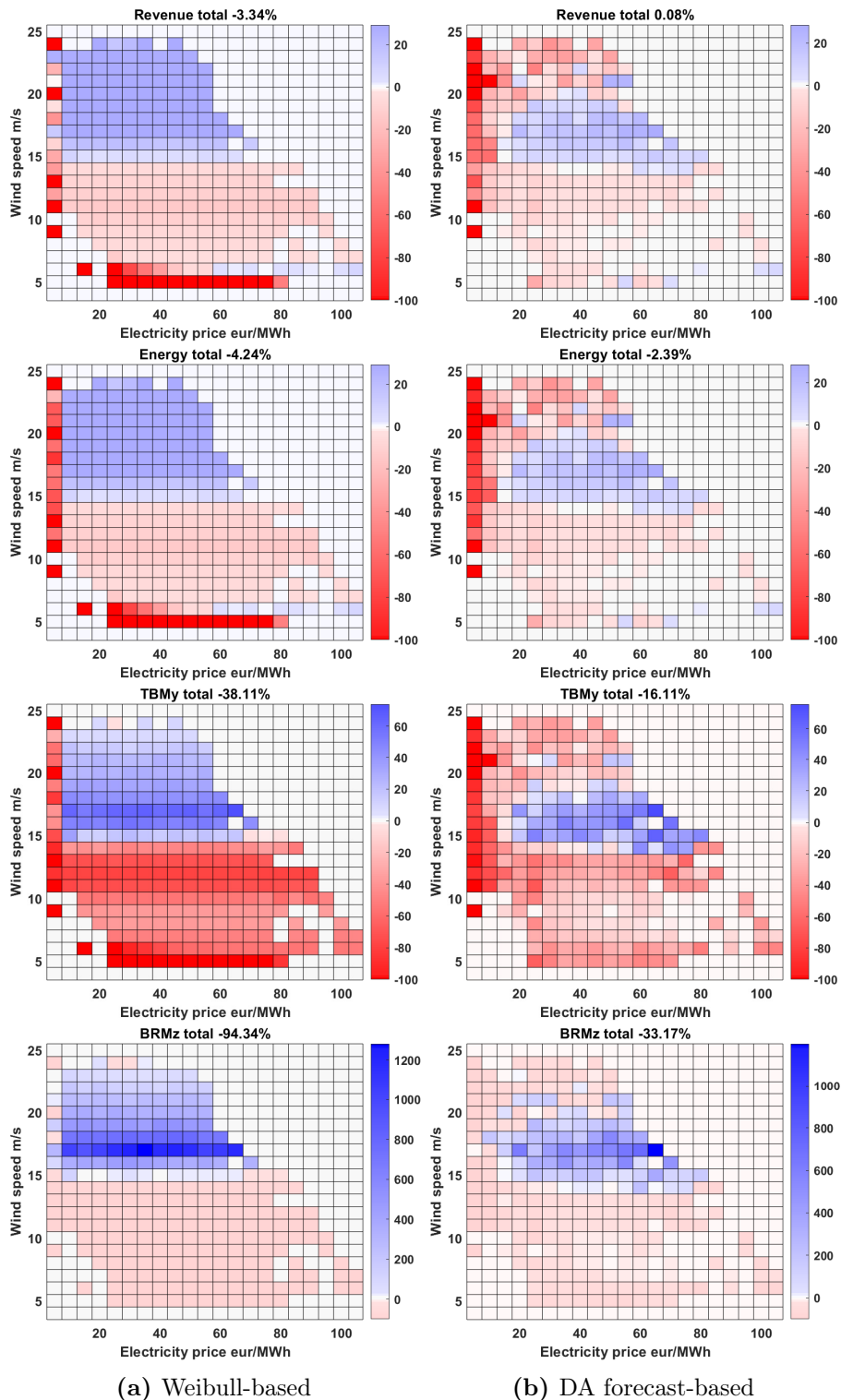
The previous discussion underscores the significance of various factors in influencing the effectiveness of the distribution-based approach under fluctuating prices. These factors include the selection of the fixed price value, the correlation between prices and wind speeds, the variability of turbulence intensity across wind speeds, and the overall fluctuations in wind and prices over time. In contrast, the forecast-based approach exhibits greater resilience to these variations but, concurrently, demonstrates reduced potential for fatigue reduction due to its limited ability to harness advantageous conditions in the long term, stemming from the short optimization horizon used.

To gain a deeper insight into the differences between the two optimization approaches, the relative differences in revenue, energy production, and cumulative fatigue damage compared to the baseline for the binned wind speed-electricity price conditions within the DK\_2019 dataset are presented as an illustrative example, in figure 7.27. These results, in combination with the baseline contributions detailed in section 7.1.1, can shed light on the strengths and weaknesses of each approach.

The revenue and energy results show that the power level scheduling derived based on the mean wind speed distribution is more aggressive in reducing revenue across the entire price spectrum for a specific wind speed. This approach proves effective in mitigating fatigue damage. However, the increase of power levels during high wind speeds cannot adequately offset the revenue reductions, as the combination of high prices and high wind speeds occurs less frequently. Under fixed prices, this power increase showed to be able to compensate for the revenue loss in lower wind speeds due to the constant and higher price. Conversely, the DA approach prioritizes lower prices within the same wind speed range to achieve load reduction through down-regulation. This strategy capitalizes on the greater influence of high-price occurrences on revenue but comes at the expense of fewer reductions in fatigue damage.

Moreover, the revenue threshold for the selective shutdown, derived with fixed prices set at 80 eur/MWh, is relatively high compared to the spot electricity price levels. This leads to shutdown for most of the instances with wind speeds below 6 m/s, regardless of the price level. While this leads to some load reductions, it has a more pronounced impact on revenue and energy production. On the other hand, the DA-based optimization restricts selective shutdown mainly to instances characterized by low prices across all wind speeds. This approach is effective in load reduction with less revenue and energy losses. These two aspects primarily contribute to the discrepancies between the two approaches.

The differences between the cumulative energy and revenue results are mainly driven by the price dynamics. Specifically, the degree of correlation between prices and wind energy production plays a pivotal role. In cases where high prices coincide less frequently with high wind speeds, there tends to be a more substantial reduction in energy production. This is valid for both the forecast- and distribution-based approaches, as exemplified by the results for



(a) Weibull-based

(b) DA forecast-based

**Figure 7.27:** Relative differences of revenue, energy, and fatigue damage for the TBM and BRMz loads to the baseline per wind speed-price bin for the DK 2019 data considering the revenue-neutral load minimization scenario under fluctuating prices. Results with the wind distribution-based optimization are shown in column (a) and results using the DA forecasts of price and wind speeds in column (b). The titles report the cumulative value difference. A maximum power level of 130% and the constTSR down-regulation trajectory is used for both cases

DK\_2020 presented in figure 7.26, which shows the highest energy reduction in all cases, even when revenue neutrality is achieved. As seen in figure 7.27, the DA approach tends to decrease power production or initiate shutdowns at high wind speeds when prices are low. As energy production is not a direct optimization objective, these reductions favor revenue and loads, the actual objectives. This leads to higher reductions in energy output as the power generated at higher wind speeds is larger in volume. For the distribution-based approach, the energy loss is also higher when the prices are more correlated to wind speeds. This results from a higher frequency of cases featuring both high wind speeds and low prices, leading to revenue falling below the shutdown threshold. This effect is particularly pronounced as the overall price level decreases, causing a greater reduction in energy compared to revenue.

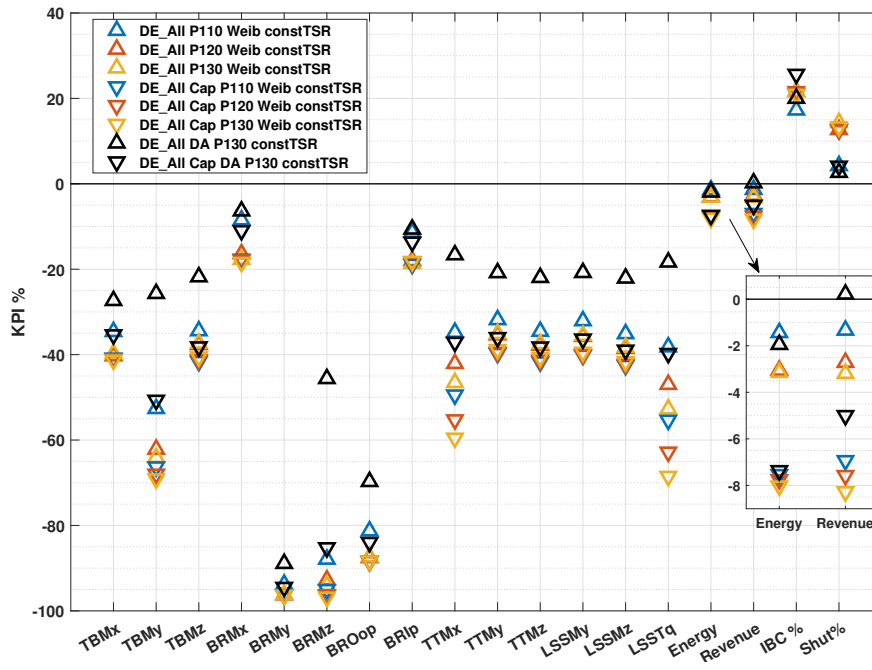
### **Fatigue damage minimization with a revenue loss cap under fluctuating prices**

This section examines the potential of additional cumulative fatigue damage reductions by incorporating a 5% cumulative revenue decrease cap under fluctuating market prices. The results compared to the baseline for various power levels, both down-regulation trajectories and both optimization approaches for the DE\_all dataset are presented in figure 7.28.

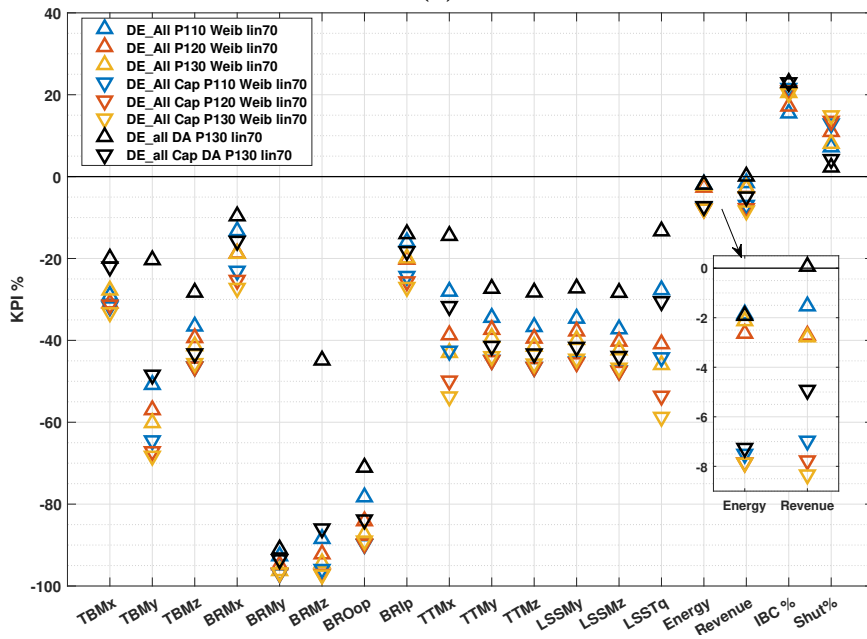
The additional fatigue reductions achieved with the Weibull-based approach are, also in this case, closely aligned with the findings for fixed prices shown in section 7.2.1. This similarity arises because the loads depend only on wind speeds, and the method does not account for price variations. The additional fatigue reductions are minimal for all trajectories and power levels, indicating that implementing the cap offers no noticeable advantages within this optimization approach. The DA forecast-based optimization also yields outcomes akin to the fixed prices scenario in terms of fatigue reduction magnitudes, exhibiting substantial additional load decreases compared to the revenue-neutral case. The discrepancy in outcomes between optimization with DA wind forecasts under fixed prices and optimization with DA wind and price forecasts under fluctuating market prices is found to be lower than 5% for both the revenue-neutral and capped scenarios.

As in the revenue-neutral case, the main difference between the two optimization approaches lies in their response with respect to revenue. The forecast-based approach is able to accurately track the revenue decrease constraint, while with the Weibull-based approach, the revenue reduction is between 6.5% and 8.5% for all power levels and trajectories. The energy production is reduced by 7-8% for all cases, including the DA-based approach.

The relevant results for the DK\_all dataset are presented in figure 7.29. Similar behavior is observed in this case, with the load reduction magnitudes closely resembling those obtained under fixed prices. The additional load reductions with the distribution-based approach are minimal, while the forecast-based approach leads to significant additional reductions. For the



(a)



(b)

**Figure 7.28:** KPIs for load minimization cases including a revenue reduction cap of 5% under fluctuating prices for the DE site. Both trajectories for the whole period considered and different maximum power levels 110%-130% (a) constTSR, (b) lin70

DK\_all dataset, the maximum load reductions are similar for both optimization approaches and both down-regulation trajectories.

Concerning the revenue decrease constraint, it is once again only achieved with the DA approach. The Weibull-based approach results in revenue reductions ranging from 6% to 9% across both trajectories and all power levels, accompanied by corresponding energy reductions

in the range of 8% to 10%. Conversely, the forecast-based approach incurs a reduction of approximately 8% in energy production for both trajectories.

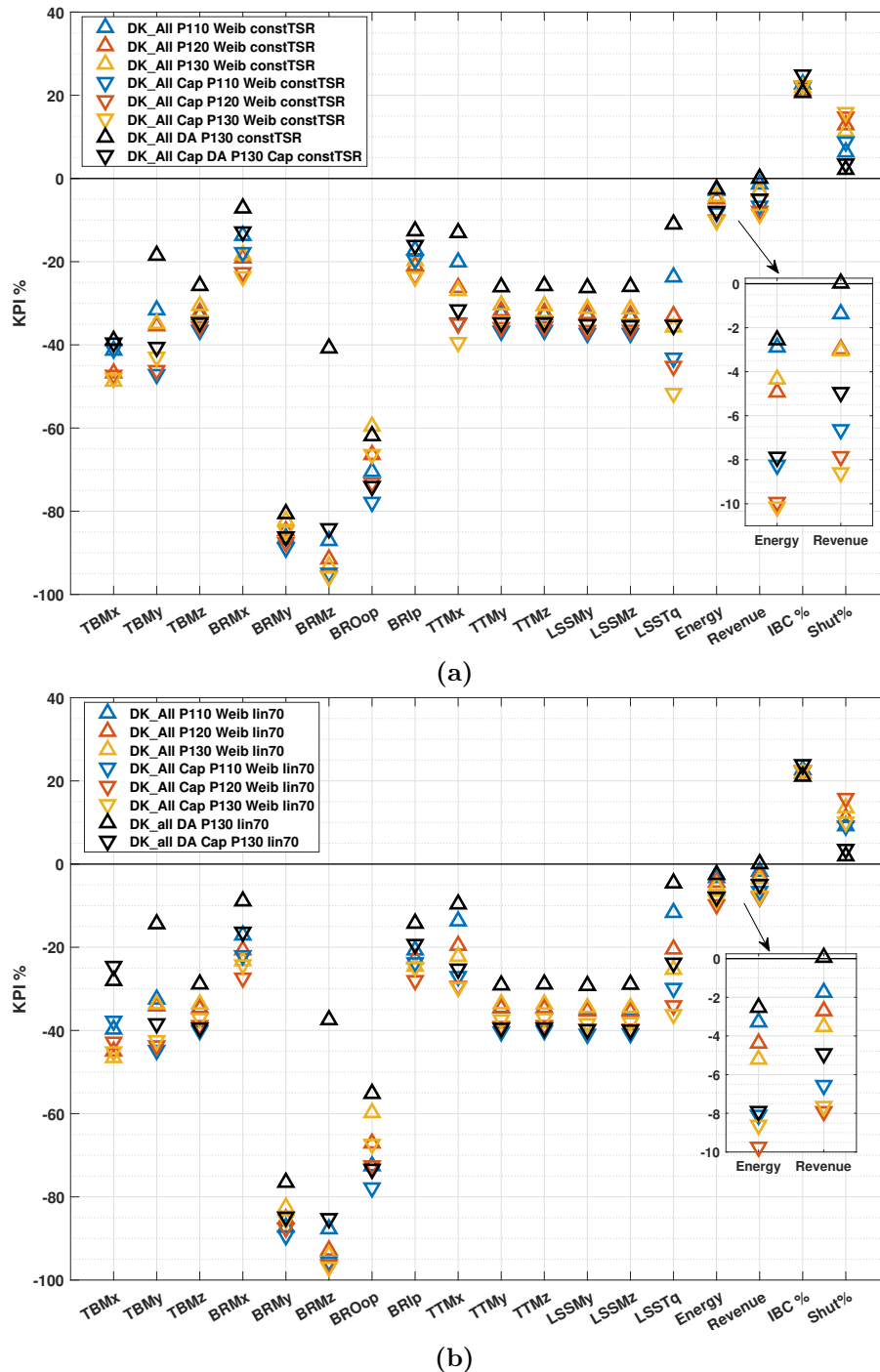
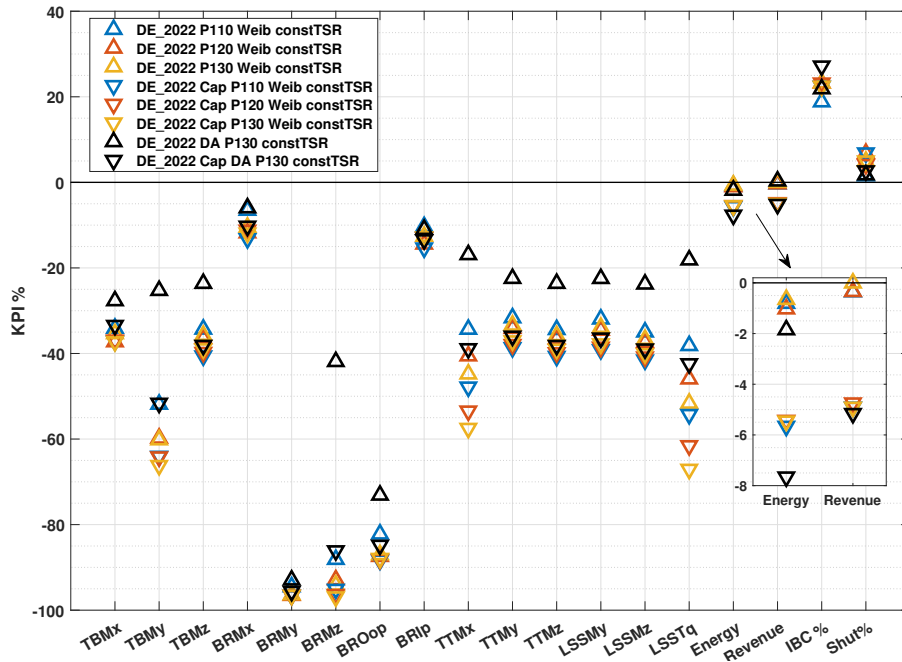


**Figure 7.29:** KPIs for load minimization cases including a revenue reduction cap of 5% under fluctuating prices for the DK site. Both trajectories for the whole period considered and different maximum power levels 110%-130% (a) constTSR, (b) lin70

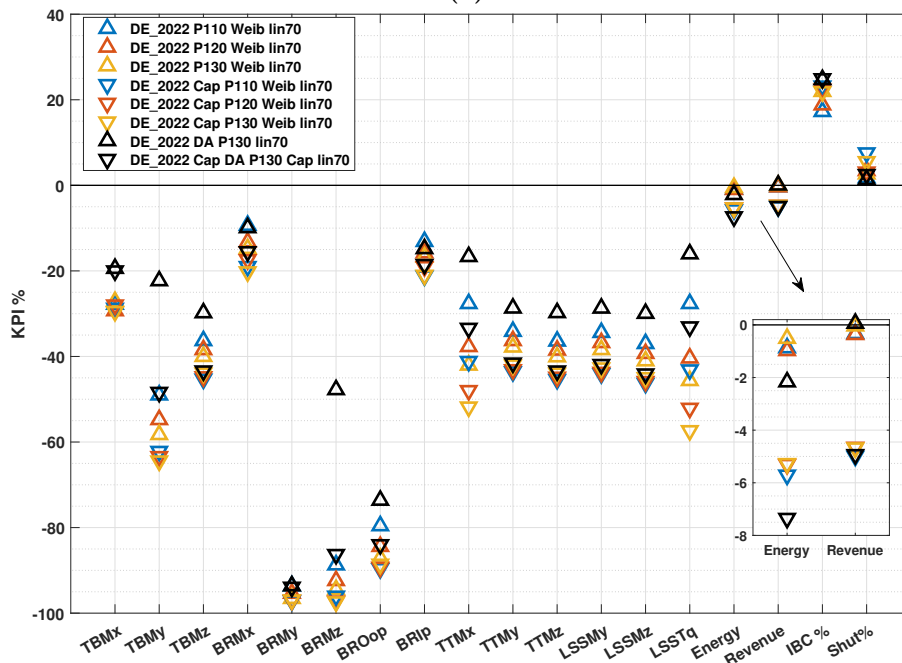
Figure 7.30 presents the results for the DE\_2022 dataset, where notable changes in trends emerge due to differing market price behavior. Fatigue reductions display similar trends to the DE\_all dataset for all cases. However, the revenue decrease constraint of 5% is satisfied

with both optimization approaches for this dataset. Moreover, energy reductions are less pronounced, ranging between 5% and 6% for the Weibull-based approach, and are found to be approximately 7.5% for the DA-based approach. The correlation between wind speeds and prices in the DE\_2022 is weak, resulting in lower tradeoffs between revenue and loads, rendering the Weibull-based approach more effective. Furthermore, the much higher overall price levels cancel out the effect of the shutdown threshold, derived for the Weibull-based approach under fixed prices, as indicated by the reduced downtime. These two factors lead to both approaches being effective under the DE\_2022 conditions. These findings show that the proposed operational management method becomes more robust and efficient under such market conditions.

Overall, the findings of this section showed that revenue-neutral cumulative fatigue damage minimization under fluctuating market prices, for most cases, is only possible with the forecast-based approach, which includes the price forecast as input. With this method, the fatigue reductions across all loads considered are found in the range of 20-30%, with exceptions noted for the BRMx and BRIp loads, which exhibit lower reductions, and the blade BRMy, BROop, and BRMz loads, which demonstrate higher reductions due to the influence of IBC. Similarly, the introduction of an additional revenue decrease cap proves effective exclusively within the DA-based optimization approach, leading to further load reductions. The total energy production is decreased for all cases employing both optimization approaches, showing that revenue and energy production objectives behave differently. The results for the special DE\_2022 case highlight that both optimization approaches are significantly influenced by the wind and market boundary conditions. The considerably higher prices with greater variability, coupled with the weak correlation between prices and wind speeds, lead to the revenue constraint being satisfied and the energy production less reduced with both optimization approaches for both revenue-neutral and capped cases.



(a)



(b)

**Figure 7.30:** KPIs for load minimization cases including a revenue reduction cap of 5% under fluctuating prices for the DE2022 dataset. Both trajectories for the whole period considered and different maximum power levels 110-130% (a) constTSR, (b) lin70

### 7.3.2 Revenue maximization under fluctuating market prices

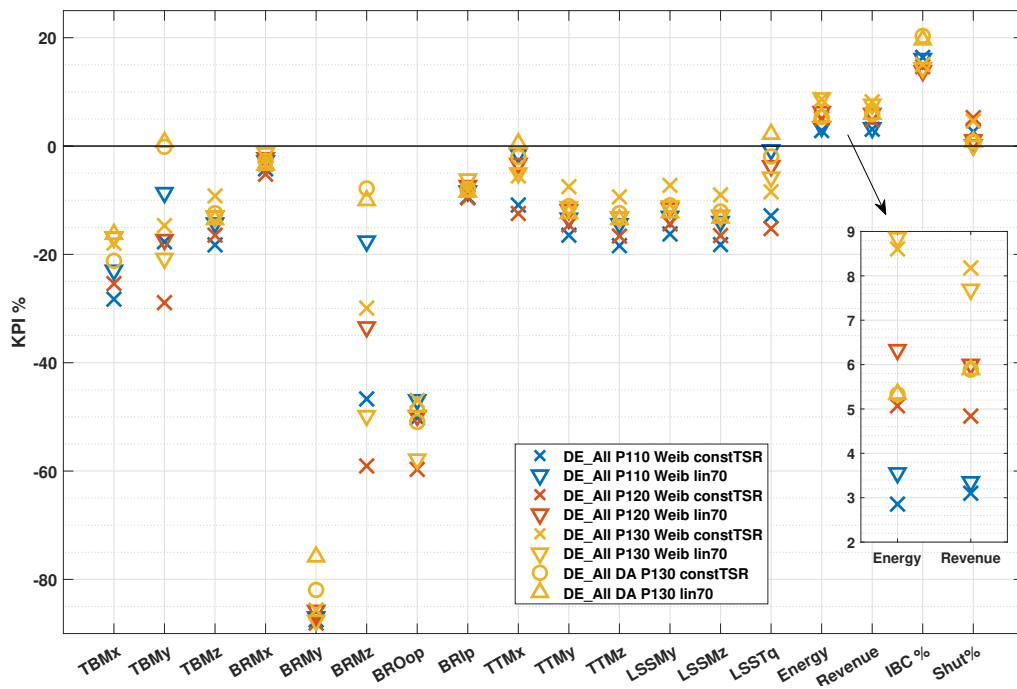
In this section, the findings relevant to accumulated revenue maximization under fluctuating market prices are presented. Figure 7.31 includes the results of load-neutral revenue maximization for the DE\_all and DK\_all datasets considering the entire period. Both optimization approaches are utilized, incorporating various maximum power boosting levels.

For all cases across both datasets, the revenue is increased compared to the baseline, while the fatigue damage does not exceed the baseline levels in most cases. The revenue increases for the DE\_all dataset are higher for all cases compared to the DK\_all dataset. Specifically, using the Weibull-based approach at a 110% maximum power boosting level for the DE site, revenue increases fall within the range of 3-3.5%, rise to 5-6% at 120%, and peak at approximately 8% at 130%. Meanwhile, with the DA-based optimization approach, a revenue increase of around 6% is achieved for both trajectories at a maximum power level of 130%. For the DK\_all dataset employing the Weibull-based approach, the revenue increases are at a level of 2.5%, 3.5-4%, and 4.5% for the 110%, 120%, and 130% maximum power levels, respectively. The forecast-based approach with a maximum power level of 130% yields lower revenue increases in the range of 3-3.5%.

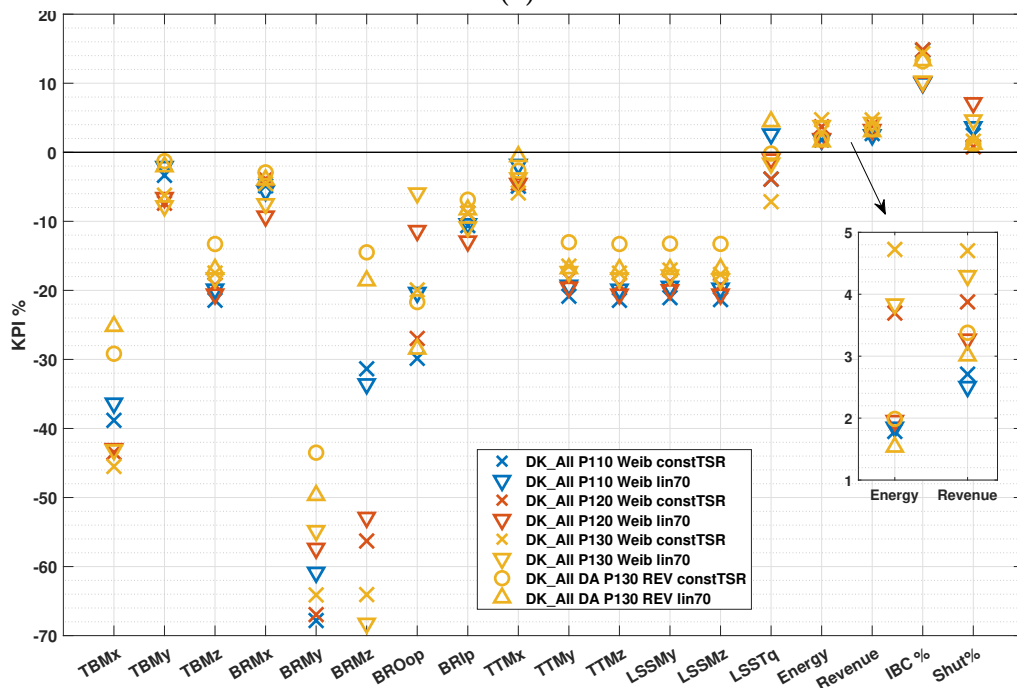
The corresponding results in total energy production are close to the revenue results with less than 0.5% difference for all cases and both datasets, except for the DA-based optimization for the DK\_all dataset where the energy increase is 1.5% lower than the revenue increase. Comparatively, revenue increases achieved through wind distribution-based optimization are generally lower than those under fixed prices for all cases. Conversely, with the forecast-based approach, the increases closely align with the fixed price optimization levels.

The choice of down-regulation trajectory has a marginal impact on revenue and energy production when the DA approach is used. For the forecast-based approach, the constTSR trajectory yields higher increases up to 0.5% for the revenue and 1% for energy production for the DK site. For the DE conditions, the lin70 trajectory leads to higher revenue and energy increases up to 1% compared to the constTSR. In the context of load-neutral revenue maximization under fluctuating prices with the distribution-based approach, the choice of down-regulation set points exerts a higher impact on revenue compared to scenarios with fixed prices. Thus, selecting the optimal set points according to the boundary conditions and the maximum power level can have a modest yet measurable enhancement in the efficiency of the proposed method.

For most cases within both datasets, IBC activation is slightly decreased compared to scenarios with fixed prices for the Weibull-based approach by 2-3%. Notably, this reduction is more pronounced for the DK dataset. It's important to note that the same IBC activation threshold is applied in both cases, and the differences arise from increased selective shutdowns



(a)



(b)

**Figure 7.31:** KPIs for load-neutral revenue maximization cases under fluctuating prices using both trajectories for the entire period considered for both locations and different maximum power levels. Cases based on wind speed distribution and electricity prices are denoted as Weib and cases based on day-ahead forecasts of wind speeds are denoted as DA. P110, P120, and P130 denote the maximum power level allowed for each case. (a) DK\_all, (b) DE\_all

at higher wind speeds when coupled with exceptionally low prices. For the DA-based approach in fluctuating prices, IBC activation is significantly increased for the DK dataset from 13% to 18% and 24% for the lin70 and constTSR trajectories, respectively, in comparison to the fixed prices cases. These values translate to increased blade pitch travel by 100% and 140% compared to the baseline.

For the DE conditions, the IBC activation is not changed compared to the results for fixed prices with the DA-based optimization. IBC is active for approximately 20% of the time for both cases, leading to an increase in blade pitch travel of 340% compared to the baseline case. The different behavior between the two datasets stems, once again, from the higher correlation of wind speeds to prices for the DK conditions along with the elevated TI levels. These factors lead to more frequent power-boosting in wind speed regions that are particularly influential for the loads, requiring higher IBC activation to counterbalance the load increase.

The duration of selective shutdowns is minimal with the DA-based optimization approach, accounting for approximately 1% of the time. In contrast, with the Weibull-based approach, this duration extends up to 5% for the DE dataset with the constTSR trajectory and up to 8% for the DK dataset with the lin70 trajectory, while in the rest of the cases, it remains consistently below 2%. This variation occurs due to the different aeroelastic responses of the turbine to each down-regulation trajectory in combination with the specific wind conditions at each site. Consequently, this divergence in load response led the optimizer to define lower shutdown thresholds in order to compensate for the load increases, resulting in a higher frequency of shutdowns when the same threshold is applied under fluctuating prices.

The fatigue constraint considered in this scenario is, in most cases, satisfied across the entire load ensemble. For the DE conditions, the constraint is only exceeded for the DA-based optimization with a maximum power level of 130%, employing the constTSR trajectory, where the cumulative fatigue damage of the LSSTq load increases by 3%. For the DK conditions, the baseline threshold is exceeded for the DA-based approach with a power level of 130% and the Weibull-based approach with a power level of 110%. In both cases, the LSSTq load exceeds the threshold by 4%.

These findings highlight the differences compared to optimization under fixed prices, where the baseline levels, particularly for the LSSTq load, were exceeded for both sites with the DA approach. Additionally, for the DK site, the baseline was surpassed in all cases employing the lin70 trajectory. This suggests that under fluctuating prices, both optimization methods perform better in terms of achieving the load-neutral constraint for all cases. This is due to the price fluctuations over time. For the Weibull-based approach, these fluctuations result in more frequent selective shutdowns due to low prices, particularly for wind speeds within the rated wind speed region, which is critical for most loads. Furthermore, within the DA-based approach, the variability in prices leads to a higher occurrence over time of situations where

down-regulation or shutdown is feasible in this region, allowing for more effective balancing of loads and revenue.

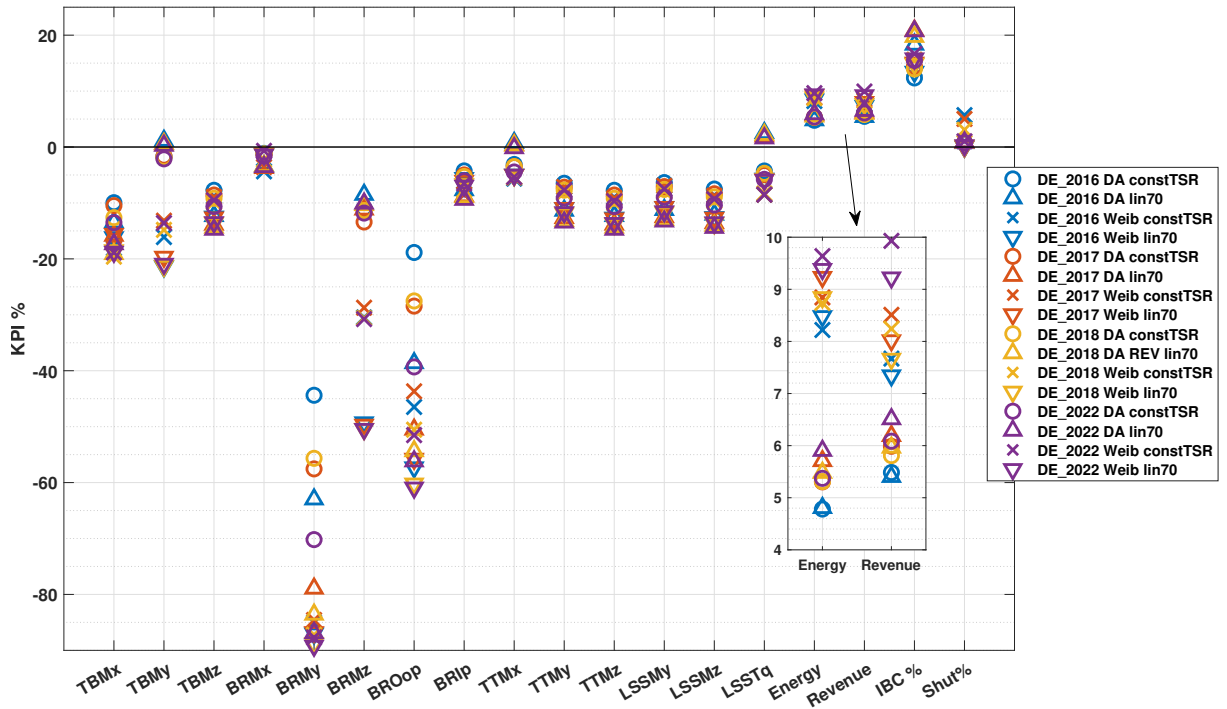
The loads reaching the baseline fatigue threshold and, thus, limiting the revenue maximization are TBMy, TTMx, and LSSTq. This is in agreement with the findings under fixed prices, confirming that the turbine and controller design determine which loads will impose the limit, rather than the boundary conditions. For the remaining loads considered, fatigue margins are generated within the load-neutral revenue maximization scenario.

For the forecast-based approach, the fatigue reductions are similar, within 5%, to those obtained under fixed prices. The only exceptions are the BRMy and BROop loads, which show higher deviations of up to 15% between the two scenarios. These loads consistently experience the most significant reductions, and the higher variations in the responses occur due to their high sensitivity to both IBC and down-regulation. Utilizing the forecast-based approach, the corresponding fatigue margins are similar to the results under fixed prices, with deviations up to 5% for most cases. Comparing the two optimization approaches, the most significant deviations in damage margins are found for the BRMz load for both sites. For the DE conditions, the TBMy load also displays substantial deviations. The BRMz and TBMY loads can only be effectively reduced by lowering the power level, a strategy that can be more efficiently implemented across the entire wind speed range when optimization is conducted based on the mean wind speed distribution.

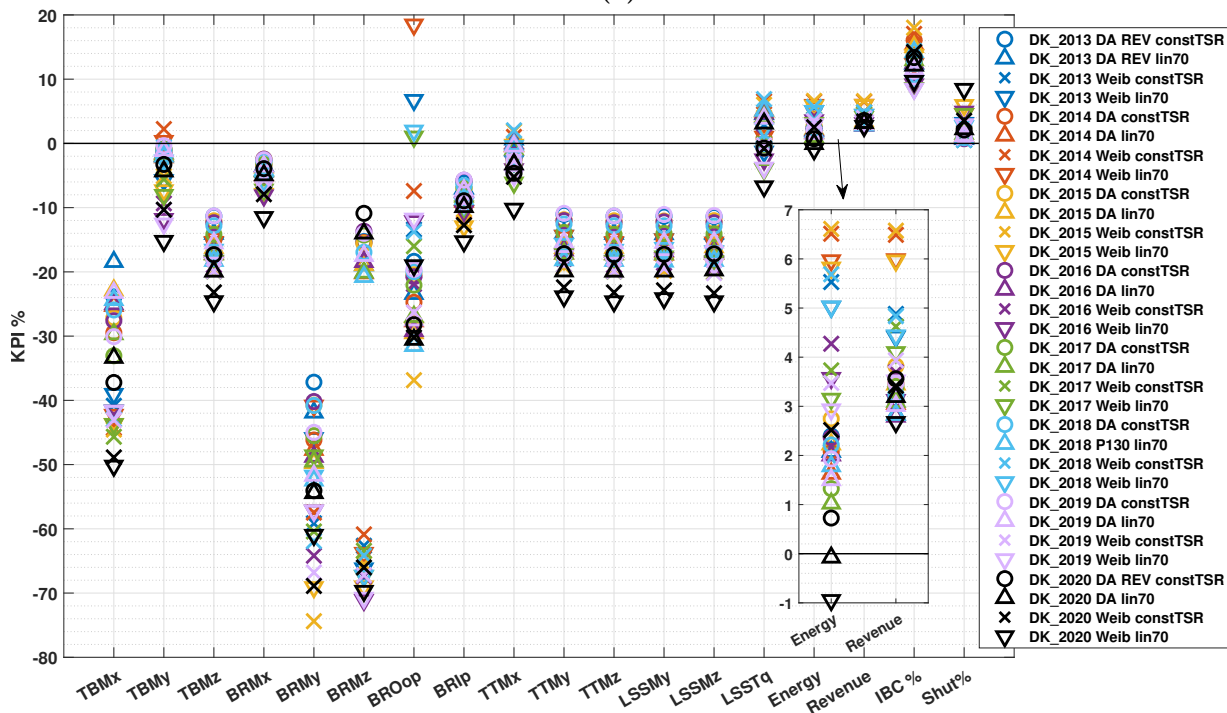
The results of load-neutral revenue maximization for each year, with a maximum power level of 130%, including the DE\_2022 dataset, are presented in figure 7.32. The higher inter-annual variability is also observed in these results, especially looking at the response of the loads, which exhibit greater variations for the DK site. Notably, for the BROop load, the cumulative fatigue damage for the years 2013, 2014, 2017, and 2018 increased by up to 20% compared to the baseline. Nevertheless, as seen in figure 7.31, the total damage for the entire period considered is still reduced by 5% in total. Moreover, for the year 2020, the energy production is reduced compared to the baseline when using both optimization approaches with the lin70 down-regulation trajectory, while the revenue gain remains at a level of 3%.

This discussion underscores the impact of the inter-annual variability as well as the limitations of the Weibull-based approach, which lacks flexibility in adapting to changing conditions. Large deviations in optimization results may occur if the method is applied with a short-term horizon in mind. Moreover, the DK wind and price conditions lead to less distinct variations between the trajectories and the optimization approaches in terms of load responses. In terms of revenue and energy, the differences between the optimization approaches are evident for both sites. The DA-based optimization approach shows consistently lower increases in all cases.

The findings for the DE\_2022 dataset, demonstrate that the Weibull-based optimization approach is more effective in leveraging favorable conditions for revenue optimization. The



(a)



(b)

**Figure 7.32:** KPIs for load-neutral revenue maximization under fluctuating prices using both trajectories per year. Cases based on wind speed distribution are denoted as Weib and cases based on day-ahead forecasts are denoted as DA. The maximum power level allowed is 130% for all cases. (a) DE, (b) DK

revenue results show 1.5-2% higher revenue compared to the year 2018, utilizing the same wind data. With the DA approach, this difference is less than 0.5%. This difference is observed only for the energy and revenue metrics, while in terms of loads, IBC activation, and selective shutdown, the results between 2018 and 2022 are very close.

The effects of the two optimization approaches are further examined by analyzing the relative differences compared to the baseline per wind speed and price bin. Figure 7.33 presents the results for the year 2015 at the DK site using the constTSR trajectory with a maximum power level of 130%. Cumulative revenue is increased by 6.6% with the Weibull-based approach and by 3.8% with the forecast-based approach. The higher revenue increase is explained by the constant maximum power boosting level applied to wind speeds above 16 m/s, which is compensated by the large reductions in fatigue at the rated wind speed region. This strategy is feasible for the Weibull-based approach since the whole period is evaluated in the objective function through the long-term wind distribution, allowing for revenue maximization while generating higher damage margins.

In contrast, the results obtained through the DA-based approach suggest that, within the intraday wind and price variations, the level of power boosting is lower in order to balance loads and revenue within these short periods. Similarly, the reduction of power in the rated region is mainly happening for the lower prices. For higher prices in this region, the results show low or no reductions in loads, as the optimizer is trying to boost revenue in the cost of loads within days when these wind speeds are prevalent. This behavior leads to much lower damage margins, especially for the loads depending on down-regulation for reduction, as seen from the LSSTq and BRMz results. Additionally, it results in overall lower revenue gains when compared to the Weibull-based approach.

The corresponding results for the DE site for years 2018 and 2022 are shown in figures 7.34 and 7.35. The correlation between prices and wind speeds allows for an overall higher gain in revenue and energy compared to the DK conditions. This is because higher prices occur more often for wind speeds above the rated region where power boosting can be applied with a lower impact on loads. Moreover, the combination of wind speed distribution and TI levels at the DE site allows for higher power levels to be applied in the wind speed range of 13-15 m/s lying in the rated region, which is critical for loads but also for revenue due to its relatively high occurrence. This can be observed by the higher fatigue increase in this region for the DE site compared to the DK site. This higher increase is offset by greater load reductions in the rated and below-rated regions, which have a higher frequency of occurrence and are also more often combined with lower prices compared to the DK site. These observations are valid for both optimization approaches, with the DA-based approach showing more pronounced differences between the two sites due to the limited optimization horizons.

Comparing the two years for the DE site with the wind distribution-based approach, the

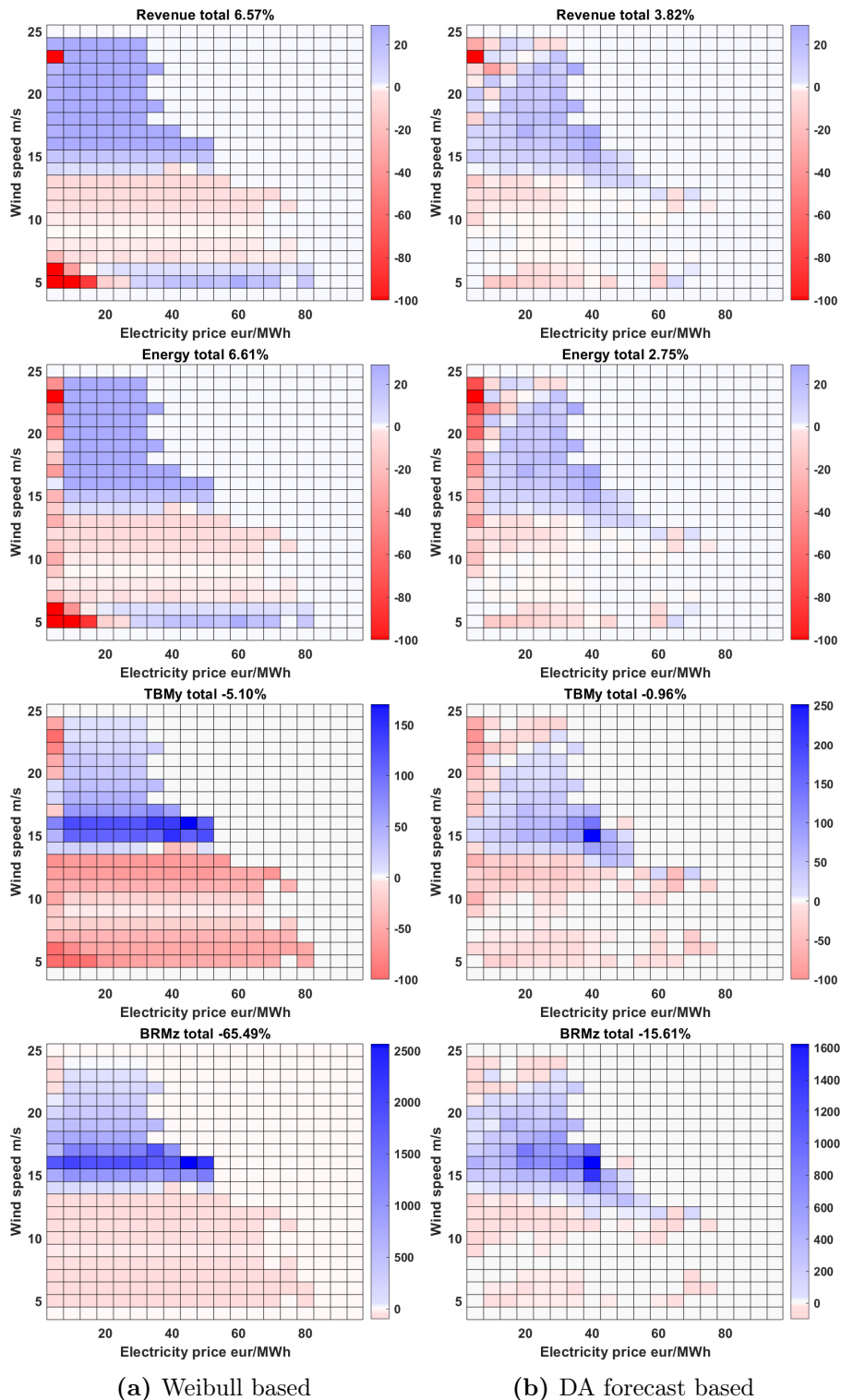


**Figure 7.33:** Relative differences of revenue, energy, and fatigue damage for the TBMz and BRMz loads to the baseline per wind speed-price bin for the DK 2015 data considering load-neutral revenue maximization under fluctuating prices. Results with the wind distribution-based optimization are shown in column (a), and with the DA forecasts in column (b). The plot titles report the cumulative value difference. A maximum power level of 130% and the constTSR down-regulation trajectory are used for both cases

discrepancies in the increase of revenue, which is 8.2% for 2018 and 9.9% for 2022, and energy, which is 8.7% for 2018 and 9.6% for 2022, are primarily driven by the higher prices occurring more often at high wind speeds. In contrast, when employing the DA-based optimization, the results between the two years are very similar. In this context, the optimizer is not aware of the frequency of occurrence of high prices in the long term as it is only driven by the daily wind speed variations.

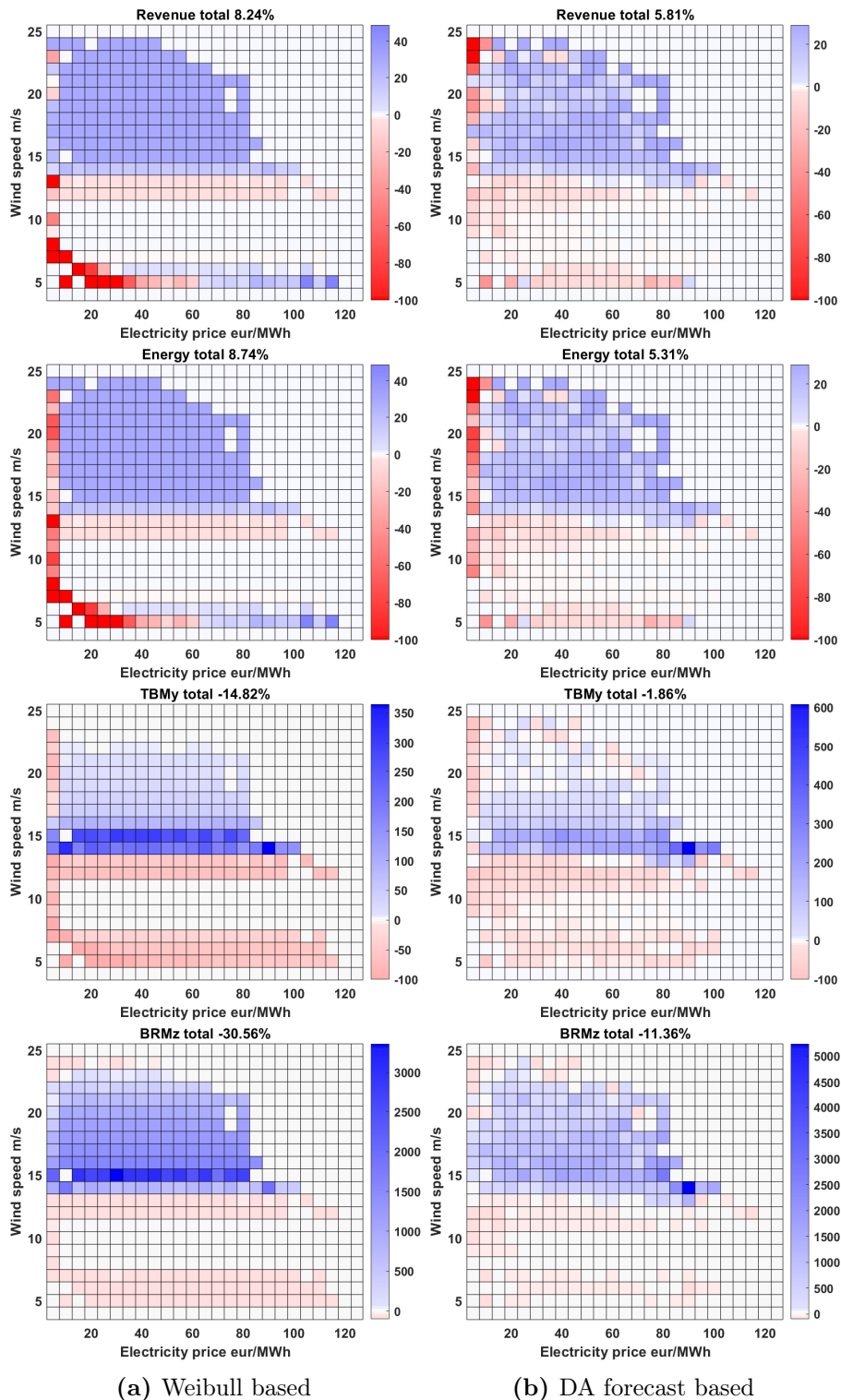


**Figure 7.34:** Relative differences of revenue, energy, and fatigue damage for the TBMz and BRMz loads to the baseline per wind speed-price bin for the DE 2018 data considering load-neutral revenue maximization under fluctuating prices. Results with the wind distribution-based optimization are shown in column (a), and with the DA forecasts in column (b). The plot titles report the cumulative value difference. A maximum power level of 130% and the constTSR down-regulation trajectory are used for both cases

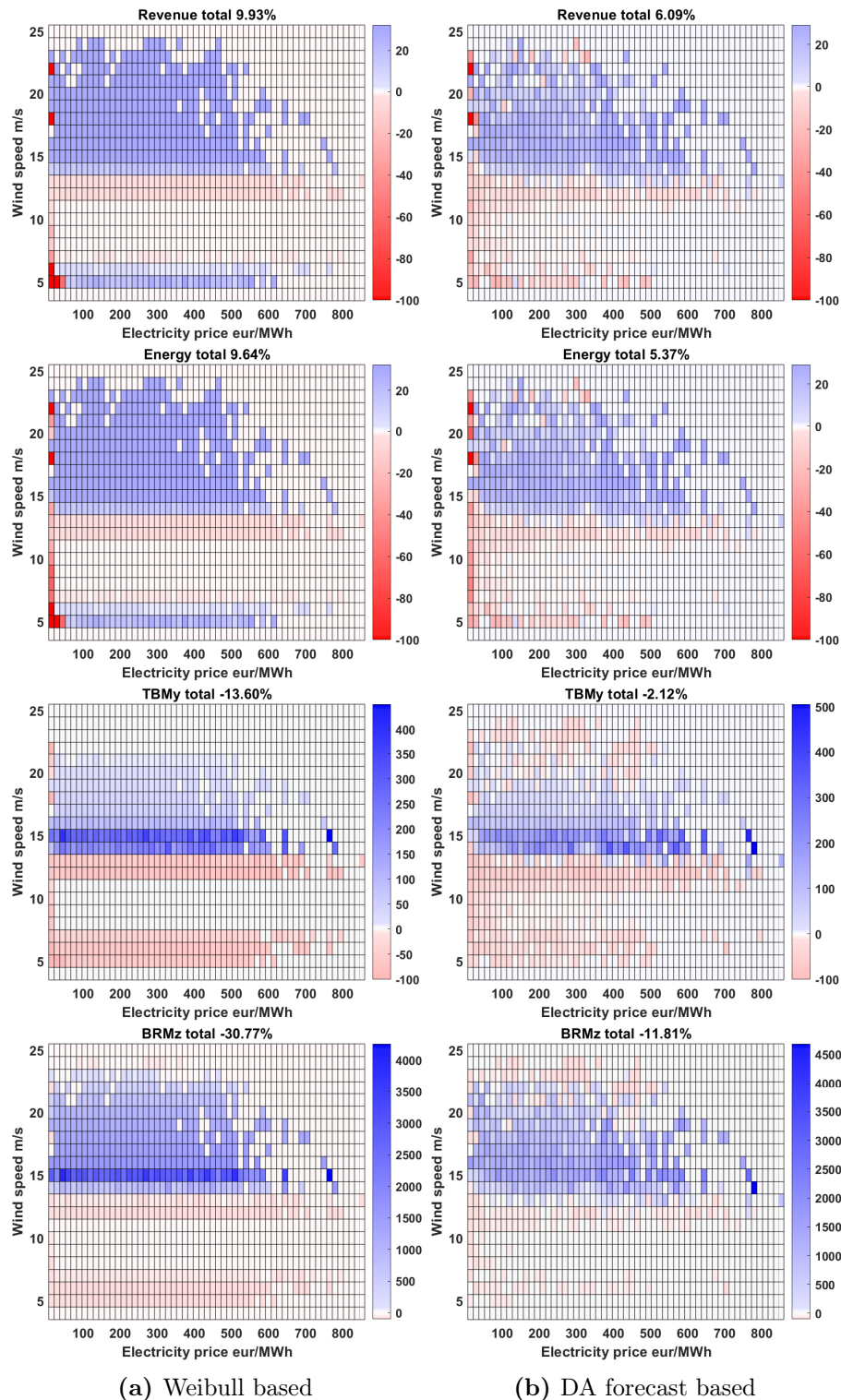


**Figure 7.35:** Relative differences of revenue, energy, and fatigue damage for the TBMy and BRMz loads to the baseline per wind speed-price bin for the DE 2022 data considering load-neutral revenue maximization under fluctuating prices. Results with the wind distribution-based optimization are shown in column (a), and with the DA forecasts in column (b). The plot titles report the cumulative value difference. A maximum power level of 130% and the constTSR down-regulation trajectory are used for both cases

### Revenue maximization with a load increase cap under fluctuating prices

The potential to increase revenue further by allowing a fatigue damage increase cap in optimization under fluctuating prices is investigated in this section. The results for the DE\_all dataset, including a 5% load increase cap, are presented in figure 7.36.

In all cases for both trajectories, additional revenue increases are achieved compared to the load-neutral case. Specifically, with the Weibull-based optimization approach employing the constTSR trajectory, additional revenue increases of 1%, 2%, and 0.2% are achieved for the maximum power levels of 110%, 120%, and 130%, respectively. When using the lin70 trajectory, these increases amount to 0.8% 1% and 1.2% for the corresponding maximum power levels. These values are at comparable levels with the additional increase reported for the fixed prices. The energy production shows additional increases at the same level as the revenue. The least additional revenue increase is found for the case using the constTSR trajectory with the 130% maximum power level. This is due to the more frequent selective shutdown. As seen from the fixed price scenarios, the shutdown threshold was set higher for this power level to offset the higher load increases stemming from the higher power boosting level. When this threshold is applied under fluctuating prices, it leads to higher shutdown frequency, which translates to lower revenue increases. Furthermore, the results regarding the IBC activation are similar to the results under fixed prices.

Regarding the DA-based optimization with a 130% maximum power level, additional increases in both revenue and energy of approximately 0.8% are observed for both down-regulation trajectories. The IBC activation is decreased compared to the revenue-neutral case by approximately 5%, which shows the opposite behavior to the results under fixed prices. This suggests that including the prices in the DA optimization, compared to using only the wind speeds, influences the optimization outcome for revenue objectives in contrast to the findings regarding fatigue minimization. The selective shutdown frequency has not changed compared to the load-neutral cases.

The loads that reach the fatigue cap and, therefore, determine the limit of revenue maximization vary depending on the down-regulation trajectory. With the constTSR trajectory, TBMy is the limiting factor, while with the lin70 trajectory, TBMy, TTMx, and LSSTq play this role. The 5% limit is satisfied for all cases except for the 110% maximum power level with both trajectories. For this power level with the constTSR trajectory, the fatigue damage of TBMy increases by 8% compared to the baseline, and with the lin70 trajectory, the BRMz load shows an increase of 8%. Notably, for the 130% maximum power level in combination with the constTSR trajectory for the Weibull-based approach, the results indicate that none of the loads exceeds the baseline levels under fluctuating prices. This highlights a limitation of the Weibull-based optimization approach applied in scenarios under fluctuating prices, where

the effect of the price levels on selective shutdowns, as well as revenue distributions (as shown in previous results), can restrict its effectiveness.

For the rest of the loads that do not reach the fatigue limit, the damage margins produced

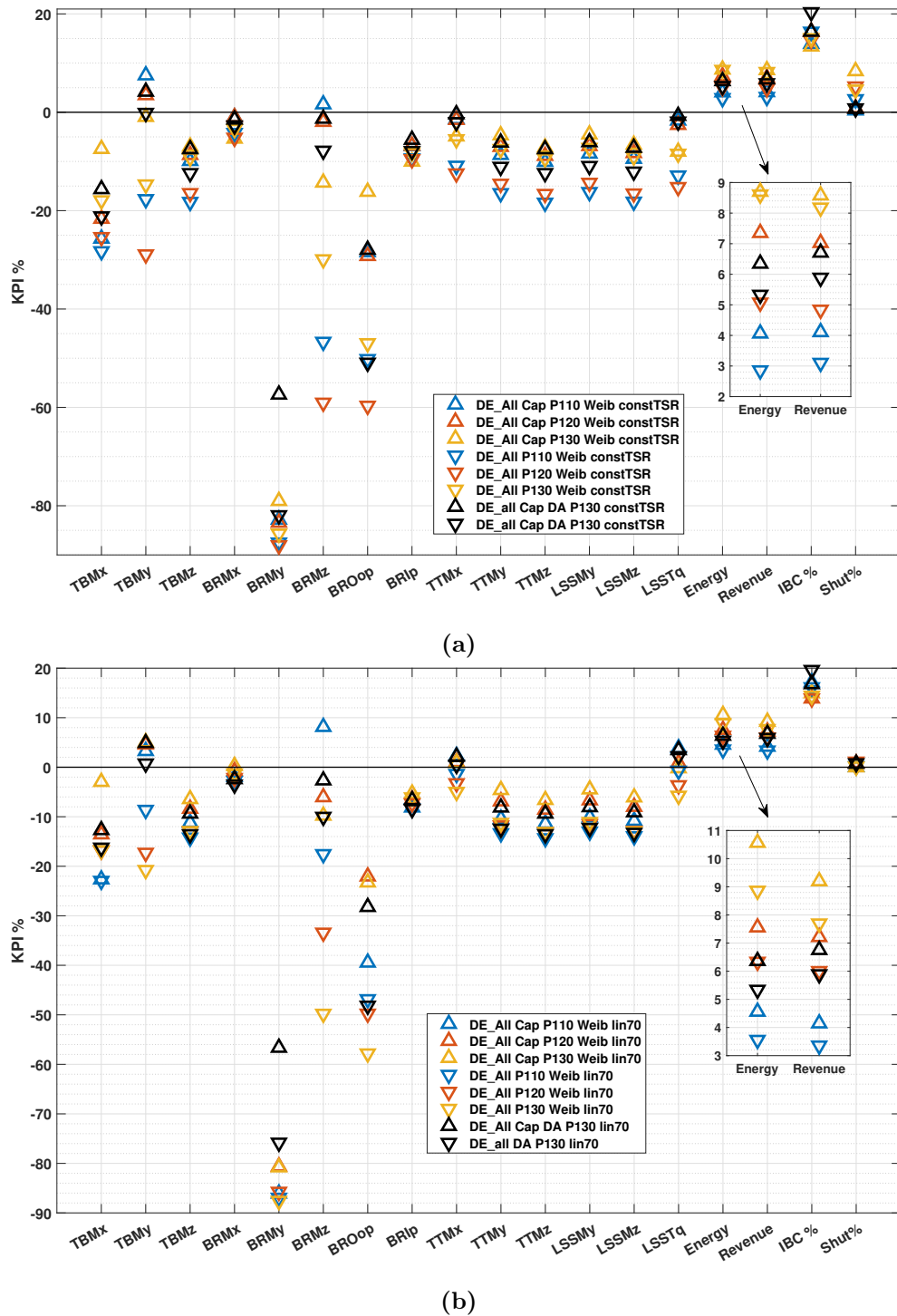


**Figure 7.36:** KPIs for revenue maximization with a load increase cap under fluctuating prices using both down-regulation trajectories for the DE site. Cases based on wind speed distribution are denoted as Weib and cases based on day-ahead forecasts are denoted as DA. The maximum power level is 130% for all cases. (a) constTSR, (b) lin70

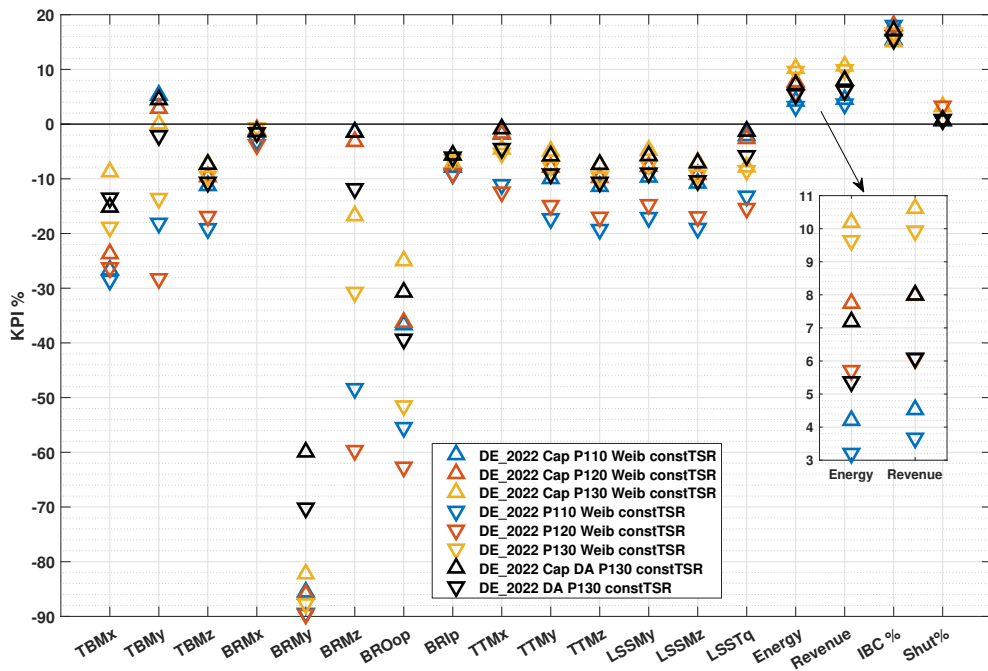
within the revenue maximization scenario with a load increase cap closely resemble the margins obtained under fixed prices, with differences of less than 3% for all cases. Considering the DA-based optimization approach with the constTSR trajectory, the damage margins are slightly decreased by approximately 2-5% compared to the fixed prices, except for the BRMy and BROop loads, where the damage margins are substantially decreased by 20-30% due to the decreased IBC activation under fluctuating prices. Nevertheless, these loads still maintain the highest damage margins. Considering the lin70 trajectory, the differences in damage margins to the fixed price scenario are smaller to a level of 2% for most loads and 10-15% for the BRMy and BROop loads.

The outcomes of revenue maximization with a 5% load increase cap for the DE\_2022 dataset are presented in 7.37. When utilizing the Weibull-based approach with the constTSR trajectory, additional revenue increases of 1%, 2%, and 0.5% are observed for the 110%, 120%, and 130% power levels, respectively. Meanwhile, with the lin70 trajectory, the corresponding increments are 0.5%, 1%, and 1.3%. In the case of the DA-based optimization approach with a maximum power level of 130%, additional revenue increases of 2% are identified with the constTSR trajectory and 1.3% with the lin70.

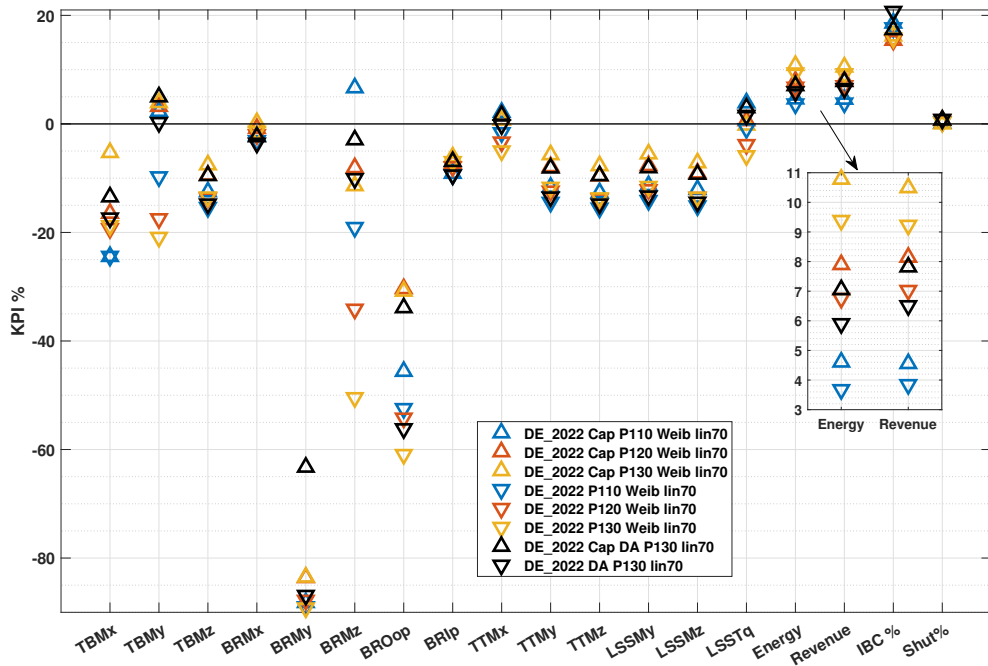
Compared to the results for the DE\_all dataset, the additional revenue increases achieved with the Weibull-based optimization are similar for the DE\_2022 dataset. However, with the DA-based optimization approach, the increase is notably higher for the DE\_2022 dataset. This observation shows that for revenue maximization scenarios, the DA-based optimization approach can more efficiently leverage the load increase cap in market conditions characterized by higher price variations and lower price-wind speed correlations. Nevertheless, the revenue increase achieved by the DA-based approach is still 2.5% lower than the increase attained with the Weibull-based approach for the same maximum power level. The 8% revenue increase achieved for the DE\_2022 case with the constTSR trajectory is the overall highest increase observed with the DA-based optimization for all cases examined in this work.

In terms of load response, the results are very close to those for the DE\_all dataset with the exception of BRMy and BROop loads, which are further reduced by 5-10%. This verifies that, across all scenarios considered, the fatigue damage outcomes within the proposed operational optimization approach are primarily influenced by the wind conditions, the controller design, and the optimization method, whereas the revenue and energy outcomes are driven by the price fluctuations and their correlation with wind conditions.

The results for the DK\_all dataset are shown in figure 7.38. For the DK conditions, employing the load cap with the Weibull-based approach in combination with the constTSR down-regulation trajectory leads to additional revenue increases of 0.5%, 0.2%, and 1% for the 110%, 120%, and 130% maximum power levels, respectively. The relatively low additional increase for the 120% case can be attributed to the relatively high, for the market price levels,



(a)



(b)

**Figure 7.37:** KPIs for revenue maximization with a load increase cap under fluctuating prices using both down-regulation trajectories for the DE2022 dataset. Cases based on wind speed distribution are denoted as Weib and cases based on day-ahead forecasts are denoted as DA. The maximum power level is 130% for all cases. (a) constTSR, (b) lin70

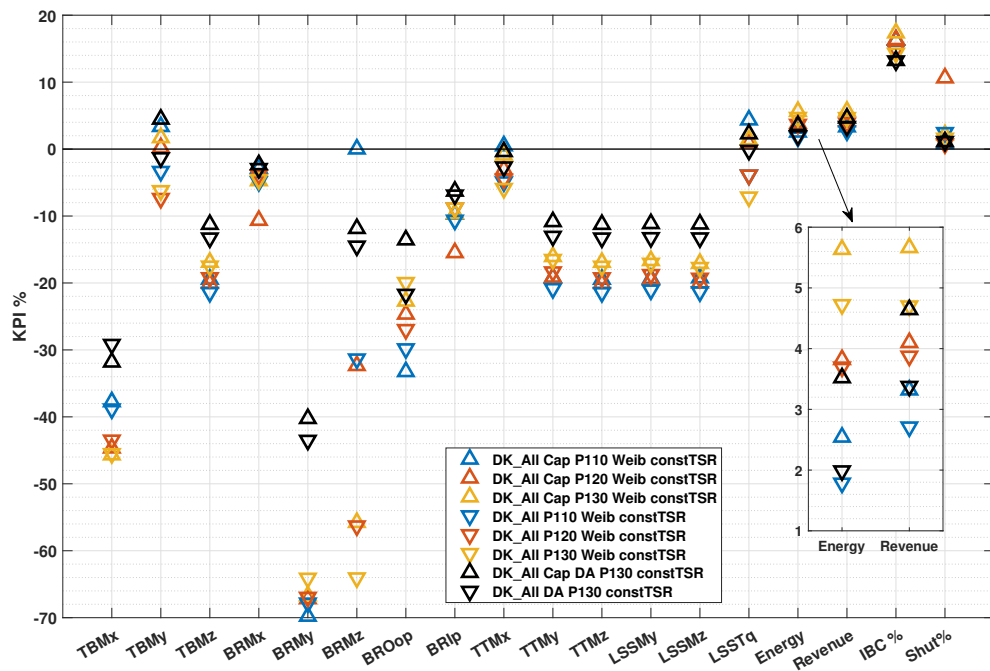
selective shutdown threshold as seen from the downtime percentage. As seen for the DE cases too, this is due to the derivation of the optimization parameters based on a higher fixed price in combination with the requirement for load and revenue balancing in the specific conditions.

For the lin70 down-regulation trajectory, the corresponding increases are found to be 0.8%, 0.5%, and 1.1% for the same maximum power levels. Employing the DA-based optimization approach, the additional revenue increase for a maximum power level of 130% is 1.3% with the constTSR trajectory and 1.1% with the lin70 trajectory. These findings underscore that under fluctuating prices, the DA-based approach, which considers both wind speeds and prices, is more effective compared to the DA optimization under fixed prices, as the load increase cap did not yield any additional revenue for the DK cases.

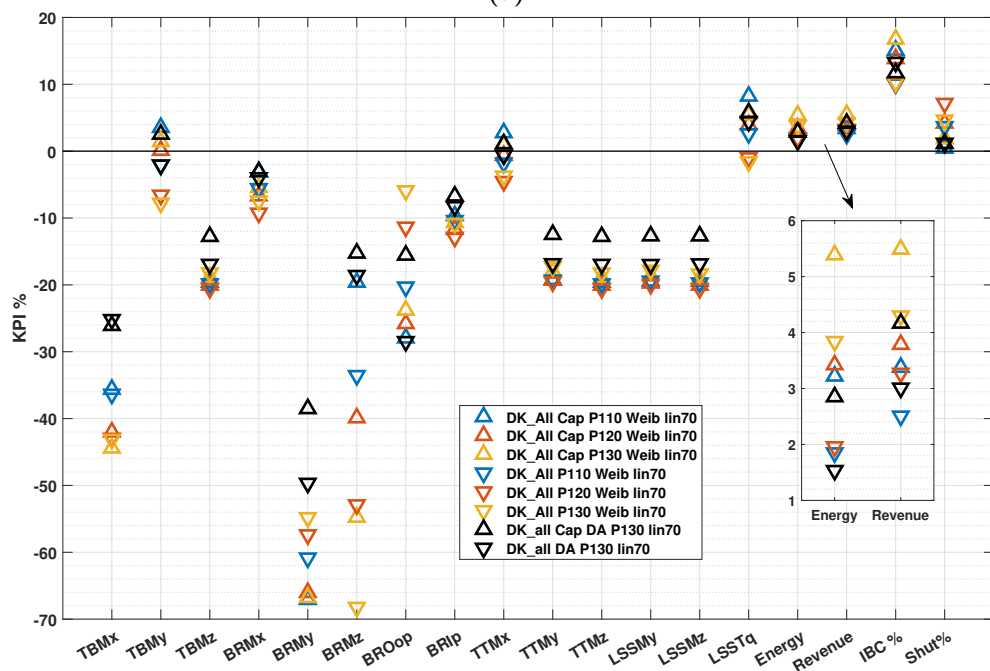
The loads approaching the fatigue cap limit are TBMy and LSSTq when the constTSR is employed and TBMy, TTMx, and LSSTq when the lin70 trajectory is used. The limit is only exceeded for the LSSTq load by 3% when the lin70 trajectory is used in combination with the lowest maximum power level considered of 110%. The resulting damage margins are similar, with the margins achieved for the optimization under fixed prices when the Weibull-based optimization approach is utilized.

Employing the DA-based approach with the constTSR trajectory, the fatigue margins are lower than the margins achieved with the Weibull-based approach. Furthermore, the fatigue margins are reduced by 1-5% for most loads compared to the same optimization scenario under fixed prices. The BRMy and BROop loads exhibit higher decreases of 20% and 30%, primarily due to the increased IBC activation. The fatigue margins for the revenue optimization with a load increase cap, relative to the baseline, for the TBMz, BRMz, BROop, TTMy, TTMz, LSSMy, and LSSMz loads range from 10% to 15% for both trajectories. The TBMx load shows a fatigue margin of 25-30%, and the BRMy load shows a margin of approximately 40%, which is the highest achieved for the DK dataset in this scenario.

Compared to the DE conditions, the DK conditions, characterized by higher variability as well as higher correlation of price and wind speeds, produce overall lower revenue gain in revenue-focused optimization cases. Moreover, more loads approach the fatigue limit, and greater differences are observed between the two down-regulation trajectories. In parallel, the DK conditions yield higher fatigue margins across the majority of loads considered, for all trajectories and power levels considered. Finally, the 110% maximum power boosting level shows, for both datasets and down-regulation trajectories, the least increase in revenue and the highest increase in fatigue with the additional load cap.



(a)



(b)

**Figure 7.38:** KPIs for revenue maximization with a load increase cap under fluctuating prices using both trajectories for the DK site. Cases based on wind speed distribution are denoted as Weib and cases based on day-ahead forecasts are denoted as DA. The maximum power level is 130% for all cases.

(a) constTSR, (b) lin70

### 7.3.3 Sensitivity to day ahead forecast uncertainty under fluctuating prices

This section investigates the sensitivity of the optimization outcomes to uncertain DA forecasts of price and wind speeds. To achieve this, the original time series of wind speed, TI, and electricity prices are modified with the addition of noise. This is implemented by generating a series of random numbers with equal length to the original time series based on a Gaussian distribution with zero mean and appropriate standard deviation values, which is superimposed on the original time series. The choice of a zero mean is based on the assumption that over time, under- and over-predictions for the different quantities cancel out. Subsequently, during the optimization process, the modified time series are input to the optimizer, and the optimization outputs are assessed within the evaluation framework using the original time series.

This is a simplified approach to investigate the uncertainty in the DA forecasts. More precise modeling of the forecast uncertainty, possibly based on historical forecasts, along with more systematic analyses, is required to gain a deeper understanding of the impact of forecast uncertainty on the operational management optimization methods proposed in this work. Nonetheless, the approach employed here can still provide initial insights into the influence of forecasting uncertainty on the optimization outcomes.

Three representative datasets with a full-year duration, chosen to avoid seasonal biases, are considered for this sensitivity analysis: DE\_2017, DE\_2022, and DK\_2015. For all cases, the standard deviation of the noise time series applied to the wind speed and TI time series is set to 0.5. This choice is based on the discussion in section 5.3, aiming for a mean absolute error of 2-15% for most days. Regarding the DA forecast of spot prices, the standard deviation of the noise time series is set to 4.3, 50, and 3.1 eur/MWh for the DE\_2017, DE\_2022, and DK\_2015 datasets, respectively. These values were chosen again based on the literature findings aiming for a 10-20% mean absolute error for each day. For the DE\_2022 dataset, this was increased to 15-30% in order to account for the increased price magnitudes and variability, as well as the more complex financial and political conditions leading to possibly higher uncertainty in market forecasting. Figure 7.39 shows an example snippet comparing the modified time series to the original time series for the DK\_2015 dataset. It should be noted that the choice of these values is a preliminary estimation, taking a conservative approach due to the wide range of reported values in the literature for DA forecasting of wind speeds and prices. These can vary highly based on factors such as the forecasting method used, site-specific characteristics, and electricity market modeling.

The results for load-neutral revenue maximization using the constTSR down-regulation trajectory and a 130% maximum power level are presented in 7.40. The figure provides a comparison of the optimization outcomes using the original and modified time series.

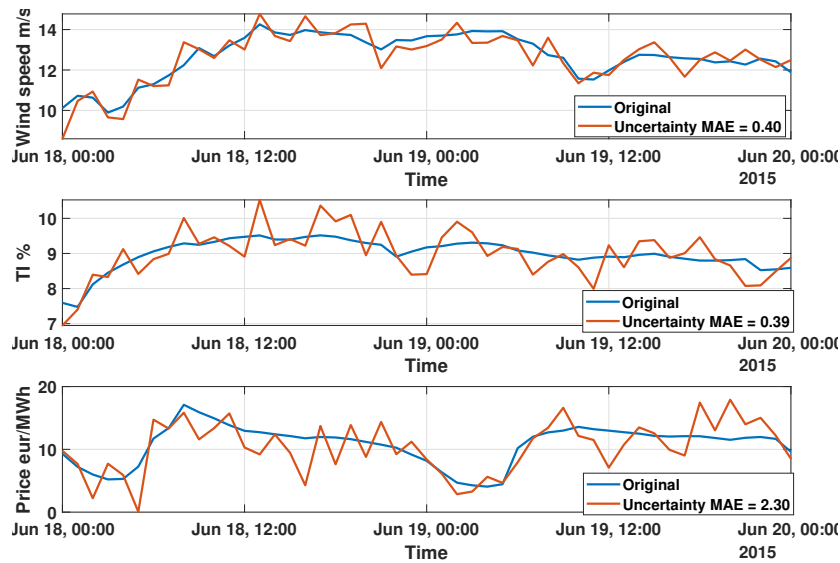


**Figure 7.39:** Example time series of wind speed, TI, and electricity prices with the added uncertainty from the DK2015 dataset. The mean absolute error (MAE) is reported in each legend for the total duration.

The results demonstrate that the forecast uncertainty has a higher impact on fatigue objectives rather than revenue objectives. The TBM<sub>y</sub> and BRM<sub>z</sub> loads exceed the baseline levels for all cases. In the case of the DE\_2022 dataset, the LSST<sub>q</sub> load also exceeds the baseline level by 4%. The loads most affected by this uncertainty are not necessarily the loads shown to limit the optimization when the original time series is used but rather loads that are less influenced by IBC. The BRM<sub>z</sub> load, which displays the highest differences, showed fatigue reductions higher than 10% with the perfect forecasts. However, in the presence of forecast uncertainty, fatigue significantly increased compared to the baseline values by 16%, 40%, and 8%, for the DE\_2017, DE\_2022, and DK\_2015 datasets, respectively. For the TBM<sub>y</sub> load, the corresponding values are 8%, 12%, and 2%. The highest impact on loads across the entire load ensemble is found for the DE\_2022 dataset. This shows that the higher uncertainty in forecasts and the higher variability in the original conditions exert the most significant influence on the optimization outcomes.

Comparing the results for DE\_2017 and DK\_2015, datasets characterized by similar levels of uncertainty and relatively stable market behavior compared to DE\_2022, it is observed that uncertainty has a more pronounced impact on the DE dataset. This could be possibly attributed to the highest intraday variability of the DK conditions acting as a dampening factor on the effects of forecast uncertainty on the optimization. However, it's essential to acknowledge that more systematic research and a more precise modeling of uncertainty are required to draw definitive conclusions regarding this matter.

On the other hand, the revenue and energy results are not significantly influenced by the uncertainty in the input forecasts. Differences within a range of up to 1.2% are observed for

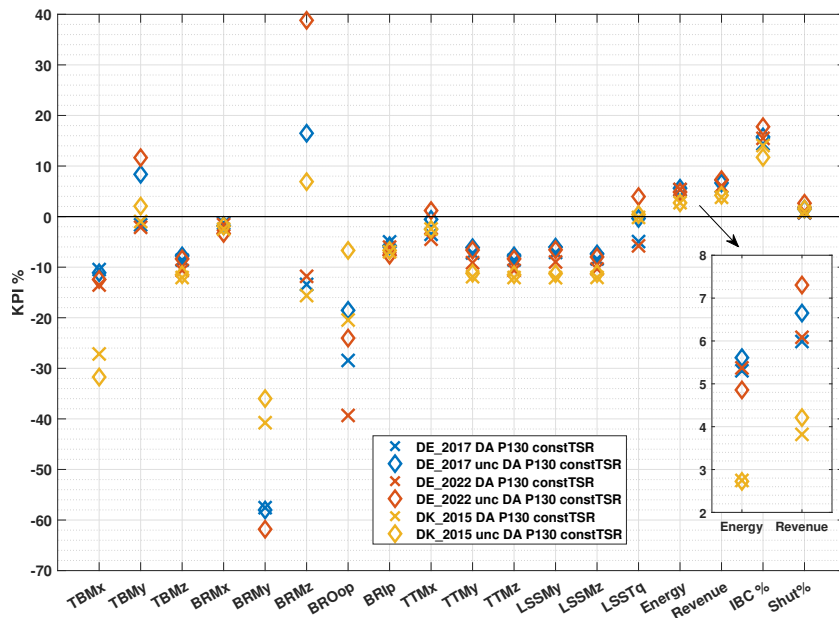


**Figure 7.40:** Comparison of results of load neutral cumulative revenue maximization based on DA forecasts under fluctuating prices with and without uncertainty in the forecast. All results are shown as relative differences to the baseline. Cases with uncertain DA forecasts are denoted as unc.

all cases. The highest discrepancies are observed for the DE\_2022 dataset, while for DE\_2017 and DK\_2015, they are less than 0.5%. This observation, coupled with the fact that loads dependent only on down-regulation for load balancing are found to be the most sensitive to the uncertainty, indicates that the forecasting uncertainty influences mostly the fatigue objective through the high sensitivity of some loads to specific wind conditions. In contrast, the revenue objective is still adequately captured, as it is less sensitive to specific wind speed ranges.

Figure 7.41 presents the relevant results for a revenue-neutral fatigue minimization case, comparing the optimization outcomes with the original and uncertain time series. The maximum power level is 130%, utilizing the constTSR down-regulation trajectory for all cases.

The revenue constraint is minimally influenced by the forecast uncertainty, resulting in a revenue reduction of less than 0.5% for the DE\_2017 and DK\_2015 cases, while for the DE\_2022 case, the revenue reduction is 0.8%. The energy production is also decreased in the presence of forecast uncertainty by less than 1% for DE\_2017 and DK\_2015 and by 2.4% for DE\_2022.

The forecast uncertainty has minimal impact on the fatigue reductions achieved for most loads, with the exceptions being the TBMy and BRMz loads. For the TBMy load, the fatigue reductions decrease from 25% to 15% for the DE cases, while for the DK case, the forecast uncertainty has no influence. The BRMz load shows lower fatigue reductions by 5% for the DK\_2015 dataset and 7% and 25% for the DE\_2017 and DE\_2022 cases when uncertain forecasts are considered. Nevertheless, the BRMz is one of the loads exhibiting the highest fatigue reductions even when forecasting uncertainty is considered. Similar to the

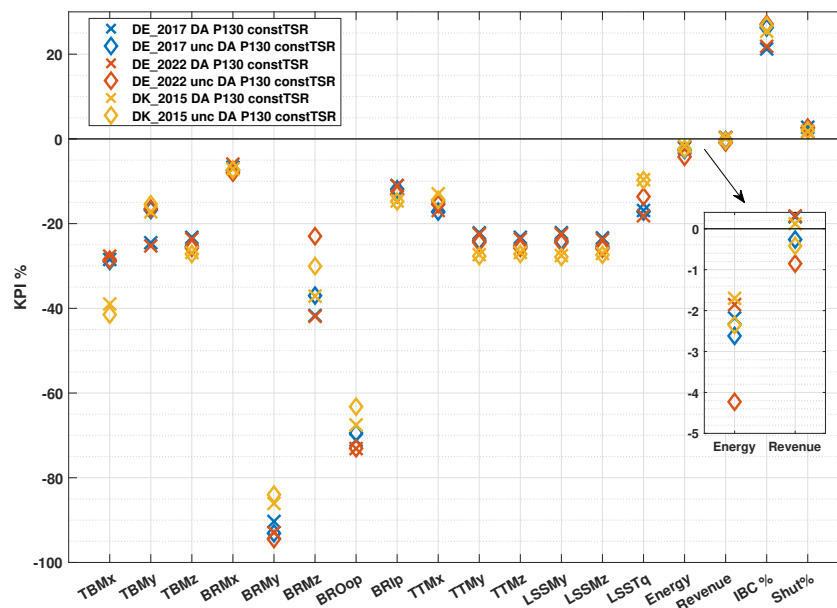


**Figure 7.41:** Comparison of results for revenue-neutral cumulative fatigue damage minimization based on DA forecasts under fluctuating prices with and without uncertainty in the forecast. All results are shown as relative differences to the baseline. Cases with uncertain forecast inputs are denoted as unc.

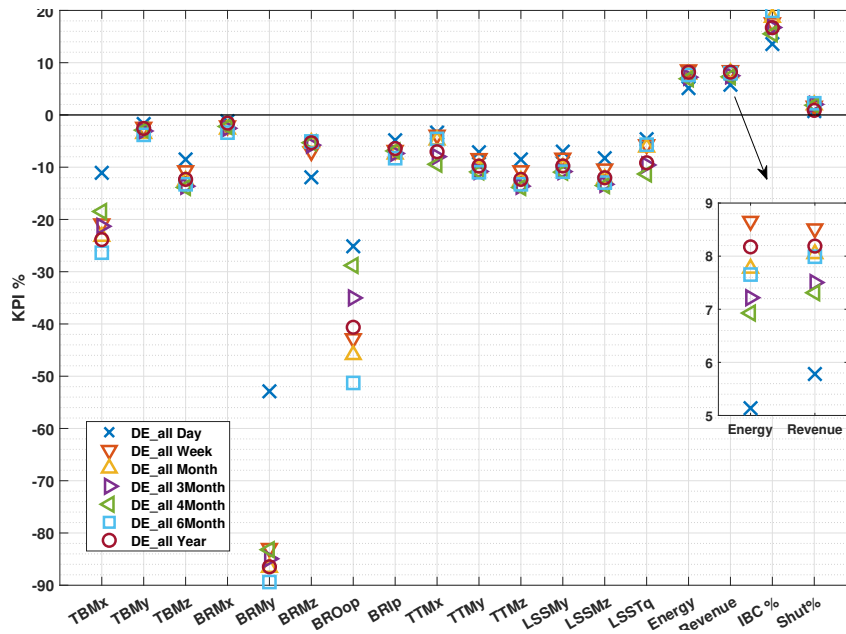
revenue maximization scenario, the most influenced loads are the ones that rely mainly on down-regulation for fatigue reductions.

Overall, the uncertainty in forecast inputs has a higher impact on the optimization outcome in scenarios focused on revenue maximization rather than fatigue minimization. This effect is primarily driven by the substantial trade-offs between power production and loads when down-regulation is employed. Loads that rely solely on down-regulation for load mitigation are more sensitive to the mismatch between the actual conditions and the optimization inputs. This sensitivity becomes more prominent in revenue maximization cases where load margins are smaller and power boosting is employed more often, requiring a more precise offsetting of the additional loads.

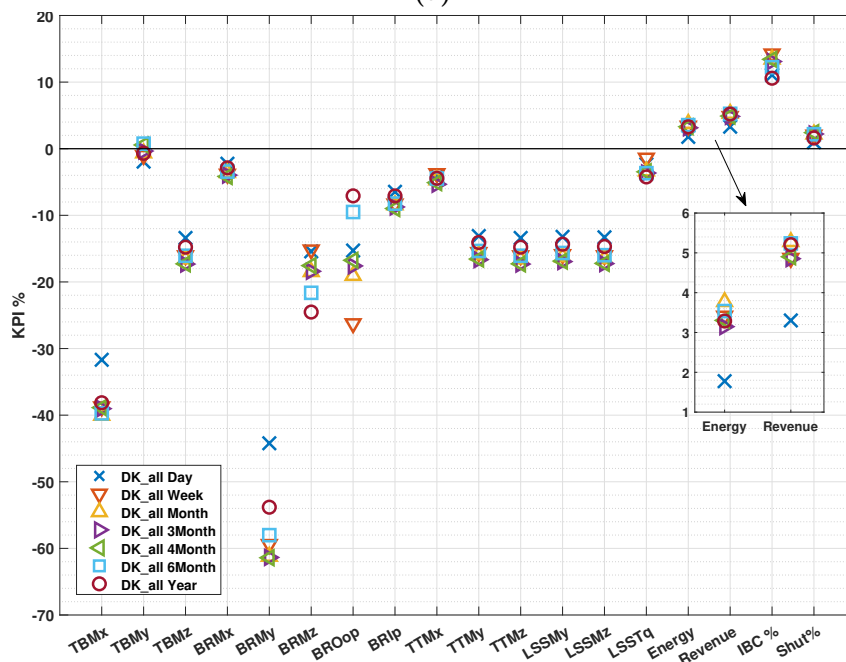
### 7.3.4 Sensitivity to forecast horizon length under fluctuating prices

The discussion on the results presented earlier in this chapter showed that one weakness of the DA-based optimization approach, which limits its efficiency compared to the wind distribution-based approach, is the length of the forecast horizon. To investigate this further, the effect of the length of the forecast horizon on the optimization results is examined in this section. This assessment is carried out by using the optimization settings found to work best for the single day-ahead forecast horizon and running the optimization again with forecast horizon lengths varying from one week to a full year. The forecast is considered perfect without uncertainty in all cases. It's important to note that this is a theoretical exercise to evaluate

the impact of the horizon length. In practice, even short forecast horizons typically introduce uncertainty, while extremely long horizons, such as several months or a year, are infeasible to forecast.



(a)



(b)

**Figure 7.42:** Results of optimization cases for load-neutral revenue maximization compared to baseline operation in fluctuating prices using varying forecast horizon lengths. The constTSR trajectory is used with a maximum power level of 130% (a) DE\_all (b) DK\_all

Figure 7.42 presents the optimization results for a load-neutral revenue maximization case using the constTSR down-regulation trajectory with a maximum power level of 130% for the

DE\_all and DK\_all datasets considering varying forecast horizon lengths. The findings clearly illustrate the high impact of the forecast horizon length. All horizons longer than a day achieve significantly higher revenue for both datasets while simultaneously producing slightly larger fatigue damage margins.

For the DK\_all dataset, the revenue is further increased from 3.3% with the DA horizon to 4.9-5.3% for all other horizon lengths. This range surpasses the 4.7% achieved with the Weibull-based approach using the same controller settings. Moreover, the total energy production also increases from 1.8% to 3.2-3.8% with the longer horizons, albeit still lower than the 4.7% achieved with the Weibull-based optimization approach. In terms of loads, all fatigue margins increase except for the TBMy load, which reaches the baseline level with the longer horizons. Additionally, the BROop load displays the highest variation, with damage margins decreasing compared to the day ahead horizon for the 6-month and 1-year horizons, while for the rest of the horizons considered, the damage margins increase. The load margins obtained by the longer horizons are in a similar range with the results obtained with the Weibull-based approach except for the BRMz load, which shows significantly lower margins with the forecast-based approach by 30% or more.

Regarding the DE\_all dataset, the revenue increases from 5.8% with the DA horizon to a range of 7.3-8.5% with the longer forecast horizons. The revenue gain obtained with the Weibull-based approach for the same settings was 8.2 %, surpassed only by the cases with 1-week and 1-year horizons. Energy production is further increased by 1.8-3.6% when the longer horizons are considered. The loads show higher fatigue reductions, also for the DE conditions, when longer horizons are employed. The only exception is the BRMz load, which increases by approximately 6% compared to the DA case while still maintaining fatigue margins higher than 4% for all cases.

For both datasets, the IBC activation and the frequency of selective shutdowns increase with an extended forecast horizon. As observed in previous cases, particularly when the Weibull-based optimization is employed, these increases can potentially decrease revenue and increase fatigue for the loads that are adversely affected by IBC. The current findings suggest that when utilizing a forecast-based approach with longer horizons, the optimizer can more effectively balance the tradeoffs in loads and revenue by applying IBC and selective shut-downs with greater precision, thus avoiding negative impacts.

These results could potentially be enhanced through the fine-tuning of optimization settings tailored to each forecast horizon. Especially for horizons exceeding one week, where prices and wind speeds are provided as binned inputs to the optimizer, as discussed in section 5.2, improvements can be expected by precise tuning of the optimization and objective function parameters. Thus, the presented results are on the conservative side regarding the potential but still serve the purpose of showing the general trends associated with increasing the forecast

horizon.

The main outcome of this investigation is that increasing the forecast horizon beyond a single day to longer periods significantly improves the optimization results, while the differences between the various extended horizons considered are relatively small. For both datasets, the improvements don't show to be proportional to the horizon length. The fact that the results for the week-ahead and year-ahead horizons are very close shows that the length of the horizon is not the decisive parameter. The DA-based optimization is limited due to the very short horizons, and increasing the horizon even by a few days can potentially improve its efficiency. Overall, the full potential of the forecast-based optimization approach is higher than that of the Weibull-based approach, but it is practically bounded by the forecasting uncertainty as the forecast horizon length increases.

### 7.3.5 Sensitivity to wind distribution uncertainty under fluctuating prices

This section delves into the sensitivity of the optimization's efficiency to uncertainty in the input wind speed distribution under fluctuating prices. The employed methodology mirrors the sensitivity analysis conducted under fixed prices, as outlined in section 7.2.3.

As the revenue-oriented scenarios showed the highest sensitivity under fluctuating prices, the present analysis focuses on these cases. The results, considering the modified Weibull distributions as optimization inputs, for a load-neutral revenue maximization case using the DE\_all dataset and a revenue maximization case with a load increase cap for the DK\_all dataset are presented in figure 7.43. In both cases, the constTSR down-regulation trajectory is employed with a maximum power level of 130%.

For the DE\_all dataset, the uncertain wind distribution input leads to a reduction in revenue and energy gains for most cases. The observed revenue reductions are up to 1%, and the maximum energy reduction is 1.5%. For the DK conditions, the revenue varies in the range of -1% to 1% compared to the results obtained with the original distribution. However, energy production decreases for most cases, with the maximum reduction being approximately 3%. The cases where decreases in revenue and higher decreases in energy are observed for the DK\_all dataset are correlated with the overestimation of the scale parameter of the Weibull distribution. No such correlation is observed for the DE site in terms of revenue and energy KPIs.

The changes in IBC activation are correlated to the type of uncertainty in the Weibull distribution. As the shape parameter increases and the scale parameter decreases, the IBC activation increases and vice versa. Downtime due to selective shutdowns increases in most cases due to the modified inputs, with no pattern of correlation to the type of uncertainty

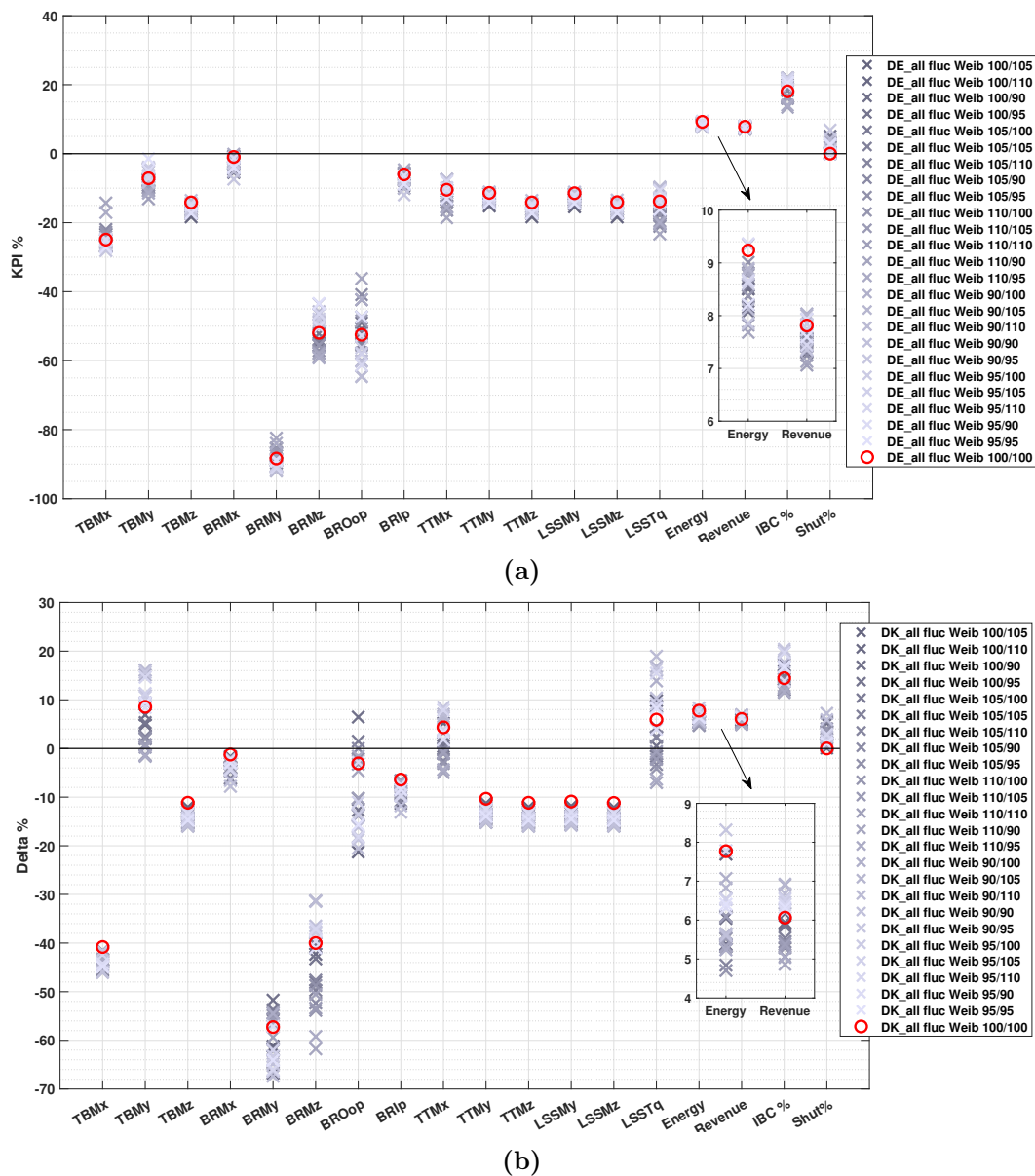


**Figure 7.43:** KPIs of revenue maximization cases under fluctuating prices using the modified Weibull distributions representing the uncertainty in wind speed distribution estimation. The values in the legend indicate the percentages of the unmodified parameters. The first value refers to the scale ( $A$ ) and the second to the shape ( $k$ ) parameter. The cases with red denote the results obtained using the unmodified Weibull distributions. (a) DE\_all, (b) DK\_all

observed.

The sensitivity of the optimization results to the Weibull uncertainty in terms of cumulative fatigue is very similar to the response obtained under fixed prices. This is expected since, as discussed in this chapter, when the Weibull-based optimization approach is employed, the differences in fatigue outcomes between fixed and fluctuating price scenarios are small. Load neutrality is achieved for all the cases using the DE\_all dataset, which exhibits overall smaller variations compared to the DK conditions. For the DK\_all dataset, the variations in the

fatigue results are higher for the TBMy, BROop, TTMx, and LSSTq loads, which reach or exceed the cap limit, showing a higher sensitivity to the uncertain input. For a more detailed analysis of the load responses, the reader is referred to section 7.2.3.

Overall, the uncertainty in the wind distribution input has a greater impact on the fatigue objectives than on the energy and revenue objectives, also under fluctuating prices. Boundary conditions with less variability and lower correlation between wind speeds and prices tend to be more robust to this type of uncertainty. Nevertheless, the observed sensitivity of the fatigue objectives suggests that the uncertainty in the wind distribution input should be taken into account in a possible implementation of the proposed method, especially in revenue-focused scenarios where the resulting fatigue response can have a large impact on the business case.

## 7.4 Discussion

The proposed method for operational optimization of wind turbines for revenue and fatigue objectives was evaluated in this chapter. Two scenarios were investigated, each representing a potential business case, focusing on cumulative revenue maximization and cumulative fatigue damage minimization. The investigation encompassed the operation of wind turbines under both fixed prices and market spot prices. Three historical datasets, spanning over several years and representing distinct boundary conditions in terms of wind and electricity prices, were employed to realistically evaluate the proof of concept. Based on this investigation, overall conclusions about the efficiency of the method and its sensitivity to controller design, optimization approach, boundary conditions, and uncertainty to the inputs are drawn and critically discussed in this section.

Based on the findings, the most efficient optimization approaches for cumulative fatigue minimization are the distribution-based approach with a low power boosting level for scenarios under fixed prices and the forecast-based approach for scenarios under fluctuating prices. The fatigue is reduced across all components, which suggests that the proposed method can potentially enable lifetime extension for the entire system. The fatigue reductions are, in most cases, higher with the wind distribution-based approach. However, with this approach under fluctuating prices, the revenue constraint cannot be satisfied. Incorporating a revenue decrease cap significantly enhances fatigue reductions with the forecast-based optimization approach in all cases, in contrast to the distribution-based approach. To improve the efficiency of the distribution-based approach under fluctuating prices, adjusting the fixed price level used as input to the optimization to reflect expected long-term price levels could be considered.

The findings regarding the revenue maximization scenario showed that the distribution-based approach is able to produce higher increases in all cases, with the increase in revenue being proportional to the maximum power level. Nevertheless, when applied to fluctuating prices,

depending on the controller design and the boundary conditions, it showed limitations in the efficient restriction of the loads to the set limit. The application of a load increase cap showed that it is possible to moderately increase revenue in most cases. However, the efficiency and efficacy of this method showed high sensitivity to all parameters, i.e., controller design, wind and price conditions, maximum power level, and optimization approach.

The combination of IBC, power boosting, down-regulation, and selective shutdowns allowed for a more effective distribution of power production and fatigue damage across the wind speed range with the optimization approach based on the site's mean wind speed distributions. On the other hand, the optimization based on day-ahead forecasts demonstrated reduced effectiveness, primarily due to the constraints of limited optimization windows that hinder the exploitation of mid- and long-term variations in wind and prices.

The outcomes of cumulative revenue maximization were found to be more sensitive to all parameters influencing the proposed method, and the tuning of the optimization variables proved more complicated and time-consuming in these cases. Conversely, cumulative fatigue minimization proved to be more robust to the different parameters and boundary conditions. Additionally, the load constraint could not be as effectively tracked as the revenue constraint in most cases. This stems from the fact that fatigue loads are strongly correlated to wind speeds, whereas revenue depends on the correlation between wind speed and prices. Moreover, the formulation of the objective function and the optimization setup add an additional layer of complexity in tracking the fatigue loads. This could be potentially improved by a different formulation of the objective function in combination with a suitable optimization algorithm.

The controller design, in terms of down-regulation set points, has a higher impact in revenue maximization scenarios rather than fatigue damage minimization scenarios. In fatigue damage minimization scenarios, only minor differences are found in the magnitudes of reduction of the loads, which can only be mitigated with down-regulation. Exploring down-regulation trajectories that further lower the rotational speed may prove beneficial if specific load reductions are a priority. Otherwise, the constant TSR approach showed to be, in general, slightly more effective and robust. In revenue maximization scenarios, the controller design can impact the revenue increase and also influence the load response in terms of loads reaching or exceeding the fatigue constraint.

The most significant sensitivity of the proposed method was observed in response to variations in wind and price boundary conditions. Factors such as the wind speed distribution, TI levels, wind condition variability (both intra- and inter-annually), price variability, and the correlation between prices and wind speeds were all found to affect the optimization outcomes in various ways, as extensively discussed in previous sections.

The complex interplay between the wind turbine's aeroelastic response to the controller design with the wind conditions and price conditions in the context of optimally balancing fatigue

and revenue can significantly influence the optimization outcome. Hence, it is recommended to derive the controller set points considering the site-specific conditions and to utilize sufficiently long datasets for evaluating the optimization method's potential on a specific site.

The impact of wind speed distribution uncertainty on the optimization outcome is highly dependent on the specific boundary conditions. Generally, the fatigue objectives are more sensitive to this uncertainty compared to the revenue objective, with the sensitivity increasing in wind conditions with higher variability. Uncertainty in day-ahead forecasts of price and wind speeds has a significant impact on revenue maximization scenarios, with some loads significantly exceeding the fatigue constraint. On the other hand, it has a low impact on fatigue minimization scenarios where the fatigue reductions proved robust to this kind of uncertainty, while the revenue objective is slightly influenced. Nonetheless, further research is required in the modeling of uncertainty in order to draw definitive conclusions about the overall impact of input uncertainty on the proposed operational management approach.

It is important to note that the scenarios examined represent the boundary cases in terms of optimization objectives. Instead of focusing solely on revenue maximization or fatigue minimization, a combination of them can be considered where the results are expected to fall within the boundaries presented here. This combined approach can also enhance the optimization's robustness to uncertainty. For instance, in a load minimization scenario, the revenue objective weight can be increased along with possibly employing a revenue increase cap. This adjustment may lead to slightly lower fatigue reductions but provides a buffer to ensure that revenue does not decrease below the specified constraint.

The IBC loop proved to be an important component of the proposed method driving significant load reductions, particularly for the blade loads, and enabling the application of power boosting. Additionally, the combination of IBC and down-regulation demonstrated its ability to influence the entire load ensemble. Moreover, in the context of the proposed optimization, IBC activation is less frequent compared to applying IBC as a standard control feature, while the majority of potential fatigue reductions are still realized. This suggests that the proposed operational optimization method can leverage technologies like IPC and showcase their potential to create added value in practical terms, including monetary benefits and the possibility of extending the turbine's lifetime, beyond the typically considered reduction of manufacturing costs.

The computational time is not discussed in detail, as it would not be a significant consideration in an actual implementation. The accumulation of values over time is computationally cheap and straightforward with the evaluation framework. The optimization with the distribution-based approach would be done offline. The forecast-based optimization, executed within rolling horizon windows, is not expected to impose a high computational burden due to the limited number of variables involved. Studies like those presented in this work, including the tuning

of the optimization parameters, are computationally expensive as the optimization has to be repeated for the entire dataset. The main computational cost arises from calling the surrogate model to obtain the turbine response within the optimization loop. Indicatively, 300-360 minutes of wall time were required for the optimization of a single year using day-ahead forecast horizons with 36 cores available for parallelization.

The two optimization approaches developed in this work have distinct benefits and shortcomings. The distribution-based approach performs better in terms of optimization objectives for most scenarios analyzed, besides revenue-neutral load minimization in fluctuating prices. However, it can not adapt to switching objectives over time and requires long-term horizons to realize the optimization benefits, making it a long-term investment. On the other hand, the DA-based approach is limited in its efficiency due to the short horizons, which can significantly be improved if a longer forecast horizon can be realistically achieved. Nevertheless, the short-term nature of the optimization with the rolling horizon allows it to be more agile in switching objectives over time, which can be beneficial in order to adjust to the evolving objectives of the various stakeholders during the lifecycle of a wind farm.

Furthermore, the distribution-based approach is potentially more robust to uncertainty, particularly for sites with large existing measurement datasets, as the long-term Weibull distribution can be more accurately determined compared to the wind and price forecasts. The forecast would typically have varying uncertainty according to conditions such as seasonality, market conditions, etc., and would increase with the forecast horizon length.

Another distinction between the two optimization approaches is the cost of implementation. Assuming the costs for the blade load sensors, and adapting the controller's software are equal, the costs of applying the forecast-based optimization, including the procurement of reliable forecasts and the possible involvement of human decision-making in daily optimization objectives, would generally be more costly compared to deriving a one-time operational plan that only requires periodic revisions.

Moreover, the results reveal a significant distinction in how energy production is influenced by the two optimization approaches. Energy production is shifted towards higher wind speeds in the case of the distribution-based optimization approach and towards higher wind speeds combined with higher prices within the forecast-based optimization. This suggests that the forecast-based approach will tend to shift energy production towards instances with higher demand, assuming that the market price signals reflect the demand. This is expected to be beneficial for the electricity grid, as it can lead to a more efficient utilization of wind energy resources and support higher penetration of wind energy in the generation mix. With the distribution-based approach, the energy is shifted only towards higher wind speeds with no correlation to the demand. This suggests that the distribution-based approach may be more beneficial for the wind farm operator in the sense of better optimization results, lower

uncertainty, and lower implementation costs. However, it does not inherently contribute to grid-level demand response.

This is a general issue of the fixed pricing mechanisms applied as support mechanisms to renewables. Traditional electricity market structures are built around conventional producers having high marginal costs due to fuel prices and high flexibility in output volumes. In contrast, wind energy is far less flexible and has very low marginal costs. Consequently, there is no incentive for the turbines to follow the demand. More recent pricing mechanisms focusing on premiums to the market prices could be more effective in encouraging renewables to align with demand. In order to accommodate further any possible flexibility by wind energy, such as the flexibility resulting from the operational approach proposed here, the monetary incentive should prioritize the demand as well as not penalize as heavily the possible imbalances in energy clearing.

# Chapter 8

## Conclusions

### 8.1 Summary

The goal of this work was to develop and evaluate an operational management method for the optimization of long-term revenue and fatigue objectives for wind turbines through adaptive control. Achieving this goal required a multidisciplinary approach. The basis was the development of a simple and robust controller with multiple modes, requiring no additional actuators and sensors. The controller allows adjusting the power output within the range of 50-130% of the baseline level as well as optionally applying an individual blade control loop. Two distinct approaches in performing down-regulation were considered to investigate their impact on reducing fatigue loads across all major components. The first approach was based on only blade pitch adjustment, and the second on combining pitch and torque adjustments.

Furthermore, a surrogate model was developed, based on mid-fidelity aeroelastic simulations, able to capture the response of the wind turbine, including the fatigue loads of major components as well as power and other performance metrics, for all control modes and wind conditions encompassing mean wind speed and turbulence intensity. Dense factorial sampling was employed to create the training dataset. Moreover, two methods with increasing cost and complexity, spline-based interpolation and Gaussian process regression, were employed and compared.

The surrogate model was utilized to create a framework able to track the accumulation of relevant metrics over time, similar to a data-driven digital twin. Within this framework, an optimization methodology was introduced aiming to optimize the control mode of the turbine at each time block in order to achieve the long-term objectives. Two optimization

approaches were developed with the framework, one utilizing the wind speed distributions as input and the other using forecasts of wind speeds and electricity prices. Due to the nature of the problem, heuristic optimization algorithms, specifically the genetic algorithm and particle swarm optimization, were employed.

The concept was evaluated based on scenarios relevant to potential business case applications. The boundary scenarios of revenue maximization with fatigue damage constraints and fatigue minimization with revenue constraints were considered. These scenarios were evaluated considering fixed electricity pricing, resembling a case where a subsidy scheme or fixed PPA exists, and fluctuating market prices, assuming that the entire production is traded in the day ahead electricity market. Moreover, two historical datasets of wind and electricity prices were used to evaluate the impact of the boundary conditions in terms of wind conditions and market dynamics on the proposed methods. The impact of control design choices, optimization, and boundary conditions, as well as input uncertainty on the efficacy and performance of the proposed method, were evaluated.

The evaluation-optimization framework, the surrogate models, and the wind and price datasets used are publicly available. The relevant repositories can be found in appendix A.1.

## 8.2 Conclusions

The main research objective of this work was the development and evaluation of an operational management approach for wind turbines aiming to optimize long-term revenue and fatigue damage objectives. The application of the proposed method showed that it is possible to manage revenue and fatigue over time by adjusting power levels, applying the IBC loop, and selectively shutting down according to projected revenue. Combining these approaches, it was demonstrated that it is possible to effectively redistribute revenue and fatigue damage along the wind speeds and prices based on optimization. Detailed discussion and conclusions about each of the research topics included in the thesis can be found in the relevant chapter. A high-level overview of these conclusions is included here.

The surrogate modeling of the turbine's response was based on mid-fidelity simulation with an hourly duration using FAST. The training set was created based on dense factorial sampling of the input space consisting of wind speeds, turbulence intensity, and controller mode. A spline-based regression and a Gaussian process regression were used to obtain the surrogate model's predictions. The uncertainty quantification analysis showed that the methods have similar accuracy, with errors below 4% for most cases. The highest uncertainty for both models, across most metrics, was found in low wind speeds close to cut-in and close to the rated wind speeds. The main difference between the two methods, with respect to the present application, was found in the computational time for predictions, which is significantly higher with the

more complex GPR model. The high computational cost and the similar performance of the two methods motivated the use of spline-based regression for the applications presented in this work. Nevertheless, as indicated by the literature review, with higher dimensions for the surrogate that would lead to sparser sampling, GPR may perform better. Moreover, the GPR model can inherently provide uncertainty estimation on the predictions, which can be useful for further uncertainty propagation studies.

The detailed aeroelastic analysis performed revealed the impact of the controller design on the aeroelastic response of the turbine under normal operation conditions. For most loads, the wind speed around rated is the most sensitive with higher fatigue loads. For the majority of loads, the highest fatigue reductions are achieved by down-regulation until a power level of 90%. Beyond this range, further reductions have a diminished impact on load mitigation. The tradeoff between load reduction and power output showed that, for the specific turbine design, down-regulation until 85% is sufficient for fatigue minimization, while for revenue maximization, down-regulation until 90% is sufficient. Furthermore, down-regulation is most effective in reducing fatigue loads primarily in wind speeds around the rated region and, to a lesser extent, to the below-rated region, while in higher wind speeds, it has a low impact.

The application of IBC has the greatest influence on out-of-plane and flap-wise blade loads. It is also able to reduce, albeit to a lesser extent, the majority of loads considered except for the tower fore-aft moment, nacelle roll moment, blade torsion, and low-speed shaft torque. These loads either remained unaffected or slightly increased, particularly when IBC was implemented at wind speeds in the rated region. However, these loads can be significantly reduced by down-regulation, demonstrating the synergistic effect of the two methods. Along with the blade torsion, these are the loads that increase the most with power-boosting, thus making them the most sensitive loads, often defining the boundaries of optimization. Moreover, as seen from the optimization outcomes, selectively applying IBC only in higher wind speeds, above the rated region, the major load reductions from IBC can still be achieved while mitigating the adverse effects in some of the loads and also reducing the impact on the blade pitch actuator.

The distinction between performing the down-regulation solely through pitching or by a combination of pitching and reducing rotational speeds showed to be small in terms of fatigue reductions. Reducing the rotational speed is more effective in load reductions in above-rated conditions, although the magnitude of reductions is low. In rated and below-rated wind speeds, down-regulation based on pitching only performs slightly better in reducing loads. In the context of the operational optimization method, the combination of the wind and price boundary conditions with the choice of down-regulation trajectory has an impact on the distribution of fatigue reductions across all loads considered. Moreover, it showed to have a higher impact on the optimization outcomes in revenue maximization scenarios as it can limit the revenue increase by influencing specific loads that reach the fatigue constraint. As the

effects of the trajectory choice for deriving the down-regulation set points depend highly on the turbine design and can influence the optimization depending on wind and price dynamics, it is recommended that the set points are derived according to the application and the specific objectives.

The application of the method to the two datasets demonstrated load-neutral revenue increases, compared to the baseline operation, up to 10.5% and 6.8% with a maximum power level of 130% under fixed prices and 8.2% and 4.6% under fluctuating market prices using the wind distribution-based optimization approach. The forecast-based approach, employing day-ahead forecasts, achieved revenue increases up to 6.3% and 3% under fixed prices and 6% and 3.4% under fluctuating prices with a maximum power level of 130%. The magnitude of revenue increase proved to be proportional to the maximum power level considered. The introduction of a 5% fatigue increase cap resulted in moderate additional increases in the revenue objective. However, the magnitude of additional increases showed high dependency, in both efficacy and performance, on the maximum power boosting level, optimization approach, and site- and market-specific conditions. Under fluctuating prices, the fatigue cap constraint could not be accurately tracked with the distribution-based optimization approach. The loads reaching the fatigue constraint and thus limiting the revenue maximization were found to be the tower bottom fore-aft moment, the tower top roll moment, and the low-speed shaft torque in most cases. Additionally, in all cases, it was observed that besides the critical loads reaching the defined fatigue constraints, the rest of the loads still exhibited some fatigue reductions. This can be potentially leveraged to combine or adjust objectives over time in order to achieve lifetime goals while aiming for revenue maximization as the main objective.

In revenue-neutral fatigue damage minimization scenarios, the application of the method to the two datasets showed significant load reductions, compared to the baseline operation, surpassing 25% for most loads with variations in the magnitude across all loads considered. The in-plane blade loads are an exception to this trend, displaying low sensitivity to all controller modes. The blade out-of-plane and torsional loads showed the most substantial reductions due to their high sensitivity to both IBC and down-regulation. The two optimization approaches showed, in general, similar fatigue reduction performance, with the distribution-based approach performing slightly better in terms of fatigue reductions. However, under fluctuating prices, the revenue constraint would not be satisfied with this approach, resulting in revenue losses of up to 3.5% for both sites, while the forecast-based approach was able to track it accurately. Considering a revenue loss cap of 5% proved impactful in further reducing fatigue only with the forecast-based approach under both fixed and fluctuating prices. Furthermore, the differences observed by considering varying maximum power boosting levels are low. Thus, the lowest power boosting level of 10% considered is sufficient to yield the major benefits of the method. These findings suggest that it is possible to achieve substantial lifetime extension, from a

fatigue reliability perspective, for the entire system while maintaining the baseline revenue.

Comparing the optimization methods developed in this work, significant differences can be found. The distribution-based approach performs better under fixed prices and also in fluctuating prices when revenue constraints are not included. It performs better due to the fact that the optimizer is informed of the long-term conditions and is able to leverage better the long-term fluctuations in wind speeds. Additionally, its implementation is simpler, more straightforward, and possibly cheaper. On the other hand, it lacks the ability to react to price fluctuations as prices are not considered. Moreover, it is more sensitive to inter- and intra-annual variability since the input assumes a constant mean wind distribution of the site. Hence, the optimization benefits are realized in the long term, and adapting the optimization regularly over time is not possible.

With this optimization approach, the main mechanism to achieve the objectives, both fatigue and revenue, is by reducing the power levels in rated and below-rated wind speeds. For higher wind speeds, the power level increases until it reaches the maximum power boost level and then stays constant. This shows that in order to balance fatigue and revenue objectives, the power level, and consequently revenue, is increased at the highest end of the wind speed spectrum. Conversely, the increase in fatigue by power boosting is compensated by the application of IBC in the higher wind speeds above the rated region and by down-regulation primarily in wind speeds close to the rated region and, to a lesser extent, at the lower spectrum of wind speeds.

The forecast-based optimization utilizing day-ahead forecast horizons showed lower performance in most cases, with its best performance observed under fluctuating prices. The inclusion of prices in the optimization inputs allows it to achieve the revenue constraint under all scenarios and pricing mechanisms. This method offers greater flexibility in adjusting optimization objectives over time as the horizon of each optimization is short. Furthermore, it enables more potential use cases, such as including the intra-day or balancing markets in the optimization, which is not possible with the distribution-based approach. Furthermore, the forecast-based approach shifts energy production more towards instances with higher electricity prices, which can have benefits for grid integration purposes as it shifts the increased production towards higher demand. This is not possible with the distribution-based approach.

A sensitivity analysis showed that including longer horizons to a week-ahead level can improve the performance of the method significantly, reaching or exceeding the distribution-based approach. Nevertheless, this result was obtained assuming a perfect forecast. Its applicability in real-world applications has to be further investigated, taking into account the associated uncertainty.

Overall, cases focusing on fatigue minimization proved to be more straightforward to achieve for all scenarios, datasets, and trajectories. On the other hand, revenue maximization cases required more tuning in the optimization parameter setup and longer optimization duration

due to significantly more iterations required. This is explained by the fact that managing fatigue accumulation is only dependent on wind speeds, while revenue is dependent on the combination of wind speeds and prices, which leads to more pronounced tradeoffs in fatigue and revenue objectives.

The sensitivity analyses on the uncertainty of input wind distribution showed that the uncertainty is more pronounced under fluctuating prices, with the fatigue objectives being more sensitive than the revenue objective. Additionally, examining the two sites considered, the influence of this uncertainty was found to be higher for the site with greater variability in conditions and a higher correlation between prices and wind speeds. The impact of the uncertainty to input day-ahead forecasts also showed a higher impact on the fatigue objectives. The impact across the different loads considered varies highly, with loads relying more on down-regulation for reduction, exhibiting the highest sensitivity. It should be noted that the modeling of forecast uncertainty used in this work is rather simplistic, and further research is required on the topic.

The boundary conditions of wind speeds, TI, and prices, as well as their correlation, demonstrated the greatest impact on the efficacy and performance of the proposed method. In revenue maximization scenarios, conditions with less variability of wind conditions over time, lower inter-annual variability, and lower correlation between wind speeds and prices were found to hold more potential for optimization. This was verified by an example using the 2022 electricity market prices, which, due to the energy crisis, had high variability along with low correlation to wind speeds. This case demonstrated the highest revenue increases regardless of the optimization approach and controller setup. In fatigue minimization scenarios, the boundary conditions mainly affect the distribution of fatigue reductions across the various components.

Overall, the interaction of controller configuration, wind and price site-specific dynamics, and optimization approach was shown to influence the performance of the method across multiple dimensions. Consequently, the analyses conducted in this study reveal that no single setting or approach universally outperforms the others. Nevertheless, there is potential to achieve long-term optimization objectives through the proposed operational management method. Thus, it is recommended that these aspects should be considered simultaneously, along with the specific use case requirements, in order to determine the feasibility and optimal configuration.

### 8.3 Recommendations for future work

This section provides recommendations for further research on the topic of operational optimization of wind turbines. More details on specific topics can be found in the discussion and conclusion sections of the corresponding chapters.

- As this work serves as the proof of concept for the proposed method, the assumptions considered should be further investigated. The most important, from a technical point of view, would be the implications of power boosting. While this work focused on managing fatigue loads, evaluating ultimate loads is equally essential to ensure the structural reliability of the system. Moreover, the overload capacity of the power electronics and the electrical system has to be further investigated in order to assess the realistic limits of power boosting.
- In order to evaluate the full potential of the method in the context of the entire wind plant, the farm flow effects have to be considered. Extending the method to incorporate wake interactions within a farm is a logical progression. As a first approach, simplified models such as FLORIS or the effective turbulence approximation recommended by the IEC standard can be employed to derive surrogate models for the farm flow effects on a per-turbine and per-operational point basis, factoring in wind conditions and flow interactions. This can be further extended by creating surrogate models for the entire farm based on mid-fidelity models, like FAST.farm, and using these in place of the single turbine surrogates to obtain more accurate results. In this case, the main challenge would be creating the surrogate model due to the high dimensionality.
- Additional control strategies can be incorporated into the method to improve further the optimization effectiveness. One particularly relevant strategy is wind farm flow control, which can impact power production and fatigue loading across all the wind turbines within the farm. Wind farm flow control primarily comes into play in the below-rated wind speed region and is anticipated to have synergistic effects when combined with the methods proposed in this work.
- A limited uncertainty analysis was conducted in this work. Further uncertainty quantification analyses are required to determine the robustness of the proposed method. This involves a more precise modeling of uncertainties, potentially including historical forecasts. Additionally, the uncertainty propagating from the surrogate model to the optimization process has to be further investigated. The Gaussian process regression method introduced in this work, or a similar method able to provide uncertainty estimates alongside predictions, can be employed for this purpose.
- In this work, the controller design was done independently of the optimization process. Two distinct down-regulation approaches were considered, demonstrating that the derivation of the controller setpoints has an impact on the optimization outcomes. This highlights the potential for further enhancements by enabling a co-design of the controller along with the optimization. Exploring various setpoints for down-regulation and power boosting, as well as different settings for the IBC loop, can influence the optimization results, potentially improving the objectives and altering the damage distribution across

the various loads considered.

- The financial implications of the proposed optimization have to be further examined to draw conclusions regarding the practical benefits. While the method has demonstrated the potential to impact revenue generation and potentially extend the lifetime of the wind turbine, additional economic evaluation is necessary. Comprehensive analyses, including the CAPEX and OPEX costs, the additional implementation costs associated with the proposed method, and its impact on OPEX, as well as potential extensions in the turbine's operational lifetime, including related projected costs and revenue, are required to determine the potential added value.
- Similar to technologies such as lidar-assisted control or wind farm control, the certification aspect of the proposed method has to be considered. In order to ensure the bankability of a project, such methods require certification by the relevant bodies. One viable approach could involve certifying each operational mode individually, thereby generating a map of power production and structural loading for each component in every mode. These maps can then be used in conjunction with an overall fatigue budget, defined per component, to ensure that operational strategies applied do not lead to surpassing this predefined limit. This is a complex issue that involves multiple stakeholders and necessitates further attention and exploration.
- The proof of concept demonstrated the method's potential for improving the specified objectives. There is room for exploration in terms of additional optimization objectives, constraints, and approaches, as suggested in chapters 6 and 7. Building upon the foundation established in this work, further research can address diverse business cases and expand the scope of application.

# Appendix

## A.1 Code and data availability

The surrogate model data, including the raw dataset, the smoothened dataset, the trained GPR models, as well as relevant reading scripts, are available at:

<https://doi.org/10.5281/zenodo.10092271>

The evaluation-optimization framework is available at:

[https://github.com/SWE-UniStuttgart/WT\\_Operational\\_Optimization](https://github.com/SWE-UniStuttgart/WT_Operational_Optimization)

A subset of the optimization results are available at:

<https://doi.org/10.5281/zenodo.10580236>

## A.2 Publications

Peer-reviewed publications related to the present thesis:

1. Pettas V., Cheng P. W.: Operational optimization of wind turbines for revenue and fatigue objectives considering wind conditions and electricity prices, in preparation, Wind Energy 2024
2. Pettas V., Cheng P. W.: Surrogate modeling and aeroelastic analysis of a wind turbine with down-regulation, power boosting, and IBC capabilities, under review, Energies 2023
3. Kölle K., Göçmen T., T., Eguinoa, I., Alcayaga Roman, L. A., Aparicio-Sanchez, M., Feng, J., Meyers, J., Pettas, V., and Sood, I.: FarmConnors market showcase results: wind farm flow control considering electricity prices, Wind Energ. Sci., 7, 2181–2200, <https://doi.org/10.5194/wes-7-2181-2022>, 2022.
4. Kölle K., Göçmen T., Garcia-Rosa P. B., Petrović V., Eguinoa I., Vrana T. K., Long Q., Pettas V., Anand A., Barlas T. K., Cutululis N., Manjock A., and Tande J. O.: Towards integrated wind farm control: interfacing farm flow and power plant control, Advanced Control for Applications: Engineering and Industrial Systems, 4( 2):e105, <https://doi.org/10.1002/adc2.105>, 2022
5. Pettas V., & Cheng P. W. (2018). Down-regulation and individual blade control as

lifetime extension enablers. *Journal of Physics: Conference Series*, 1102, 012026. <https://doi.org/10.1088/1742-6596/1102/1/012026>

6. Pettas V., Salari M., Schlipf D., & Cheng P. W. (2018). Investigation on the potential of individual blade control for lifetime extension. *Journal of Physics: Conference Series*, 1037, 032006. <https://doi.org/10.1088/1742-6596/1037/3/032006>

Peer-reviewed publications during the PhD project, not related to the present thesis:

1. Costa F., Peña A., Pettas V., and Cheng P. W. (2023). Impact of Probe Volume and Peak Detection Methods on Lidar Rotor Effective Wind Speed and Turbulence Intensity Estimations. *Journal of Physics: Conference Series* 2626 (1): 012020. <https://doi.org/10.1088/1742-6596/2626/1/012020>
2. Gräfe, M., Pettas, V., Gottschall, J., and Cheng, P. W.: Quantification and correction of motion influence for nacelle-based lidar systems on floating wind turbines, *Wind Energ. Sci.*, 8, 925–946, <https://doi.org/10.5194/wes-8-925-2023>, 2023.
3. Gräfe M., Pettas V., Cheng PW (2022). Wind field reconstruction using nacelle based lidar measurements for floating wind turbines, *Journal of Physics: Conference Series*, 2265(4), 042022. <https://doi.org/10.1088/1742-6596/2265/4/042022>
4. Pettas V., Kretschmer M., Clifton A., and Cheng P. W.: On the effects of inter-farm interactions at the offshore wind farm Alpha Ventus, *Wind Energ. Sci.*, 6, 1455–1472, <https://doi.org/10.5194/wes-6-1455-2021>, 2021.
5. Kretschmer M., Jonkman J., Pettas, V., and Cheng P. W.: FAST.Farm load validation for single wake situations at alpha ventus, *Wind Energ. Sci.*, 6, 1247–1262, <https://doi.org/10.5194/wes-6-1247-2021>, 2021.
6. Conti D., Pettas V., Dimitrov N., and Peña A.: Wind turbine load validation in wakes using wind field reconstruction techniques and nacelle lidar wind retrievals, *Wind Energ. Sci.*, 6, 841–866, <https://doi.org/10.5194/wes-6-841-2021>, 2021.
7. Pettas V., Costa García F, Kretschmer M, Rinker JM, Clifton A, Cheng P. W. (2020). A numerical framework for constraining synthetic wind fields with lidar measurements for improved load simulations. In: *AIAA SciTech 2020 Forum*. American Institute of Aeronautics and Astronautics; 2020:1-6. <https://doi.org/10.2514/6.2020-0993>
8. Kretschmer M., Pettas V., & Cheng P. W. (2019). Effects of Wind Farm Down-Regulation in the Offshore Wind Farm Alpha Ventus. *ASME 2019 2nd International Offshore Wind Technical Conference*. <https://doi.org/10.1115/IOWTC2019-7554>
9. Khaniki M. S., Schlipf D., Pettas V., & Cheng P. W. (2018). Control Design For Disturbance Rejection in Wind Turbines. *2018 Annual American Control Conference (ACC)*, 1515–1519. <https://doi.org/10.23919/ACC.2018.8431637>

# Bibliography

- [1] J. Hu, R. Harmsen, W. Crijns-Graus, E. Worrell, and M. van den Broek, “Identifying barriers to large-scale integration of variable renewable electricity into the electricity market: A literature review of market design,” *Renewable and Sustainable Energy Reviews*, vol. 81, no. March 2017, pp. 2181–2195, jan 2018. [Online]. Available: <https://doi.org/10.1016/j.rser.2017.06.028>
- [2] P. Pinson, “What May Future Electricity Markets Look Like?” *Journal of Modern Power Systems and Clean Energy*, vol. 11, no. 3, pp. 705–713, 2023. [Online]. Available: <https://ieeexplore.ieee.org/document/10049815/>
- [3] L. Blickwedel, F. Harzendorf, R. Schelenz, and G. Jacobs, “Future economic perspective and potential revenue of non-subsidized wind turbines in Germany,” *Wind Energy Science*, vol. 6, no. 1, pp. 177–190, feb 2021. [Online]. Available: <https://wes.copernicus.org/articles/6/177/2021/>
- [4] M. Jansen, I. Staffell, L. Kitzing, S. Quoilin, E. Wiggelinkhuizen, B. Bulder, I. Riepin, and F. Müsgens, “Offshore wind competitiveness in mature markets without subsidy,” *Nature Energy*, vol. 5, no. 8, pp. 614–622, jul 2020. [Online]. Available: <https://www.nature.com/articles/s41560-020-0661-2>
- [5] S. Malleret, M. Jansen, A. S. Laido, and L. Kitzing, “Winner’s Curse or Blessing? The Changing Profitability of Offshore Wind from Auction to Final Investment Decision,” *SSRN Electronic Journal*, 2023. [Online]. Available: <http://dx.doi.org/10.2139/ssrn.4415948>
- [6] F. Gaffney, J. Deane, and B. Gallachóir, “Reconciling high renewable electricity ambitions with market economics and system operation: Lessons from Ireland’s power system,” *Energy Strategy Reviews*, vol. 26, no. July, p. 100381, nov 2019. [Online]. Available: <https://linkinghub.elsevier.com/retrieve/pii/S2211467X19300744>
- [7] H. Algarvio, F. Lopes, A. Couto, and A. Estanqueiro, “Participation of wind power producers in day-ahead and balancing markets: An overview and a simulation-based study,” *Wiley Interdisciplinary Reviews: Energy and Environment*, vol. 8, no. 5, 2019. [Online]. Available: <https://doi.org/10.1002/wene.343>
- [8] C. Edmunds, S. Martín-Martínez, J. Browell, E. Gómez-Lázaro, and S. Galloway, “On the participation of wind energy in response and reserve markets in Great Britain and

- Spain,” *Renewable and Sustainable Energy Reviews*, vol. 115, no. March, p. 109360, nov 2019. [Online]. Available: <https://doi.org/10.1016/j.rser.2019.109360>
- [9] L. Ziegler, E. Gonzalez, T. Rubert, U. Smolka, and J. J. Melero, “Lifetime extension of onshore wind turbines: A review covering Germany, Spain, Denmark, and the UK,” *Renewable and Sustainable Energy Reviews*, vol. 82, no. September 2017, pp. 1261–1271, feb 2018. [Online]. Available: <http://dx.doi.org/10.1016/j.rser.2017.09.100>
- [10] J. Simpson, E. Loth, and K. Dykes, “Cost of Valued Energy for design of renewable energy systems,” *Renewable Energy*, vol. 153, pp. 290–300, 2020. [Online]. Available: <https://doi.org/10.1016/j.renene.2020.01.131>
- [11] K. Dykes, “Optimization of Wind Farm Design for Objectives Beyond LCOE,” *Journal of Physics: Conference Series*, vol. 1618, no. 4, p. 042039, sep 2020. [Online]. Available: <https://iopscience.iop.org/article/10.1088/1742-6596/1618/4/042039>
- [12] I. Eguinoa, T. Göçmen, P. B. Garcia-Rosa, K. Das, V. Petrović, K. Kölle, A. Manjock, M. J. Koivisto, and M. Smailes, “Wind farm flow control oriented to electricity markets and grid integration: Initial perspective analysis,” *Advanced Control for Applications*, vol. 3, no. 3, pp. 1–28, 2021. [Online]. Available: <https://doi.org/10.1002/adc2.80>
- [13] J. Meyers, C. Bottasso, K. Dykes, P. Fleming, P. Gebraad, G. Giebel, T. Göçmen, and J.-W. van Wingerden, “Wind farm flow control: prospects and challenges,” *Wind Energy Science*, vol. 7, no. 6, pp. 2271–2306, nov 2022. [Online]. Available: <https://wes.copernicus.org/articles/7/2271/2022/>
- [14] H. Canet, A. Guilloré, and C. L. Bottasso, “The eco-conscious wind turbine: design beyond purely economic metrics,” *Wind Energy Science*, vol. 8, no. 6, pp. 1029–1047, jun 2023. [Online]. Available: <https://wes.copernicus.org/articles/8/1029/2023/>
- [15] L. Hirth and S. Müller, “System-friendly wind power-How advanced wind turbine design can increase the economic value of electricity generated through wind power,” *Energy Economics*, vol. 56, pp. 51–63, may 2016. [Online]. Available: <http://dx.doi.org/10.1016/j.eneco.2016.02.016>
- [16] P. Pinson, C. Chevallier, and G. N. Kariniotakis, “Trading Wind Generation From Short-Term Probabilistic Forecasts of Wind Power,” *IEEE Transactions on Power Systems*, vol. 22, no. 3, pp. 1148–1156, aug 2007. [Online]. Available: <http://ieeexplore.ieee.org/document/4282048/>
- [17] A. Papakonstantinou, G. Champeri, S. Delikaraoglou, and P. Pinson, “Trading wind power through physically settled options and short-term electricity markets,” *Wind Energy*, vol. 22, no. 11, pp. 1487–1499, nov 2019. [Online]. Available: <https://onlinelibrary.wiley.com/doi/10.1002/we.2383>
- [18] T. Soares, P. Pinson, T. V. Jensen, and H. Morais, “Optimal Offering Strategies

- for Wind Power in Energy and Primary Reserve Markets,” *IEEE Transactions on Sustainable Energy*, vol. 7, no. 3, pp. 1036–1045, jul 2016. [Online]. Available: <https://ieeexplore.ieee.org/document/7399764/>
- [19] P. Chen and T. Thiringer, “Analysis of Energy Curtailment and Capacity Overinstallation to Maximize Wind Turbine Profit Considering Electricity Price–Wind Correlation,” *IEEE Transactions on Sustainable Energy*, vol. 8, no. 4, pp. 1406–1414, oct 2017. [Online]. Available: <http://ieeexplore.ieee.org/document/7879327/>
- [20] E. Rebello, D. Watson, and M. Rodgers, “Performance Analysis of a 10 MW Wind Farm in Providing Secondary Frequency Regulation: Experimental Aspects,” *IEEE Transactions on Power Systems*, vol. 34, no. 4, pp. 3090–3097, jul 2019. [Online]. Available: <https://ieeexplore.ieee.org/document/8606157/>
- [21] M. Lutz, P. Görg, S. Faulstich, R. Cernusko, and S. Pfaffel, “Monetary-based availability: A novel approach to assess the performance of wind turbines,” *Wind Energy*, vol. 23, no. 1, pp. 77–89, jan 2020. [Online]. Available: <https://onlinelibrary.wiley.com/doi/10.1002/we.2411>
- [22] D. McInnis and M. Capezzali, “Managing Wind Turbine Generators with a Profit Maximized Approach,” *Sustainability*, vol. 12, no. 17, p. 7139, sep 2020. [Online]. Available: <https://www.mdpi.com/2071-1050/12/17/7139>
- [23] K. Kölle, T. Göçmen, I. Eguinoa, L. A. Alcayaga Román, M. Aparicio-Sanchez, J. Feng, J. Meyers, V. Pettas, and I. Sood, “Farmconners market showcases results: Wind farm flow control considering electricity prices and revenue,” *Wind Energy Science Discussions*, vol. 2022, pp. 1–29, 2022. [Online]. Available: <https://wes.copernicus.org/preprints/wes-2022-25/>
- [24] E. Simley, D. Millstein, S. Jeong, and P. A. Fleming, “The value of wake steering wind farm control in U.S. energy markets,” *Wind Energy Science*, 2023. [Online]. Available: <https://doi.org/10.5194/wes-2023-12>
- [25] A. C. Kheirabadi and R. Nagamune, “A quantitative review of wind farm control with the objective of wind farm power maximization,” *Journal of Wind Engineering and Industrial Aerodynamics*, vol. 192, no. March, pp. 45–73, sep 2019. [Online]. Available: <https://doi.org/10.1016/j.jweia.2019.06.015>
- [26] L. E. Andersson, O. Anaya-Lara, J. O. Tande, K. O. Merz, and L. Imsland, “Wind farm control - Part I: A review on control system concepts and structures,” *IET Renewable Power Generation*, vol. 15, no. 10, pp. 2085–2108, jul 2021. [Online]. Available: <https://onlinelibrary.wiley.com/doi/10.1049/rpg2.12160>
- [27] S. Kanev, F. Savenije, and W. Engels, “Active wake control: An approach to optimize the lifetime operation of wind farms,” *Wind Energy*, vol. 21, no. 7, pp. 488–501, jul 2018.

- [Online]. Available: <http://doi.wiley.com/10.1002/we.2173>
- [28] E. Bossanyi, “Combining induction control and wake steering for wind farm energy and fatigue loads optimisation,” *Journal of Physics: Conference Series*, vol. 1037, no. 3, p. 032011, jun 2018. [Online]. Available: <https://iopscience.iop.org/article/10.1088/1742-6596/1037/3/032011>
- [29] I. Sood, C. d. F. et D’Espierres, and J. Meyers, “Quasi-static closed-loop wind-farm control for combined power and fatigue optimization,” *Preprint*, pp. 1–24, may 2023. [Online]. Available: <http://arxiv.org/abs/2305.11710>
- [30] J. Gonzalez Silva, R. Ferrari, and J.-W. van Wingerden, “Wind farm control for wake-loss compensation, thrust balancing and load-limiting of turbines,” *Renewable Energy*, vol. 203, no. September 2022, pp. 421–433, feb 2023. [Online]. Available: <https://doi.org/10.1016/j.renene.2022.11.113>
- [31] N. Beganovic and D. Söffker, “Structural health management utilization for lifetime prognosis and advanced control strategy deployment of wind turbines: An overview and outlook concerning actual methods, tools, and obtained results,” *Renewable and Sustainable Energy Reviews*, vol. 64, pp. 68–83, 2016. [Online]. Available: <http://dx.doi.org/10.1016/j.rser.2016.05.083>
- [32] S. Loew, D. Obradovic, and C. L. Bottasso, “Economic nonlinear model predictive control of fatigue—Formulation and application to wind turbine control,” *Optimal Control Applications and Methods*, no. April 2021, pp. 1–30, 2022. [Online]. Available: <https://doi.org/10.1002/oca.2870>
- [33] N. Beganovic, J. Njiri, and D. Söffker, “Reduction of Structural Loads in Wind Turbines Based on an Adapted Control Strategy Concerning Online Fatigue Damage Evaluation Models,” *Energies*, vol. 11, no. 12, p. 3429, dec 2018. [Online]. Available: <https://doi.org/10.3390/en11123429>
- [34] P. F. Odgaard, “On usage of pareto curves to select wind turbine controller tunings to the wind turbulence level,” in *2015 European Control Conference (ECC)*. IEEE, jul 2015, pp. 1534–1539. [Online]. Available: <http://ieeexplore.ieee.org/document/7330756/>
- [35] S. J. Johnson, S. Larwood, G. McNerney, and C. Dam, “Balancing fatigue damage and turbine performance through innovative pitch control algorithm,” *Wind Energy*, vol. 15, no. 5, pp. 665–677, jul 2012. [Online]. Available: <https://onlinelibrary.wiley.com/doi/10.1002/we.495>
- [36] P. Loepelmann and B. Fischer, “Lifetime extension and opex reduction by adapting the operational strategy of wind farms,” *Journal of Physics: Conference Series*, vol. 2257, no. 1, p. 012014, apr 2022. [Online]. Available: <https://iopscience.iop.org/article/10.1088/1742-6596/2257/1/012014>

- [37] N. Requate and T. Meyer, “Active Control of the Reliability of Wind Turbines,” in *IFAC-PapersOnLine*, vol. 53, no. 2. Elsevier Ltd, 2020, pp. 12 789–12 796. [Online]. Available: <https://doi.org/10.1016/j.ifacol.2020.12.1941>
- [38] N. Requate, T. Meyer, and R. Hofmann, “From wind conditions to operational strategy: Optimal planning of wind turbine damage progression over its lifetime,” *Wind Energy Science Discussions*, 2023. [Online]. Available: <https://doi.org/10.5194/wes-2022-99>
- [39] M. Miner, “Cumulative Damage in Fatigue,” *Journal of Applied Mechanics*, vol. 3, no. 3, pp. 159–164, 1945.
- [40] I. Rychlik, “A new definition of the rainflow cycle counting method,” *International Journal of Fatigue*, vol. 9, no. 2, pp. 119–121, apr 1987. [Online]. Available: <https://linkinghub.elsevier.com/retrieve/pii/0142112387900545>
- [41] K. Thomsen, “The statistical variation of wind turbine fatigue loads,” DTU Risoe-R-1063(EN), Tech. Rep., 1998. [Online]. Available: <https://orbit.dtu.dk/en/publications/the-statistical-variation-of-wind-turbine-fatigue-loads-3>
- [42] J. P. Blasques and A. Natarajan, “Mean load effects on the fatigue life of offshore wind turbine monopile foundations,” in *Proceedings of the 5th International Conference on Computational Methods in Marine Engineering, MARINE 2013*, 2013. [Online]. Available: [https://backend.orbit.dtu.dk/ws/portalfiles/portal/54008700/Mean\\_load\\_effects.pdf](https://backend.orbit.dtu.dk/ws/portalfiles/portal/54008700/Mean_load_effects.pdf)
- [43] J. M. Jonkman and M. L. J. Buhl, “FAST User’s Guide - Updated August 2005,” National Renewable Energy Laboratory (NREL), Golden, CO, Tech. Rep. 6, oct 2005. [Online]. Available: <https://doi.org/10.2172/15020796>
- [44] “NREL FAST v8,” 2016. [Online]. Available: <https://www.nrel.gov/wind/nwtc/fastv8.html>
- [45] NREL, “Turbsim legacy web page.” [Online]. Available: <https://www.nrel.gov/wind/nwtc/turbsim.html>
- [46] C. Bak, F. Zahle, R. Bitsche, A. Yde, L. C. Henriksen, A. Nata, and M. H. Hansen, “Description of the DTU 10 MW Reference Wind Turbine DTU Wind Energy Report-I-0092,” DTU, Roskilde, Tech. Rep. July, 2013.
- [47] M. Borg, M. Mirzaei, and H. Bredmose, “LIFES50+ Deliverable D1.2 Wind turbine models for the design,” LIFES50+, Tech. Rep., 2015. [Online]. Available: <https://lifes50plus.eu/results/>
- [48] T. Burton, N. Jenkins, D. Sharpe, and E. Bossanyi, *Wind Energy Handbook*. Wiley, may 2011. [Online]. Available: <https://onlinelibrary.wiley.com/doi/book/10.1002/9781119992714>
- [49] J. F. Manwell, J. G. McGowan, and A. L. Rogers, *Wind Energy Explained*.

- Wiley, dec 2009. [Online]. Available: <https://onlinelibrary.wiley.com/doi/book/10.1002/9781119994367>
- [50] M. Hansen, *Aerodynamics of Wind Turbines*, 2nd ed. Routledge, may 2015, vol. 44, no. 8. [Online]. Available: <https://www.taylorfrancis.com/books/9781317671039>
- [51] A. D. Wright and L. J. Fingersh, “Advanced Control Design for Wind Turbines Part I: Control Design, Implementation, and Initial Tests,” National Renewable Energy Lab (NREL), Tech. Rep. March, 2008. [Online]. Available: <https://doi.org/10.2172/927269>
- [52] J. Jonkman, S. Butterfield, W. Musial, and G. Scott, “Definition of a 5-MW Reference Wind Turbine for Offshore System Development,” National Renewable Energy Laboratory (NREL), Golden, CO, Tech. Rep., feb 2009. [Online]. Available: <http://www.osti.gov/servlets/purl/947422-nhrlni/>
- [53] E. A. Bossanyi, “The Design of closed loop controllers for wind turbines,” *Wind Energy*, vol. 3, no. 3, pp. 149–163, jul 2000. [Online]. Available: <http://doi.wiley.com/10.1002/we.34>
- [54] Morten Hartvig Hansen ; Lars Christian Henriksen, “Basic DTU Wind Energy controller,” DTU Energy E No. 0028, Tech. Rep. January, 2013. [Online]. Available: [https://backend.orbit.dtu.dk/ws/portalfiles/portal/56263924/DTU\\_Wind\\_Energy\\_E\\_0028.pdf](https://backend.orbit.dtu.dk/ws/portalfiles/portal/56263924/DTU_Wind_Energy_E_0028.pdf)
- [55] N. J. Abbas, D. S. Zalkind, L. Pao, and A. Wright, “A reference open-source controller for fixed and floating offshore wind turbines,” *Wind Energy Science*, vol. 7, no. 1, pp. 53–73, jan 2022. [Online]. Available: <https://wes.copernicus.org/articles/7/53/2022/>
- [56] L. Brandetti, Y. Liu, S. Mulders, C. Ferreira, S. Watson, and J. van Wingerden, “On the ill-conditioning of the combined wind speed estimator and tip-speed ratio tracking control scheme,” *Journal of Physics: Conference Series*, vol. 2265, no. 3, p. 032085, may 2022. [Online]. Available: <https://iopscience.iop.org/article/10.1088/1742-6596/2265/3/032085>
- [57] S. Mulders and J. van Wingerden, “Delft Research Controller: an open-source and community-driven wind turbine baseline controller,” *Journal of Physics: Conference Series*, vol. 1037, no. 3, p. 032009, jun 2018. [Online]. Available: <https://iopscience.iop.org/article/10.1088/1742-6596/1037/3/032009>
- [58] N. J. Abbas, A. Wright, and L. Pao, “An Update to the National Renewable Energy Laboratory Baseline Wind Turbine Controller,” *Journal of Physics: Conference Series*, vol. 1452, no. 1, p. 012002, jan 2020. [Online]. Available: <https://iopscience.iop.org/article/10.1088/1742-6596/1452/1/012002>
- [59] P. A. Fleming, A. Peiffer, and D. Schlipf, “Wind Turbine Controller to Mitigate Structural Loads on a Floating Wind Turbine Platform,” *Journal of Offshore Mechanics and Arctic Engineering*, vol. 141, no. 6, dec 2019. [Online]. Available: <https://asmedigitalcollection.asme.org/offshoremechanics/article/doi/10.1115/>

- 1.4042938/727486/Wind-Turbine-Controller-to-Mitigate-Structural
- [60] M. Mirzaei, C. Tibaldi, and M. H. Hansen, “PI controller design of a wind turbine: evaluation of the pole-placement method and tuning using constrained optimization,” *Journal of Physics: Conference Series*, vol. 753, no. 5, p. 052026, sep 2016. [Online]. Available: <https://iopscience.iop.org/article/10.1088/1742-6596/753/5/052026>
- [61] C. Tibaldi, M. H. Hansen, and L. C. Henriksen, “Optimal tuning for a classical wind turbine controller,” *Journal of Physics: Conference Series*, vol. 555, no. 1, p. 012099, dec 2014. [Online]. Available: <https://iopscience.iop.org/article/10.1088/1742-6596/555/1/012099>
- [62] L. C. Henriksen, “Model-based predictive control of wind turbines,” PhD thesis, Technical University of Denmark, 2011. [Online]. Available: [https://backend.orbit.dtu.dk/ws/portalfiles/portal/5505252/phd244\\_larh.pdf](https://backend.orbit.dtu.dk/ws/portalfiles/portal/5505252/phd244_larh.pdf)
- [63] C. Bottasso and A. Croce, “Advanced control laws for variable-speed wind turbines and supporting enabling technologies,” Politecnico di Milano, Tech. Rep. February, 2009. [Online]. Available: [http://www.aero.polimi.it/bottasso/downloads/CLBottasso\\_ACroce\\_2009a.pdf](http://www.aero.polimi.it/bottasso/downloads/CLBottasso_ACroce_2009a.pdf)
- [64] M. Geyler and P. Caselitz, “Robust Multivariable Pitch Control Design for Load Reduction on Large Wind Turbines,” *Journal of Solar Energy Engineering*, vol. 130, no. 3, aug 2008. [Online]. Available: <https://asmedigitalcollection.asme.org/solarenergyengineering/article/doi/10.1115/1.2931510/469296/Robust-Multivariable-Pitch-Control-Design-for-Load>
- [65] D. Schlipf, “Lidar-assisted control concepts for wind turbines,” Phd Thesis, Stuttgart University, 2016. [Online]. Available: <https://doi.org/10.18419/OPUS-8796>
- [66] T. K. Barlas and G. A. M. van Kuik, “Review of state of the art in smart rotor control research for wind turbines,” *Progress in Aerospace Sciences*, vol. 46, no. 1, pp. 1–27, 2010. [Online]. Available: <http://dx.doi.org/10.1016/j.paerosci.2009.08.002>
- [67] V. Pettas, T. Barlas, D. Gertz, and H. A. Madsen, “Power performance optimization and loads alleviation with active flaps using individual flap control,” *Journal of Physics: Conference Series*, vol. 749, no. 1, p. 012010, sep 2016. [Online]. Available: <http://stacks.iop.org/1742-6596/749/i=1/a=012010?key=crossref.d13ce7e3184e1e16dcafb186ca1bfc20>
- [68] E. A. Bossanyi, “Individual Blade Pitch Control for Load Reduction,” *Wind Energy*, vol. 6, no. 2, pp. 119–128, apr 2003. [Online]. Available: <https://onlinelibrary.wiley.com/doi/10.1002/we.76>
- [69] E. A. Bossanyi, “Further load reductions with individual pitch control,” *Wind Energy*, vol. 8, no. 4, pp. 481–485, 2005. [Online]. Available: <https://doi.org/10.1002/we.166>

- [70] W. H. Lio, B. L. Jones, Q. Lu, and J. A. Rossiter, “Fundamental performance similarities between individual pitch control strategies for wind turbines,” *International Journal of Control*, vol. 90, no. 1, pp. 37–52, 2017. [Online]. Available: <http://dx.doi.org/10.1080/00207179.2015.1078912>
- [71] E. A. Bossanyi, P. A. Fleming, and A. D. Wright, “Validation of Individual Pitch Control by Field Tests on Two- and Three-Bladed Wind Turbines,” *IEEE Transactions on Control Systems Technology*, vol. 21, no. 4, pp. 1067–1078, jul 2013. [Online]. Available: <http://ieeexplore.ieee.org/document/6515638/>
- [72] D. Ossmann, P. Seiler, C. Milliren, and A. Danker, “Field testing of multi-variable individual pitch control on a utility-scale wind turbine,” *Renewable Energy*, vol. 170, pp. 1245–1256, jun 2021. [Online]. Available: <https://linkinghub.elsevier.com/retrieve/pii/S096014812100207X>
- [73] G. Bir, “Multi-Blade Coordinate Transformation and its Application to Wind Turbine Analysis,” in *46th AIAA Aerospace Sciences Meeting and Exhibit*. Reston, Virginia: American Institute of Aeronautics and Astronautics, jan 2008. [Online]. Available: <http://arc.aiaa.org/doi/10.2514/6.2008-1300>
- [74] R. P. Coleman and A. M. Feingold, “Theory of self-excited mechanical oscillations of helicopter rotors with hinged blades,” NACA Technical Report TR 1351, Tech. Rep., 1958. [Online]. Available: <https://ntrs.nasa.gov/citations/19930092339>
- [75] C. L. Bottasso, A. Croce, C. E. Riboldi, and M. Salvetti, “Cyclic pitch control for the reduction of ultimate loads on wind turbines,” *Journal of Physics: Conference Series*, vol. 524, no. 1, 2014. [Online]. Available: <https://iopscience.iop.org/article/10.1088/1742-6596/524/1/012063>
- [76] V. Petrović, M. Jelavić, and M. Baotić, “MPC framework for constrained wind turbine individual pitch control,” *Wind Energy*, vol. 24, no. 1, pp. 54–68, 2021. [Online]. Available: <https://doi.org/10.1002/we.2558>
- [77] Y. Han and W. E. Leithead, “Combined wind turbine fatigue and ultimate load reduction by individual blade control,” *Journal of Physics: Conference Series*, vol. 524, no. 1, 2014. [Online]. Available: <https://iopscience.iop.org/article/10.1088/1742-6596/524/1/012062>
- [78] Y. Han and W. E. Leithead, “Comparison of Individual Blade Control and Individual Pitch Control for Wind Turbine Load Reduction,” *EWEA 2015*, no. October, 2016.
- [79] V. Pettas and P. W. Cheng, “Down-regulation and individual blade control as lifetime extension enablers,” *Journal of Physics: Conference Series*, vol. 1102, p. 012026, oct 2018. [Online]. Available: <https://iopscience.iop.org/article/10.1088/1742-6596/1102/1/012026>
- [80] W. E. Leithead, V. Neilson, S. Dominguez, and A. Dutka, “A novel approach to structural load control using intelligent actuators,” *17th Mediterranean Conference*

- on Control & Automation*, no. June, pp. 1257–1262, 2009. [Online]. Available: [http://ieeexplore.ieee.org/xpls/abs/\\_all.jsp?arnumber=5164719](http://ieeexplore.ieee.org/xpls/abs/_all.jsp?arnumber=5164719)
- [81] D. Astrain Juangarcia, I. Eguinoa, and T. Knudsen, “Derating a single wind farm turbine for reducing its wake and fatigue,” *Journal of Physics: Conference Series*, vol. 1037, p. 032039, jun 2018. [Online]. Available: <http://stacks.iop.org/1742-6596/1037/i=3/a=032039?key=crossref.1423606afb0ae9b058a8522695ce0cfhttps://iopscience.iop.org/article/10.1088/1742-6596/1037/3/032039>
- [82] W. H. Lio, M. Mirzaei, and G. C. Larsen, “On wind turbine down-regulation control strategies and rotor speed set-point,” *Journal of Physics: Conference Series*, vol. 1037, p. 032040, jun 2018. [Online]. Available: <http://stacks.iop.org/1742-6596/1037/i=3/a=032040?key=crossref.011cc406dd4baff3fcf3ee684120d898https://iopscience.iop.org/article/10.1088/1742-6596/1037/3/032040>
- [83] C. Galinos, T. J. Larsen, and M. Mirzaei, “Impact on wind turbine loads from different down regulation control strategies,” *Journal of Physics: Conference Series*, vol. 1104, no. 1, p. 012019, oct 2018. [Online]. Available: <https://iopscience.iop.org/article/10.1088/1742-6596/1104/1/012019>
- [84] D.C. van der Hoek; and S. Kanev, “Reducing Wind Turbine Loads with Down-Regulation,” ECN-E-17-032, Tech. Rep. ECN-E-17-032, 2017. [Online]. Available: <http://resolver.tudelft.nl/uuid:fc6658f8-106b-4cf0-8d67-50c99cb895aa>
- [85] J. Aho, P. Fleming, and L. Y. Pao, “Active power control of wind turbines for ancillary services: A comparison of pitch and torque control methodologies,” in *2016 American Control Conference (ACC)*. IEEE, jul 2016, pp. 1407–1412. [Online]. Available: <http://ieeexplore.ieee.org/document/7525114/>
- [86] M. Kretschmer, V. Pettas, and P. W. Cheng, “Effects of Wind Farm Down-Regulation in the Offshore Wind Farm Alpha Ventus,” *ASME 2019 2nd International Offshore Wind Technical Conference*, nov 2019. [Online]. Available: <https://asmedigitalcollection.asme.org/OMAE/proceedings/IOWTC2019/59353/St.Julian’s,Malta/1072002>
- [87] V. Pettas, M. Salari, D. Schlipf, and P. W. Cheng, “Investigation on the potential of individual blade control for lifetime extension,” *Journal of Physics: Conference Series*, vol. 1037, p. 032006, jun 2018. [Online]. Available: <https://iopscience.iop.org/article/10.1088/1742-6596/1037/3/032006>
- [88] A. Solum and M. Leijon, “Investigating the overload capacity of a direct-driven synchronous permanent magnet wind turbine generator designed using high-voltage cable technology,” *International Journal of Energy Research*, vol. 31, no. 11, pp. 1076–1086, sep 2007. [Online]. Available: <https://onlinelibrary.wiley.com/doi/10.1002/er.1301>
- [89] Siemens Gamesa AS. (2020) Siemens Gamesa Power Boost technol-

- ogy. Brochure; "<https://www.siemensgamesa.com/products-and-services/offshore/wind-turbine-sg-14-222-dd>". [Online]. Available: <https://www.siemensgamesa.com/products-and-services/offshore/wind-turbine-sg-14-222-dd>
- [90] Vestas. Vestas Power Uprate. [Online]. Available: <https://nozebra.ipapercms.dk/Vestas/Communication/Productbrochure/ProductImprovements/PowerUprate/>
- [91] Siemens. Siemens Energy Thrust. [Online]. Available: <https://www.siemensgamesa.com/products-and-services/service-wind/energy-thrust>
- [92] A. I. J. Forrester, A. Sóbester, and A. J. Keane, *Engineering Design via Surrogate Modelling*. Wiley, jul 2008. [Online]. Available: <https://onlinelibrary.wiley.com/doi/book/10.1002/9780470770801>
- [93] N. Dimitrov, M. C. Kelly, A. Vignaroli, and J. Berg, "From wind to loads: wind turbine site-specific load estimation with surrogate models trained on high-fidelity load databases," *Wind Energy Science*, vol. 3, no. 2, pp. 767–790, oct 2018. [Online]. Available: <https://wes.copernicus.org/articles/3/767/2018/>
- [94] R. M. Slot, J. D. Sørensen, B. Sudret, L. Svenningsen, and M. L. Thøgersen, "Surrogate model uncertainty in wind turbine reliability assessment," *Renewable Energy*, vol. 151, pp. 1150–1162, may 2020. [Online]. Available: <https://linkinghub.elsevier.com/retrieve/pii/S096014811931794X>
- [95] K. Müller, "Probabilistic Fatigue Load Assessment for Floating Wind Turbines," PhD Thesis, University of Stuttgart, 2019.
- [96] A. N. Robertson, K. Shaler, L. Sethuraman, and J. Jonkman, "Sensitivity analysis of the effect of wind characteristics and turbine properties on wind turbine loads," *Wind Energy Science*, vol. 4, no. 3, pp. 479–513, sep 2019. [Online]. Available: <https://wes.copernicus.org/articles/4/479/2019/>
- [97] P. Bortolotti, H. Canet, C. L. Bottasso, and J. Loganathan, "Performance of non-intrusive uncertainty quantification in the aeroservoelastic simulation of wind turbines," *Wind Energy Science*, vol. 4, no. 3, pp. 397–406, jul 2019. [Online]. Available: <https://wes.copernicus.org/articles/4/397/2019/>
- [98] H. S. Toft, L. Svenningsen, W. Moser, J. D. Sørensen, and M. L. Thøgersen, "Assessment of wind turbine structural integrity using response surface methodology," *Engineering Structures*, vol. 106, pp. 471–483, jan 2016. [Online]. Available: <http://dx.doi.org/10.1016/j.engstruct.2015.10.043>
- [99] J. M. Rinker, "Calculating the sensitivity of wind turbine loads to wind inputs using response surfaces," *Journal of Physics: Conference Series*, vol. 753, no. 3, p. 032057, sep 2016. [Online]. Available: <https://iopscience.iop.org/article/10.1088/1742-6596/753/3/032057>

- [100] J. P. Murcia, P.-E. Réthoré, N. Dimitrov, A. Natarajan, J. D. Sørensen, P. Graf, and T. Kim, “Uncertainty propagation through an aeroelastic wind turbine model using polynomial surrogates,” *Renewable Energy*, vol. 119, pp. 910–922, apr 2018. [Online]. Available: <https://linkinghub.elsevier.com/retrieve/pii/S0960148117306985>
- [101] R. Teixeira, A. O’Connor, M. Nogal, N. Krishnan, and J. Nichols, “Analysis of the design of experiments of offshore wind turbine fatigue reliability design with Kriging surfaces,” *Procedia Structural Integrity*, vol. 5, pp. 951–958, 2017. [Online]. Available: <http://dx.doi.org/10.1016/j.prostr.2017.07.132>
- [102] T. Barlas, N. Ramos-García, G. R. Pirrung, and S. González Horcas, “Surrogate-based aeroelastic design optimization of tip extensions on a modern 10 MW wind turbine,” *Wind Energy Science*, vol. 6, no. 2, pp. 491–504, mar 2021. [Online]. Available: <https://wes.copernicus.org/articles/6/491/2021/>
- [103] N. Dimitrov, “Surrogate models for parameterized representation of wake-induced loads in wind farms,” *Wind Energy*, vol. 22, no. 10, pp. 1371–1389, oct 2019. [Online]. Available: <https://onlinelibrary.wiley.com/doi/10.1002/we.2362>
- [104] N. Dimitrov and A. Natarajan, “Wind farm set point optimization with surrogate models for load and power output targets,” *Journal of Physics: Conference Series*, vol. 2018, no. 1, p. 012013, sep 2021. [Online]. Available: <https://iopscience.iop.org/article/10.1088/1742-6596/2018/1/012013>
- [105] P. Hulsman, S. J. Andersen, and T. Göçmen, “Optimizing wind farm control through wake steering using surrogate models based on high-fidelity simulations,” *Wind Energy Science*, vol. 5, no. 1, pp. 309–329, mar 2020. [Online]. Available: <https://wes.copernicus.org/articles/5/309/2020/>
- [106] C. M. J. Debusscher, T. Göçmen, and S. J. Andersen, “Probabilistic surrogates for flow control using combined control strategies,” *Journal of Physics: Conference Series*, vol. 2265, no. 3, p. 032110, may 2022. [Online]. Available: <https://iopscience.iop.org/article/10.1088/1742-6596/2265/3/032110>
- [107] G. Gasparis, W. H. Lio, and F. Meng, “Surrogate Models for Wind Turbine Electrical Power and Fatigue Loads in Wind Farm,” *Energies*, vol. 13, no. 23, p. 6360, dec 2020. [Online]. Available: <https://www.mdpi.com/1996-1073/13/23/6360>
- [108] L. Schröder, N. Krasimirov Dimitrov, and D. Robert Verelst, “A surrogate model approach for associating wind farm load variations with turbine failures,” *Wind Energy Science*, vol. 5, no. 3, pp. 1007–1022, 2020. [Online]. Available: <https://doi.org/10.5194/wes-5-1007-2020>
- [109] X.-L. Li, J.-G. Park, and H.-B. Shin, “Comparison and Evaluation of Anti-Windup PI Controllers,” *Journal of Power Electronics*, vol. 11, no. 1, pp. 45–50, jan 2011. [Online].

- Available: <http://koreascience.or.kr/journal/view.jsp?kj=E1PWAX&py=2011&vnc=v11n1&sp=45>
- [110] R. Ungurán and M. Kühn, “Combined individual pitch and trailing edge flap control for structural load alleviation of wind turbines,” in *2016 American Control Conference (ACC)*. IEEE, jul 2016, pp. 1–9. [Online]. Available: <http://ieeexplore.ieee.org/document/7524879/>
- [111] L. Ljung, *System identification (2nd ed.): theory for the user*. Prentice Hall PTR, 1999.
- [112] W. Larimore, “Canonical variate analysis in identification, filtering and adaptive control.” in *Proceedings of the 29th IEEE Conference on Decision and Control*. IEEE, dec 1990.
- [113] International Electrotechnical Commission (IEC), “Wind turbines Part 1: Design requirements 61400-1 , 3rd edition,” International Electrotechnical Commission (IEC), Switzerland, Tech. Rep., 2005.
- [114] K. Q. Ye, “Orthogonal Column Latin Hypercubes and Their Application in Computer Experiments,” *Journal of the American Statistical Association*, vol. 93, no. 444, pp. 1430–1439, dec 1998. [Online]. Available: <http://www.tandfonline.com/doi/abs/10.1080/01621459.1998.10473803>
- [115] M. D. McKay, R. J. Beckman, and W. J. Conover, “A Comparison of Three Methods for Selecting Values of Input Variables in the Analysis of Output from a Computer Code,” *Technometrics*, vol. 21, no. 2, p. 239, may 1979. [Online]. Available: <https://www.jstor.org/stable/1268522?origin=crossref>
- [116] C. E. Rasmussen and C. K. I. Williams, *Gaussian Processes for Machine Learning*. The MIT Press, 2005. [Online]. Available: <https://direct.mit.edu/books/book/2320/gaussian-processes-for-machine-learning>
- [117] V. Pettas, M. Kretschmer, A. Clifton, and P. W. Cheng, “On the effects of inter-farm interactions at the offshore wind farm Alpha Ventus,” *Wind Energy Science*, vol. 6, no. 6, pp. 1455–1472, nov 2021. [Online]. Available: <https://doi.org/10.5194/wes-2021-50>
- [118] T. W. Athan and P. Y. Papalambros, “A note on weighted criteria methods for compromise solutions in multi-objective optimization,” *Engineering Optimization*, vol. 27, no. 2, pp. 155–176, sep 1996. [Online]. Available: <http://www.tandfonline.com/doi/abs/10.1080/03052159608941404>
- [119] J. R. R. A. Martins and A. Ning, *Engineering Design Optimization*. Cambridge University Press, nov 2021. [Online]. Available: <https://www.cambridge.org/core/product/identifier/9781108980647/type/book>
- [120] Z. Ugray, L. Lasdon, J. Plummer, F. Glover, J. Kelly, and R. Martí, “Scatter Search and Local NLP Solvers: A Multistart Framework for Global Optimization,” *INFORMS Journal on Computing*, vol. 19, no. 3, pp. 328–340, aug 2007. [Online]. Available:

- <https://pubsonline.informs.org/doi/10.1287/ijoc.1060.0175>
- [121] L. C. W. Dixon and G. P. Szegő, *Towards global optimisation 2*. Amsterdam New York: North-Holland Pub. Co, 1978.
- [122] S. Katoch, S. S. Chauhan, and V. Kumar, “A review on genetic algorithm: past, present, and future,” *Multimedia Tools and Applications*, vol. 80, no. 5, pp. 8091–8126, feb 2021. [Online]. Available: <http://link.springer.com/10.1007/s11042-020-10139-6>
- [123] D. E. Goldberg, *Genetic Algorithms in Search, Optimization, and Machine Learning*. New York: Addison-Wesley, 1989.
- [124] J. Kennedy and R. Eberhart, “Particle swarm optimization,” in *Proceedings of ICNN’95 - International Conference on Neural Networks*, vol. 4. IEEE, 1995, pp. 1942–1948. [Online]. Available: <http://ieeexplore.ieee.org/document/488968/>
- [125] R. Eberhart and J. Kennedy, “A new optimizer using particle swarm theory,” in *MHS’95. Proceedings of the Sixth International Symposium on Micro Machine and Human Science*. IEEE, 1995, pp. 39–43. [Online]. Available: <http://ieeexplore.ieee.org/document/494215/>
- [126] E. Mezura-Montes and C. A. Coello Coello, “Constraint-handling in nature-inspired numerical optimization: Past, present and future,” *Swarm and Evolutionary Computation*, vol. 1, no. 4, pp. 173–194, dec 2011. [Online]. Available: <https://linkinghub.elsevier.com/retrieve/pii/S2210650211000538>
- [127] M. E. Hvas Pedersen, “Good parameters for particle swarm optimization,” Hvas Laboratories, Technical Report HL1001, Tech. Rep., 2010. [Online]. Available: [https://www.researchgate.net/profile/Mohamed\\_Mourad\\_Lafifi/post/Which-is-the-best-swarm-size-in-PSO/attachment/5b5b6f85b53d2f89289c14e1/AS%3A653084896288769%401532718981208/download/Good+Parameters+for+Particle+Swarm+Optimization.pdf](https://www.researchgate.net/profile/Mohamed_Mourad_Lafifi/post/Which-is-the-best-swarm-size-in-PSO/attachment/5b5b6f85b53d2f89289c14e1/AS%3A653084896288769%401532718981208/download/Good+Parameters+for+Particle+Swarm+Optimization.pdf)
- [128] R. Weron, “Electricity price forecasting: A review of the state-of-the-art with a look into the future,” *International Journal of Forecasting*, vol. 30, no. 4, pp. 1030–1081, oct 2014. [Online]. Available: <http://dx.doi.org/10.1016/j.ijforecast.2014.08.008>
- [129] G. Giebel, R. Brownsword, G. Kariniotakis, M. Denhard, and C. Draxl, “The State-Of-The-Art in Short-Term Prediction of Wind Power A Literature Overview,” *Technical Report, ANEMOS.plus*, pp. 1–109, 2011. [Online]. Available: <papers://6470de79-5287-45a9-8e4f-b629919aff7a/Paper/p5443>
- [130] J. Yan, C. Möhrlen, T. Göçmen, M. Kelly, A. Wessel, and G. Giebel, “Uncovering wind power forecasting uncertainty sources and their propagation through the whole modelling chain,” *Renewable and Sustainable Energy Reviews*, vol. 165, no. May, p. 112519, 2022. [Online]. Available: <https://doi.org/10.1016/j.rser.2022.112519>
- [131] E. O’Brien and A. Ralph, “Operational Evaluation of a Wind-farm Forecasting

- System,” *Energy Procedia*, vol. 76, pp. 216–222, aug 2015. [Online]. Available: <http://dx.doi.org/10.1016/j.egypro.2015.07.903>
- [132] C.-M. Huang, S.-J. Chen, S.-P. Yang, and H.-J. Chen, “One-Day-Ahead Hourly Wind Power Forecasting Using Optimized Ensemble Prediction Methods,” *Energies*, vol. 16, no. 6, p. 2688, mar 2023. [Online]. Available: <https://www.mdpi.com/1996-1073/16/6/2688>
- [133] J. Lago, G. Marcjasz, B. De Schutter, and R. Weron, “Forecasting day-ahead electricity prices: A review of state-of-the-art algorithms, best practices and an open-access benchmark,” *Applied Energy*, vol. 293, no. December 2020, p. 116983, jul 2021. [Online]. Available: <https://doi.org/10.1016/j.apenergy.2021.116983>
- [134] S. C. Pryor, T. J. Shepherd, and R. J. Barthelmie, “Interannual variability of wind climates and wind turbine annual energy production,” *Wind Energy Science*, vol. 3, no. 2, pp. 651–665, sep 2018. [Online]. Available: <https://wes.copernicus.org/articles/3/651/2018/>
- [135] New European Wind Atlas. [Online]. Available: <https://map.neweuropeanwindatlas.eu/>
- [136] J. S. Rodrigo, R. A. Chávez Arroyo, B. Witha, M. Dörenkämper, J. Gottschall, M. Avila, J. Arnqvist, A. Hahmann, and T. Sile, “The New European Wind Atlas Model Chain,” *Journal of Physics: Conference Series*, vol. 1452, p. 012087, jan 2020. [Online]. Available: <https://iopscience.iop.org/article/10.1088/1742-6596/1452/1/012087>
- [137] SMARD. Electricity market data download. [Online]. Available: <https://www.smard.de/en/downloadcenter/download-market-data>
- [138] TotalControl. Advanced integrated supervisory and wind turbine control for optimal operation of large Wind Power Plants EU project. [Online]. Available: <https://cordis.europa.eu/project/id/727680>
- [139] FarmConnors. FarmConnors - Paving the Way for Wind Farm Control in Industry EU project. [Online]. Available: <https://cordis.europa.eu/project/id/857844>
- [140] TotalControl, “Reference Wind Power Plant D1.03,” Tech. Rep., 2018. [Online]. Available: <https://cordis.europa.eu/project/id/727680/results>
- [141] M. Koivisto, K. Das, F. Guo, P. Sørensen, E. Nuño, N. Cutululis, and P. Maule, “Using time series simulation tools for assessing the effects of variable renewable energy generation on power and energy systems,” *WIREs Energy and Environment*, vol. 8, no. 3, may 2019. [Online]. Available: <https://onlinelibrary.wiley.com/doi/10.1002/wene.329>
- [142] M. Koivisto, G. M. Jónsdóttir, P. Sørensen, K. Plakas, and N. Cutululis, “Combination of meteorological reanalysis data and stochastic simulation for modelling wind generation variability,” *Renewable Energy*, vol. 159, pp. 991–999, oct 2020. [Online]. Available: <https://linkinghub.elsevier.com/retrieve/pii/S0960148120309277>

- [143] Energinet. Energi data service. [Online]. Available: <https://www.energidataservice.dk/tso-electricity/nordpoolmarket>